

DISS. ETH No. 25398

MODELING HAZARDS RELATED TO LARGE WOOD IN RIVERS

A thesis submitted to attain the degree of
DOCTOR OF SCIENCES of ETH ZURICH
(Dr. sc. ETH Zurich)

presented by

ISABELLA SCHALKO

Dipl.-Ing., University of Natural Resources and Life Sciences, Vienna

born on 22.11.1986

citizen of Austria

accepted on the recommendation of

Prof. Dr. Robert M. Boes

Dr. Lukas Schmocker

Prof. Dr. Markus Stoffel

Dr. Volker Weitbrecht

Prof. Dr. Ellen Wohl

2018



Model large wood accumulation at a retention rack with a movable bed

Acknowledgements

This doctoral thesis was written during my employment at the Laboratory of Hydraulics, Hydrology and Glaciology (VAW) at ETH Zurich. The project was funded by the Swiss Federal Office for the Environment (FOEN), Grant 15.0018.PJ / O192-0202, and was part of the research project *WoodFlow*. I would like to thank all who contributed to the present work with particular acknowledgment to

- VAW director and examiner Prof. Dr. Robert Boes for his continuous support, helpful discussions, and detailed review of this thesis.
- My supervisors and co-examiners Dr. Volker Weitbrecht and Dr. Lukas Schmocker for initiating this doctoral thesis, their scientific and moral support, and invaluable advice during the past three years.
- Prof. Dr. Markus Stoffel, University of Geneva, co-examiner, for the review and interesting discussions during our WoodFlow meetings.
- Prof. Dr. Ellen Wohl, Colorado State University, co-examiner, for the review and for introducing me to real wood accumulations during my research visit at CSU.
- WoodFlow team for the helpful discussions and exchange; in particular to Dr. Virginia Ruiz-Villanueva for her invaluable support using 'IberWood'.
- My Master and project theses students Karin Bertram, Carmen Lageder, Nicole Schärer, and Daniel Schaller for their conscientious work.
- Technical infrastructure team of VAW including workshop, electronics workshop, photographer, and graphic designers for their excellent work.
- Dr. Michael Plötze (Institute for Geotechnical Engineering, ETH Zurich) for the help during the density measurements, Grün Stadt Zürich and Fritz Graber (Facility Management, ETH Zurich) for the model wood.
- All my colleagues at VAW and friends, in particular Cristina Rachelly and Claudia Beck, for the interesting discussions, helpful input, and motivation.

- My family and especially my parents, Renate and Werner, for enabling my education, and for their continuous encouragement and support.
- Finally, I thank my partner Helge Fuchs for his precious support and the wonderful time together so far.

Zurich, October 2018

Isabella Schalko

Table of contents

Acknowledgements	III
Abstract	IX
Kurzfassung	XI
1 Introduction	1
1.1 Motivation	1
1.2 Objectives.....	3
1.3 Thesis outline	4
2 Background	5
2.1 Overview	5
2.2 Terminology	5
2.3 Wood in river ecosystems	6
2.4 Estimation of large wood volume	7
2.4.1 Overview	7
2.4.2 Empirical formulae.....	8
2.4.3 Recruitment process analysis	10
2.5 Large wood movement.....	15
2.5.1 Entrainment	15
2.5.2 Transport	18
2.5.3 Deposition	20
2.6 Selected past floods with extensive large wood transport.....	20
2.6.1 Switzerland, 1987.....	20
2.6.2 Switzerland, 2005.....	21
2.6.3 Italy – Magra river basin, 2011	21
2.6.4 Switzerland – Zug and Emme River basins, 2012	23
2.6.5 Japan – Northern Kyushu, 2012.....	24
3 Literature review	25
3.1 Overview	25
3.2 Large wood accumulation probability.....	25
3.3 Large wood accumulation characteristics	31
3.4 Hazards due to large wood accumulations at river infrastructures	34
3.4.1 Backwater rise	34
3.4.2 Local scour	37
3.5 Large wood accumulation risk reduction measures	43
3.6 Numerical studies on large wood in rivers.....	47

3.7	Summary and identified research gaps	50
4	Methodology	53
4.1	Overview.....	53
4.2	Similitude and scale effects	53
4.3	Accuracy and error analysis.....	56
4.4	Tests I: Large wood accumulation probability at bridge piers	57
4.4.1	Model flume I – tilting flume	57
4.4.2	Instrumentation.....	58
4.4.3	Model large wood and sediment.....	59
4.4.4	Test procedure and program	59
4.4.5	Test repetitions and reproducibility	61
4.5	Tests II: Large wood accumulation characteristics – Backwater rise and local scour	65
4.5.1	Model flume II – small flume.....	65
4.5.2	Model flume III – large flume	66
4.5.3	Instrumentation.....	67
4.5.4	Model large wood and organic fine material.....	67
4.5.5	Sediment.....	68
4.5.6	Test procedure and program	69
4.5.7	Test reproducibility.....	75
4.6	Tests III: Measures for large wood accumulation risk reduction	77
4.6.1	Test procedure and program	77
4.7	Numerical modeling of large wood accumulation.....	80
4.7.1	Model setup and test program.....	80
5	Results and discussion	83
5.1	Overview.....	83
5.2	Large wood accumulation probability	83
5.2.1	General process description: Incipient log detachment	83
5.2.2	General process description: Log transport	87
5.2.3	Approach flow conditions and log dimensions	89
5.2.4	Pier characteristics.....	93
5.2.5	Large wood characteristics	97
5.2.6	Movable bed	102
5.2.7	Normalized large wood accumulation probability: Design equation	105
5.3	Large wood accumulation characteristics – Backwater rise and local scour	110
5.3.1	Backwater rise	110
5.3.1.1	Approach flow conditions.....	110
5.3.1.2	Large wood accumulation characteristics.....	112
5.3.1.3	Organic fine material	115

5.3.1.4	Scale series	119
5.3.1.5	Natural large wood accumulation.....	123
5.3.1.6	Bed material.....	130
5.3.1.7	Normalized backwater rise: Design equations.....	132
5.3.2	Local scour	142
5.3.2.1	Approach flow conditions and bed material	142
5.3.2.2	Normalized local scour depth: Design equation	149
5.4	Measures for large wood accumulation risk reduction	154
5.4.1	Large wood fin	154
5.4.2	Bottom sills	158
5.5	Numerical modeling of large wood accumulation	162
5.5.1	Large wood accumulation probability at bridge piers.....	162
5.5.2	Backwater rise at a retention rack	165
5.5.3	Evaluation of ‘IberWood’	167
6	Computational example.....	169
7	Conclusions and outlook.....	175
7.1	Conclusions	175
7.2	Outlook.....	181
	Notation.....	183
	References	191
	Curriculum Vitae	207

Abstract

During floods, transported large wood (LW) may accumulate at river infrastructures or is retained intentionally at retention structures. In both cases, LW accumulation results in backwater rise and local scour. Especially the 2005 flood in the Alpine regions in Europe demonstrated the hazard potential of transported and accumulated LW. Despite recent research, knowledge of the hydraulic and geomorphic effects due to LW accumulations is still limited. Previous studies on LW accumulation probability focused mainly on the effect of a bridge deck. The formulae for backwater rise apply mostly to a specific LW retention rack placement. In addition, interactions between backwater rise and local scour due to LW accumulations have not been studied so far.

Physical model tests were performed to investigate (1) LW accumulation probability at bridge piers, (2) LW accumulation characteristics, resulting backwater rise and local scour at transverse river structures, and (3) design of suitable measures for LW accumulation risk reduction at bridge piers. For model evaluation, selected physical model tests on LW accumulation were simulated with the 2D numerical program 'IberWood'. For the LW accumulation probability, the effect of varying approach flow conditions, LW and pier characteristics, and a movable bed was investigated. The LW accumulation characteristics with particular focus on backwater rise were analyzed in three test series, comprising a predefined versus natural LW accumulation, and a fixed versus movable bed. The effects of varying approach flow conditions, LW characteristics, organic fine material, and bed material on backwater rise were studied. Furthermore, a scale series was investigated on backwater rise due to LW accumulations. The analysis of local scour due to LW accumulations included the variation of approach flow conditions and uniform bed material. The efficiency of LW fins and bottom sills to reduce accumulation probability was studied for various approach flow conditions and LW characteristics.

The main results of the present work include a prediction equation for LW accumulation probability at bridge piers for uncongested and semi-congested LW transport. Design equations are proposed to estimate both backwater rise and local scour due to LW accumulations. In addition, the effect of varying LW volume on backwater rise and local scour are considered in the design equations, allowing for a sensitivity analysis. The present work adds to the process understanding of LW accumulations at river infrastructures and contributes to an improved design of LW retention structures.

Kurzfassung

Während Hochwasserereignissen kann transportiertes Schwemmholz bei Querbauwerken verklausen oder wird bewusst mit Hilfe von Rückhaltebauwerken zurückgehalten. In beiden Fällen führt die Schwemmholzverklausung zu Aufstau und lokalem Kolk. Vor allem das Hochwasserereignis im Jahr 2005 im europäischen Alpenraum verdeutlichte das erhöhte Gefahrenpotenzial infolge Schwemmholztransport und –verklausungen. Das Verständnis hydraulischer und geomorphologischer Auswirkungen von Schwemmholzverklausungen ist immer noch begrenzt. Frühere Untersuchungen zur Verklausungswahrscheinlichkeit konzentrierten sich hauptsächlich auf den Einfluss einer Brückenträgers. Die Gleichungen für die Abschätzung des Aufstaus infolge einer Schwemmholzverklausung beziehen sich grösstenteils auf bestimmte Rechenkonfigurationen. Weiter wurde die Wechselwirkung zwischen Aufstau und lokalem Kolk infolge Schwemmholzverklausung bisher vernachlässigt.

Mit Hilfe von physikalischen Modellversuchen wurden die folgenden Aspekte untersucht: (1) Verklausungswahrscheinlichkeit an Brückenpfeilern, (2) Verklausungseigenschaften sowie resultierender Aufstau und lokaler Kolk an Querbauwerken und (3) Dimensionierung von Massnahmen zur Reduktion des Verklausungsrisikos an Brückenpfeilern. Zur Modellevaluation wurden einzelne physikalische Modellversuche zur Verklausungswahrscheinlichkeit und zum Aufstau mit Hilfe des numerischen 2D Simulationsprogramms 'Iber Wood' simuliert. Für die Verklausungswahrscheinlichkeit wurde der Einfluss verschiedener Zuflussbedingungen, Holz- und Pfeilereigenschaften und einer beweglichen Sohle untersucht. Die Verklausungseigenschaften und speziell der Aufstau infolge Schwemmholzverklausung wurden im Rahmen von drei Versuchsserien untersucht. Diese beinhalten eine vordefinierte im Vergleich zu einer natürlichen Verklausung sowie eine bewegliche Sohle. Der Einfluss verschiedener Zuflussbedingungen, Holzeigenschaften, Feinmaterialien und Sohlenmaterialien auf den Aufstau wurde für stationäre Fliessbedingungen untersucht. Weiter wurde eine Massstabsfamilie zum Aufstau infolge Schwemmholzverklausung durchgeführt. Im Rahmen der Modellversuche zu lokalem Kolk infolge Schwemmholzverklausung wurden die Zuflussbedingungen und das Einkornmaterial der Sohle variiert. Die Wirksamkeit von Schwemmholzabweisern und Sohlenschwellen auf die Reduktion der Verklausungswahrscheinlichkeit wurde für ausgewählte Zuflussbedingungen und Holzeigenschaften untersucht.

Die Hauptergebnisse der vorliegenden Arbeit umfassen Gleichungen zur Verklauungswahrscheinlichkeit an Brückenpfeilern für Einzel- und schubweisen Schwemholztransport. Weiter können sowohl Aufstau als auch lokaler Kolk infolge Schwemholzverklauung mit Hilfe von Gleichungen abgeschätzt werden. Zusätzlich wird der Einfluss des Schwemholzvolumens auf Aufstau und Kolk berücksichtigt und somit eine Sensitivitätsanalyse ermöglicht. Die vorliegende Arbeit verbessert das Prozessverständnis von Schwemholzverklauungen an Querbauwerken und erleichtert die Dimensionierung von Schwemholzrechen.

1 Introduction

1.1 Motivation

Wood is a significant part of a river ecosystem and influences its morphology, biodiversity, and hydraulics (Gurnell *et al.* 2002). Logs with a diameter ≥ 0.1 m and length ≥ 1 m are referred to as large wood (LW) (Wohl and Jaeger 2009). In rivers, LW may appear as single log pieces or in bulk, i.e. LW accumulations or log jams. LW accumulations increase the flow resistance and create heterogeneous hydraulic conditions (Gippel 1995). The connectivity between the channel and the floodplain, and between water, sediments, and nutrients can consequently significantly improve due to log pieces or jams (Wohl *et al.* 2016). Besides these positive ecological aspects, LW may pose a considerable hazard during floods. Transported LW can accumulate at river infrastructures such as bridges or weirs. The LW accumulation reduces the flow cross-section, leading to backwater rise and consequently to a flooding of the surrounding area (Figure 1.1). In addition, a LW accumulation affects the geomorphic conditions. Local scour may occur at river infrastructures, thereby damaging the infrastructure itself. Furthermore, an accumulation can foster the disruption of the sediment continuity. The 2005 flood in Switzerland transported 30,000 t of LW, demonstrating its high hazard potential (Bezzola and Hegg 2007, VAW 2008, Waldner *et al.* 2009). The estimation of the probability and characteristics of LW accumulations at river infrastructures are deemed necessary for an integrated flood hazard assessment.

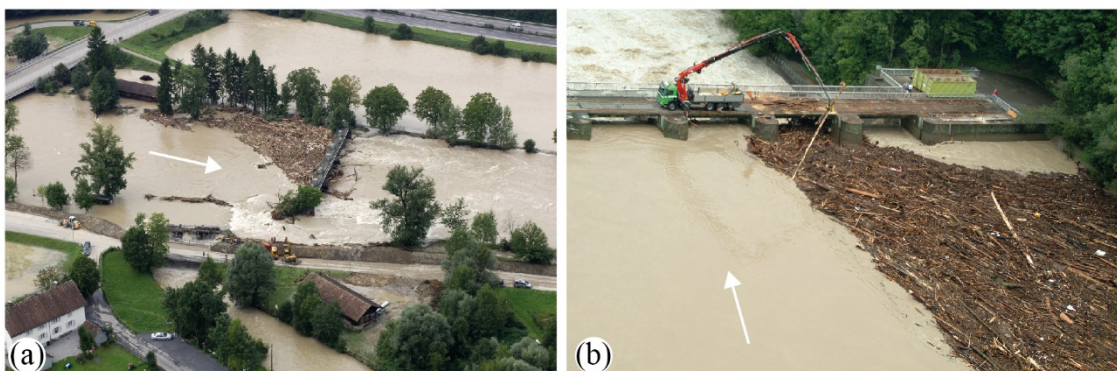


Figure 1.1 LW accumulations during the 2005 flood in Switzerland, (a) Weir Perlen (Photo: Swiss Air Force, adapted), (b) Weir Bremgarten (Photo: Canton police Aargau, adapted)

To account for the tradeoff between ecological benefit and natural hazard, the Swiss approach to LW management is to convey LW downstream wherever possible and to retain LW only when necessary. To mitigate the risk and impact of LW accumulations at river infrastructures, both passive and active measures are possible. Passive measures include organizational measures such as early warning systems or evacuation plans. Active measures are either maintenance works within the catchment area (i.e. forest maintenance, or bank erosion prevention) or structural measures such as retention structures and measures for the safe downstream conveyance of wood (Lange and Bezzola 2006). Retention racks or nets are a common method to retain LW (Perham 1987, Hartlieb and Bezzola 2000, Schmocker and Weitbrecht 2013). However, the intended LW accumulation also leads to backwater rise and possible local scour at the retention structure. To prevent LW from overtopping the rack, backwater rise is the governing parameter to determine the required rack height.

The investigations on the role of LW during floods have increased within the last decades. The combination of steep, afforested catchment areas and the frequency of floods implies the relevance of this topic for Switzerland. The Laboratory of Hydraulics, Hydrology and Glaciology (VAW) of ETH Zurich has been involved in LW research since the 1987 flood in Switzerland. A series of case studies was conducted for LW retention structures in Switzerland (e.g. Gürbe River, Kleine Emme River) in addition to fundamental research on LW accumulation characteristics. Based on completed studies on LW at VAW, Lange and Bezzola (2006) summarized the aspects of LW entrainment, transport, accumulation, and retention. In addition, they recommended potential engineering measures to mitigate the risk of LW accumulations at river infrastructures. Bezzola *et al.* (2002) and Schmocker and Hager (2011) studied LW accumulation probability of single logs and single rootstocks at different bridge deck constructions (e.g. truss, baffle, or railing bridge). Schmocker and Weitbrecht (2013) introduced a novel LW retention rack configuration with the objective to reduce backwater rise and maintain sediment continuity. They presented the so-called bypass retention where LW is retained parallel to the main stream in a bypass channel. Further experiments on backwater rise at a LW rack were conducted by Schmocker and Hager (2013). They defined the governing parameters to generalize the accumulation process and to simplify small-scale model tests. Furthermore, research on LW process was likewise conducted in the neighboring Alpine countries by e.g. Knauss (1995), Rimböck (2003), Hartlieb (2015), or Bocchiola *et al.* (2006a).

Despite recent research, knowledge of LW accumulation probability and characteristics is still limited and the results are partially contradictory. The effects of bridge piers, multiple logs, and a movable bed on the accumulation probability have not been considered in detail. The available formulae for backwater rise were established for a limited number of tests and apply mostly to a specific rack placement. In addition, previous model tests neglected organic fine material as leaves and branches as well as the interactions between backwater rise and a movable riverbed. Given the high damage potential due to LW transport during floods, a detailed understanding of the LW accumulation process and its impact is required.

1.2 Objectives

The present work aims to analyze the LW accumulation process at river infrastructures and its hydraulic and geomorphic impact using primarily physical modeling. The physical model tests were conducted in three different flumes at the Laboratory for Hydraulics, Hydrology and Glaciology (VAW) of ETH Zurich. In addition, a numerical simulation on LW accumulation probability and backwater rise was performed for model evaluation. This study focuses on four main parts:

- LW accumulation probability – Flume I (tilting flume)
Physical model tests were performed to identify the governing parameters of LW accumulation probability at bridge piers. The model tests comprise the effect on the accumulation probability of varying approach flow conditions, LW and pier characteristics, and a movable bed.
- LW accumulation characteristics – Flume II and III (small and large flume)
The general process understanding of LW accumulations was studied in two different flumes and allowed the investigation of scale and model effects. Special emphasis was put on investigating the effect of accumulation shape and organic fine material (branches, leaves) on backwater rise. Additional flume experiments were conducted with a movable bed to study the interactions between backwater rise and scour due to LW accumulations.
- Measures for LW accumulation risk reduction at bridge piers – Flume I (tilting flume)
A typical bridge pier cross-section was modeled in a flume to test the efficiency of existing measures and investigate new measures.

- Numerical modeling of LW accumulation
Selected experimental results on LW accumulation probability and backwater rise were used to evaluate the 2D numerical simulation model ‘IberWood’.

The objectives of this study contribute to flood safety and risk assessment. The main results will be summarized in a design guideline in cooperation with the Swiss Federal Office for the Environment (FOEN). This study is part of the interdisciplinary research project *WoodFlow* on LW management in rivers in Switzerland (Ruiz-Villanueva *et al.* 2016a).

1.3 Thesis outline

This doctoral thesis consists of 7 chapters. Chapter 2 provides a general background on LW in rivers, including previous floods with extensive LW transport. The current state-of-the-art of LW accumulation research is summarized in Chapter 3, followed by the experimental setup and methods in Chapter 4. The results of the hydraulic and numerical model tests are presented in Chapter 5, followed by a discussion of LW accumulation probability, characteristics, hazards, and measures at bridge piers. To demonstrate the practical application of this work, a computational example is provided in Chapter 6. The conclusions and an outlook are presented in Chapter 7.

2 Background

2.1 Overview

This section gives an overview of the processes prior to LW accumulations at river infrastructures. It provides the basis for an improved understanding of the experimental setup, data analysis, and discussion of the results of this study. The used terminology is introduced in Section 2.2. The historic and current role of wood in river ecosystems, and its ecological and morphological aspects are described in Section 2.3. The research on estimating LW volumes on a reach and catchment scale is summarized in Section 2.4. The entrainment, transport, and deposition of LW in rivers are discussed in Section 2.5. Selected past floods with extensive LW transport are described in Section 2.6.

2.2 Terminology

Wood (e.g. trees, logs, and rootstocks) in a fluvial corridor is hereafter specified as large wood (LW). Large wood is defined as single logs with a diameter ≥ 0.1 m and a length ≥ 1.0 m. This definition has been commonly used in literature (Keller and Swanson 1979, Nakamura and Swanson 1994, Wohl and Jaeger 2009, Ruiz-Villanueva *et al.* 2016b). Related terms are drift or driftwood, referring to the type of transport, in-stream wood, or in-channel wood. The definition of wood in rivers as woody debris, coarse woody debris (CWD), or large woody debris (LWD) was widely used in the past. Given the negative connotation of the term ‘debris’, the use is perceived as inappropriate (Wohl *et al.* 2016, Ruiz-Villanueva *et al.* 2016b). Any flow with wood can be defined as ‘wood-laden flow’ (Ruiz-Villanueva *et al.* 2018). Transported wood may also include branches, needles, or leaves. These components are defined as organic fine material *FM*. Selected wood types from different sources are further classified in Table 2.1.

Table 2.1 Definition of wood types (Ruiz-Villanueva *et al.* 2016b)

Term	Definition
Deadwood	Old or dead wood in the channel bed
Green / fresh wood	Fresh wood recently entrained into the river
In-stream / In-channel wood	Wood located in the river
Timber / construction wood	Wood from lumberyards or silviculture

2.3 Wood in river ecosystems

Wood provides various benefits for river ecosystems. Single log pieces and wood accumulations enhance the variability of morphological structures, species, and flow conditions (Figure 2.1). According to Keller and Swanson (1979), LW accumulations in small mountain streams provide in-channel sediment storage and vary channel morphology. As the presence of LW in rivers is crucial for their ecosystems, LW removal should be limited (Young 1991). Hence, the removal of LW decreases the flow resistance and obstruction, thereby increasing the tendency of bed erosion (Shields and Gippel 1995, Gippel 1995). Studies on benefits of LW for the river ecosystems were conducted, amongst others, by Gurnell *et al.* (2002), Wohl (2011), Kramer and Wohl (2015), Gurnell (2015) and Bertoldi *et al.* (2015).



Figure 2.1 Natural LW accumulation at River Thur, Switzerland (Photo: VAW, F. Maager)

Wohl *et al.* (2016) give an overview of the current knowledge on the benefits of LW on different scales:

- *Catchment scale*: In mountainous catchment areas, single pieces of LW can create steps and pools or represent flow obstructions. The accumulation of wood allows the storage of fine sediments and organic matter. Additionally, accumulations provide overhead cover and create habitat for fish, or invertebrates. In lowland rivers, wood improves the exchange within the hyporheic zone, creates pools and riffles,

and provides cover and habitat. Furthermore, it improves the connectivity between channel and floodplain. LW transport may increase bank erosion and further creates multi-thread channels.

- *Reach scale*: The positive effects on a reach scale include the formation of secondary or multiple channels. Transported logs may increase bank scour, form obstructions, thereby creating backwater pools. The areas upstream of log jams allow for storage of fine sediments and organic matter.
- *Channel unit scale*: Given a log jam, backwater rise increases habitat diversity, as it promotes the retention of finer sediments and organic matter. Transported wood may increase overbank flow and sedimentation. Due to the hyporheic exchange, the water chemistry and habitat for invertebrates improves. The variability of flow velocities, flow depths, and morphology provides an enhanced habitat for various fish species.

From an ecological point of view, removal of wood from the river should therefore be kept at a minimum.

2.4 Estimation of large wood volume

2.4.1 Overview

The estimation of the available LW volume in a fluvial system is crucial for the flood hazard assessment and can be assessed on both a reach- and catchment scale. Common methods include empirical formulae or a quantitative LW recruitment process analysis of the catchment area, e.g. with the aid of geographical information systems (GIS), remote sensing tools, field examinations, or a combination thereof. A distinction is made between the potential and effective LW volume. The potential (subscript pot) LW volume V_{pot} is the stock of wood in the catchment area that can theoretically be entrained into the river during a flood. In comparison, the effective (subscript eff) LW volume V_{eff} is the actual LW volume entrained during a flood.

2.4.2 Empirical formulae

Rickenmann (1997) derived empirical formulae based on surveyed LW volumes during floods in Switzerland (1987 and 1993), USA, Germany, and Japan (Ishikawa 1990) to estimate both V_{pot} and V_{eff} . The data base was further extended by Steeb *et al.* (2017) including LW volumes of the 2005 flood in Switzerland. Ishikawa (1990) and Uchiogi *et al.* (1996) also established empirical formulae for V_{pot} and V_{eff} . The empirical formulae for LW volumes V [m³] are a function of the following characteristics of the catchment area or the flood:

- *Size of catchment area* (Rickenmann 1997 and Steeb *et al.* 2017):

$$V_{\text{eff}} = b \cdot A_{\text{catch}}^{2/3}, \quad (2.1)$$

as solid (subscript *s*) LW volume V_s with $b = 21$ for data provided by Rickenmann (1997) and $b = 113$ for data of the 2005 flood in Switzerland (Steeb *et al.* 2017), A_{catch} as catchment (subscript *catch*) area [km²] and with an application range for $A_{\text{catch}} = 0.054 - 6'273$ km². To obtain loose (subscript *l*) LW volumes V_l , V_s is corrected with the so-called bulk factor a . It is the ratio between V_l and V_s and describes the compactness of an accumulation. Given a rather compact accumulation, $a \approx 2$ resulting in $b_l = 45$ for data provided by Rickenmann (1997) and $b_l = 242$ for data of the 2005 flood (Steeb *et al.* 2017).

- *Discharge volume* (Rickenmann 1997):

$$V_{\text{eff}} = 4 \cdot V_d^{2/5}, \quad (2.2)$$

as V_l with V_d as discharge (subscript *d*) volume of a flood hydrograph [m³] and valid for $V_d = 21.6 \cdot 10^3 - 390 \cdot 10^6$ m³.

- *Sediment load* (Ishikawa 1990, Uchiogi *et al.* 1996):

$$V_{\text{eff}} = 0.02 \cdot SL, \quad (2.3)$$

as V_l with SL as sediment load during a flood [m³] for $SL = 380 - 50'000$ m³.

- *Type of vegetation* (Ishikawa 1990 und Uchiogi *et al.* 1996):

$$V_{\text{pot}} = C \cdot A_{\text{catch}}, \quad (2.4)$$

as V_l with C = dimensionless coefficient as a function of the vegetation type in the catchment area. It can be distinguished between a coniferous ($10 < C < 1000$) and a deciduous forest ($10 < C < 100$). The equation is valid for $A_{\text{catch}} < 100$ km².

- *Forested catchment area* (Rickenmann 1997):

$$V_{\text{pot}} = 90 \cdot A_{\text{f,catch}}, \quad (2.5)$$

as V_l with $A_{f,catch}$ as forested catchment (subscript f,catch) area [km^2] and valid for $A_{catch} = 0.76 - 78 \text{ km}^2$ and $A_{f,catch} = 0.3 - 21.1 \text{ km}^2$.

- *Forested stream length* (Rickenmann 1997):

$$V_{\text{pot}} = 40 \cdot L_f^2, \quad (2.6)$$

as V_l with L_f as forested (subscript f) stream length [km] and for $L_f < 20 \text{ km}$.

Note that, Eqs. (2.1)-(2.3) describe V_{eff} , whereas Eqs. (2.4)-(2.6) V_{pot} . As the main data base for these empirical formulae are collected LW volumes after floods, the magnitude of V_{eff} and V_{pot} is rather similar (Figure 2.2). Figure 2.2 compares the resulting LW volume obtained with different empirical equations (Eqs. (2.1)-(2.6)) for the Swiss mountain river Renggbach in Canton Lucerne. For Eq. (2.1), the constant b is ≈ 5.5 times higher for the 2005 flood data compared to the previous obtained data (1987, 1990, and 1993), indicating an upper limit for b . For Eq. (2.4), the vegetation type coefficient C has a strong influence on the resulting LW volume. $C = 400$ seems to be an upper limit for the observed LW volumes in Switzerland (SCD, 2017). The empirical formulae for V_{pot} are a function of the forested stream length (L_f) and the type of vegetation (C , $A_{f,catch}$) in the catchment area. Hence, the results do not correspond to the overall potentially mobilized stock of wood in the catchment area and tend to underestimate V_{pot} .

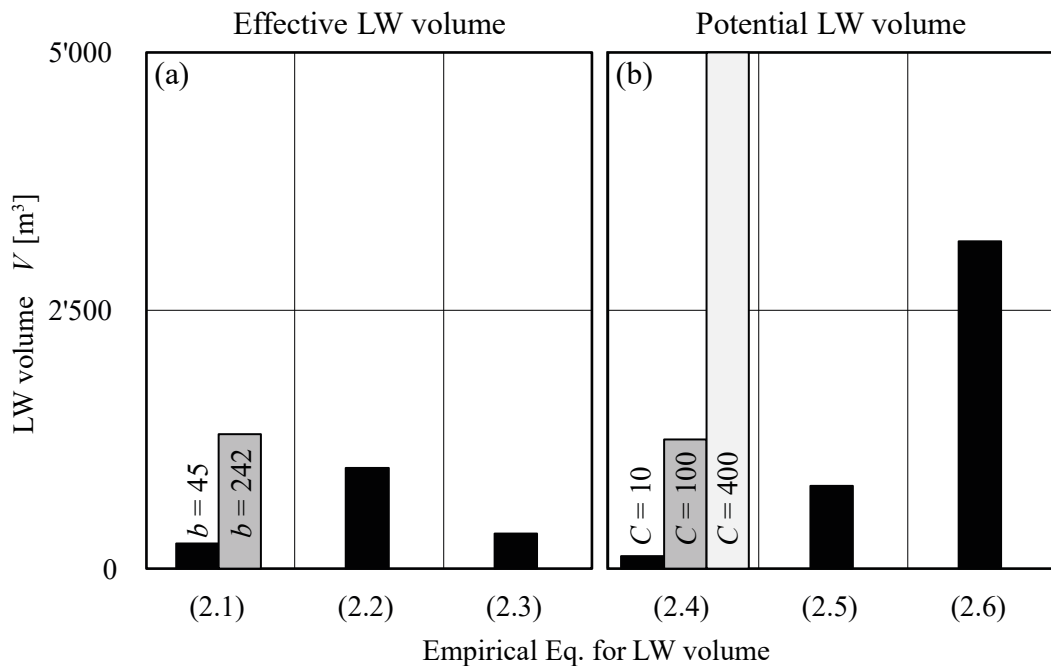


Figure 2.2 Comparison of LW volume using Eqs. (2.1)-(2.6) for the Swiss mountain river Renggbach in Canton Lucerne with $A_{catch} = 12.5 \text{ km}^2$ (adapted from Schalko *et al.* 2017)

None of the above formulae combines some of the main parameters affecting LW volume as e.g. $A_{f,catch}$ and V_d . The application results in a rough estimate, but a detailed analysis of the catchment is required to obtain reliable results.

2.4.3 Recruitment process analysis

During a flood, LW can be recruited and entrained into the fluvial corridor due to different processes in the catchment area. The so-called wood budgeting was first introduced by Keller and Swanson (1979). A wood budget is comprised of input, output, and decay dynamics for a specific domain, commonly defined as the catchment area. Keller and Swanson (1979) carried out case studies in Indiana, North Carolina, and Western Oregon (USA) to develop a conceptual and qualitative wood budget for streams. They distinguished between the governing processes for LW recruitment in low (Indiana and North Carolina) compared to high (Western Cascades, Oregon) gradient streams. In low gradient streams, the recruitment processes were identified to be bank failure, blowdown due to high winds, and collapse of trees due to icing during winter storms. In high gradient streams, wood can additionally be recruited due to snow avalanches and various soil mass movements.

Benda and Sias (2003) further advanced this concept by introducing a quantitative and more detailed framework for the mass balance of wood in rivers. Their approach can be compared to water or sediment mass balances. The data base included various field measurements over a 20 year period for the Pacific Northwest region in the USA. The objective was to estimate the wood mass balance over a long time period. The mass balance is described similar to the wood budget as input, output, and decay processes with:

$$\frac{\Delta LW}{\Delta t} = LW_{in} - LW_{out} + \frac{Q_{LW,in}}{\Delta x} - \frac{Q_{LW,out}}{\Delta x} - LW_{dc}. \quad (2.7)$$

The change in large wood storage is defined as ΔLW [m^3/m] within a river reach of length Δx over the time interval Δt . The input (subscript *in*) or lateral wood recruitment LW_{in} [$m^3/(m \cdot s)$] is the sum of various input processes, including forest mortality, downfall of trees due to fire or windstorms, bank erosion, landslides, debris flow, snow avalanches, and buried wood pieces or jams. The output or loss (subscript *out*) of large wood is described by LW_{out} [$m^3/(m \cdot s)$] including the overbank deposition during a flood. The fluvial transport of large wood (subscript *LW*) involves the transport into the river reach length Δx ($Q_{LW,in}$) and out of Δx ($Q_{LW,out}$) [m^3/s]. The large wood decay (subscript *dc*) processes

are included in LW_{dc} [$\text{m}^3/(\text{m}\cdot\text{s})$]. Benda and Sias (2003) carried out a sequential analysis of the wood mass balance including the following steps: (1) definition of forest death and growth cycles, (2) decay of wood, (3) bank erosion, (4) mass loss, and (5) fluvial transport. The individual parameters are defined in detail in Benda and Sias (2003).

Lucía *et al.* (2015) and Comiti *et al.* (2016) adapted Eq. (2.7) for shorter durations such as a flood. Consequently, the large wood decay processes LW_{dc} can be neglected and the change in large wood storage $\Delta LW / \Delta t$ is assumed constant. The equation then simplifies to:

$$\frac{Q_{LW, out}}{\Delta x} = LW_{in} - LW_{out} + \frac{Q_{LW, in}}{\Delta x}. \quad (2.8)$$

The large wood input parameter LW_{in} was further specified by LW recruitment from the fluvial corridor ($LW_{in, FC}$) due to bank erosion and LW recruitment from the hillslopes ($LW_{in, HS}$) due to landslides, debris flow, or snow avalanches (Figure 2.3).

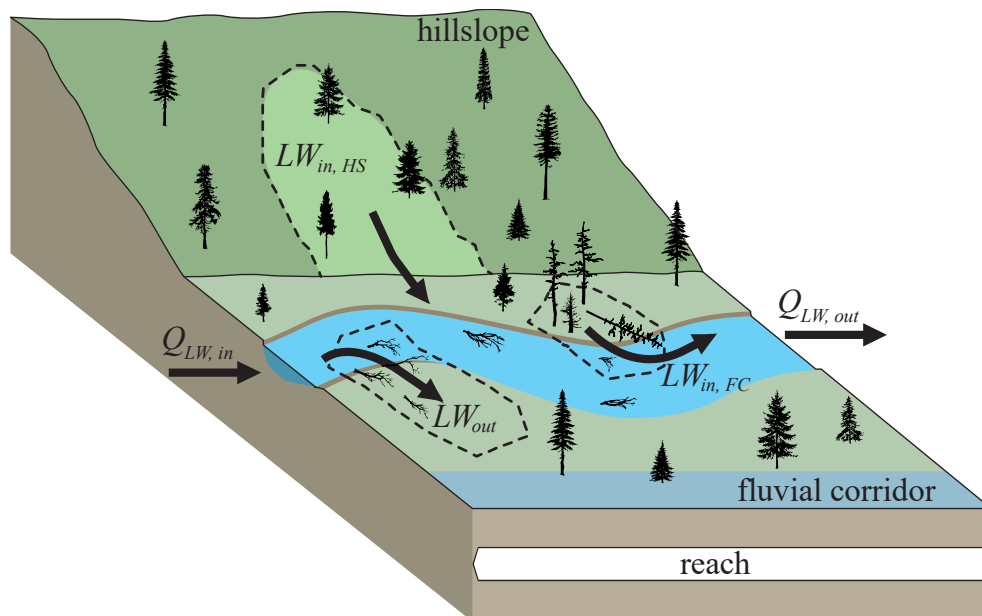


Figure 2.3 Conceptual LW dynamics in a river reach during a short time period, e.g. a flood (adapted from Lucía *et al.* 2015)

Similar wood dynamic processes were identified by Swanson (2003), Rickli and Bucher (2006), Mazzorana *et al.* (2009), Ruiz-Villanueva *et al.* (2014a), and Steeb *et al.* (2017). The wood dynamic processes may vary depending on the relation between channel width and log length. LW recruitment due to landslides or debris flows are more likely to occur in confined mountain streams or torrents and are mostly triggered due to continuous rain. The vegetation or channel widening play a more significant role in lowland

rivers or unconfined mountain rivers, though (Comiti *et al.* 2016). In general, an analysis of the river reach and catchment area is required to estimate the potential volumes for the LW mass balance (or wood budget). The approaches vary from aerial surveys, LiDAR (light detection and ranging), to GIS.

Rimböck (2001) estimated the LW potential based on aerial surveys. The recruitment areas and the stock of wood are determined using aerial images. The potential LW volume V_{pot} is defined as:

$$V_{\text{pot}} = \sum_{i=1}^n A_{\text{rec},i} \Omega_{\text{LW},i} f_i, \quad (2.9)$$

with A_{rec} as the recruitment (subscript rec) area for a certain quantity i [m^2], Ω_{LW} as the stock of large wood [m^3/m^2], and f as the reduction ratio $[-]$ (compare Eq. (2.12)). The aerial images were used to generate a digital elevation model with a resolution of about 10 m. Based on the digital elevation model, the recruitment processes and areas were determined. Rimböck (2001) investigated bank erosion, landslides, snow avalanches, wind throw, and in-stream wood storage. The reduction ratios for the different recruitment processes were estimated based on literature data and previous floods with extensive LW transport. The presented tool was applied to different catchment areas in Germany and showed plausible results.

Bertoldi *et al.* (2013) investigated wood recruitment due to bank erosion and in-channel wood volume for two study sites at the Tagliamento, Italy. They analyzed airborne LiDAR surveys from 2005 and 2010, hourly photographs of the two study sites, field measurements of trees (standing and deposited) in 2010, and hydrological information from a gauging station. The airborne LiDAR data provided information on the tree height, vegetation density, extent of the riparian forest due to erosion, and bed morphology of areas with previously deposited trees. The hourly photographs were used to obtain changes in bank position and to quantify the number and position of deposited trees after floods. The field observations focused on the measurement of standing and deposited tree characteristics (e.g. species, density, and dimensions). The data analysis was conducted within three steps. First, the field observations of 2010 were evaluated to describe the characteristics of the standing trees close to eroding banks and compare them with deposited trees in the fluvial corridor. Second, the impact of floods on the wood budgets at the two study sites were analyzed. By comparing the 2005 with the 2010 data (LiDAR and photographs), information was gained regarding the deposited and retained wood in the fluvial corridor. Third, the flow conditions, the riverbed topography, and the

photographs of the tree positions were evaluated, allowing for an analysis of wood retention.

Several studies on LW volumes have been conducted using a GIS approach. A detailed description of the required steps and formulae are summarized in Mächler (2009), Mazzorana *et al.* (2009), Meyer and Rimböck (2014), or Ruiz-Villanueva *et al.* (2014a). Considering landslides and bank erosion as the main wood recruitment processes, the required steps to estimate the potential LW volume are the following (adapted from Mächler 2009, Meyer and Rimböck 2014, Schalko *et al.* 2017):

1. **Acquire basic information:** Collection of the required basic data sets (e.g. elevation model, maps of the forested area, stream network) and definition of the perimeter.
2. **Slope gradients:** Definition of decisive slope gradients. During the 2005 flood in Switzerland, the majority of landslides occurred at slope gradients varying from $20^\circ \dots 50^\circ$ (Bezzola and Hegg 2008). Since landslides at slope gradients higher than 20° do not stop immediately once the slope decreases, it is necessary to include a buffer zone of ≈ 25 m (Rickli *et al.* 2008).
3. **Sub-catchment area size:** The discharge capacity of the river is decisive for whether LW can be transported or not. It is assumed that sub-catchment areas with a size ≥ 1 km² are capable of transporting LW (Waldner *et al.* 2009).
4. **Forested area:** The forested area of the perimeter should be defined.
5. **Hazard areas due to landslides:** The hazard areas due to landslides (subscript LS) A_{LS} [m²] are defined as the forested areas (Step 4) with slope gradients varying from $20^\circ \dots 50^\circ$ (Step 2) located within the reach of sub-catchment area with ≥ 1 km² (Step 3). Due to the stabilizing effect of tree roots, it is assumed that not all landslides within the hazard area will be triggered during a flood. This is considered with the so-called landslide reduction ratio f_{LS} . Based on recommendations by Rimböck (2003), f_{LS} can vary between $0.1 \dots 0.8$ depending on the slope instability within the perimeter.
6. **Hazard areas due to bank erosion:** Considering a natural, low gradient river, the regime width is reached at HQ_{5-10} leading to LW recruitment due to bank erosion. For natural high gradient rivers the corresponding flood is roughly HQ_{30-100} . The regime width B_{Parker} [m] can be calculated using the empirical formula by Parker (1979)

$$B_{\text{Parker}} = 4.4 \cdot \sqrt{\frac{Q}{g \cdot (s-1) \cdot d_{50,AL}}}, \quad (2.10)$$

with Q as discharge [m³/s] for HQ_{5-10} for low gradient and HQ_{30-100} for high gradient rivers, g = gravity acceleration [m/s²], s = relative sediment density ≈ 2.65 [–], and

$d_{50,AL}$ = characteristic grain size diameter of the armor layer [m]. During a flood, either landslide or bank erosion lead to LW recruitment (Rimböck 2003). To avoid a double consideration of hazard areas, the unobstructed, forested stream length L_f should be identified only for sections with risks of bank erosion. The hazard areas due to bank erosion (subscript BE) A_{BE} are defined as:

$$A_{BE} = L_f \cdot (B_{\text{Parker}} - \bar{B}), \quad (2.11)$$

with \bar{B} as the average channel width [m].

7. Potential LW volume: The potential LW volume V_{pot} results to:

$$V_{\text{pot}} = \Omega_{LW} \cdot ((A_{LS} \cdot f_{LS}) + A_{BE}), \quad (2.12)$$

with Ω_{LW} as the wood stock within the perimeter [m^3/m^2].

8. Effective LW volume: The potential LW volume is the theoretical amount of wood that can be entrained into the river during a flood. The effective LW volume can be estimated based on recorded LW volumes in similar catchment areas of past floods. Considering a reduction factor f_{eff} , the effective LW volume V_{eff} [m^3] can be estimated to:

$$V_{\text{eff}} = V_{\text{pot}} \cdot f_{\text{eff}} \quad (2.13)$$

The 8 steps represent a simplified estimation approach for the potential and effective LW volume of a selected perimeter (e.g. sub- or catchment area).

Ruiz-Villanueva *et al.* (2014a) described a more detailed GIS-approach with different scenarios for a likely, intermediate, and maximum wood recruitment. In addition to the different LW entrainment processes, the vegetation stage (mature, mid-successional, young, or re-forested) and species (conifer, deciduous, or riparian) were included to consider the vegetation resistance (e.g. the ability of the vegetation to oppose a potential recruitment). A volume correction factor then reduces the potential wood volume for areas with high vegetation resistance.

A detailed literature study on LW recruitment is provided by Comiti *et al.* (2016). Case studies for a specific (sub-)catchment area were conducted by Nakamura and Swanson (1994), Wyzga and Zawiejska (2005), Comiti *et al.* (2006), Lassetre *et al.* (2008), Mazzorana *et al.* (2009), Hassan *et al.* (2016), and Steeb *et al.* (2017).

2.5 Large wood movement

The movement of LW during a flood is of primary importance to estimate the interaction between wood and river infrastructures, and the resulting hazards. The state-of-the-art of this subsection will be structured in the order of LW (1) entrainment, (2) transport, and (3) deposition. Due to the scope of this work, the presented research focuses on theoretical approaches and physical experiments. The variety of field measures to observe LW movement has increased within the last decades, though. MacVicar *et al.* (2009) provide an overview of the existing measurement techniques, including field and aerial surveying, ^{14}C dating, visual and tag tracking, and monitoring (video or wood removal). Other field investigations on wood dynamics are provided by Curran (2010), Merten *et al.* (2010), Mazzorana *et al.* (2011), Dixon and Sear (2014), Schenk *et al.* (2014), and Ravazzolo *et al.* (2015a).

2.5.1 Entrainment

Lienkamper and Swanson (1987) studied the dynamics of LW transport initiation (i.e. incipient motion) at a study site in Oregon (USA). Based on their observations, the LW mobility characteristics can be described by the ratios of log dimensions and channel dimensions (i.e. log length to channel width). Logs with lengths less than the channel width were more likely to be transported.

Braudrick and Grant (2000) studied the entrainment and transport of large wood by combining a theoretical approach with hydraulic flume experiments. The entrainment process was described by the force balance acting on wood in streams. Their model applies for cylindrical logs in uniform flow lying on a smooth impermeable riverbed. The log movement can be defined by the balance of downstream and upstream force components (Figure 2.4). The downstream components are the normal force F_N (force balance of buoyancy F_B and gravitation F_G) and drag force F_{drag} , whereas the upstream component is the friction force F_{friction} . As logs are commonly not submerged, the lift force F_{lift} can be neglected. The forces are defined as:

- Normal force F_N :

$$F_N \sin \beta = (F_G - F_B) \sin \beta = \left(g \rho_L L_L \frac{\pi d_L^2}{4} - g \rho_W L_L A_{\text{sub}} \right) \sin \beta \quad (2.14)$$

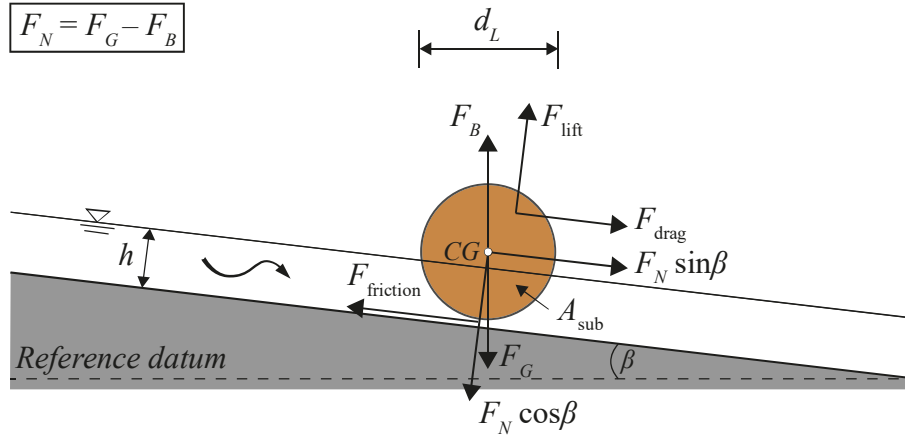


Figure 2.4 Forces acting on a cylindrical log oriented normal to the flow (cross-section) with $CG =$ center of gravity (adapted from Braudrick and Grant 2000)

The normal force F_N equals the effective log weight in downstream direction with $F_G - F_B =$ effective log weight (gravitation force minus buoyant force), $\beta =$ bed angle in flow-parallel plane, $g =$ gravitational acceleration, $\rho_L =$ log density, $L_L =$ log length, $d_L =$ log diameter, $\rho_W =$ water density, and $A_{\text{sub}} =$ submerged area of the log perpendicular to piece length exposed to drag. For a cylindrical log, A_{sub} resolves to

$$A_{\text{sub}} = \left\{ 2 \cos^{-1} \left(1 - \frac{2h}{d_L} \right) - \sin \left[2 \cos^{-1} \left(1 - \frac{2h}{d_L} \right) \right] \right\} \frac{d_L^2}{8}. \quad (2.15)$$

- Friction force F_{friction} :

$$F_{\text{friction}} = F_N \cos \beta \mu_{\text{bed}} = \left(g \rho_L L_L \frac{\pi d_L^2}{4} - g \rho_W L_L A_{\text{sub}} \right) \cos \beta \mu_{\text{bed}} \quad (2.16)$$

The friction force is a function of the normal force F_N acting on the log $F_N = (F_G - F_B) \cos \beta$ and the bed friction coefficient μ_{bed} .

- Drag force F_{drag} :

$$F_{\text{drag}} = -\frac{v^2}{2} \rho_W C_d (L_L h \sin \gamma + A_{\text{sub}} \cos \gamma) \quad (2.17)$$

The drag force equals the downstream drag exerted on the log by moving water with $v =$ flow velocity, $C_d =$ drag coefficient of wood in water, $h =$ flow depth, $\gamma =$ log position angle relative to the flow with $\gamma = 0^\circ$ for logs oriented parallel to the flow and $\gamma = 90^\circ$ for logs oriented normal to the flow. The drag coefficients for cylindrical logs were investigated with flume experiments by Wallerstein *et al.* (2002) and Gippel *et al.* (1996). In addition, field measurements were conducted by Hygelund and Manga (2003), and

Shields and Alonso (2012). For cylindrical logs C_d strongly depends on γ and the blockage ratio. Values in literature range from $C_d = 0.4$ for $\gamma = 15^\circ$, $C_d = 0.8$ for $\gamma = 90^\circ$ up to $C_d = 1.4$ for $\gamma = 0^\circ$.

The force balance can then be summarized as:

$$F_{friction} - F_N \sin \beta = F_{drag}, \text{ and} \quad (2.18)$$

$$\left(g \rho_L L_L \frac{\pi d_L^2}{4} - g \rho_W L_L A_{sub} \right) (\cos \beta \mu_{bed} - \sin \beta) = \frac{v^2}{2} \rho_W C_d (L_L h \sin \gamma + A_{sub} \cos \gamma) \quad (2.19)$$

Based on Eq. (2.19), the entrainment process is a function of log characteristics (diameter, length, density, log orientation relative to the flow), channel characteristics (flow velocity, flow depth, and channel slope), and drag- and friction coefficients.

According to Braudrick *et al.* (1997), log transport, i.e. flotation, starts if the buoyant depth h_B is equal to the flow depth h . Given a log without rootstock, entrainment or beginning of transport is defined by:

$$F_G = F_B \rightarrow g \rho_L L_L \frac{\pi d_L^2}{4} = g \rho_W L_L A_{sub} \quad (2.20)$$

The physical experiments by Braudrick *et al.* (1997) showed that the flow depth at the beginning of transport is nearly a linear function of the log diameter, i.e. logs with a smaller diameter are sooner mobilized.

Bocchiola *et al.* (2006a) and Crosato *et al.* (2013) further studied the entrainment process of logs using hydraulic flume experiments. They stated that the entrainment condition cannot be simplified by the balance of drag and friction forces, as also the flow around the logs highly affects this process. Due to few experimental data, their findings were nor parameterized.

The incipient motion of LW can further be described by the ratio between flow depth h and log diameter d . According to Lange and Bezzola (2006), logs with a density of $\approx 500 \text{ kg/m}^3$ may be transported, if $h > d/2$. Flume experiments at VAW (2001) extended this recommendation for supercritical flow conditions (flow Froude number $F_o \approx 2$) and logs without branches to $h > 1.0 \dots 1.2 d$ and with branches to $h > 1.2 \dots 1.5 d$.

2.5.2 Transport

Jegorow (1941) conducted flume experiments on LW transport and stated that logs oriented parallel to the flow are more stable than logs normal to the flow. Braudrick and Grant (2000) tested the stability of transported logs as a function of their position relative to the flow and confirmed the findings of Jegorow (1941). Based on their flume experiments, logs oriented in flow direction are more stable than logs oriented normal to the flow or with an angle of $\gamma = 45^\circ$. This was observed for all logs independent of their length, diameter, or existence of rootstock. Braudrick and Grant (2001) further investigated the position of transported logs with flume experiments. The log orientation relative to the flow was mainly a function of the velocity distribution. Logs oriented normal to the flow were observed for non-uniform flow velocity distributions. Still, they observed the tendency that logs were transported in the thalweg and oriented parallel to the flow with increasing transport distance.

Braudrick *et al.* (1997) classified LW transport in rivers in three different transport regimes: (1) uncongested, (2) congested, and (3) semi-congested LW transport (Figure 2.5). For uncongested LW transport, single logs move independently without contact. In contrast, congested LW transport represents a single mass movement of logs, e.g. as a LW carpet. Hence, the movement of a single log depends on the other logs. Semi-congested LW transport is an intermediate regime. Some logs are then transported in clumps and others as individuals. Congested LW transport is common for low-order streams, and uncongested LW transport for higher-order streams. Ruiz-Villanueva *et al.* (2018) extended this classification and included ‘hypercongested’ as an additional LW transport regime. In this regime, unsaturated logs are transported in bulk at the front of a flood wave. The wood front is either dry (rolling or sliding logs), or wet (floating logs). The different transport regimes are a function of the so-called log input rate. It is defined as the ratio of the wood input rate $Q_{LW,in}$ to the approach flow (subscript o) discharge Q_o , resulting in hypercongested or congested LW transport for high ratios of $Q_{LW,in} / Q_o > 0.10$. This was further confirmed by the flume experiments of Bertoldi *et al.* (2014). The correlations between water, sediment, and wood-laden flows are plotted in Figure 2.6a. According to Ruiz-Villanueva *et al.* (2018), hypercongested and congested LW transport were observed at the rising limb of the flood hydrograph, whereas uncongested LW transport commonly occurred after the flood crest (Figure 2.6b).

The different transport modes of LW are resting, rolling or sliding, and floating. According to Haga *et al.* (2002) the modes depend on both the ratio of the flow depth to

the log diameter, and the ratio of hydrodynamic forces to resistance forces, i.e. $(F_{\text{friction}} - F_N) / F_{\text{drag}}$ (compare Eq. (2.19)). The beginning of log transport, i.e. floating, is hereby defined if $h \geq d_L$.

The wood characteristics highly affect the LW transport modes. Ruiz-Villanueva *et al.* (2016c) investigated the influence of different wood densities on LW transport. The density difference of decayed in-stream wood compared to fresh green wood were studied during field campaigns and accompanying flume experiments. During their experiments, the log density ρ_L resulted in 800 kg/m^3 for green wood and 660 kg/m^3 for in-stream wood. Logs with a lower density were more likely being transported compared to logs with a higher density. Additionally, the travelled distance of logs with a lower density was higher. Ruiz-Villanueva *et al.* (2016c) concluded that LW dynamics or movement should not be estimated based on the standard wood density value of $\rho_L = 500 \text{ kg/m}^3$ found in literature.

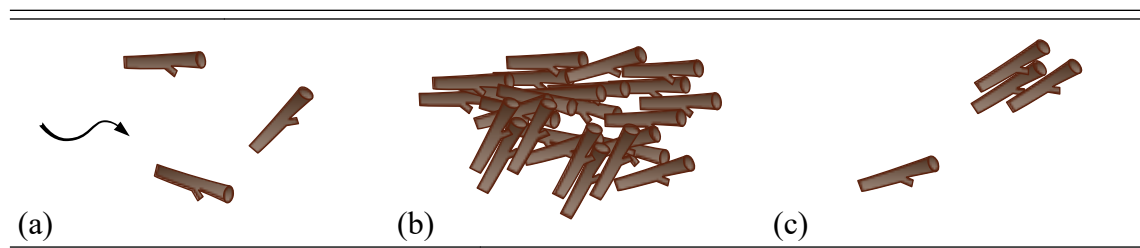


Figure 2.5 Large wood transport regimes, (a) uncongested, (b) congested, and (c) semi-congested (adapted from Braudrick *et al.* 1997)

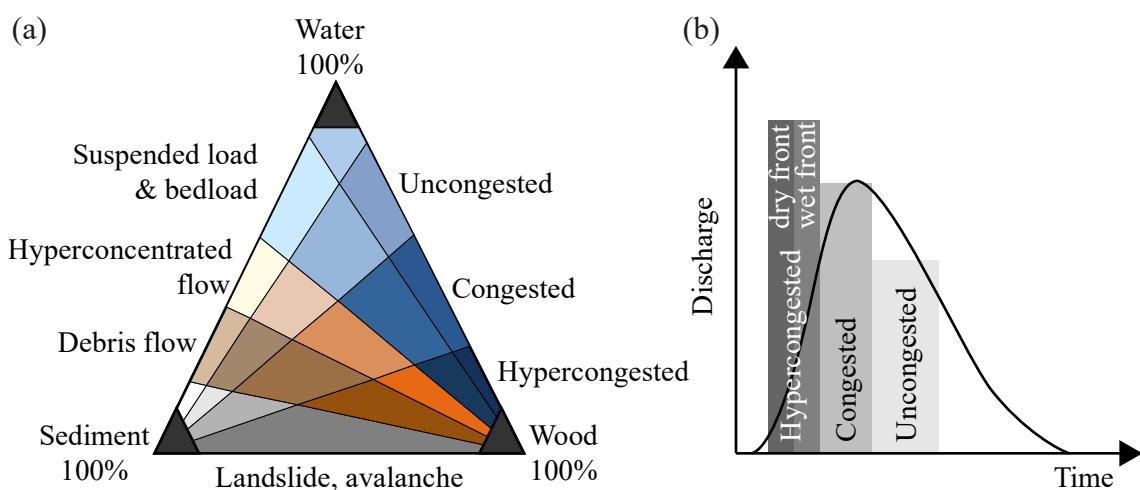


Figure 2.6 (a) Water, sediment, and wood-laden flows and (b) LW transport regimes for a flood (adapted from Ruiz-Villanueva *et al.* 2018)

2.5.3 Deposition

This section refers to natural deposition of single logs, whereas deposition at river infrastructures is described in Section 3.3. According to Braudrick *et al.* (1997), wood is mainly deposited in the shallowest areas and oriented normal to the flow for both uncongested and semi-congested LW transport. Braudrick and Grant (2001) confirmed the findings and commented that during their flume experiments, logs were deposited at mid-channel bars, in shallow zones, and on the outside of river bends. The so-called debris roughness DR , similar to the hydraulic roughness, describes the factors promoting LW deposition in a river. DR is a reach-average dimensionless index that can be described by channel characteristics, i.e. channel width, depth, and sinuosity, and log characteristics, i.e. log length and diameter. DR was theoretically evaluated as high for low-gradient headwater streams compared to large streams. The factors influencing the deposition are similar to the factors for incipient motion, described by Lienkamper and Swanson (1987). The ratio of log length to channel width is a governing parameter describing LW deposition. In contrast to the incipient motion of logs, Braudrick and Grant (2001) observed larger logs to be transported for longer distances compared to shorter logs. Longer logs may not be strongly affected by local hydraulic variations and exhibit a higher momentum to not be deposited at obstacles, leading to a more stable log transport.

2.6 Selected past floods with extensive large wood transport

2.6.1 Switzerland, 1987

In 1987, several floods occurred in the Alpine regions of Switzerland and Austria. In Switzerland, the damage sum amounted to 1'200 Mio. Swiss Francs. In addition to the high water and sediment discharges, a large volume of wood was entrained, transported, and deposited during the flood (Figure 2.7). According to Bänziger (1989), approximately 41'000 m³ of LW was accumulated and the maximum measured water discharge at the River Rhine (Diepoldsau, Canton St. Gallen) amounted to 2'660 m³/s ($\approx HQ_{150}$). Even though the damage due to LW accumulations was rather low, the incidence led to a detailed analysis of the LW processes that occurred. The analysis focused on the quantification of LW volumes, sources, and size distributions in various Swiss catchment areas. It was conducted based on aerial images and individual LW records. In the Swiss Canton Valais, the majority of entrained LW was classified as deadwood, construction wood, and

fresh wood due to landslides. The analysis of the flood led to the study and design of measures for LW retention and safe downstream conveyance.



Figure 2.7 1987 flood in Switzerland in (a) Canton Grisons, Trun (Photo: Community archive Trun) and (b) Canton Grisons, Poschiavo (Photo: Public works service Grisons)

2.6.2 Switzerland, 2005

The 2005 flood in Switzerland transported approximately 110'000 m³ and 30'000 t of LW, respectively (Bezzola and Hegg 2007, VAW 2008, Waldner *et al.* 2009). The property damage amounted to 3 billion Swiss Francs. The return period of the flood at the northern edge of the Swiss Alps was estimated to be ≈ 80 years. During the flood mainly fresh wood (50-75%) was entrained in mountainous catchment areas due to landslides and bank erosion (Bezzola and Hegg 2007) and transported to areas with lower channel slopes and various river infrastructures, leading to numerous accumulations at bridges and weirs (Figure 2.8). This resulted in severe problems due to backwater rise upstream of the blocked cross-sections and consequently flooding of the surrounding area. The negative impact of transported LW led to a detailed analysis of the LW entrainment, transport, and deposition processes for three different catchment areas (i.e. River Kander, River Kleine Emme, and River Grosse Melchaa) in Switzerland. The results were used for future action planning and risk evaluation and triggered several research projects, as for example the LW retention rack at the River Kleine Emme in Canton Lucerne (Schmocker and Weitbrecht 2013).

2.6.3 Italy – Magra river basin, 2011

In 2011, high precipitation events led to flash floods ($HQ_{200-300}$) in the Magra River basin in the north-western part of Italy (Lucía *et al.* 2015, Rinaldi *et al.* 2016). The flash floods

caused bank erosion due to channel widening. The channel bed width was enlarged by a factor of 20. Therefore, the majority of LW was entrained due to bank erosion (70-80%). This resulted in a LW transport of 1'270 m³/km and various LW accumulations (Figure 2.9). After the flood, the dynamics of LW during flash floods were investigated for two highly affected mountainous catchment areas (Lucía *et al.* 2015). The geomorphic changes and their effect on LW transport were analyzed by Rinaldi *et al.* (2016). Both studies highlight the difficulty in predicting LW budgets, LW-related hazards, and morphological modifications.

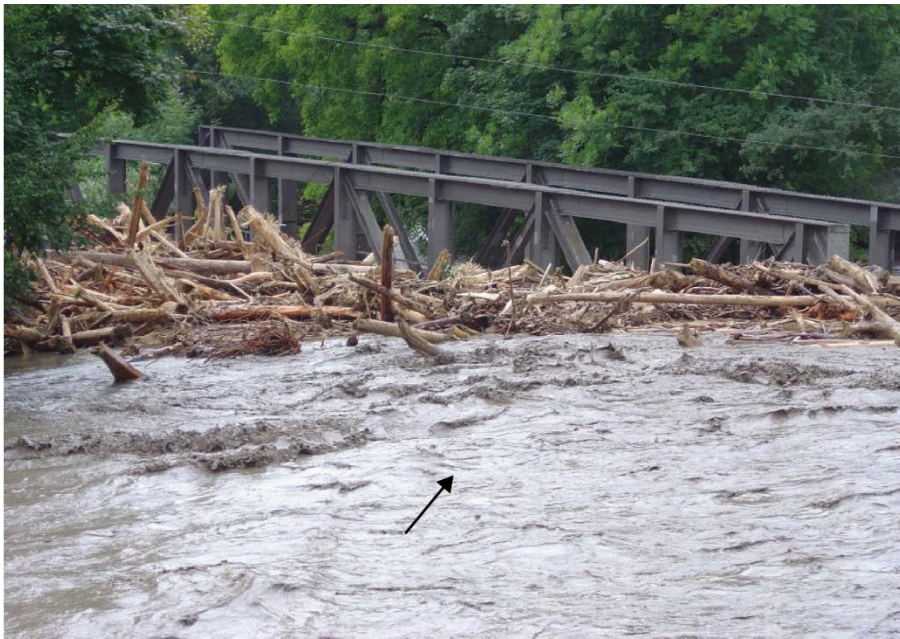


Figure 2.8 2005 flood in Switzerland, LW accumulation at a bridge in Canton Obwalden (Photo: belop GmbH)



Figure 2.9 2011 flood in Italy with LW accumulations in (a) Pignone and (b) Borghetto di Vara (Photos: guatebaffi, Panoramio.com)

2.6.4 Switzerland – Zulg and Emme River basins, 2012

In 2012, a regional flood ($\approx HQ_{100}$) with extensive LW transport occurred in the catchment area of the Rivers Emme and Zulg, affecting the downstream regions River Aare (Figure 2.10) and Lake Biel. The transported LW volume was low compared to the flood in 2005 and therefore caused less damage. In the River Zulg, approximately 1'000 m³ of fresh- and deadwood were entrained due to bank erosion and landslides (Flussbau AG 2012). The precipitation mainly occurred in the upper catchment area and the base flow was rather low. This combination resulted in a low flow depth at the front of the flood wave. Due to the bottom friction, the reduced flow velocity led to backwater rise and to the formation of a surge wave with a distinct bore front. LW was transported at the front of the surge wave, forming a compact LW carpet that further increased backwater rise. This phenomenon was observed both at the Rivers Zulg and Emme and can be described as hypercongested LW transport (Section 2.5.2; River Emme in Figure 2.10a). At the River Zulg, maximum backwater rise amounted to ≈ 2 m and was observed at the beginning of the flood (Flussbau AG 2012). LW accumulated mainly in the river channel. Consequently, maintenance works were increased to reduce the potential of LW accumulations. In addition, a LW retention rack is planned and physical experiments were conducted at the University of Applied Sciences Rapperswil to test the setup and retention efficiency.



Figure 2.10 2012 flood in Switzerland, (a) LW transport in the River Emme (Photo: energisch.ch), (b) LW accumulation in the River Aare in Bern due to LW recruitment in the River Zulg (Photo: derbund.ch)

2.6.5 Japan – Northern Kyushu, 2012

In 2012, an extreme flood occurred in the northern part of Kyushu in the prefectures of Kumamoto, Oita, Fukuoka, and Saga. The flood caused property damage of approximately 200 billion JPY (≈ 2 billion CHF). In the coastal area, the accumulated LW amounted to 17'500 m³ (Yano *et al.* 2015). Due to LW accumulations, several bridges were clogged and subsequently damaged (Figure 2.11).



Figure 2.11 2012 flood in Taketa (prefecture Oita in northern Kyushu, Japan), (a) LW accumulation at a bridge (Photo: dailymail.co.uk) and (b) debris flow with LW (Photo: democraticunderground.com)

3 Literature review

3.1 Overview

This section provides an overview of the current knowledge on large wood accumulations at river infrastructures. It focuses on literature that is directly related to the present work. Based on the literature review, the research gaps are identified. The review supports the investigational approach and highlights the main objectives of this thesis. The research on large wood accumulation probability at river infrastructures with special emphasis on bridges is presented in Section 3.2. The characteristics of large wood accumulations in rivers are described in Section 3.3. In Section 3.4, the current state-of-the-art regarding hazards due to LW accumulations at river infrastructures is summarized, focusing on backwater rise and local scour. The existing engineering measures for LW accumulation risk reduction at bridges are depicted in Section 3.5. The recent numerical simulation approaches for large wood entrainment, transport, and deposition are described in Section 3.6. Finally, Section 3.7 identifies the research gaps based on the literature review and summarizes the objectives of this study.

3.2 Large wood accumulation probability

Transported LW can accumulate at river infrastructures like bridges or weirs. The estimation of the LW accumulation probability is crucial for an integrated flood hazard assessment, as it directly affects the damage potential. Several case studies on LW accumulation probability for a specific bridge or weir exist, but only a few systematic investigations have been conducted so far. This section will focus on LW accumulation probability at river bridges. Literature regarding other infrastructures such as weirs, spillways, or check dams are summarized in Lange and Bezzola (2006), Hartlieb (2012), Hartlieb (2015), Piton and Recking (2015), SCD (2017), or Furlan *et al.* (2018).

Bezzola *et al.* (2002) conducted flume experiments on the LW accumulation probability p of single logs, single rootstocks, and wood mixtures at different bridge deck constructions (e.g. truss, baffle, or railing bridge). The flume experiments were conducted in a 13 m long and 0.6 m wide channel with a fixed channel bed at VAW. The bridge deck geometry was kept constant, while the flume was adjusted to model rectangular and various trapezoidal cross-sections. The tested hydraulic conditions included subcritical-,

supercritical flow, and a hydraulic jump at the location of the bridge deck. The approach flow conditions were defined by the approach flow Froude number $F_o = v_o/(gh_o)^{1/2} = 0.3 \dots 1.1$ with v_o = approach flow velocity, h_o = approach flow depth, and g = gravitational acceleration, and the ratio of the approach flow depth to the bridge clearance height $h_o/H_{\text{Bridge}} = 0.5 \dots 1.0$. The model LW consisted of single logs and single rootstocks (Figure 3.1), and was transported both uncongested and congested. The experiments were repeated $N =$ three times, resulting in a total of 1'200 test runs. According to Bezzola *et al.* (2002), the accumulation probability p is mainly a function of the LW dimensions (length and diameter) in combination with the cross-sectional geometry, whereas the approach flow conditions (relative approach flow depth h_o/H_{Bridge} and F_o) were of minor importance. The maximal (subscript max) accumulation probability $p_{\text{max}} \approx 80 \dots 100\%$ was observed for the trapezoidal cross-section with congested LW transport including rootstocks, compared to $p_{\text{max}} = 30\%$ for the rectangular cross-section. Single rootstocks resulted in $p_{\text{max}} \approx 50 \dots 70\%$ for trapezoidal cross-sections, compared to $p_{\text{max}} = 25\%$ for the rectangular cross-section. The minimum (subscript min) accumulation probability $p_{\text{min}} \approx 0 \dots 20\%$ was observed for single logs independent of the cross-section. The results for uncongested transport were combined in design equations and the accumulation probability for single logs p_L can be described as:

$$p_L = 0 \quad \text{for } \frac{L_L}{B} < 0.5, \text{ and} \quad (3.1)$$

$$p_L = 0.133 \frac{L_L}{B} - 0.066 \quad \text{for } \frac{L_L}{B} \geq 0.5, \quad (3.2)$$

with B as bridge width [m]. The accumulation probability of single rootstocks (subscript R) p_R depends on the mean dimensions of the rootstock and clearance height, with

$$p_R = 0 \quad \text{for } \frac{d_{R^*}}{H_{\text{Bridge}}} < 0.6, \quad (3.3)$$

$$p_R = 1 \quad \text{for } \frac{d_{R^*}}{H_{\text{Bridge}}} \geq 1.0, \text{ and} \quad (3.4)$$

$$p_R = 2 \frac{d_{R^*}}{H_{\text{Bridge}}} - 1.2 \quad \text{for } 0.6 \leq \frac{d_{R^*}}{H_{\text{Bridge}}} < 1.0, \quad (3.5)$$

with d_{R^*} as the geometric mean of the maximum and minimum dimensions of the rootstock and the attached log length $d_{R^*} = (d_{R\text{max}} d_{R\text{min}} L_L)^{1/3}$ [m]. The experiments with congested transport resulted in higher p compared to the uncongested transport but were not summarized in a design equation due to the limited number of experiments.

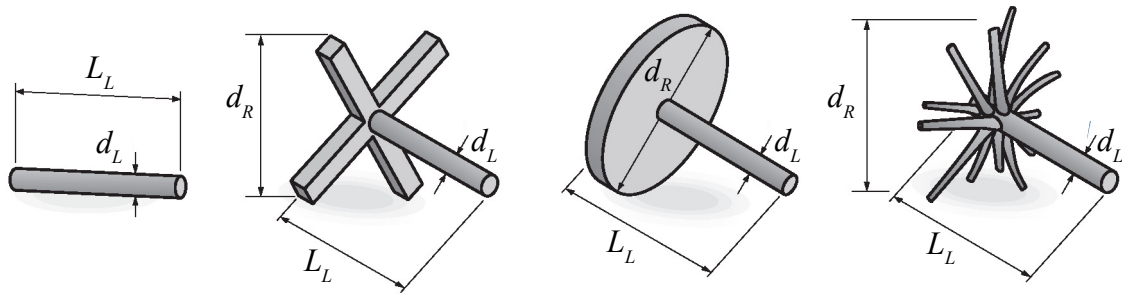


Figure 3.1 Model LW and model rootstocks (adapted from Bezzola *et al.* 2002)

The effect of different bridge deck types (Figure 3.2) on p for uncongested transport was studied by Schmocker and Hager (2011). The flume experiments were conducted in a 13 m long and 0.6 m wide flume at VAW with approach flow conditions varying from $h_o/H_{\text{Bridge}} = 0.9, 1.0, 1.07$ and $F_o = 0.3 \dots 1.2$. The model LW consisted of logs with different lengths and various types of rootstocks. A single log or rootstock was randomly added 5 m upstream of the model bridge. It was tested, whether the log or rootstock accumulated at the bridge deck or not. One test run consisted of $N = 8$ repetitions to obtain the accumulation probability p . Increasing p was observed for increasing log dimensions, decreasing F_o , and decreasing relative freeboard ($1 - (h_o/H_{\text{Bridge}})$). For a plain bridge deck without railings (Figure 3.2a and d), single logs and $h_o/H_{\text{Bridge}} = 0.9$, p was always zero, whereas $p = 30 \dots 100\%$ for $h_o/H_{\text{Bridge}} = 1.07$, respectively. Bridge decks with a truss or railings (Figure 3.2b and c) resulted in higher p . The maximum accumulation probability for single logs $p_{L, \max}$ was defined as a function of the approach flow conditions and can be described for $0.3 \leq F_o \leq 0.8$ as follows:

$$p_{L, \max} = 0 \quad \text{for } \frac{h_o}{H_{\text{Bridge}}} \leq 0.9, \quad (3.6)$$

$$p_{L, \max} = 0.25z + (4 - z)(F_o - 0.8)^2 \quad \text{for } \frac{h_o}{H_{\text{Bridge}}} = 1, \quad (3.7)$$

$z = 2$ for bridge type a-c
 $z = 0$ for bridge type d

$$p_{L, \max} = 1 - z + (F_o - 0.3)^2 \quad \text{for } \frac{h_o}{H_{\text{Bridge}}} = 1.07, \quad (3.8)$$

$z = 1.0$ for bridge type a-c
 $z = 2.5$ for bridge type d

with $z = \text{constant}$ based on the bridge type [–]. According to Schmocker and Hager (2011), the maximum accumulation probability of single rootstocks $p_{R, \max}$ is only a function of F_o and can be described for $0.5 \leq F_o \leq 1.2$ with:

$$p_{R, \max} = 1.17 - 0.55F_o \quad \text{for bridge type a-c, and} \quad (3.9)$$

$$p_{R, \max} = 0.91 - 0.69F_o \quad \text{for bridge type d.} \quad (3.10)$$

The accumulation probability for various flow conditions, bridge types, and LW dimensions can then be calculated using $p_{L, \max}$ or $p_{R, \max}$. Compared to the results of Bezzola *et al.* (2002), the governing parameters for p highly differ. According to Bezzola *et al.* (2002), F_o has a minor effect on p , whereas Schmocker and Hager (2011) identified F_o as the governing parameter.

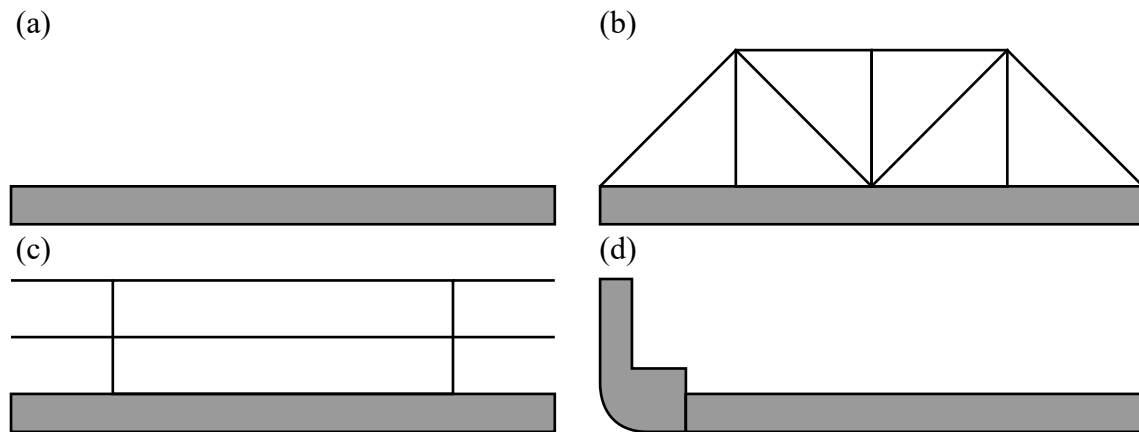


Figure 3.2 Tested bridge types; Frontal view of (a) reference bridge, (b) truss bridge, (c) railing bridge, and side view of (d) baffle bridge (adapted from Schmocker and Hager 2011)

Bocchiola *et al.* (2006b) conducted flume experiments on LW transport in the presence of obstacles. The test setup consisted of ≈ 30 obstacles made of wood rods with a diameter of 0.01 m placed vertically on a fixed channel bed. The obstacles were randomly distributed and represented in-channel vegetation or structures. Based on 810 test runs (15 starting positions, 6 log types, 3 transportation types, and $N = 3$ repetitions), p of a single log was calculated for each wood rod. The spatial distribution of p varied for the different transportation types (rolling, partially floating, and fully floating). The accumulation probability at a wood rod varied between 0...50%. Long and fully floating logs resulted in the highest p . The majority of the transported logs accumulated at the beginning of the obstacle area. The probability distribution was not parameterized, as the sample size was too small.

The LW accumulation probability at bridge decks (type railing bridge) including a circular bridge pier was investigated by Gschnitzer *et al.* (2013). The model LW consisted of logs with and without branches, a constant diameter, and five different log lengths. The experiments were conducted for congested (addition of 10 logs at the same time) and

uncongested LW transport. The logs were inserted parallel to the flow 6.5 m upstream of the bridge pier. An accumulation was defined, if one log accumulated at the bridge for more than 30 seconds. To obtain p , each test run was repeated $N = 8$ times. For the experiments, F_o was varied between 0.60, 0.80, and 1.20, resulting in 1'440 test runs. Similar to previous studies, their findings indicate an increasing p for increasing log length, congested transport, logs with branches, and increasing h_o . The results of Gschnitzer *et al.* (2013) were not summarized in a design equation.

The LW accumulation probability p at a single bridge pier was tested by Lyn *et al.* (2003) for various approach flow conditions (h_o , F_o , and approach flow velocity v_o). The modeled rounded bridge pier had a width of 0.0125 m and a streamwise bridge pier length of 0.105 m (Figure 3.3). The model LW consisted of logs ($d_L = 0.006$ m and $L_L = 0.1$ m) with and without branches. For selected tests, the effect of a modeled ‘sand bar’ in front of the bridge pier was tested on p_L . In addition, model tests were conducted on the effect of possible countermeasures to reduce p_L . The countermeasures included a submerged groin-like structure and a vertical cylindrical deflector positioned ≈ 0.40 m upstream of the bridge pier. Within one test run, 70 single logs were inserted 6 m upstream of the bridge pier in random orientation to the flow. The accumulated logs in front of the bridge pier or deflector were counted at test end. An accumulation was defined, if at least three logs accumulated at the bridge pier for a minimum duration of 15 minutes. The tests were repeated $N = 50$ to improve statistical significance.

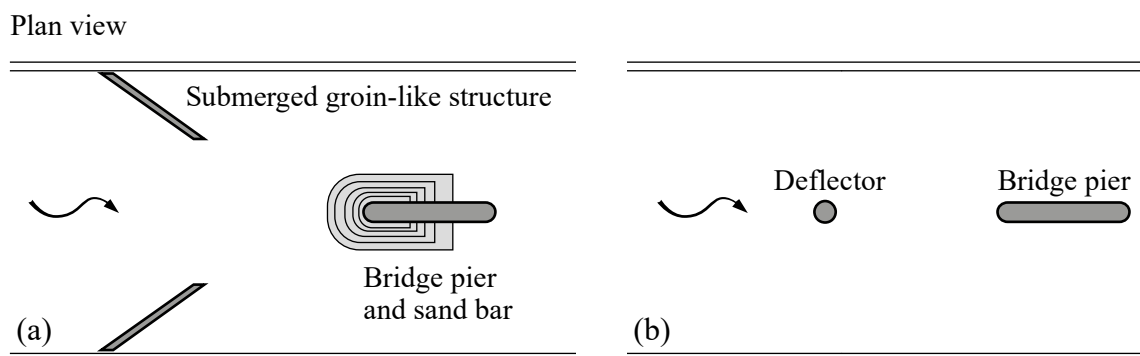


Figure 3.3 Test setup including countermeasures to reduce accumulation probability; (a) submerged groin-like structure and the sand bar, (b) deflector (not drawn to scale; adapted from Lyn *et al.* 2003)

In contrast to Schmocker and Hager (2011), no governing effect of F_o was found, but p increased with decreasing v_o and h_o . If more than six logs with branches accumulated, the

branches improved the interrelation between the single logs, thereby increasing the accumulation stability. This resulted in higher p compared to accumulations of logs without branches, which tended to disperse. In addition, p was higher for the experiments with the modeled ‘sand bar’. The vertical cylindrical deflector reduced the accumulation probability at the bridge pier. However, logs were also retained at the deflector itself. The submerged groin-like structures decreased p only for higher discharges. The test results were not parameterized. Lyn *et al.* (2003) further summarize recommendations for bridge design and countermeasures (Section 3.5).

De Cicco *et al.* (2016) and De Cicco (2017) studied the influence of different single bridge pier shapes on p . Flume experiments were conducted for uniform logs, steady flow conditions ($F_o = 0.3$ and 0.5), congested and uncongested LW transport, and a fixed channel bed. The modeled pier included square, round, triangular, ogival, and trapezoidal shapes and was placed in the centerline of the 5 m long and 0.30 m wide flume. The model log length varied in relation to the channel width B , resulting in small ($L_L = 20\%$ of B), medium ($L_L = 30\%$ of B), and large ($L_L = 50\%$ of B) model logs. The logs were inserted randomly ≈ 3 m upstream of the bridge pier. To model congested LW transport, a total of 125 logs with various lengths were inserted in bulks of 25 logs every 20 seconds with $N = 10$ repetitions. For uncongested LW transport, 50 small model logs were individually added to the flow every 5 seconds with $N = 5$. The logs were not removed until test end. Three different types of accumulation probabilities were defined in the study:

- *Blockage probability p_1* : $p_1 = 0$ was assigned, if none of the added logs accumulated at the pier. In contrast, $p_1 = 1$, if at least one of the added logs accumulated. The accumulation probability for one configuration was then calculated as the ratio between the sum of p_1 and the number of repetitions N . For uncongested LW transport with $N = 5$, p can be estimated in 20%-steps ($1/5 \dots 5/5 p$). For congested LW transport, p can be specified in 10%-steps. For $F_o = 0.3$, $p_{1,\max} = 60\%$ for uncongested and $p_{1,\max} = 40\%$ for congested LW transport were observed for the trapezoidal pier. For uncongested LW transport and $F_o = 0.3$, p_1 was zero for all other pier shapes. For $F_o = 0.5$, a square pier exhibited $p_{1,\max} = 40\%$ for uncongested and $p_{1,\max} = 90\%$ for congested LW transport. Given an ogival pier, p_1 was zero for all tested F_o and LW transport types.
- *Effective blockage probability p_2* : The effective blockage probability p_2 was defined as the ratio between the number of accumulated logs after a test run and the number of added logs. The result was then averaged over N . For all tested F_o and

LW transport types, p_2 varied between 0...5% for the different pier shapes. Due to these small differences, no governing effect of the pier shape on p_2 can be deduced.

- *Potential blockage probability p_3* : The potential blockage probability p_3 was the ratio between the number of logs touching the pier and the number of added logs, averaged over N . The results are contrary compared to previous studies, as p increased with increasing F_o for all tested pier shapes. For $F_o = 0.5$, $p_3 \approx 20\%$ for all tested pier shapes with deviations of $\pm 5\%$. In contrast, $p_3 \approx 10\%$ for $F_o = 0.3$ and all tested pier shapes with deviations of $\pm 10\%$. As the deviations of p_3 are in the range of $\pm 10\%$, it is rather difficult to derive a governing effect of the pier shape on p_3 .

The governing parameters to describe LW accumulation probability are partially contradictory (Table 3.1). The required test repetitions N to obtain statistically significant p were defined from $N = 3...50$. According to Furlan *et al.* (2018), $N \geq 30$ is recommended for statistically significant p . The existing design equations for p are only valid for bridge decks. Systematic studies on the accumulation probability at bridge piers exist, but the results were not parameterized.

Table 3.1 Governing parameters on LW accumulation probability determined in past studies.

Type	Literature	Approach flow Froude number F_o	Approach flow depth h_o	Approach flow velocity v_o	LW dimensions	LW with branches	Congested LW transport	Cross-section or pier geometry	Number of repetitions N
Bridge deck	Bezzola <i>et al.</i> 2002				X		X	X	3
	Schmocker & Hager 2011	X	X		X				8
Bridge pier	Gschnitzer <i>et al.</i> 2013		X		X	X	X		8
	Lyn <i>et al.</i> 2003		X	X	X	X	X		50
	De Cicco 2017	X						X	5-10

3.3 Large wood accumulation characteristics

A LW accumulation is commonly described by its shape (cross-section and longitudinal section), volume and porosity. The LW accumulation characteristics depend on the

amount of entrained and transported LW (Section 2.4 and Section 2.5), the hydraulic and topographic conditions, and the accumulation probability (Section 3.2). In river reaches without infrastructures, LW accumulations are commonly formed in areas of low flow depths and flow velocities, due to in-channel obstructions, or at river bends (Nakamura and Swanson 1994, Braudrick and Grant 2001, Bocchiola *et al.* 2006b, Bocchiola *et al.* 2008). Those natural LW accumulations highly increase the ecological functions of a river (Section 2.3, Keller and Swanson 1979, Gurnell *et al.* 2002, Wohl *et al.* 2016).

LW accumulations consist of a so-called ‘key member’ or ‘key log’, which can be described as a long piece of wood (with or without branches or rootstocks) initiating and stabilizing the accumulation (Nakamura and Swanson 1994, Wallerstein *et al.* 1996, Abbe and Montgomery 2003, Manners and Doyle 2008, Davidson *et al.* 2015). Diehl (1997) introduced the concept of the ‘design-log-length’ equal to the potential LW accumulation width. It can be defined based on the smallest value of either the channel width upstream of the river infrastructure, the maximum length of stable logs, or $9 \text{ m} + \frac{1}{4}$ of the upstream channel width. Only one study, by Manners *et al.* (2007), has actually quantified the proportions of different materials making up natural LW accumulations. The Manners study did this for 3 jams in the eastern United States. Based on the findings of that study, we here assume that an accumulation volume consists of approximately 69% LW (with 45% key logs), 17% medium wood (MW, with a trunk diameter 0.01...0.1 m), 5% small wood (SW, with a trunk diameter ≤ 0.01 m), 7% leaves, and 2% soil. The organic fine material *FM* ranges from 3...15% (for leaves and SW). An accumulation body can be described by its porosity or void fraction ϕ with

$$\phi = \frac{V_l - V_s}{V_l}, \quad (3.11)$$

or the bulk factor a

$$a = \frac{1}{1 - \phi} = \frac{V_l}{V_s} \quad (3.12)$$

with V_l as the loose LW volume [m^3] and V_s as the solid LW volume [m^3]. The flow through the accumulation body is comparable to seepage flow in porous media. According to field measurements after floods in Switzerland, the bulk factor of LW accumulations varied between $a = 2...5$ (Lange and Bezzola 2006, Waldner *et al.* 2009), equivalent to $\phi = 0.5...0.8$. A bulk factor of $a = 5$ describes a rather loose accumulation, and $a = 2$ corresponds to a dense accumulation.

The formation of a LW accumulation at a retention rack perpendicular to the flow was investigated by Schmocker and Hager (2013). Approximately the first 5% to 20% of the LW accumulation volume generate the main increase of backwater rise Δh (Section 3.4.1), whereas the following $\approx 80\%$ form a LW carpet, leading only to a small additional increase of Δh (Figure 3.4).

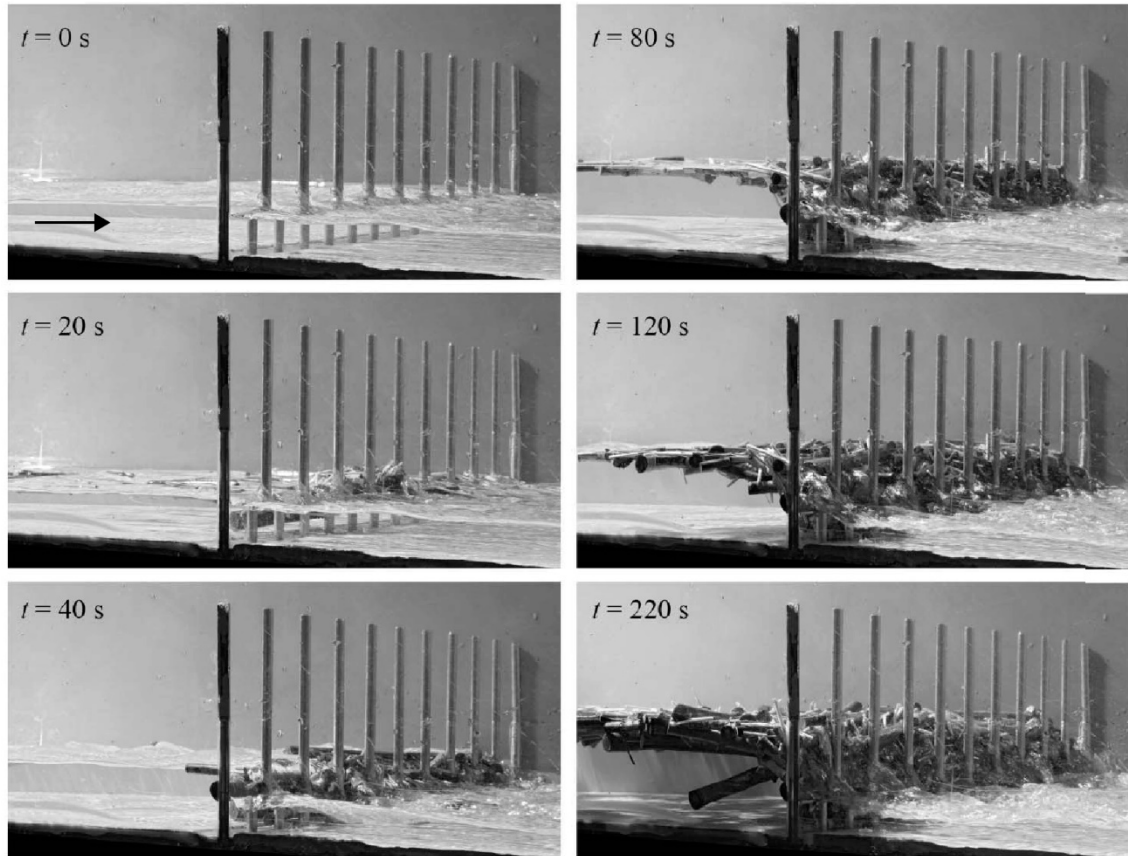


Figure 3.4 Temporal development of a LW accumulation at a retention rack (adapted from Schmocker and Hager 2013)

Schmocker and Hager (2013) normalized the length of the LW carpet (subscript C) L_C using the retention rack (subscript r) width B_r . A higher approach flow Froude number leads to a more compact LW accumulation body (i.e. lower bulk factor a), a higher backwater rise and a shorter LW carpet. The dimensionless length of the LW carpet was defined for $F_o = 0.5 \dots 1.5$ as:

$$\frac{L_C}{B_r} = 6.6 - 2.6 F_o. \quad (3.13)$$

The longitudinal shape of LW accumulations at retention structures in a vertical plane parallel to the approach flow is triangular or trapezoidal in shape. The initial LW accumulation volume can be approximated to a box-shape.

For LW accumulations at a single bridge pier (Diehl 1997, Panici and de Almeida 2017) the cross-sectional shape of LW accumulations can be described as a horseshoe. According to Panici and de Almeida (2017), the accumulation process at a single bridge pier can be divided into three phases. The first phase is characterized by an unstable growth of the accumulation body, with logs alternately clogging and resolving from the accumulation. The second phase describes a stable accumulation, followed by the third and critical phase involving the detachment of the accumulation from the pier.

Natural LW accumulation characteristics were studied at various field sites and are provided by Piégay and Gurnell (1997), Gurnell and Sweet (1998), Gurnell *et al.* (2000), Andreoli *et al.* (2007), Wohl and Goode (2008), and Ravazzolo *et al.* (2015b).

3.4 Hazards due to large wood accumulations at river infrastructures

Large wood accumulations at river infrastructures can lead to backwater rise and consequently to flooding of the surrounding area. In addition, local scour may occur at the river infrastructure. The current research on these two hazards will be summarized in the following subsections.

3.4.1 Backwater rise

Backwater rise Δh due to LW accumulation was investigated in various studies. Knauss (1995) tested different LW retention rack configurations (Figure 3.5) and examined the effect of LW dimensions on Δh using physical modeling. According to Knauss (1995), Δh can be described with the normalized height difference α :

$$\alpha = \frac{h - h_o}{\frac{v_o^2}{2g}} = \frac{\Delta h}{\frac{v_o^2}{2g}}, \quad (3.14)$$

with h = flow depth with LW accumulation [m], h_o = approach flow depth without LW accumulation [m], v_o = approach flow velocity representing uniform flow without LW accumulation [m/s], and g = gravitational acceleration [m/s²]. The value of α equals

$\alpha = 1.5$ for large wood and increases up to $\alpha \approx 2.3$ for small wood. Compared to a rectangular rack, a V-shaped rack (Figure 3.5, B and C) results in smaller Δh due to its larger rack length. The LW pile up at a V-shaped rack is reduced, which results in smaller Δh and favors the development of a LW carpet. Furthermore, Knauss (1995) observed an increase of Δh with increasing approach flow Froude number F_o representing uniform flow conditions without a LW accumulation, which was varied between 1.5 and 2. Even though different rack types and LW characteristics were investigated within the study, the parameter range is still rather small. Therefore, the estimation of backwater rise with respect to the normalized height difference α is not transferrable to other LW retention structures. In principle, Δh depends on v_o , LW dimensions, and rack configuration.

Plan view

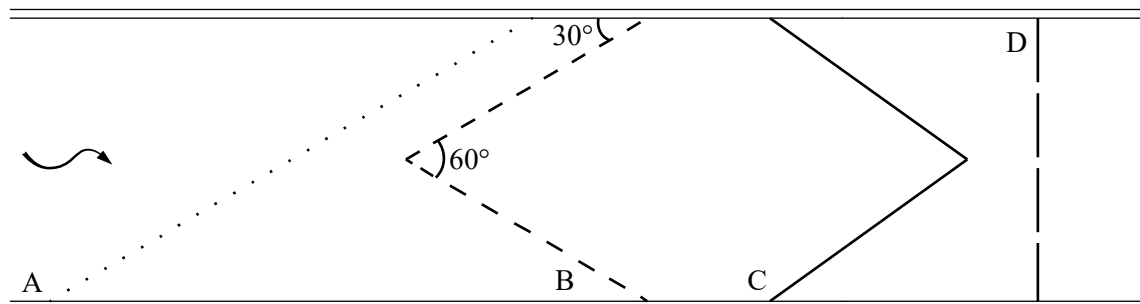


Figure 3.5 Large wood retention rack configurations with A = diagonal rack, B = V-shaped rack against flow direction; C = V-shaped rack in flow direction, D = rectilinear rack (adapted from Knauss, 1995)

Rimböck (2003) conducted flume and field experiments on the design of rope net constructions for LW retention. The governing parameters for Δh were identified as LW characteristics (mixture and wood type), discharge Q , bottom slope J_o , and channel roughness. To reduce Δh and prevent LW from overtopping the net, the flow velocity at the upper end of the LW carpet should not exceed 0.8...1 m/s. Rimböck (2003) further compared the rope net placement in a straight channel to a setup in a river bend, resulting in a smaller Δh for the setup in the river bend. However, this configuration was not further investigated due to the load concentration at the outer bend and the resulting negative aspects for the rope net dimensioning.

A different rack configuration with the objective to reduce Δh was introduced by Schmocker and Weitbrecht (2013). They presented the so-called bypass retention where LW is retained parallel to the main stream in a bypass channel. The bypass channel is located at the outer bend of a river and the rack is placed parallel to the river axis. Due to

the secondary currents in the bend, LW is transported at the outer bend and into the bypass channel. The approach flow is parallel to the LW retention rack, which leads to smaller Δh . As the bed load remains in the main channel, the bypass retention has further a positive effect on the sediment continuity.

Further flume experiments on Δh due to LW accumulation at a rectilinear rack were conducted by Schmocker and Hager (2013). The objectives were to identify the governing parameters for the accumulation process and to simplify small-scale model tests. The effect of the rack pole diameter d_r , LW watering time t_w , loose LW volume V_l , test duration t_T , F_o , and LW characteristics (including mixtures) on Δh were investigated. The experimental results identified F_o and V_l as the governing parameters for the accumulation process. The resulting backwater rise Δh can be estimated for $F_o = 0.5 \dots 1.5$ with:

$$\Delta h + h_o = (1.4 + 1.9F_o) h_o, \quad (3.15)$$

Based on Eq. (3.15), Δh is primarily a function of the approach flow conditions. In contrast, neither the pole diameter, nor the watering time, or test duration had an influence on Δh . The floatability of the model logs only changed after watering the logs for approximately one week. Furthermore, the accumulation process and Δh were almost independent of the tested LW mixtures. However, no *FM* was included in the mixtures.

Hartlieb (2015) performed a dimensional analysis to parameterize Δh due to LW accumulation and evaluated various experimental results and field observations of LW accumulations at hydraulic structures. As a result, F_o and the compactness of the LW accumulation were identified as the governing parameters for Δh . The compactness of the LW accumulation is affected by F_o and the log density. The higher these two parameters, the higher the compactness and the higher Δh . For one LW accumulation test run with $F_o = 0.35$, Hartlieb (2015) additionally added *FM* (small branches, leaves, spruce needles) to the flow. Due to the *FM*, the accumulation body was considerably less permeable, and the relative backwater rise $\Delta h/h_o$ at least 35% higher compared to test runs without *FM*. As the addition of *FM* was limited to a single test run, no general conclusions could be drawn.

Case studies for Δh due to a LW accumulation at a specific river infrastructure were summarized amongst others by the following authors: Elliot *et al.* (2012) calculated the potential effects of LW accumulations on Δh and bridge scour for a study site in the USA using a 2D numerical program. Ruiz-Villanueva *et al.* (2014b) described the influence of LW during a flood in 1997 in Central Spain. The extensive LW transport led to a bridge clogging, resulting in Δh and a flooding of the adjacent area.

Table 3.2 summarizes the governing parameters for Δh due to a LW accumulation identified in previous studies. The existing formulae to estimate Δh are limited to a certain parameter range and are not consistent in terms of the different governing parameters. The effect of FM on Δh was neglected in the majority of previous studies mentioned above. Branches and leaves may change the accumulation characteristics and therefore affect Δh . Furthermore, the majority of the studies was conducted with a fixed bed. Hence, the knowledge on the interactions between Δh and scour is still limited. A movable bed may decrease Δh , while the resulting scour may damage the river infrastructure itself.

Table 3.2 Summary of relevant parameters for backwater rise due to LW accumulation

Literature	Approach flow Froude number F_o	Discharge Q	Bottom slope J_o	Channel roughness	Compactness of accumulation	LW dimensions and wood type	LW volume V_s	LW retention rack configuration
Knauss, 1995	X	X				X		X
Rimböck, 2003		X	X	X		X		
Schmocker & Weitbrecht, 2013	X				X			X
Schmocker & Hager, 2013	X						X	
Hartlieb, 2015	X				X			

3.4.2 Local scour

Erosion and deposition are common processes for flows with a movable riverbed. Due to local changes of the geometry or flow conditions, additional erosion processes occur, defined as local scour (Graf and Altinakar 2017). Local scour may result due to hydraulic structures, constriction, or vertical or horizontal jets and may be considerably affected due to LW accumulations. The presented studies herein were conducted under clear-water conditions (i.e. no sediment feeding).

Local scour at bridge piers can be described as an abrupt decrease of the channel bed elevation around the pier. Chiew (1984) described the mechanisms of local scour based on the vortices-system created around the bridge pier (Figure 3.6). They can be divided into (1) downflow in front of the pier, (2) horseshoe vortex, (3) wake vortex, and (4) trailing vortex in case the pier is submerged. A bridge pier changes the flow pattern

causing an adverse pressure gradient. Hence, part of the approach flow is directed downward in front of the bridge pier. According to literature, the downward movement is the main cause of local scour.

The dimensions and temporal evolution of local scour at bridge piers were studied in detail in various flume experiments (Chiew 1984, Hager and Unger 2010). According to Melville and Chiew (1999), the resulting scour depth is approached asymptotically. Oliveto and Hager (2002) proposed an equation to predict temporal scour evolution for steady approach flow. The equation has been further developed for unsteady approach flow conditions by Hager and Unger (2010).

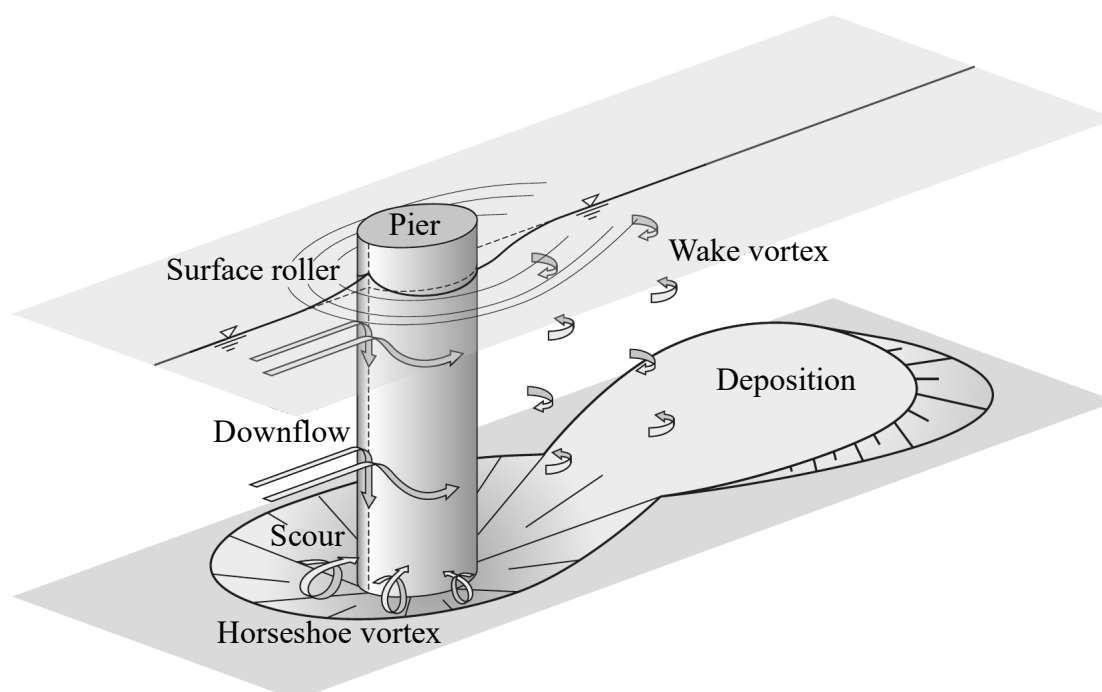


Figure 3.6 Vortex system around a bridge pier (adapted from Bezzola 2017 based on Melville and Coleman 2000)

Only a few studies have investigated the influence of LW accumulations on local scour, thereby focusing mainly on bridge pier scour. Laursen and Toch (1956) studied local scour around bridge piers and abutments using physical modeling, focusing on scour depth for various bridge pier shapes commonly used in Iowa (USA) at that time. Additional model tests included LW transport and accumulation, and the qualitative effect on local scour. The LW accumulation was either formed naturally or predefined. For the naturally formed accumulation, a certain LW volume was continuously added to the flow upstream of the bridge pier. The predefined accumulation consisted of single logs tied

together with cloth strips to account for different porosities (Figure 3.7). Some tests were conducted using Masonite boards to model an almost impervious LW accumulation. The LW accumulation at the bridge pier changed the approach flow conditions and led to deeper and larger scour holes. The results are only qualitative, as the influence of the permeability and dimensions of the accumulation were not investigated in detail.

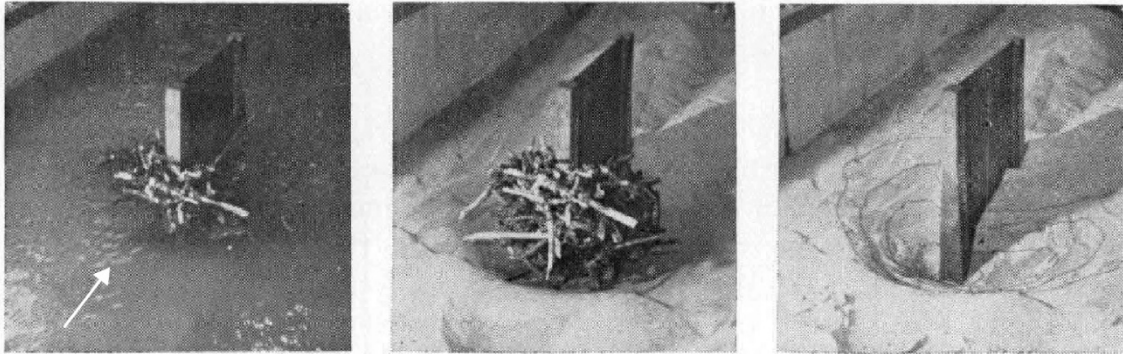


Figure 3.7 Bridge pier scour pattern due to large wood accumulation (adapted from Laursen and Toch 1956)

Melville and Dongol (1992) modeled a LW accumulation at a bridge pier as a raft with smooth, impermeable, regular shapes. The raft was mounted on the bridge pier at water level height. The raft shapes varied between cylindrical, conical, and elliptical; the cylindrical shape resulted in the largest scour. Melville and Dongol (1992) introduced the effective pier diameter d_{eff} (Figure 3.8), defined as:

$$d_{\text{eff}} = \frac{0.52h_A d_A + (h_o - 0.52h_A)d_P}{h_o}, \quad (3.16)$$

with h_A as effective height of LW accumulation [m], d_A as diameter of the LW accumulation [m], h_o as approach flow depth [m], and d_P as pier diameter [m]. To estimate the scour depth S , d_P is replaced by d_{eff} using the proposed scour equation by Melville and Sutherland (1988). The local scour reached the maximum magnitude for $h_o/d_P = 4$ and decreased again for higher values of h_o/d_P . In summary, local scour was mainly affected by the LW accumulation characteristics, the approach flow depth and velocity, sediment size and grading, as well as pier size, shape, and orientation to the flow.

Lagasse *et al.* (2010) conducted flume experiments with different accumulation porosities (impermeable versus 25% porosity). According to Lagasse *et al.* (2010), the concept of the effective pier diameter by Melville and Dongol (1992) tends to overestimate local scour. In addition, it does not consider the effect of the LW accumulation shape or

carpet. Lagasse *et al.* (2010) proposed a modification of the effective pier diameter formulae d_{eff}^* to:

$$d_{\text{eff}}^* = \frac{K_1 h_A d_A \left(\frac{L_A}{h_o} \right)^{K_2} + (h_o - K_1 h_A) d_P}{h_o} \quad \text{for } \frac{L_A}{h_o} > 1, \text{ and} \quad (3.17)$$

$$d_{\text{eff}}^* = \frac{K_1 h_A d_A + (h_o - K_1 h_A) d_P}{h_o} \quad \text{for } \frac{L_A}{h_o} \leq 1, \quad (3.18)$$

with L_A as the upstream length of the LW accumulation [m]. K_1 is a dimensionless accumulation shape factor with $K_1 = 0.79$ for rectangular and $K_1 = 0.21$ for triangular shape (compared to 0.52 in Eq. (3.16)). K_2 considers the intensity of the plunging flow due to the LW accumulation with $K_2 = -0.79$ for rectangular and $K_2 = -0.17$ for triangular shape. The largest scour was observed for a rectangular LW accumulation with $L_A \approx h_o$. Compared to the size, shape, and location of the LW accumulation, the porosity had only a minor effect on the resulting local scour.

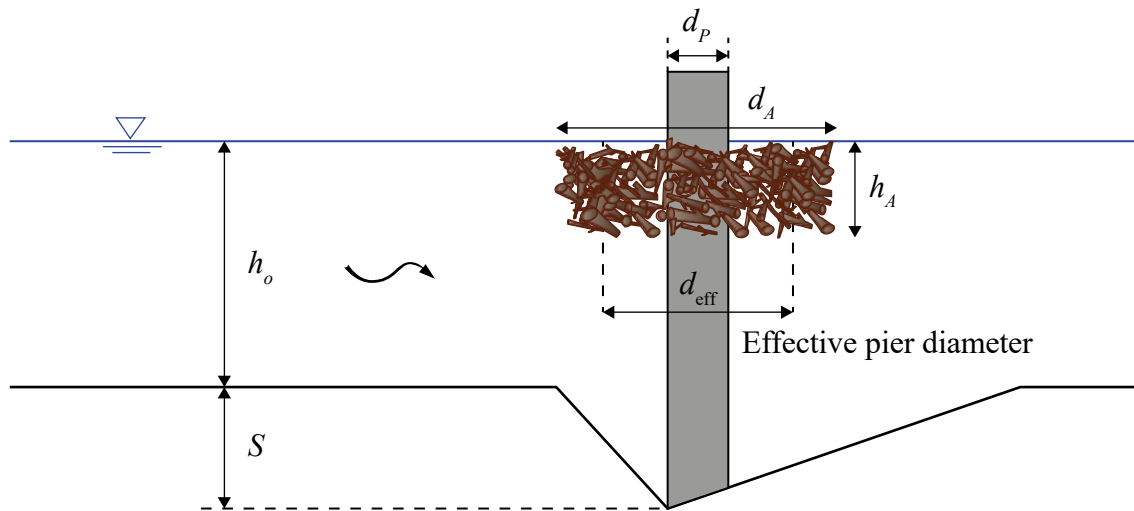


Figure 3.8 Experimental setup for local scour due to LW accumulation with S as the resulting scour depth (adapted from Melville and Dongol 1992)

Pagliara and Carnacina (2011) experimentally studied the influence of the transverse section of LW accumulations on local scour at bridge piers (Figure 3.9). The test setup is comparable to the studies of Melville and Dongol (1992) and Lagasse *et al.* (2010) (Figure 3.8). As Lagasse *et al.* (2010) stated that porosity has a minor effect on the local scour, Pagliara and Carnacina (2011) only modeled impervious accumulations. The LW accumulation was varied to account for rectangular, cylindrical, and triangular shapes (front view). They introduced the equilibrium LW contraction factor K_d as the

ratio between the maximum scour depth with ($S_{\max, A}$) and without ($S_{\max, 0}$) LW accumulation, defined as:

$$K_d = \frac{S_{\max, A}}{S_{\max, 0}},$$

$$K_d = 1 + 0.036 \Delta A^{1.5} \text{ (rect. and tr.)}, \quad (3.19)$$

$$K_d = 1 + 0.018 \Delta A^{1.5} \text{ (cylindrical)}.$$

In Figure 3.10, K_d , Eq. (3.19), and data points from Melville and Dongol (1992) are plotted versus the blockage ratio ΔA (= ratio of LW accumulation area to the flow area).

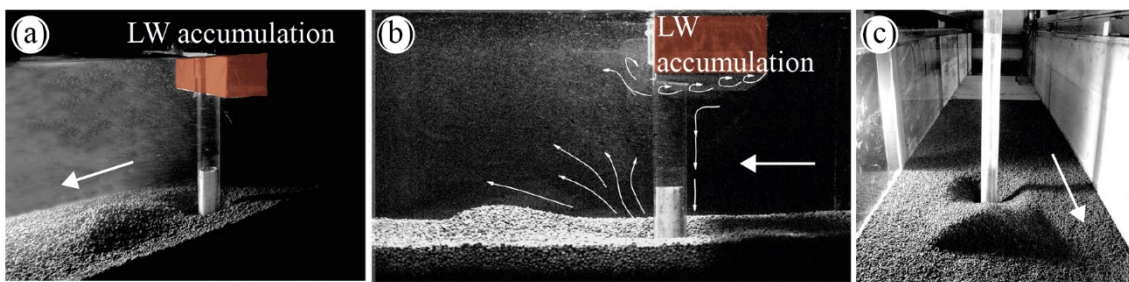


Figure 3.9 Flume experiments on local scour due to LW accumulation; (a) scour around bridge pier, (b) side view of test set-up, and (c) final scour (adapted from Pagliara and Carnacina 2011)

Note that Eq. (3.19) predicts K_d well for the different accumulation shapes. The results confirmed the findings of Melville and Dongol (1992) and Lagasse *et al.* (2010). In addition, ΔA was identified as the governing parameter affecting K_d . LW accumulations with a rectangular or triangular shape resulted in larger scours compared to a cylindrical accumulation shape. For $\Delta A < 0.03$, the LW accumulation shape had a negligible effect on K_d . As this approach mainly considered the frontal area of LW accumulations, it was suggested to further examine the effect of downstream extension of LW accumulation on local scour at bridge piers.

Wallerstein *et al.* (2001) conducted flume experiments to study constriction scour due to a partial LW blockage in sand-bed channels. The flow conditions were chosen below the threshold for incipient motion to investigate geomorphic effects solely due to the LW elements. The LW element size was the governing parameter for scour depth and size. Wallerstein (2003) developed a model to describe constriction scour due to LW accumulations. The analytical model was validated with field and experimental data from the Mississippi River (Wallerstein *et al.* 2001) and facilitates estimation of both scour rate and depth due to partial LW blockage.

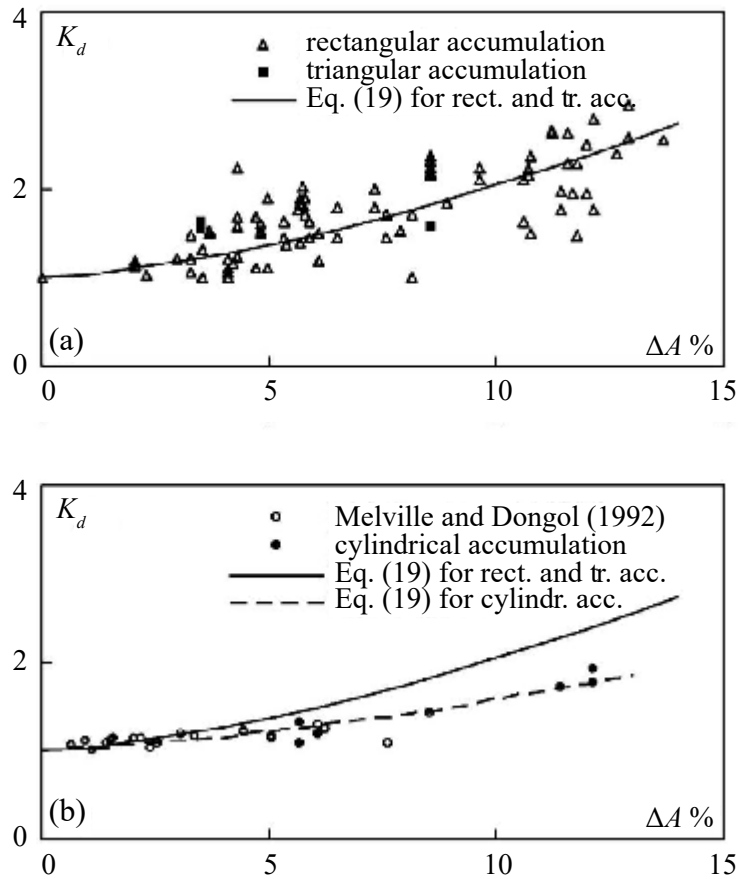


Figure 3.10 K_d versus ΔA for (a) rectangular and triangular accumulation shape and Eq. (3.19), (b) cylindrical accumulation shape, data points from Melville and Dongol (1992), and Eq. (3.19)

Studies on local scour due to LW retention racks have not been conducted so far. However, the flow through a LW accumulation at a retention rack is comparable to a horizontal jet. Local scour due to horizontal jets was described by e.g. Eggenberger and Müller (1944) as

$$S + h_2 = W \frac{\Delta h^{0.5} q^{0.6}}{d_{90}^{0.4}}, \quad (3.20)$$

with S = scour depth [m], h_2 = downstream flow depth [m], W = constant for jet type [$\text{m}^{0.3}/\text{s}^{0.6}$], Δh = difference between upstream and downstream flow depth (i.e. backwater rise) [m], q = unit discharge [m^2/s], and d_{90} = characteristic grain size diameter [mm]. For a free jet W was set to $W = 10.35$, whereas $W = 15.4$ for a submerged jet.

3.5 Large wood accumulation risk reduction measures

This section focuses on measures at river infrastructures. An overview on measures at weirs or spillways is summarized in SCD (2017), including a hazard assessment diagram. The risk of LW accumulations at river infrastructures can be mitigated using active or passive measures. Active measures are either maintenance works within the catchment area (i.e. forest maintenance, removal of deadwood, or bank erosion prevention) or structural measures such as retention structures and countermeasures to ensure the safe downstream conveyance of LW. Passive measures include organizational tasks such as early warning systems or evacuation plans, and strategic tasks including the designation of hazard zones and land use planning (Figure 3.11). An outline of possible LW accumulation risk reduction measures is provided by Zollinger (1983), Bänziger (1989), Lange and Bezzola (2006), and Schmocker and Weitbrecht (2013).

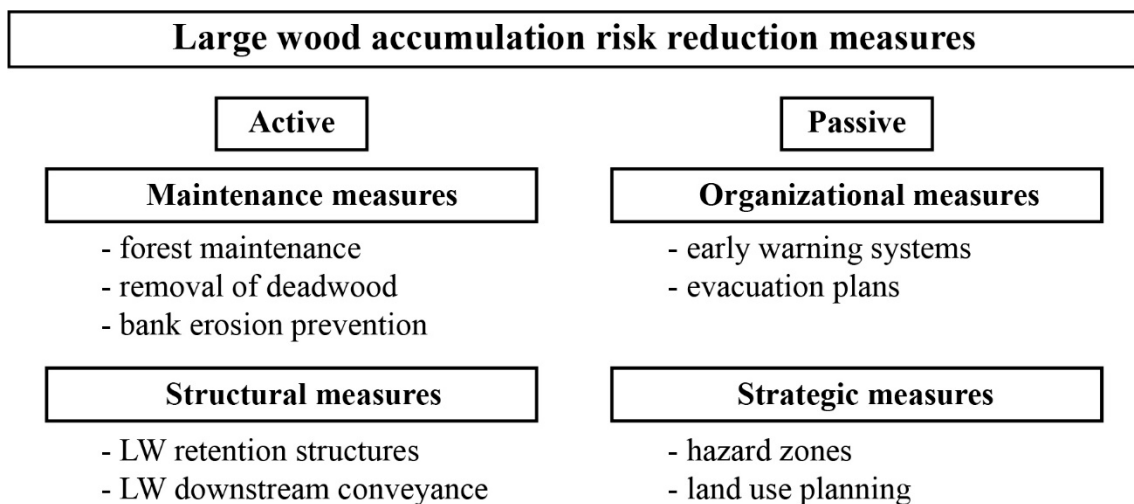


Figure 3.11 LW accumulation risk reduction measures (adapted from Lange and Bezzola 2006, Schmocker and Weitbrecht 2013)

The two strategies of active and passive measures are comparable to existing frameworks regarding flood protection in Switzerland (BWG 2001). Due to the scope of this study, the literature review on LW accumulation risk reduction measures concentrates on structural measures for a safe downstream conveyance of LW. The characteristics of LW retention structures are well documented in Perham (1987), Wallerstein *et al.* (1996, 1997), Hartlieb and Bezzola (2000), Rimböck (2003), and Schmocker and Weitbrecht (2013).

The objective of structural measures for a safe downstream conveyance of LW is the prevention of LW accumulations at river infrastructures, especially bridges. According to Bradley *et al.* (2005) the following measures are suitable to enable or improve the downstream conveyance of LW.

- *Rectifier / Fin*: A rectifier orients transported logs parallel to the flow direction (e.g. longitudinal alignment of LW). A fin is installed as an extension upstream of the bridge pier (Figure 3.12).
- *Rectifier / Deflector*: A deflector has the same purpose as a fin and orients the transported logs parallel to the flow direction. It is located upstream of the river infrastructure. The shape of a deflector may differ between ‘V-shaped pointing against flow direction’ or ‘circular’ (i.e. a pole; Figure 3.3, Lyn *et al.* 2003, Lange and Bezzola 2006). The efficiency of rectifiers was tested at VAW for a case study at the sediment bypass tunnel Campo Vallemagia (VAW 1991, Lange and Bezzola 2006). The results of the flume experiments showed that the rectifier loosens up the LW carpet. The shape of the rectifier was of minor importance.
- *Instream River Training Structures*: These structures are placed on the channel bottom to alter the flow by inducing secondary currents and thus transported logs are not accumulated at the bridge pier. Common types are micro groins (i.e. submerged sills), Iowa vanes, spurs, or meandering ramps. Micro groins may cover the entire or partial river width and are placed inclined or declined to the flow direction. The various types, their function, and applicability are summarized in Werdenberg *et al.* (2014).
- *Sweeper*: A sweeper consists of a polyethylene device mounted on a vertical beam. This construction is attached at the upstream side of the bridge pier. The vertical height of the sweeper is adjusted according to the current flow depth. The objective is to avoid LW accumulation at the bridge pier. The sweeper rotates due to the motion of water, thereby deflects transported LW (Figure 3.13).
- *Design features*: New river infrastructures should be designed to reduce the risk of LW accumulation. According to Bradley *et al.* (2005) this includes: (1) sufficient dimensions of the freeboard, (2) alignment of bridge piers to the flow direction and adequate spacing between two or more bridge piers to avoid LW accumulation, (3) design of superstructure to prevent LW accumulation at the bridge deck.

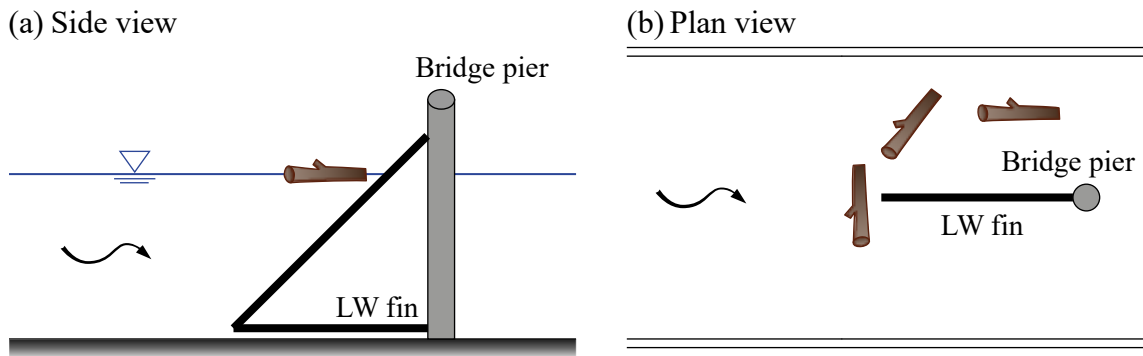


Figure 3.12 LW fin as a countermeasure to orient transported logs in flow direction, (a) side view and (b) plan view (adapted from Bradley *et al.* 2005)



Figure 3.13 Double-stacked installation of a LW sweeper at the Mississippi River, USA (adapted from Bradley *et al.* 2005)

Lange and Bezzola (2006) summarized possible measures to ensure a safe downstream conveyance of LW at bridges. In general, the following recommendations were made to prevent LW accumulations at river infrastructures:

- *Cross-section dimensions*: The bridge width should be at least two times the expected log length.
- *Bridge dimensions*: The clearance height of the bridge should be at least 1.7 times the dimension of the expected rootstocks.

Furthermore, they differentiated between permanent and temporary measures. The characteristics of permanent measures are: (1) sufficient river cross-sections, (2) smooth design of the bridge bottom and casings at the front side of the bridge (Figure 3.14), (3)

consistent design of the river cross-section (e.g. avoidance of jutting abutments), and (4) longitudinal alignment of LW (compare Figure 3.3 and Figure 3.12). Temporary measures include solutions during a flood such as LW removal using an excavator. Another possible measure is the installment of movable bridges. During a flood, the flow cross-section can be enlarged, thereby improving the downstream conveyance of LW. A movable bridge was installed in Switzerland (Canton Valais) after a flood in 1993 with extensive LW transport. The efficiency of this measure was proven during a flood in 2010 (Lange and Bezzola 2006). According to Schmocker and Hager (2011), a baffle bridge considerably favors LW passage without damage. The accumulation probability for root-stocks at a baffle bridge was almost halved compared to a truss bridge.

Franzetti *et al.* (2011) presented a protection structure for a bridge at the River Po in Italy. The bridge is characterized by two narrow parallel rows of piers. The measure consists of a plate mounted at the upstream side of the bridge piers and is built on pillars (Figure 3.15). The efficiency of the measure regarding LW accumulation reduction and bridge scour was evaluated with model tests and extended by field observations after measure completion.

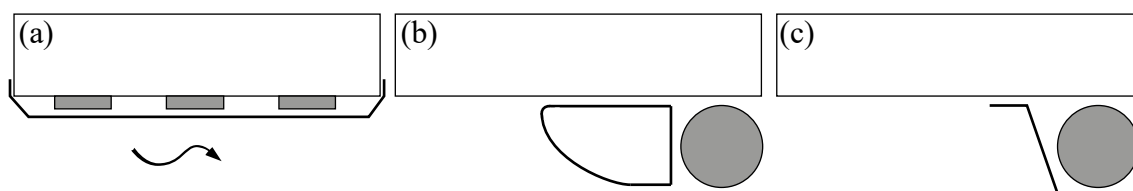


Figure 3.14 Casing countermeasures at bridges; (a) complete casing of the bridge bottom side, (b) single casing: nose, (c) single casing: baffle (adapted from Lange and Bezzola 2006)

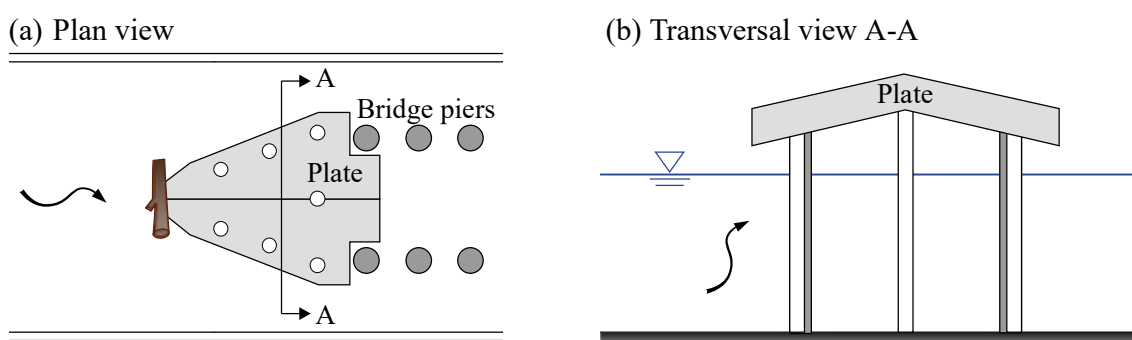


Figure 3.15 Plate as a countermeasure at bridge pier rows (adapted from Franzetti *et al.* 2011)

3.6 Numerical studies on large wood in rivers

Various researchers have recently started to numerically investigate LW entrainment, transport, and accumulation. The majority of previous studies applied a one-dimensional (1D) or two-dimensional (2D) model to estimate the hydraulic conditions, providing the basis for further calculations of LW mobilization (Section 2.5, Merten *et al.* 2010). In addition, results of flume experiments on LW accumulation served as a basis to include e.g. backwater rise due to LW accumulation in a 2D numerical model for inundation mapping (Gems *et al.* 2012).

Bocchiola *et al.* (2002) presented an analytical and numerical approach for channel flow dynamics including LW transport. The LW transport was assumed as a continuous LW carpet layer; the structure and porosity of the LW accumulation was neglected. The flow was considered as uniform, steady, and quasi two-dimensional. For turbulent flow, the Reynolds averaged Navier Stokes (RANS) equations were solved, applying the mixing length theory for closure. Their approach shows that LW transport leads to increased bed shear stress and flow velocities. As their proposed model was established for smooth surfaces, further research is deemed necessary.

How to simulate floating objects, including LW or ice blocks, was studied by Stockstill *et al.* (2009). It combines a two-dimensional depth-averaged hydrodynamic model with a three-dimensional discrete element model (DEM). The hydrodynamic model solves the 2D shallow-water equations in conservative form using finite elements. The DEM simulates floating objects as discrete elements. It solves the acting forces on the elements, i.e. gravitational, drag, buoyancy, and inter-particle contact forces. The motion of a floating object, e.g. a log, is calculated based on the total force acting on each particle, combined with the log characteristics, comprised of size, density, and stiffness. The DEM can further account for log rotation and log-log collision by computing the forces (normal and friction force) between two logs. To model the interaction between flow and floating objects, first the hydrodynamic model is solved. The flow depth and velocity for each finite element are passed to the DEM at the end of every time step. Based on these results, the drag and buoyancy forces acting on a log are calculated. These are then combined with inter-particle and gravitational forces to obtain the motion of the floating object. Then this procedure is repeated for the next time step. The coupling between the hydrodynamic and discrete element model is based on how often the information of the flow is passed to the DEM. The coupling of the DEM to the hydrodynamic

model was not included in their study. Therefore, backwater rise due to LW accumulations cannot be computed.

A similar approach to model LW entrainment, transport, and deposition is represented by the 2D hydro-numerical model 'Iber' (Bladé *et al.* 2014) with an implemented sub-module called 'IberWood' (Ruiz-Villanueva 2012). An extensive summary of 'IberWood' is provided by Ruiz-Villanueva *et al.* (2014c). 'Iber' can be used to model free-surface flows, morphodynamics, and transport processes in rivers. It was developed by the International Center of Numerical Methods in Engineering (CIMNE), the Water and Environment Engineering Group (GEAMA), and the Flumen Research Institute (Universitat Politècnica de Catalunya, Spain). 'Iber' has three computational modules, namely hydrodynamic, turbulence, and sediment transport module. The hydrodynamic module solves the 2D shallow-water equations. The turbulence model includes the turbulent stresses in the hydrodynamic computations using e.g. the k - ε -model. The sediment transport module solves the Exner sediment conservation equation as well as (suspended) bedload transport equations. The three modules are solved using the finite volume method with a second order, time explicit scheme (extension of Roe's upwind scheme). 'IberWood' can be used to simulate single or multiple cylindrical logs (without branches) and is coupled with 'Iber' by a Lagrangian discretization. For every time step, the flow is calculated with the hydrodynamic module. Based on the results, the position and velocity of the logs is calculated. In contrast to Stockstill *et al.* (2009), the effect of logs on hydrodynamics can also be included. LW entrainment and transport is based on the force balance at incipient motion for a cylindrical log on the riverbed (Figure 2.4 and Section 2.5.1). The LW movement always depends on the force balance, which is continuously re-calculated. Depending on the LW density, the model logs are either floating or sliding. For the present thesis, all logs are considered floating and LW entrainment, rolling, or sliding has not been studied. The common log transport method is kinematic, assuming the velocity of floating logs to be equal to the flow velocity. Based on the log velocity, the log position can be calculated for every time step. Transported logs may turn, if one log end is transported faster than the other log end. To account for this rotation and to obtain log orientation, velocities at the two log ends are calculated. Log orientation further depends on the mesh size in relation to the log size, as a finer mesh may lead to a log rotation, as the two log ends are positioned in different mesh elements. To model the effect of LW on the hydrodynamics, an additional shear stress is included in the 2D shallow-water equations. The additional shear stress is defined as $\tau_{\text{Wood}} = F_{\text{drag}}/A$. The drag

force is calculated for every log at every finite volume or mesh element, and is divided by the area of mesh elements containing a log. The model further includes the interaction between logs and channel topography (Figure 3.16) by adapting the log velocity. Given a collision of two logs, the resulting log velocity changes as a function of a restitution coefficient, assuming elastic interaction. If a log touches a wall, it either bounces off or slides, depending on the angle between log and boundary, with a threshold value of 45° . Hydraulic structures can be modeled as an internal condition or by adapting the geometry. The log dimensions, position, number, angle, and density as well as the drag coefficient of the log have to be entered as an initial condition and can be varied for a scenario-based analysis. This 2D numerical approach was applied for different case studies and validated with physical experiments (Ruiz-Villanueva *et al.* 2014b, Ruiz-Villanueva *et al.* 2014c, Ruiz-Villanueva *et al.* 2016d, Bladé *et al.* 2016).

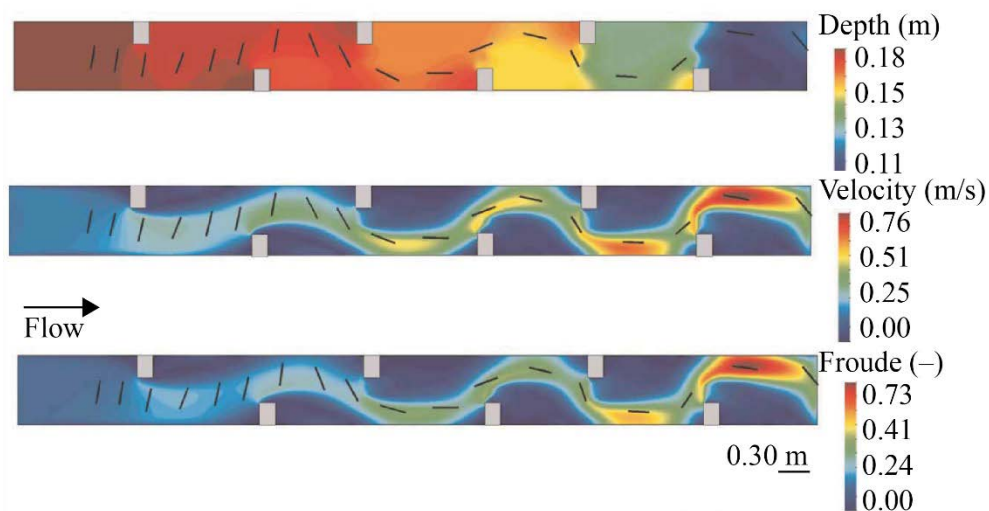


Figure 3.16 Example of LW transport (black lines) simulated with ‘IberWood’. The flow depth, flow velocity, and Froude number are illustrated (adapted from Ruiz-Villanueva *et al.* 2014c)

A three-dimensional (3D) model was presented by Xu and Liu (2016) to simulate the streamflow resistance due to LW. The objective of this study was to analyze turbulent flow around LW with branches and twigs. The numerical simulation was carried out with the open access program OpenFOAM and the two-phase solver interFOAM using the Volume of Fluid (VOF) method. Besides the continuity and momentum equation, an equation regarding the volume fraction of the fluid phase has to be solved (Ferziger and Peric 2008). The two-equation $k-\omega$ SST turbulence model, a mixture of the $k-\omega$ - and $k-\varepsilon$ -model, was applied. The model approach was validated with flume experiments, placing

a 3D printed tree on the channel bottom. The angle of the LW placed at the channel bottom was varied and the resulting drag force calculated. The drag force was estimated by the momentum equation and the pressure integral. The results of the drag force highly vary, but the wave patterns induced by the tree were modeled correctly using the 3D numerical simulation.

3.7 Summary and identified research gaps

The presented literature review highlights the past studies on hazards related to large wood in rivers. Given a certain LW volume transported in the river, the related hazard at river infrastructures comprises the three interconnected topics: (1) LW accumulation probability, (2) LW accumulation characteristics, resulting backwater rise and local scour, and (3) design of suitable measures for LW accumulation risk reduction.

Previous studies on LW accumulation probability focused mainly on the effect of the bridge deck. Design equations were elaborated for single log and single rootstock transport, but the governing parameters of the existing approaches highly vary. A series of case studies were conducted on LW accumulation at single bridge piers, but the results have not been parameterized. Furthermore, the effects of more than one bridge pier, a movable bed, or multiple logs on the accumulation probability have not been considered so far.

The number of investigations on natural LW accumulation characteristics have increased, but a systematic analysis of the influence of various LW accumulation shapes, rates, or composition on backwater rise is still missing. The available formulae for backwater rise were established for a limited number of tests and apply mostly to a specific LW retention rack placement. To further improve the estimation of backwater rise, the effect of organic fine material (e.g. branches and leaves) in LW accumulations must be considered. It is hypothesized that organic fine material changes the LW accumulation characteristics and increases backwater rise.

Only a few physical experiments have examined local scour due to LW accumulation. Existing studies focused on bridge piers and simplified the LW accumulation body as a rectangular or triangular shape. In addition, the interactions between backwater rise and local scour due to LW accumulations have not been studied so far.

Measures to ensure the safe downstream conveyance of LW are necessary to reduce the accumulation risk at bridges, especially at bridge piers. A detailed analysis of existing measures, i.e. fins or instream river training structures, may increase their efficiency.

The objectives of the present work can be described as follows:

- Establish physical model test setup to investigate LW accumulations at river infrastructures
- Improve general process understanding of LW accumulations
- Determine governing parameters for LW accumulation probability
- Examine LW accumulation shape
- Investigate scale and model effects for backwater rise due to LW accumulation
- Provide estimates for backwater rise due to LW accumulation
- Study local scour due to LW accumulation and effect on backwater rise
- Analyze the efficiency of measures for LW accumulation risk reduction at bridge piers
- Compare experimental results with numerical simulation results for evaluation

Physical experiments in three different flumes and 2D numerical simulations with ‘IberWood’ were performed to achieve these objectives. Systematic parametrical and additional analytical analyses were conducted to describe accumulation probability, backwater rise, and local scour due to LW accumulations.

4 Methodology

4.1 Overview

The research questions of this thesis were investigated using mainly physical modeling, complemented by a 2D numerical simulation. Similitude and scale effects of the physical model tests are discussed in Section 4.2. The test accuracy and error analysis are depicted in Section 4.3. Then the experimental setup including instrumentation, model large wood, test program, and procedure is described for the investigation of LW accumulation probability (Section 4.4), -characteristics (Section 4.5), and measures for LW accumulation risk reduction (Section 4.6). The setup of the numerical simulation with 'IberWood' is summarized for the LW accumulation probability and backwater rise in Section 4.7.

4.2 Similitude and scale effects

The objective of a physical scale model is to perform similarly to the prototype, achieved by maintaining geometric, kinematic, and dynamic similitude (Hughes 2005). The relation between prototype and model is described by the scale factor λ :

$$\lambda = \frac{\text{Prototype value}}{\text{Model value}}. \quad (4.1)$$

For geometric similitude, the length, area, and volume are scaled according to the selected λ , the premise for building a scale model in the laboratory. Kinematic similitude implies geometric similitude and a constant ratio of parameters of motion and time, e.g. flow velocity or acceleration (Heller 2011). In order to achieve perfect similitude, dynamic similitude has to be met as well. This includes the identical translation of all acting forces, e.g. gravity, viscosity, or pressure. Perfect similitude would further comprise the scaling of g , or atmospheric pressure and could only be achieved in a miniature universe (Heller 2011). Therefore, physical scale models are based on one governing scaling law. In open-channel flow, the common scaling law is according to Froude, with inertia as the retaining and gravity as the driving force. The Froude number is defined as:

$$F = \sqrt{\frac{\text{Inertia}}{\text{Gravity}}} = \frac{v}{\sqrt{gL}}, \quad (4.2)$$

with v = flow velocity [m/s], g = gravitational acceleration [m/s²], and L = characteristic length [m], defined as the flow depth h in rectangular open-channel flow. Other scaling

laws typically used in hydraulic engineering are according to Reynolds or Weber. The Reynolds number is defined by the ratio of inertia and viscosity, i.e.:

$$R = \frac{\text{Inertia}}{\text{Viscosity}} = \frac{\nu L}{\nu}, \quad (4.3)$$

with ν = kinematic viscosity = $1.01 \cdot 10^{-6}$ m²/s for T = 20°C. This scaling law is commonly used for modeling intake structures or air models, where the viscous force is predominant (Heller 2011). Given the surface tension as governing force, the Weber number (ratio of inertia and surface tension) is chosen as the scaling law.

The physical experiments in this thesis were scaled according to Froude similitude (Table 4.1). By selecting this scaling law, the other force ratios (e.g. inertia to viscosity or surface tension) are not identical and scale effects occur. However, model and prototype similitude may still be achieved by quantifying scale effects or by defining limiting criteria to neglect them (Heller 2011).

Table 4.1 Scale factors according to Froude similitude

Parameter	Scale factor
Length	λ
Area	λ^2
Volume	λ^3
Time	$\lambda^{1/2}$
Velocity	$\lambda^{1/2}$
Discharge	$\lambda^{5/2}$
Force	λ^3

Scale effects can be quantified by investigating a scale series, which was herein performed for backwater rise due to a predefined LW accumulation (Section 4.5). The physical experiments were conducted for $\lambda = 6$ (close-to-prototype), $\lambda = 30$, and $\lambda = 50$. In addition, backwater rise due to a natural LW accumulation was investigated for $\lambda = 6$ (close-to-prototype) and $\lambda = 30$ to further enable the analysis of model and scale effects. The setup is described in Section 4.5.1 and 4.5.2, and the final results of the scale series are discussed in Section 5.3.1.4.

To enable the upscaling of the experimental results, the dimensions of the model LW, percentage of *FM*, and the compactness of LW accumulations were based on natural observations (Bezzola and Hegg 2007, Manners *et al.* 2007). However, natural wooden

dowels were used to model LW, leading to an overestimation of the strength characteristics (tensile, bending, and flexural), and the Young's modulus of the model logs. Model LW is consequently too stiff and shows a different fracture and deformation behavior compared to prototype. Accumulated logs in prototype may break in smaller pieces, thereby increasing the compactness of the accumulation. In addition, transported logs may break when hitting bridge piers, thereby decreasing the accumulation probability. This was not observed during the physical experiments. The higher the prototype log stiffness, e.g. for logs with a large diameter, the smaller the scale effects when using natural wood in small-scale model tests (Hartlieb 2015). For the experimental setup with a predefined LW accumulation, the compactness was defined. Therefore, scale effects due to equal tensile strengths and Young's moduli in model and prototype are estimated to be negligible for this specific test setup.

To avoid viscosity and surface tension effects, Reynolds number $R = v_o \cdot 4R_h / \nu > 10^4$ (Hughes 2005) and $h_o \geq 0.05$ m (Heller 2011) were selected for the experiments on LW accumulation probability, respectively, where $R_h = Bh_o / (B + 2h_o)$ = hydraulic radius. The flow is in the rough turbulent regime for $R > 10^4$; and the viscous force is therefore independent of R (Hughes 2005). For the experiments on backwater rise due to LW accumulation, possible viscosity and surface tension effects were examined in the scale series and the results are presented in Section 5.3.1.4.

For the experiments with a movable bed (Section 4.4.3 and 4.5.5), scale effects due to cohesion can be neglected, as the model mean grain size diameter d_m was chosen to be > 2.0 mm and is significantly higher than the proposed limit of 0.22 mm by Zarn (1992).

To generalize the results of the physical experiments, the governing parameters describing (1) LW accumulation probability p , (2) backwater rise Δh and (3) scour S due to LW accumulation were identified with a dimensional analysis based on the Buckingham theorem Π (Buckingham 1914). According to Heller (2011), a physical problem is described by independent parameters n with reference dimensions r ([M] mass, [L] length, [T] time), resulting in $n - r = \Pi_1, \Pi_2, \dots, \Pi_{n-r}$ non-dimensional parameters. To obtain similitude, the non-dimensional parameters have to be identical in model and prototype. The dimensional analyses for p , Δh , and S are presented in Section 5.2.7, Section 5.3.1.7, and Section 5.3.2.2, respectively.

4.3 Accuracy and error analysis

The test setup, test procedure, and measurement systems all inhibit a certain error, classified in systematic and random errors (Martin and Pohl 2015). Systematic errors are caused by the test setup and procedure and can be summarized for the present experiments as:

• Flume geometry	± 2 mm
• Flume slope	$\pm 0.1\%$
• Ultrasonic distance sensors UDS	± 0.3 mm
• Laser distance sensors LDS	± 1 mm
• Point gauge	± 0.1 mm
• Traverse	± 1 mm
• Magnetic inductive flow meter IDM	$\pm 1\%$
• Bulk factor a	$\pm 10\%$
• Mean log diameter d_{Lm}	± 0.5 mm
• Organic fine material FM	$\pm 5\%$
• Accumulation length L_A	± 1 mm
• Personal errors	indeterminable
• Temperature variation of ± 2 C°	indeterminable
• Atmospheric pressure variation	indeterminable

Systematic errors are reduced by improving the test setup and procedure, or with calibration. Random errors are caused by indeterminable variations of the measurement systems or analysis. They are reduced with increasing test repetitions N , until converging to the expected value \bar{x} . The total error e_x is the sum of systematic and random errors, and describes the confidence interval. A certain measured quantity x therefore consists of the expected value \bar{x} and the total error e_x :

$$x = \bar{x} \pm e_x. \quad (4.4)$$

The relative standard error e^* is a common measure to assess the quality of the data series (test reproducibility, Section 4.5.7) and is defined as:

$$e^* = \frac{e_s}{\bar{x}} = \frac{\sigma_n}{\bar{x}\sqrt{n}}, \quad (4.5)$$

with e_s = standard error, \bar{x} = mean value, σ_n = standard deviation of sample, and n = number of samples.

A target value X can be calculated based on the measured parameters x . In order to determine the error of the target value e_x , an error propagation analysis is required. The error propagation law is defined as (Martin and Pohl 2015):

$$e_x = \sqrt{\left(\frac{\partial X}{\partial x_1} e_{x1}\right)^2 + \left(\frac{\partial X}{\partial x_2} e_{x2}\right)^2 + \dots + \left(\frac{\partial X}{\partial x_n} e_{xn}\right)^2}, \quad (4.6)$$

with e_{xn} = total error of measured parameter x_n . The error propagation analysis will be applied to the following target values of this thesis: LW accumulation probability p , back-water rise Δh , and local scour S . The results are presented and discussed in Section 5.2.7, Section 5.3.1.7, and Section 5.3.2.2, respectively.

4.4 Tests I: Large wood accumulation probability at bridge piers

The main objective of this part is to analyze the LW accumulation probability as a function of (1) the approach flow conditions, (2) the bridge pier characteristics with different pier roughness, -shape, -diameter, -number, (3) the LW characteristics, involving various log lengths, log diameters, log densities, LW with and without branches, and uncongested versus (semi-)congested LW transport, and (4) the channel bed, i.e. fixed versus movable bed.

4.4.1 Model flume I – tilting flume

The experiments were conducted in a 10.7 m long, 1.0 m wide, and 0.8 m deep tilting flume at VAW (Figure 4.1). The 2.0 m long intake is equipped with a flow straightener to generate undisturbed inflow. The channel has a fixed bed ($k_{St_Prototype} \approx 30 \text{ m}^{1/3}/\text{s}$) and side walls made of glass and PVC. The channel slope can be varied between $0 \leq J_o \leq 15\%$. The downstream flow conditions are regulated with a flap gate. A filtering basket was installed at the flume outlet to collect wood and sediment. For the movable bed experiments, a 1.0 m long ramp of boulders with a diameter of $\approx 0.10 \text{ m}$ was installed 3.5 m downstream of the inlet to provide a smooth flow transition. The movable bed (subscript b) had a height $h_b = 0.20 \text{ m}$, length $L_b = 3.0 \text{ m}$, and was fixed at the downstream end using a 2.5 m long plate with a roughness coat. The tests were performed according to Froude similitude with a model scale factor of $\lambda \approx 20$.

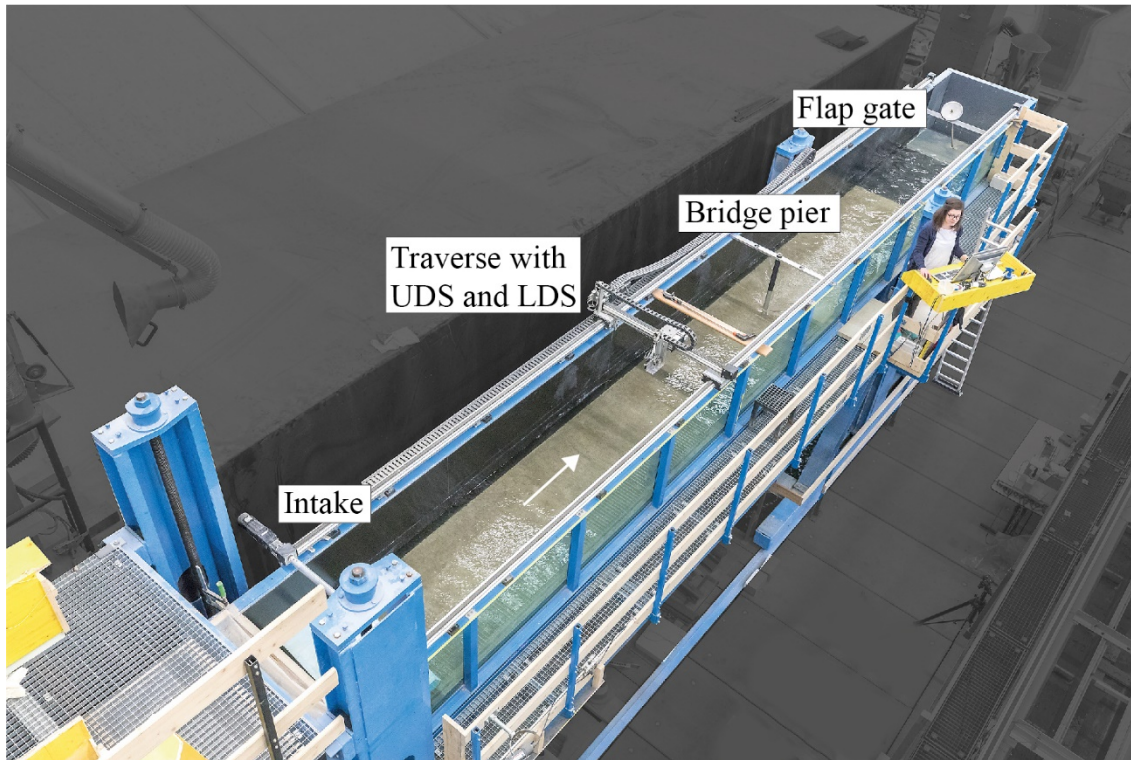


Figure 4.1 Photo of model flume I (tilting flume) at VAW with UDS = Ultrasonic Distance Sensor and LDS = Laser Distance Sensor

4.4.2 Instrumentation

The model flume I is equipped with two pumps of a combined maximum discharge capacity of $Q = 265$ l/s. The inflow discharge Q is measured in the supply pipes with an electromagnetic flow meter (IDM) and regulated with a valve. The approach flow conditions (subscript o) are controlled by adapting J_o , Q , and the downstream flap gate and are characterized by h_o , $v_o = Q/(Bh_o)$, and $F_o = v_o/(gh_o)^{1/2}$, with B = channel width, and g = gravitational acceleration. An Ultrasonic Distance Sensor (UDS) ‘UNAM 30’ and a Laser Distance Sensor (LDS) ‘ODAM 21’, both manufactured by Baumer Electric, Switzerland, were placed on an automated traverse. The UDS was used to measure h_o . For the experiments with a movable bed, the bed topography was scanned in a 2.5×2.5 cm² grid with the LDS. For selected approach flow conditions, 3D flow velocity measurements for transverse and longitudinal cross-sections were conducted using an Acoustic Doppler Velocimeter (ADV) ‘Nortek AS Vectrino 3D water velocity sensor Lab Probe’ with an accuracy of $\pm 1\%$ of the measured value ± 1 mm/s and a sampling rate of 25 Hz.

4.4.3 Model large wood and sediment

The model LW consisted of natural wooden logs with and without branches. The log lengths varied between $L_L = 0.08$ m, 0.10 m, 0.20 m, and 0.40 m and the log diameter $d_L = 0.015$ m, 0.03 m, and 0.004 m. Two different types of logs with branches were used for the experiments: The “2D” type corresponds to logs with alternate branches on two sides, whereas the “3D” type has alternate branches on four sides (Figure 4.2). The branches were 0.04...0.05 m long and 0.004 m thick. For the majority of the tests, the model LW was not watered and always fully floating. Hence, the transported logs did not interact with the channel bed. To investigate the effect of the log density on the accumulation probability, the logs were watered for durations of $t_W = 2 \dots 5$ months. The movable bed model tests were conducted with uniform material with a mean grain size diameter $d_m = 5.6$ mm.

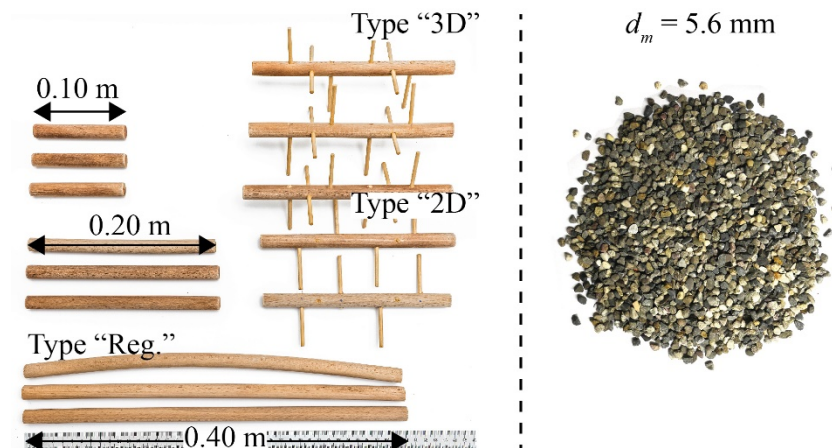


Figure 4.2 Model large wood with $d_L = 0.015$ m and model sediment

4.4.4 Test procedure and program

The LW accumulation probability p was examined within six test series (A-F, Table 4.2), comprising a total of 153 tests and 10'020 added logs. The test setup is illustrated in Figure 4.3. The basic experimental setting included a single circular bridge pier with a diameter $d_P = 0.05$ m placed 5 m downstream of the inlet in the channel centerline. The material of the bridge pier was aluminum (i.e. smooth bridge pier). The approach flow conditions were set by adapting Q and slope J_o . The approach flow Froude number F_o varied between 0.2, 0.5, 0.8, and 1.2 to model common flow conditions during floods ranging

from subcritical to slightly supercritical flow. For a selected range of approach flow conditions, the effect of different bridge pier shapes, number of piers, LW characteristics, LW transport types, and a movable bed on p was tested. For the movable bed experiments, an initial equilibrium scour was induced around the bridge pier for $F_o = 0.8$ and non-dimensional bed shear stress $\theta = 0.061$. The accumulation probability p was then tested for $F_o = 0.8, 0.5,$ and 0.2 .

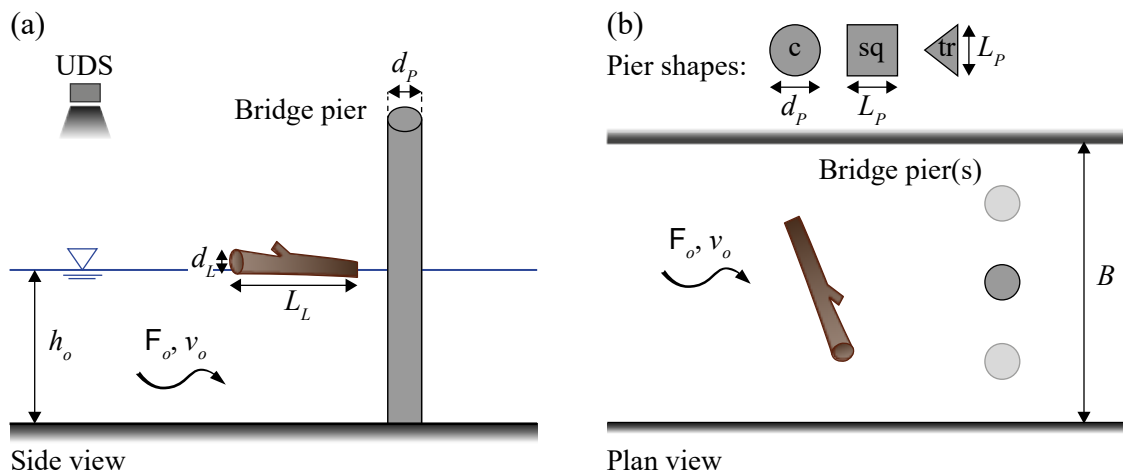


Figure 4.3 Experimental setup with notation of model tests on LW accumulation probability with (a) side and (b) plan view; c = circular, sq = square, tr = triangular bridge pier, d_P = bridge pier diameter, and L_P = bridge pier length

To model the worst-case scenario of p , the logs were added perpendicular to the flow (log position angle $\gamma = 90^\circ$) 1 m upstream of the bridge pier. Whether the log accumulated at the bridge pier was noted, and then the log was extracted from the flume. The following effects were investigated in test series A:

- Given the experimental randomness, the required number of repetitions to obtain statistically significant accumulation probabilities were studied in test A1 (Table 4.2).
- The reproducibility was evaluated by conducting four tests with identical approach flow conditions twice (A2-A9).
- The effect of $\gamma = 0^\circ, 45^\circ$ and 90° on p was investigated in tests A10-A18.

Test series B studied the effect of the approach flow conditions, L_L , and d_L on p . Various combinations of v_o and h_o were investigated for each value of $F_o = 0.2, 0.5, 0.8,$ and 1.2 :

- For $F_o = 0.2, 0.5,$ and 0.8 (B2-B36), L_L was varied to 0.10 m, 0.20 m, and 0.40 m.

- For $F_o = 0.08$ and slightly supercritical flow (B1, B37-B39), L_L was kept constant to 0.20 m.
- The effect of a wide range of h_o with a constant v_o was tested in B40-B43.
- The log diameter d_L was kept constant for B1-B43 with $d_L = 0.015$ m, and varied to $d_L = 0.004$ m and 0.03 m in B44-B55.

In test series C, the experiments were conducted for selected approach flow conditions. The bridge pier characteristics were studied in series C:

- The pier roughness was increased to model concrete material (i.e. rough bridge pier), with an equivalent sand roughness of $k_{s_Prototype} \approx 3$ mm (C1-C4).
- For tests C5-C37, the test setup was adapted to model two circular bridge piers with $d_P = 0.05$ m (C5-C16), a single triangular bridge pier with a length $L_P = 0.10$ m and square bridge pier with $L_P = 0.05$ m (C17-C28, Figure 4.3b), and single circular pier with $d_P = 0.01$ m and 0.025 m (C29-C37).

Different types of LW were investigated in test series D, including two types of logs with branches (D1-D7) and logs with higher density (D8-D11).

Test series E focused on the impact of wood transport on p :

- For the experiments with semi-congested LW transport, a bulk of 3 or 5 logs was added simultaneously to the flow 1 m upstream of the bridge pier (E1-E17).
- To model continuous LW transport, 40 logs were added consecutively to the flow (E18-E21).
- For congested LW transport, 40 logs were added simultaneously to the flow (E22-E25).

Test series F studied the effect of a movable bed and the respective scour around the bridge pier on p (F1-F6).

4.4.5 Test repetitions and reproducibility

To obtain statistically significant results for the LW accumulation probability p , the required number of test repetitions N is essential. In previous studies, N was defined in a wide range ($N = 3 \dots 50$, Table 3.1), without quantifying the standard deviation σ of p .

Furlan *et al.* (2018) recommended $N \geq 30$. For the current study, the required N_{req} was investigated in test run A1 (Table 4.2). A single log with $L_L = 0.20$ m was inserted into the flume $N = 300$ times for $F_o = 0.2$, $h_o = 0.15$ m, and $v_o = 0.24$ m/s. Figure 4.4a shows p and the corresponding σ as a function of N . The standard deviation σ increases to a maximum of $\sigma \approx 0.20$ for $N = 6$, and decreases to $\sigma = 0.05$ for $N = 300$. The accumulation probability p depends on the corresponding N and varied between 0% and 50%, converging to $p = 34\%$ for $N = 300$. To guarantee statistically significant results, a maximum standard deviation of $\sigma = 0.10$ was defined. This results in test repetitions of $N = 40$, which is feasible regarding test effort. Selected tests were repeated $N = 60$, if $\sigma \geq 0.10$ for $N = 40$. The experiments on continuous and congested LW transport (E18-E25) were repeated $N = 3$ times.

The test reproducibility was investigated with various L_L for four approach flow conditions (A2-A9). In Figure 4.4b, p is plotted as a function of N for tests A6-A7, and B27. All three tests converge to a final value $p \approx 25\%$ with $\sigma = 0.01$. Test reproducibility is consequently confirmed. Note that if N is selected to $N \leq 10$, a value used in previous studies, the accumulation probability would range between 0% and 67%.

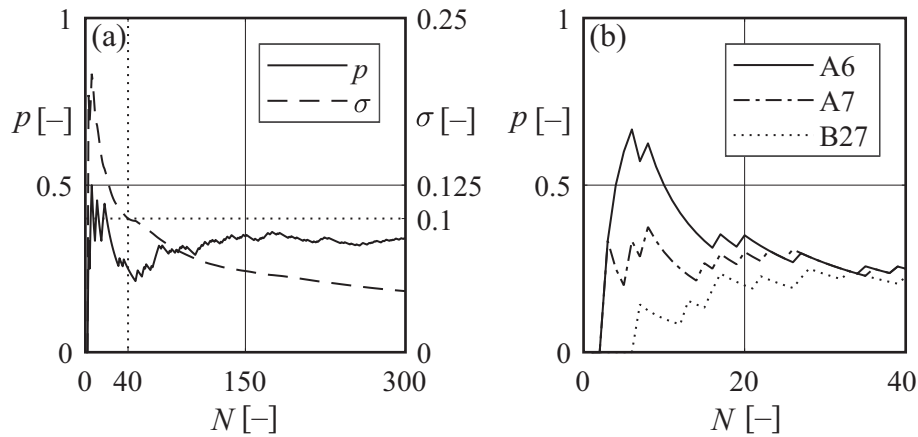


Figure 4.4 Test results of (a) p and σ versus N for test A1, (b) p versus N for reproducibility tests A6, A7, and B27

Table 4.2 Test program of test series A-F on LW accumulation probability; varied parameters are marked in bold. Parameter definition is shown in Figure 4.3.

Tests	Tested effect	F_o [-]	h_o [m]	v_o [m/s]	d_L [m]	L_L [m]	N [-]	LW	Pier					
A1	N_{req}	0.2	0.15	0.24	0.015	0.20	300							
A2-3	Repr.	0.2	0.05	0.14	0.015	0.10	40	1×Reg. $\gamma = 90^\circ$	1×c					
A4-5		0.5	0.05	0.35		0.20								
A6-7		0.8	0.05	0.56		0.40								
A8-9		0.2	0.20	0.28		0.20								
A10-12	γ	0.2	0.10	0.20	0.015	0.40	40	1×Reg. $\gamma = 0^\circ, 45^\circ, 90^\circ$						
A13-15		0.5	0.10	0.50										
A16-18		0.8	0.10	0.79										
B1	h_o, v_o, F_o, L_L	0.08	0.10	0.08	0.015	0.20	40	1×Reg. $\gamma = 90^\circ$	1×c					
B2-4			0.05	0.14	0.015	0.10-0.40	40							
B5-7		0.2	0.10	0.20	0.015	0.10-0.40								
B8-9		0.15	0.24	0.015	0.10+0.40									
B10-12		0.20	0.28	0.015	0.10-0.40									
B13-15		0.05	0.35	0.015	0.10-0.40	40								
B16-18		0.5	0.10				0.50							
B19-21		0.15	0.61											
B22-24		0.20	0.70	0.015	0.10-0.40	40								
B25-27		0.05	0.56											
B28-30	0.8	0.10	0.79											
B31-33	0.15	0.97												
B34-36	0.20	1.12	0.015	0.10-0.40	40									
B37		0.05				0.84								
B38	F_o	1.2				0.10	1.19	0.015	0.20	40				
B39						0.15	1.46		20 ^{a)}					
B40	h_o, v_o	0.2	0.52	0.45	0.015	0.20	40							
B41		0.3	0.23	0.45										
B42		0.5	0.08	0.45										
B43		0.7	0.04	0.45										
B44-45	d_L	0.2	0.10	0.20	0.015	0.20+0.40	40							
B46-47		0.5	0.10	0.50				0.004						
B48-49		0.5	0.15	0.61										
B50-51		0.2	0.10	0.20										
B52-53		0.5	0.10	0.50				0.03						
B54-55		0.5	0.15	0.61										
C1	Pier type		0.05	0.35	0.015	0.20	40	1×Reg. $\gamma = 90^\circ$	rough 1×c					
C2		0.5	0.10	0.50										
C3			0.15	0.61										
C4			0.20	0.70										
C5-7		0.2	0.10	0.20										
C8-10		0.5	0.10	0.50						0.015	0.40	40	1/3/5×Reg. $\gamma = 90^\circ$	2×c
C11-13		0.8	0.10	0.79										
C14-16		0.8	0.15	0.97										
C17-18	0.2	0.10	0.20	0.015	0.20+0.40	40	1×Reg. $\gamma = 90^\circ$	1×tr						
C19-20	0.5	0.10	0.50											
C21-22	0.8	0.10	0.79											

Tests	Tested effect	F_o [-]	h_o [m]	v_o [m/s]	d_L [m]	L_L [m]	N [-]	LW	Pier	
C23-24	Pier type	0.2	0.10	0.20	0.015	0.20+0.40	40	1×Reg. $\gamma = 90^\circ$	1×sq	
C25-26		0.5	0.10	0.50						
C27-28		0.8	0.10	0.79						
C29		0.5	0.10	0.05	0.35	0.015	0.08	40	1×Reg. $\gamma = 90^\circ$	1×c $d_P =$ 0.01 m
C30				0.50						
C31				0.15	0.61					
C32-33		0.5	0.10	0.05	0.35	0.015	0.10+0.20	40	1×Reg. $\gamma = 90^\circ$	1×c $d_P =$ 0.025 m
C34-35				0.50						
C36-37				0.15	0.61					
D1	0.05			0.35	0.015					
D2-3	LW type	0.5	0.10	0.50	0.015	0.20	60	1×2D, 1×3D $\gamma = 90^\circ$	1×c	
D4-5			0.15	0.61						
D6-7			0.20	0.70						
D8		0.5	0.05	0.35						
D9		0.5	0.10	0.50	0.015	0.20	40	1×Reg. $\gamma = 90^\circ$ $\rho_w \uparrow$		
D10		0.5	0.15	0.61						
D11		0.5	0.15	0.61						
E1-2		LW transport	0.5	0.05	0.35	0.015	0.20	40		3/5×Reg.
E3-5	0.10			0.50	3/5×Reg.					
E6-8	0.15			0.61	3×3D					
E9-11	0.20			0.70	$\gamma = 90^\circ$					
E12-13	0.5		0.10	0.20	0.015	0.40	40	3/5×Reg. $\gamma = 90^\circ$		
E14-15	0.5		0.10	0.50						
E16-17	0.8		0.10	0.79						
E18-19	0.2		0.10	0.20	0.015	0.20+0.40	3	40×Reg. Cont.		
E20-21									0.5	0.10
E22-23		0.2							0.10	0.20
E24-25		0.5							0.10	0.50
F1-2	Movable bed	0.2	0.10	0.20	0.015	0.20+0.40	40	1×Reg.	1×c	
F3-4		0.5	0.10	0.50						
F5-6		0.8	0.10	0.79						

Note:

- N_{req} = required repetitions,
 Reg. = regular smooth logs,
 Repr. = reproducibility tests,
 1×c = one circular bridge pier,
 2×c = two circular bridge piers,
 rough = rough bridge pier,
 tr = triangular bridge pier,
 sq = square bridge pier,
 Cont. = continuous addition of 40 logs with $N = 3$,
 Cong. = congested LW transport of 40 logs in $N = 3$ bulks, and
 a) test run stopped after $N = 20$, as $p = 0\%$.

4.5 Tests II: Large wood accumulation characteristics – Backwater rise and local scour

This part focuses on the characteristics of LW accumulations and in particular on their effect on backwater rise and local scour. The physical experiments were conducted in two different model flumes (small and large) at VAW and can be divided in three test series:

- **Series A** modeled a **predefined LW accumulation with a fixed bed** and studied the effect of the approach flow conditions and LW accumulation characteristics on **backwater rise Δh** in three different scales: small-scale with $\lambda = 50$ and $\lambda = 30$ (small flume) versus close-to-prototype with $\lambda = 6$ (large flume).
- **Series B** investigated a **natural LW accumulation with a fixed bed** and the effect of approach flow conditions and LW accumulation volume on **Δh** in two scales: small-scale with $\lambda = 30$ versus close-to-prototype with $\lambda = 6$.
- **Series C** studied a **natural LW accumulation with a movable bed** and the effect of approach flow conditions, LW accumulation volume, and bed material on **Δh** and **local scour S** in small-scale model tests with $\lambda = 30$.

The flume experiments were partially conducted in the context of Master and project theses at VAW by Brändli (2014), Bertram and Schärer (2015), Schaller (2015), and Lageder (2016).

4.5.1 Model flume II – small flume

The small-scale model tests were conducted in an 8.0 m long, 0.4 m wide, and 0.7 m deep channel (Figure 4.5). The intake is 0.66 m long and equipped with two flow straighteners to suppress secondary currents and surface waves. The bottom slope can be varied manually between $J_o = 0 \dots 10\%$. The downstream conditions were regulated with a sharp crested weir for the experiments with a fixed bed (series A and B) and with a needle weir for the experiments with a movable bed (series C).

For the predefined LW accumulation (series A), two rack rows were placed 3 m downstream of the intake. For the natural LW accumulation (series B and C, $\lambda = 30$), only one rack row was set 3.4 m downstream of the intake. For $\lambda = 30$, each rack row consisted of seven vertical aluminum bars with a circular cross-section of 0.008 m diameter and an axial spacing of 0.05 m. For $\lambda = 50$, each rack row consisted of eleven vertical aluminum bars with a circular cross-section of 0.005 m diameter, an axial spacing of 0.036 m, and

a distance between side wall and axis of the next bar of 0.020 m, respectively. The rack itself had a negligible effect on the approach flow conditions and did not induce backwater rise.

In series C, a 0.5 m long ramp of boulders with a diameter of 0.08 m to 0.11 m was installed at the upstream end of the flume to provide a smooth flow transition from the channel to the movable bed. The movable bed had a height $h_b = 0.35$ m, length $L_b = 5.5$ m, and was fixed at the downstream end using a 2 m long plate with a rough coating.

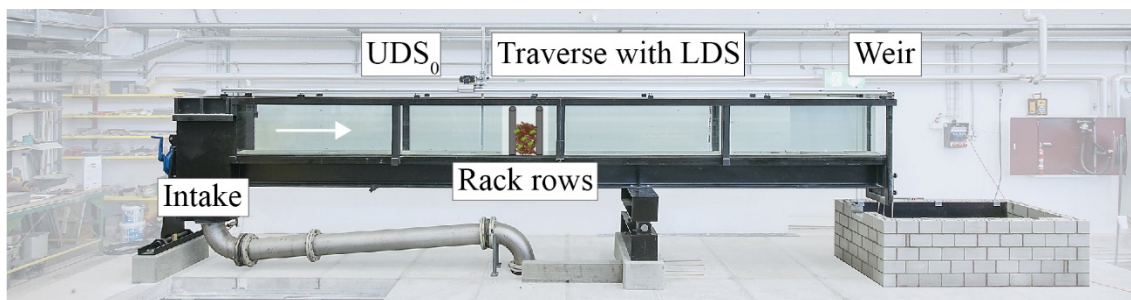


Figure 4.5 Photo of model flume II (small flume) at VAW with LDS = Laser Distance Sensor and UDS = Ultrasonic Distance Sensor

4.5.2 Model flume III – large flume

The close-to-prototype scale tests were conducted in a 30 m long, 1.50 m wide, and 1.20 m deep channel with a horizontal bottom (Figure 4.6). Two flow straighteners placed at the channel inlet suppressed secondary currents and surface waves. The downstream conditions were controlled with a flap gate to enable pseudo-uniform flow (Hager and Hutter 1984). To model a predefined LW accumulation (series A), two racks were placed 10 m downstream of the intake. For the natural LW accumulation (series B), the upstream rack row was removed. Each rack row consisted of five vertical aluminum bars with a circular cross-section of 0.04 m diameter, an axial spacing of 0.30 m, and a distance between side wall and axis of the next bar of 0.15 m, respectively. The rack itself did not induce backwater rise.

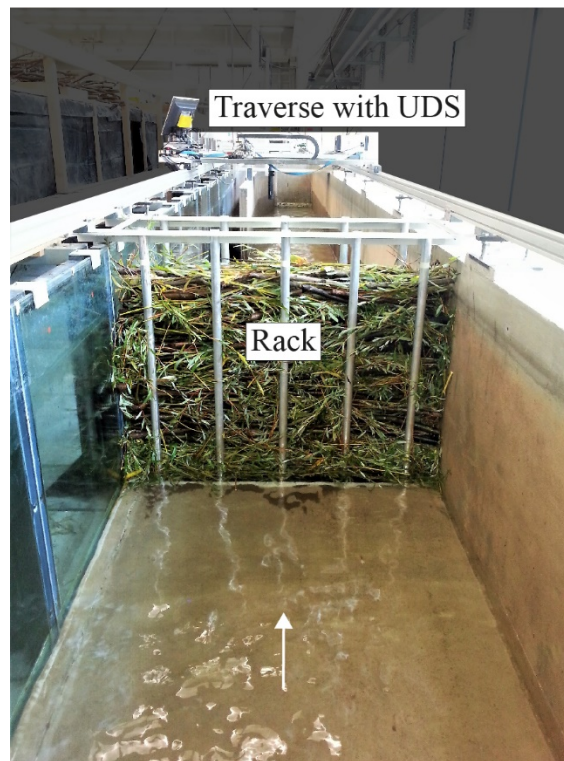


Figure 4.6 Photo of model flume III (large flume) at VAW

4.5.3 Instrumentation

The inflow discharge is measured with an IDM and regulated with a valve to a maximum of 70 l/s for the small flume and 1,200 l/s for the large flume. In both flumes, the flow depths (h_o and h = water depth with LW accumulation) were measured with UDS ('UNAM 30') and manually using a point gauge to obtain $\Delta h = h - h_o$.

In series C, the bed topography was scanned after each run in a $2.5 \times 2.5 \text{ cm}^2$ grid with an LDS ('ODAM 21') placed on a positioning system, which was manually moved in the x - (flow direction) and y -direction (spanwise direction). The origin of the x , y -coordinate system was located at the rack at the height h_b . In addition, the scour depth at the rack (subscript r) S_r was measured with a point gauge.

4.5.4 Model large wood and organic fine material

The model large wood consists of natural wooden logs without branches. For the small-scale model tests, the logs lengths varied between $L_L = 0.05 \dots 0.30 \text{ m}$ and the mean log diameter (subscript Lm) $d_{Lm} = 0.004 \dots 0.013 \text{ m}$ (Figure 4.7a). The model FM was represented by a plastic fir tree made of polyvinyl chloride (PVC). The density of the plastic fir tree $\rho_{FM,PVC}$ was measured with a powder pycnometer (GeoPyc 1360, Micrometrics

USA). Based on the average of 40 samples, $\rho_{FM,PVC}$ resulted in $1,330 \text{ kg/m}^3 (\pm 7.4 \text{ kg/m}^3)$. The plastic fir tree was selected to reduce the test effort compared to natural organic fine material. The effect of the material density can be neglected for series A, as the *FM* was manually placed and evenly distributed within the accumulation. For series B, the results will be compared to the close-to-prototype model tests, where natural material was used to model *FM*. The values of $FM = 2 \dots 8\%$ in the accumulation body were selected based on field observations by Manners *et al.* (2007). Branches and leaves in an accumulation body affect the d_{Lm} of the LW accumulation and increase the compactness (i.e., lower a). Due to the ease of measurement, d_{Lm} and a of an accumulation body were quantified prior to the addition of *FM*. Hence, the effect of *FM* was included as a separate parameter.

For the close-to-prototype model tests, L_L varied between 0.45 m to 0.90 m and $d_{Lm} = 0.035 \dots 0.065$ m. Natural willow and fir branches were used as model *FM* (Figure 4.7b). The amount of *FM* used was again selected based on natural observations by Manners *et al.* (2007), but included a wider range of $FM = 2.5 \dots 17\%$ compared to the small-scale model tests. The density of the willow (subscript w) and fir (subscript f) branches was measured with a powder pycnometer (GeoPyc 1360, Micrometrics USA) based on each 40 samples to $\rho_{FM,w} = 610 \text{ kg/m}^3 (\pm 6.2 \text{ kg/m}^3)$ and $\rho_{FM,f} = 600 \text{ kg/m}^3 (\pm 8.6 \text{ kg/m}^3)$, respectively.

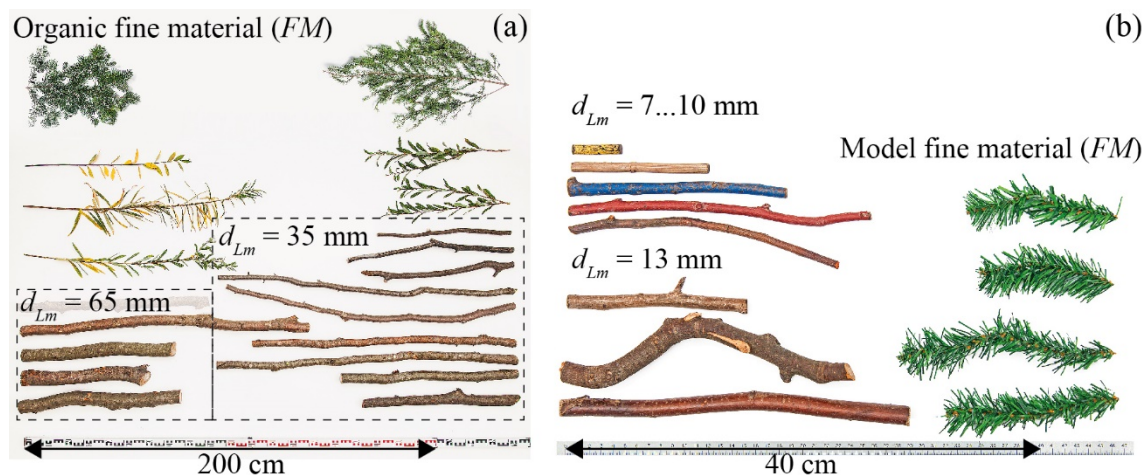


Figure 4.7 Examples of model LW (d_{Lm}) and *FM* for (a) $\lambda = 6$ and (b) $\lambda = 30$

4.5.5 Sediment

In teste series C, three different uniform grain sizes were tested in order to avoid effects due to armoring (Wallerstein *et al.* 2001, Figure 4.8). The mean grain size diameters varied from $d_m = 2.7 \text{ mm}$, 5.4 mm to 13.1 mm and were verified with a sieving analysis. The

different d_m were defined to cover both subcritical and slightly supercritical flow conditions, resulting in a range of $F_o \approx 0.5 \dots 1.5$.



Figure 4.8 Uniform bed material with standard deviation of grain size distribution $\sigma_g \approx 1.1$

4.5.6 Test procedure and program

The test setup and notation for series A, B, and C are illustrated in Figure 4.9. The test procedure and program for the different test series are described consecutively below.

Series A – predefined LW accumulation with a fixed bed

A given solid LW volume V_s ($\approx 0.0015 \text{ m}^3$ for $\lambda = 50$, $\approx 0.005 \text{ m}^3$ for $\lambda = 30$, and $\approx 0.240 \text{ m}^3$ for $\lambda = 6$) was placed between two racks, thereby representing a box-shaped accumulation. The LW accumulation has a length L_A and a constant height h_A . During all experiments, an overtopping of the accumulation was prevented. The LW accumulation consisted of logs with a mean diameter d_{Lm} and length L_L and had a compactness described by the bulk factor $a = V_l/V_s$. The bulk factor a was varied to obtain loose ($a = 4.0 \dots 5.0$), medium ($a = 3.0 \dots 4.0$), and dense ($a = 2.0 \dots 3.0$) accumulation bodies. The value range was chosen based on natural observations after floods with extensive LW transport, resulting in $a = 2 \dots 5$ (Lange and Bezzola 2006, Waldner *et al.* 2009). For selected experiments, *FM* was added to the LW accumulation as a percentage of V_s , varying from 2...17%. Different types of *FM* were used to model branches and leaves. As the densities of the different *FM* types vary for the three tested scales, the volume percentage slightly differs ($\pm 0.5\%$). The log length L_L was not systematically investigated, as it mainly affects the accumulation compactness. This was, however, accounted for with the bulk factor a .

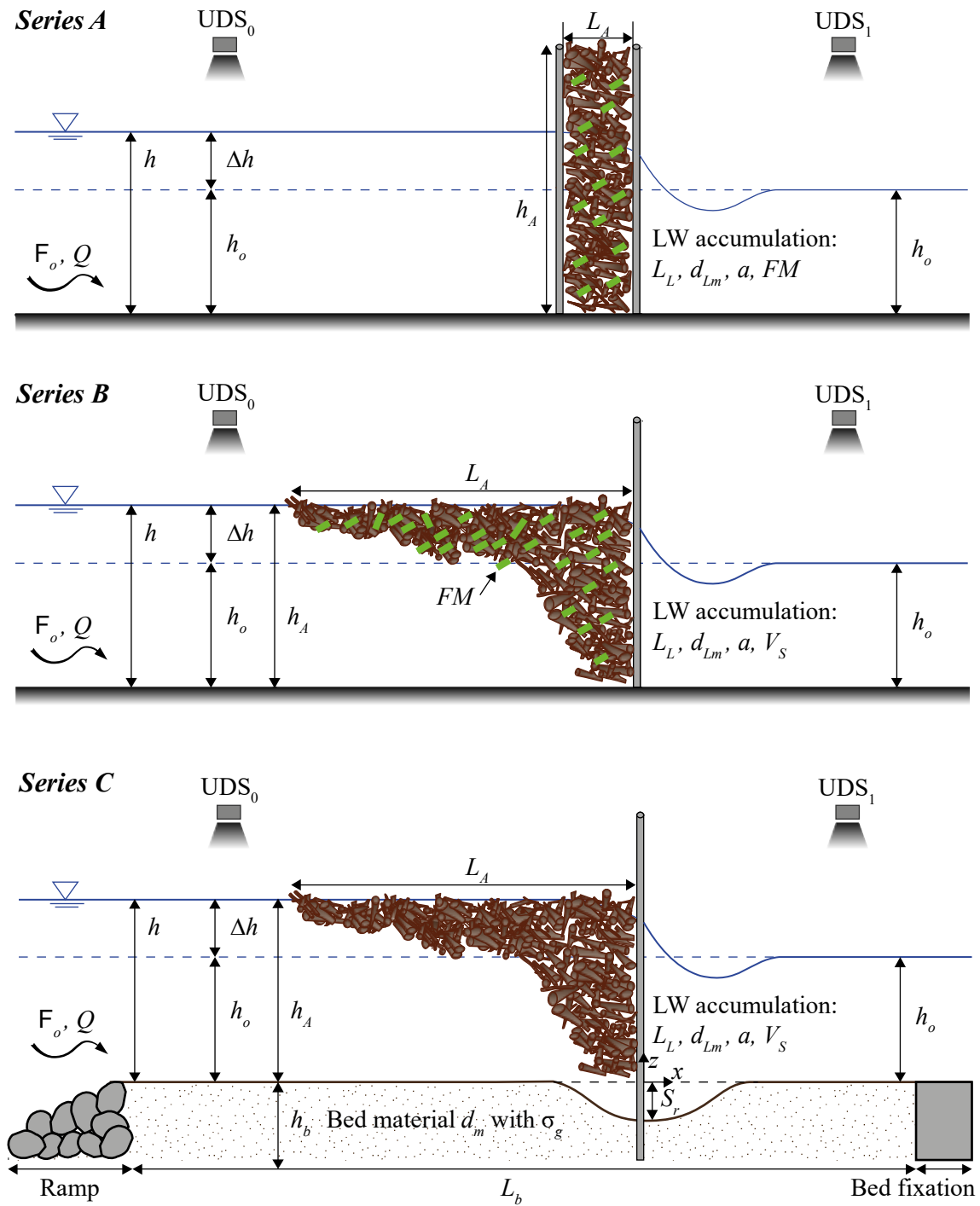


Figure 4.9 Test setup and notation for series A, B, and C. F_o , h_o , and Q were measured without LW accumulation and flow depth h was measured using UDS₀ and UDS₁. Resulting backwater rise is $\Delta h = h - h_o$. LW accumulation characteristics comprise L_A , h_A , L_L , d_{Lm} , a , FM , and V_S . Bed material characteristics are h_b , L_b , d_m , σ_g , and S_r .

The experimental procedure for series A can be described by the following steps:

- (1) measurement of approach flow depth h_o for a certain approach flow condition without LW accumulation,
- (2) addition of a specific LW accumulation between two racks with the respective L_A , d_{Lm} , a , LW volume, and FM , and
- (3) measurement of h upstream of the LW accumulation for the respective approach flow condition.

The test program for series A is listed in Table 4.3 and comprises a total of 586 test runs with three different scale factors λ . For $\lambda = 30$ (A1-A66; small flume):

- Each test (e.g. A1) consisted of three to nine test runs where F_o was continuously increased.
- The reproducibility was evaluated by conducting several tests up to three times (A1-A15).
- The effect of the approach flow characteristics h_o and F_o on Δh was analyzed with all other parameters kept constant (A16-A21).
- The LW accumulation characteristics were tested by the individual variation of a (A7-A15; A22-A29), L_A (A30-A38), d_{Lm} (A39-A43), and percentage of FM (A44-A66).
- Selected experiments were conducted for a constant F_o with increasing h_o to allow a comparison with $\lambda = 6$ (e.g. A47-A50 and A63-A66).

For $\lambda = 6$ (A67-A94; large flume):

- h_o was continuously increased from 180 mm to 440 mm for each test, as F_o could not be specifically adjusted due to the horizontal flume bottom.
- Two different tests were conducted several times (A67-A74) to verify the test repeatability.
- a was varied between 2.8 and 4.3 for two different d_{Lm} (A75-A90) to study the LW accumulation characteristics.
- The effect of FM on Δh was analyzed by varying the percentage (A75-A90) and type (A83-A86 compared to A91-A94), with all other parameters kept constant.

For $\lambda = 50$ (A95-A106; small flume), experiments with selected approach flow conditions and LW accumulation characteristics (a , L_A , d_{Lm} , and FM) were conducted to investigate

a scale series. For each test, either F_o or h_o was continuously increased to allow a comparison with both $\lambda = 30$ and $\lambda = 6$. In particular, tests A95-A106 ($\lambda = 50$) are compared with A47-A49, A63-A65 ($\lambda = 30$) and A67, A75-A76, A83-A84 ($\lambda = 6$).

Series B – natural LW accumulation with a fixed bed

For the majority of the tests, the same solid LW volume V_s as in Series A ($\approx 0.005 \text{ m}^3$ for $\lambda = 30$, and $\approx 0.240 \text{ m}^3$ for $\lambda = 6$) was now added stepwise to the flow, thereby representing a flood with a natural accumulation. The LW accumulation can be described by the length L_A and height h_A , and consisted of logs with d_{Lm} and L_L . For selected experiments, FM was added to the LW as a percentage of V_s , varying from 8...10%. The FM was modeled with both natural fir branches and a plastic fir tree made of polyvinyl chloride. The experimental procedure for series B can be described by the following steps:

- (1) measurement of h_o for a certain approach flow condition without LW accumulation,
- (2) stepwise addition of packages of 5...10% of V_s with the respective d_{Lm} , L_L , and FM ,
- (3) measurement of h upstream of the LW accumulation for the respective approach flow condition, and
- (4) determination of V_l based on side view photographs of the accumulation and determination of bulk factor $a = V_l/V_s$ after each added package of V_s .

The test program for series B is listed in Table 4.4, comprising 100 single test runs:

- The reproducibility was evaluated by conducting the same test three times (B1-B3).
- Two different model scales were analyzed with identical test setups (B1 vs. B7).
- The effect of F_o and Q on Δh was studied with all other parameters kept constant (B3+B4, B7-B9).
- The LW accumulation characteristics were tested by the individual variation of FM (B5+B6, B10).

Table 4.3 Test program for test series A on LW accumulation characteristics; varied parameters are marked in bold.

Tests	Tested effect	λ [-]	h_o [m]	F_o [-]	Q [l/s]	a [-]	L_A [m]	d_{Lm} [mm]	FM [%]				
A1-3	Repr.	30	0.05-0.10	0.2-1.2	8-48	3.6	0.10	3.7	0				
A4-6				0.2-1.4	8-56	3.8		10.3	0				
A7-8	Repr., a	30	0.05-0.10	0.2-0.8	8-32	2.5	0.10	7	0				
A9-10				0.2-1.2	8-48	3.1			0				
A11-12				0.2-1.4	8-56	4.3			0				
A13-15				0.2-0.8	8-32	3.3			0				
A16-18	h_o, F_o	30	0.05, 0.10, 0.15	0.2-1.4	8-56	3.6	0.10	3.7	0				
A19-21						3.8		10.3	0				
A22-24	a	30	0.10	0.2-1.4	8-56	2.4, 3.2, 3.6	0.10	11	0				
A25			0.05	0.2-1.4	8-56	3.3		15	0				
A26-27			0.10	0.2-1.2	8-48	3.3, 4.4		15	0				
A28-29			0.05, 0.10	0.2-1.4	8-56	3.4		2.3	0				
A30-32	L_A	30	0.05, 0.10	0.2-1.4	8-56	4.0	0.10	2.3	0				
A33-35						3.8		0.20	10.3	0			
A36-37						0.05-0.10		0.2-0.6	8-24	3.4	0.20	7	0, 2.5
A38													0.2-1.4
A39-41	d_{Lm}	30	0.10	0.2-1.4	8-56	3.6	0.10	2.3, 8.5, 14	0				
A42-43								3.8	3.7, 6	0			
A44-46	FM^a	30	0.05-0.10	0.2-0.8	8-32	2.5	0.10	7	0, 2.5, 4.5				
A47-50				0.2-1.2	8-48	3.3		7	0, 2.5, 5, 7				
A51-54				0.2-1.4	8-56	4.3		7	0, 2.5, 5, 7				
A55-58				0.2-0.8	8-32	2.8		13	0, 2, 5, 7				
A59-62				0.2-1.4	8-56	3.8		13	0, 2.5, 5, 8				
A63-66				0.2-1.4	8-56	4.2		13	0, 2.5, 5, 7.5				
A67-72				Repr.	6	0.18-0.44		0.2-0.3	85-371	3.1	0.5	35	0
A73-74												10	
A75-78	FM^b	6	0.18-0.44	0.2-0.3	85-371	4.2	0.5	35	2.5, 5, 10, 15				
A79-82								35	0, 5, 10, 15				
A83-86								65	0, 5.5, 11, 16.5				
A87-90								65	0, 5.5, 11, 16.5				
A91-94	FM^c	6	0.18-0.44	0.2-0.3	85-371	4.2	0.5	65	0, 5.5, 11, 17				

Tests	Tested effect	λ [-]	h_o [m]	F_o [-]	Q [l/s]	a [-]	L_A [m]	d_{Lm} [mm]	FM [%]
A95-97			0.06	0.2-1.4	3.6-25.7	4.3		0.08	0, 2.5, 5
A98-100	λ	50	0.03-0.06	0.2	1.3-3.6	4.3	0.06	0.08	0, 2.5, 5
A101-103			0.06	0.2-0.6	3.6-25.7	3.2		0.04	0, 2.5, 5
A104-106			0.03-0.06	0.2	1.3-3.6	3.2		0.04	0, 2.5, 5
<u>Note:</u>			Repr. =	Reproducibility tests, a) plastic fir tree, b) natural willow branches, and c) natural fir branches.					

Table 4.4 Test program for test series B on LW accumulation characteristics; varied parameters are marked in bold.

Tests	Tested effect	λ [-]	Q [l/s]	h_o [m]	F_o [-]	d_{Lm} [m]	V_s [m ³]	FM [%]
B1-B3	Repr. , λ		370.8	0.44				0
B4	Q	6	908.0	0.75	0.2-0.3	0.035	0-0.24	0
B5	FM		370.8	0.44				16^{a)}
B6	FM		620.0	0.60				10^{a)}
B7	F_o, λ		11.90		0.31			0
B8	F_o	30	23.78	0.10	0.62	0.007	0-0.0056	0
B9	F_o		55.65		1.46			0
B10	FM		23.78		0.63			8^{b)}
<u>Note:</u>	a)	Natural fir branches, and b) plastic fir tree						

Series C – natural LW accumulation with a movable bed

As in Series B, a given solid LW volume V_s ($\approx 0.023 \text{ m}^3$ for $\lambda = 30$) was added stepwise to the flow to model a natural accumulation. However, the LW volume was increased by a factor of ≈ 5 to study the effect of V_s in more detail. To investigate local scour solely due to LW accumulations, the initial flow condition (subscript IC) was chosen to represent weak transport. The bed shear stress θ_{IC} was slightly below the critical bed shear stress θ_{cr} for incipient motion ($\theta_{cr} = 0.047$ from Meyer-Peter and Müller 1948). The required value for bed shear stress was visually examined. For a given d_m and Q , the slope J_o was continuously increased until weak transport occurred. The respective θ_{IC} was determined to $\theta_{IC} = 0.04$ for $d_m = 2.7$ and 5.4 mm, and $\theta_{IC} = 0.05$ for $d_m = 13.1$ mm. The experimental procedure for series C can be described by the following steps:

- (1) measurement of h_o for a certain approach flow condition without LW accumulation,
- (2) stepwise addition of packages of 5...10% of V_s with the respective d_{Lm} and L_L

- (3) after an equilibrium scour was reached, measurement of h upstream of the LW accumulation for the respective approach flow condition,
- (4) measurement of the scour depth at the rack S_r ,
- (5) determination of accumulation compactness, i.e. bulk factor a , for each package of V_s as in Series B, and
- (6) after the addition of 100% of V_s , the bed topography was scanned in a $2.5 \times 2.5 \text{ cm}^2$ grid to obtain the scour depth S .

The test program for series C is listed in Table 4.5, comprising 200 single test runs:

- The reproducibility was evaluated by conducting the same test three times (C1-C3).
- The effect of the bed material on S and Δh was analyzed by varying d_m (C1-C12) for different approach flow conditions.

Table 4.5 Test program for test series C with $\lambda = 30$ and $d_{Lm} = 0.10 \text{ m}$ on LW accumulation characteristics; varied parameters are marked in bold.

Tests	Tested effect	Q [l/s]	J_o [%]	h_o [m]	F_o [-]	V_s [m ³]	d_m [mm]	θ_{IC} [-]
C1-C3	Repr. , d_m	20	0.70	0.08	0.74	0-0.023	5.4	0.04
C4-C5		30	0.53	0.11	0.68	0-0.023	5.4	0.04
C6-C7		40	0.45	0.13	0.65	0-0.023	5.4	0.04
C8	d_m	20	0.29	0.09	0.57	0-0.023	2.7	0.04
C9		30	0.23	0.13	0.51	0-0.023	2.7	0.04
C10		40	0.20	0.17	0.47	0-0.023	2.7	0.04
C11		20	3.00	0.05	1.53	0-0.023	13.1	0.05
C12		30	2.30	0.07	1.24	0-0.023	13.1	0.05

4.5.7 Test reproducibility

The reproducibility was evaluated for all three test series A-C by conducting a test with the same approach flow conditions several times. Tests A1-A15, A67-A74, B1-B3, C1-C3 confirmed the reproducibility of the relative backwater rise $\Delta h/h_o$ and backwater rise Δh for model scales $\lambda = 30$ and $\lambda = 6$, respectively. Due to the identical test setup for the tests with $\lambda = 50$, it is concluded that the reproducibility is likewise given. Tests C4-C5 approved the reproducibility of the scour depth at the rack S_r . In Figure 4.10a, $\Delta h/h_o$ is plotted as a function of F_o with all other parameters kept constant for tests A13-A15. In Figure 4.10b, Δh is depicted as a function of h_o with all other parameters kept constant

for tests A70-A72 (0% *FM*), and A73-74, A77 (10% *FM*). In Figure 4.10c and Figure 4.10d, $\Delta h/h_o$ is plotted as a function of V_s with all other parameters kept constant for tests B1-B3 and C1-C3. In Figure 4.10e, S_r is plotted as a function of V_s with all other parameters kept constant for tests C4-C5.

The test reproducibility was evaluated using the relative standard error e^* (Eq. (4.5), Section 4.3), and the results are summarized in Table 4.6.

Table 4.6 Evaluation of test reproducibility with relative standard error e^* for Test series A-C

Test series	λ	Parameter	Relative standard error e^*	Average relative standard error $\overline{e^*}$
A	30	Δh	0.3...15.0%	5.0%
	6	Δh	0.7...6.0%	3.4%
B	6	$\Delta h/h_o$	5.1...12.6%	9.0%
C	30	$\Delta h/h_o$	0.5...5.0%	2.5%
	30	S_r	1.6...16.7%	6.1%

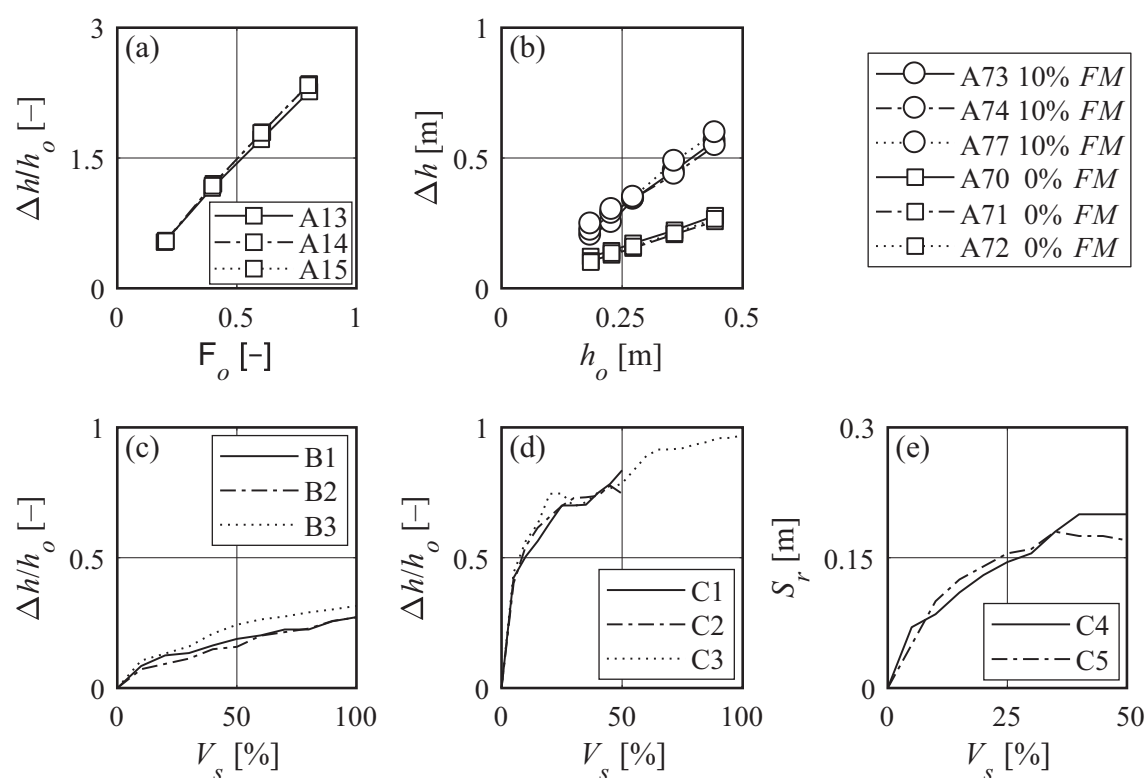


Figure 4.10 Reproducibility of (a) $\Delta h/h_o$ versus F_o for $\lambda = 30$ (A13-A15), (b) Δh versus h_o for $\lambda = 6$ (A70-A72: 0% *FM*, and A73-74, A77: 10% *FM*), (c) $\Delta h/h_o$ versus V_s in % for $\lambda = 6$ (B1-B3), (d) $\Delta h/h_o$ versus V_s in % for $\lambda = 30$ (C1-C3), (e) S_r versus V_s for $\lambda = 30$ (C4-C5)

4.6 Tests III: Measures for large wood accumulation risk reduction

The objective of this part is to examine and evaluate existing and new measures at bridge piers regarding their accumulation risk reduction. The physical experiments were conducted in model flume I (tilting flume, Section 4.4.1 and Figure 4.1). The instrumentation and model LW are described in Section 4.4.2 and 4.4.3.

4.6.1 Test procedure and program

The accumulation risk reduction was examined for two types of measures: A = LW fin mounted upstream of the bridge pier and B = bottom sill mounted on the channel bottom. The test setup is illustrated in Figure 4.11. The experiments were conducted for a selected range of approach flow conditions and LW characteristics with a model scale factor of $\lambda \approx 20$. Similar to the experiments on LW accumulation probability (Section 4.4.4), a single circular bridge pier with a diameter $d_P = 0.05$ m was placed 5 m downstream of the inlet in the channel centerline. The logs were added perpendicular to the flow ($\gamma = 90^\circ$) 1 m upstream of the bridge pier with 40 repetitions. The resulting accumulation probability p was then compared to that of the pier without measures.

The two measures comprise nine different variations (A.1-A.6, B.1-B.3, Table 4.7). Measure A is made of polyvinyl chloride (PVC). The experiments were conducted with two different vertical fin angles $\delta_1 = 45^\circ$ and 20° . The horizontal fin angle, i.e. fin position to the flow, was varied between $\delta_2 = 90^\circ$ (in flow direction) and $\delta_2 = 30^\circ$. For selected experiments, a Λ -shaped aluminum top was placed on the fin (Figure 4.11a).

Table 4.7 Definition of tested measures

Measure	Description	δ_1 [°]	δ_2 [°]	Λ -shaped top [yes/no]	Δx [m]
A.1	LW fin	45	90	no	–
A.2		45	30	no	
A.3		45	30	yes	
A.4		45	30	yes	
A.5		20	90	yes	
A.6		20	90	no	
B.1	2 declined cross sills			–	0.15
B.2	1 declined sill				0.15
B.3	2 declined serial sills			–	0.15
					0.30

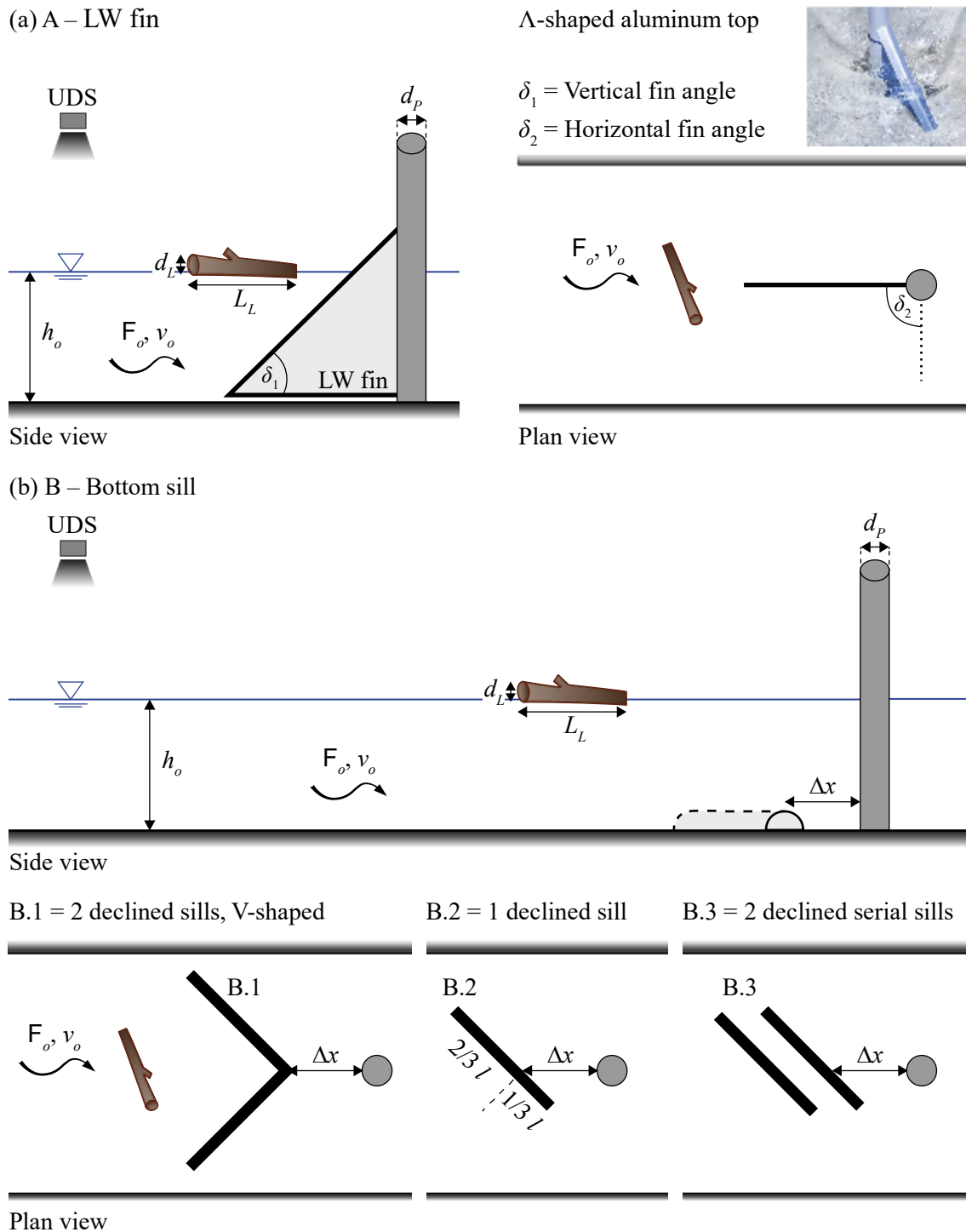


Figure 4.11 Experimental setup with notation of model tests on risk reduction measures with side and plan view of (a) measure A – LW fin versus (b) measure B – bottom sill

The bottom sills are made of PVC, half-cylinder shaped, 0.50 m long and 0.015 m high. For measure B.1, two sills were placed as a V-shape pointing in flow direction (i.e. declined) on the channel bottom. Measure B.2 consists of one declined sill, whereas this setup was further adapted for measure B.3 consisting of two consecutive declined sills. For B.3, the distance to the bridge pier Δx was varied between $\Delta x = 0$ m, 0.15 m, 0.30 m.

The test program is listed in Table 4.8, comprising 34 tests and 1'840 added logs:

- The efficiency of measure A.1 was examined for various F_o , two L_L , and single versus semi-congested LW transport (M1-M12).
- The experiments with measures A.2-A.6 were conducted for selected F_o , L_L , and single LW transport (M13-M19).
- For the measures B.1-B.3, the tests were performed for three different h_o with $F_o = 0.50$, $L_L = 0.40$ m, and single LW transport (M20-M34).
- The model tests with B.3 (M26-M34) further include the variation of $\Delta x = 0$ m, 0.15 m, and 0.30 m, whereas $\Delta x = 0.15$ m for tests M20-M25.

Table 4.8 Test program for measure A.1-A.6 and B.1-B.3 on LW accumulation risk reduction; varied parameters are marked in bold.

Tests	Measure	F_o [-]	h_o [m]	v_o [m/s]	d_L [m]	L_L [m]	N [-]	LW
M1-2	A.1	0.20		0.20				1×Reg. $\gamma = 90^\circ$
M3-4		0.50	0.10	0.50	0.015	0.20+0.40	40	
M5-6		0.80		0.79				
M7-8		0.20		0.20				
M9-10		0.50	0.10	0.50	0.015	0.20+0.40	40	
M11-12		0.80		0.79				
M13	A.2	0.20	0.10	0.20	0.015	0.20	40	1×Reg. $\gamma = 90^\circ$
M14		0.50		0.50		0.40		
M15	A.3	0.20	0.10	0.20	0.015	0.20	40	
M16	A.4	0.20	0.10	0.20	0.015	0.40	40	
M17		0.50	0.10	0.50				
M18	A.5	0.50	0.10	0.50	0.015	0.40	40	
M19	A.6	0.50	0.10	0.50	0.015	0.40	40	
M20	B.1 $\Delta x = 0.15$ m	0.71	0.05					
M21		0.50	0.10	0.50	0.015	0.40	40	
M22		0.36	0.20					
M23	B.2 $\Delta x = 0.15$ m	0.71	0.05					
M24		0.50	0.10	0.50	0.015	0.40	40	
M25		0.36	0.20					
M26	B.3 $\Delta x = 0$ m	0.71	0.05					
M27		0.50	0.10	0.50	0.015	0.40	40	
M28		0.36	0.20					
M29	B.3 $\Delta x = 0.15$ m	0.71	0.05					
M30		0.50	0.10	0.50	0.015	0.40	40	
M31		0.36	0.20					
M32	B.3 $\Delta x = 0.30$ m	0.71	0.05					
M33		0.50	0.10	0.50	0.015	0.40	40	
M34		0.36	0.20					

4.7 Numerical modeling of large wood accumulation

This part focuses on the evaluation of the 2D numerical simulation model ‘IberWood’ from a practical point of view. Selected experimental results on LW accumulation probability at bridge piers and backwater rise due to LW accumulation were compared with the results of the numerical model.

4.7.1 Model setup and test program

The 2D numerical model to simulate wood transport and deposition ‘IberWood’ is described in Section 3.6. The code is embedded in the pre- and post-processing software GiD (GiD 2012). The simulation steps can be summarized as follows:

1. **Create or import a geometry:** The geometry was created by inserting the x -, y -, z -coordinates of model flume I (tilting flume) and II (small flume). A bridge pier or retention rack was modeled by cutting out a hole to the geometry with the respective dimensions.
2. **Set the problem data:** The maximum simulation time was set to 360 s with a time interval of the results of 1 s. According to pre-tests, ≈ 100 -150 s simulation time are required to establish the approach flow conditions and to start with the modeling of LW transport. A 2nd order numerical scheme was defined and the Courant-Friedrichs-Lewy (CFL) number, the ratio between the flow velocity v and the discrete length interval Δx and time step Δt of the numerical model, was set to the default value of $CFL = v \Delta t / \Delta x < 0.45$. The Wet-Dry limit was defined as 0.001 m. The wall friction was considered with the Manning coefficient $1/k_{St}$ and set to $1/k_{St} = 0.01 \text{ s/m}^{1/3}$. The used turbulence model is k - ϵ . The simulation of wood transport was enabled with a drag coefficient $C_d = 1.4$, a common value for wood logs (Bocchiola *et al.* 2006a). The bed friction coefficient μ_{bed} (Figure 2.4) influences the incipient motion of logs. The default value of 0.47 was used, as all logs are fully floating during the simulation and the friction coefficient does not affect the results. The wall bouncing angle $= 0.78 \text{ rad} = 45^\circ$ is a threshold value, defining whether a log touching a wall or boundary is sliding (incidence angle $<$ wall bouncing angle) or bouncing off (incidence angle $>$ wall bouncing angle). The default value is based on flume experiments conducted by Ruiz-Villanueva *et al.* (2014c). The restitution coefficient describes the interactions between logs and the default value is 1, equivalent to the elastic collision of rigid bodies. The method to model LW transport is defined as kinematic, so logs

are transported with the flow velocity. For the wood initial conditions, the following parameters are entered: log number, -diameter, -length, -density, x - and y -position, $\gamma = \log$ position angle relative to the flow [rad], entering time [s], and root coefficient. For the model tests on LW accumulation probability, log density was set to $\rho_L = 480 \text{ kg/m}^3$ and for the tests on backwater rise to $\rho_L = 600 \text{ kg/m}^3$. Both values are based on density measurement of the model LW used in the physical experiments.

- 3. Define input parameters, initial and boundary conditions:** The input parameters, initial and boundary conditions are listed in Table 4.9. The roughness of the channel bottom, bridge pier, and poles were based on the physical model setup. The initial condition for the turbulence model was set to zero. The hydraulic initial and boundary conditions were defined according to the physical experiments. Two wood gauges were defined to count the passing logs up- and downstream of the pier or rack.

Table 4.9 Input parameters, initial and boundary conditions for the numerical simulation of LW accumulation probability and backwater rise

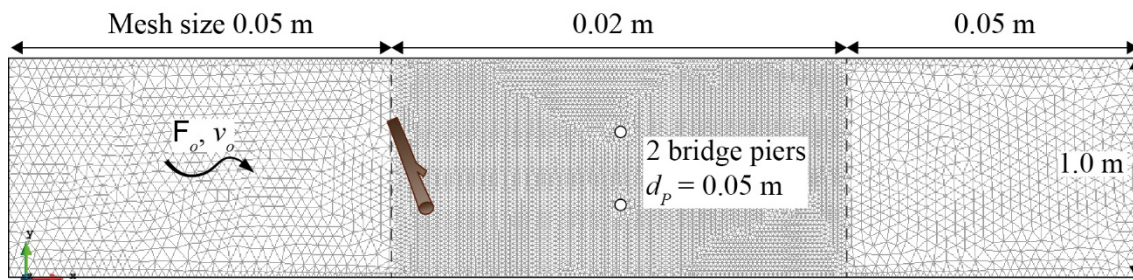
Parameter	Accumulation probability p	Backwater rise Δh
Roughness $1/k_{sr}$ [$\text{s/m}^{1/3}$]	Channel bottom = 0.017 Pier = 0.011	Channel bottom = 0.017 Rack poles = 0.011
Turbulence k- ϵ Initial conditions	Type: Uniform flow; initial conditions defined as 0 $h_o = 0.10 \text{ m}$	
Boundary conditions	Inlet: $Q_o = 0.0197 \text{ m}^3/\text{s}$ critical / subcritical Outlet: $h_o = 0.10 \text{ m}$ subcritical	Inlet: $Q_o = 0.0118 \text{ m}^3/\text{s}$ critical / subcritical Outlet: $h_o = 0.10 \text{ m}$ subcritical
Wood boundary condition	–	
Wood gauge	Up- and downstream of pier	Up- and downstream of rack

- 4. Build a numerical mesh and start the computation:** The flume geometry was divided in three parts (Figure 4.12). An unstructured mesh with a size of 0.05 m was assigned to the areas up- and downstream of the pier or rack. For the area near the pier, the mesh size was set to 0.02 m, whereas a value of 0.008 m was defined for the simulation of the retention rack.

The test program is summarized in Table 4.10. LW accumulation probability was studied for a setup with a single circular pier (N1-N2) versus two circular piers (N3). The pier diameter d_P amounts to 0.05 m. For all test setups, approach flow conditions were set to $F_o = 0.20$, $v_o = 0.20 \text{ m/s}$, and $h_o = 0.10 \text{ m}$. Log diameter was kept constant with $d_L = 0.015 \text{ m}$ and log length varied to test $L_L = 0.20 \text{ m}$ and 0.40 m . The test procedure is

comparable to the continuous addition of LW, described in Section 4.4.4. For one simulation, 40 logs were added perpendicular to the flow every 5 seconds, and 1 m or 0.20 m upstream of the bridge pier. For N1-N2, the simulation was repeated $N = 3$ times to determine accumulation probability and to compare it with the physical model test results. For N3, a single run with 40 added logs was used for the comparison. The corresponding physical model tests are E18-E19 for N1-N2, and C5 for N3 (Table 4.2 versus Table 4.10). The effect of a LW accumulation on backwater rise was numerically investigated for a selected set of approach flow conditions (N4). For N4, LW accumulation with $V_s = 0.0056 \text{ m}^3$ and $\rho_L = 600 \text{ kg/m}^3$ (Test B7, Table 4.4) was modeled using ≈ 990 logs with identical dimensions. The logs were added homogeneously across the transverse cross-section at the channel inlet with varying log position angles to simulate a full blockage of the rack.

(a) Model setup with 2 bridge piers (Tilting flume)



(b) Model setup with retention rack (Small flume)

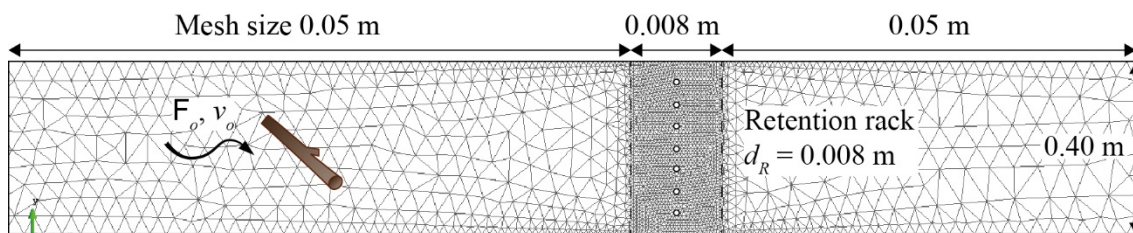


Figure 4.12 Numerical mesh for simulation of (a) tilting flume (model flume I) with two circular bridge piers and (b) small flume (model flume II) with a retention rack (drawn not to scale)

Table 4.10 Test program of numerical simulation

Tests	Tested effect	F_o [-]	h_o [m]	v_o [m/s]	d_L [m]	L_L [m]	LW	Pier/Rack	N [-]
N1	p	0.20	0.10	0.20	0.015	0.20-	40×reg. $\gamma = 90^\circ$	1×c, $d_P = 0.05 \text{ m}$	3
N2						0.40			
N3						0.40			
N4	Δh	0.30	0.10	0.30	0.007	0.15	990×reg. $\gamma = 0-90^\circ$	7 rack poles, $d_R = 0.008 \text{ m}$	1

5 Results and discussion

5.1 Overview

The LW accumulation process at river infrastructures and its impact were investigated in physical scale models to obtain information required for flood hazard assessment. The current section presents the experimental results, data analysis, and discussion, subdivided in four parts: LW accumulation probability (Section 5.2), LW accumulation characteristics with particular focus on backwater rise and local scour (Section 5.3), measures for LW accumulation risk reduction (Section 5.4), and numerical modeling of LW accumulation (Section 5.5). The results of the physical model tests contain a general process description, followed by the analysis of the governing parameters and a generalization.

5.2 Large wood accumulation probability

Parts of this subsection have been published in Schalko I. (2017): “Large wood accumulation probability at a single bridge pier”, in the proceedings of the 37th IAHR World Congress in Kuala Lumpur, Malaysia.

5.2.1 General process description: Incipient log detachment

The accumulation process of a single log with length $L_L = 0.40$ m is illustrated in Figure 5.1. The approach flow conditions (Figure 5.1a) are characterized by the flow velocity $v_o = 0.70$ m/s, flow depth $h_o = 0.20$ m, and flow Froude number $F_o = 0.50$ (Test B24, Table 4.2). The added log hits the bridge pier center at the water surface level with a log position angle $\gamma \approx 90^\circ$ and with a slight eccentricity, i.e. the log centerline is shifted ≈ 5 mm to the right of the pier centerline (Figure 5.1b). With a uniformly distributed hydraulic load acting on the log, the resulting force leads to a counter-clockwise log rotation (Figure 5.1c). If the log position angle decreases to a critical value (subscript *cr*) $\gamma \leq \gamma_{cr}$, the accumulated log detaches and is transported downstream (Figure 5.1d).

In section 2.5.1, the acting forces on a log at the channel bottom, defining incipient log transport, are described. Similar to this concept, the acting forces and the force balance at an accumulated log at a bridge pier are illustrated in Figure 5.2. The acting hydraulic force F (Figure 5.2a) can be defined as:

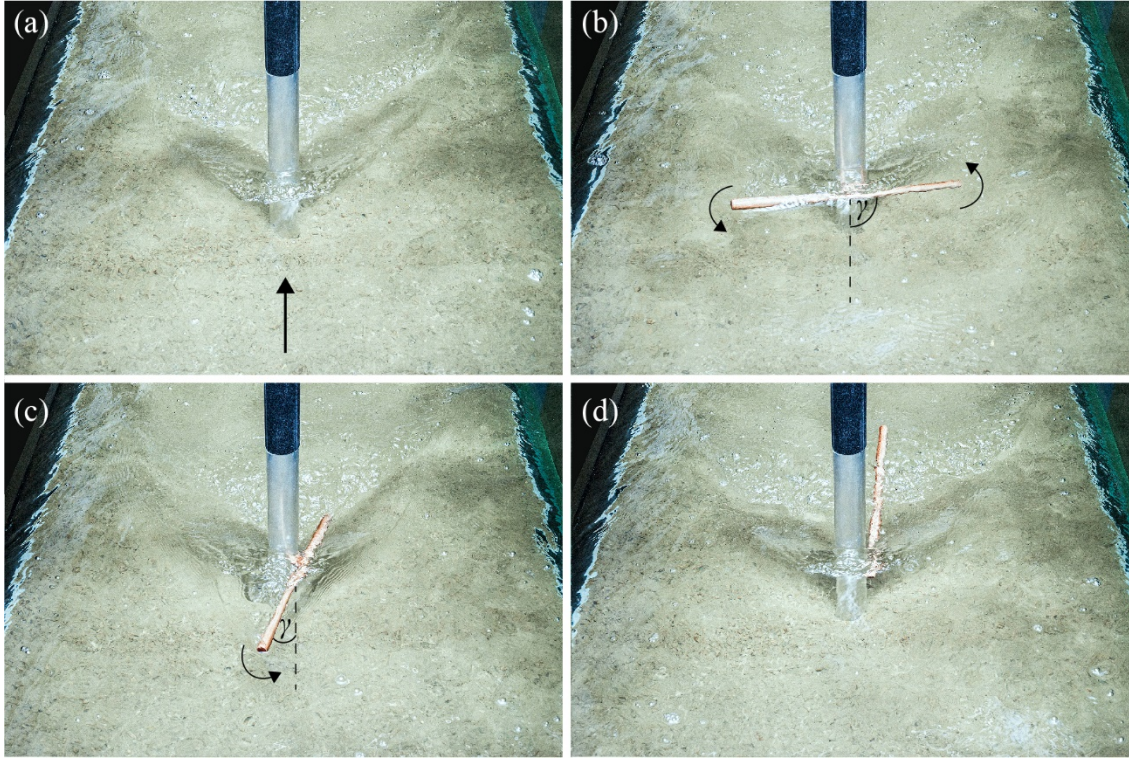


Figure 5.1 Log accumulation process with $v_o = 0.70$ m/s, $h_o = 0.20$ m, $F_o = 0.50$, and $L_L = 0.40$ m; (a) approach flow condition, (b) log accumulation with $\gamma \approx 90^\circ$, (c) $\gamma \approx 25^\circ$, and (d) log detachment (B24, Table 4.2)

$$F = \left(C_{fr} A_s \rho_w \frac{v_o^2}{2} \right) + \left(C_d A_{pr} \rho_w \frac{v_o^2}{2} \right), \text{ with } \quad (5.1)$$

$$A_s = L_L d_L \cos(\gamma) \pi \text{ and } A_{pr} = L_L d_L \sin(\gamma)$$

with C_{fr} = friction coefficient [-], C_d = drag coefficient [-], A_s = lateral area [m^2], and A_{pr} = projected area [m^2]. In literature (e.g. Schütz 2013), C_d commonly implies the friction coefficient C_{fr} , as the friction component is small compared to the drag component of the hydraulic force. Given a cylinder perpendicular to the flow, the friction component is $\sim 10\%$, whereas the drag component is 90% . Therefore, Eq. (5.1) was simplified to

$$F = C_d A_{pr} \rho_w \frac{v_o^2}{2}. \quad (5.2)$$

For C_d , the values were set as a function of γ according to Gippel (1995), ranging from $C_d = 0.90$ for $\gamma = 90^\circ$, $C_d = 0.80$ for $\gamma = 45^\circ$, $C_d = 0.50$ for $\gamma = 15^\circ$, and $C_d = 1.20$ for $\gamma = 0^\circ$. In addition, F can be described as the vector sum of the horizontal force component F_H and the normal force component F_N (Figure 5.2a). F_H increases, whereas F_N decreases with decreasing γ .

$$\vec{F} = \vec{F}_H + \vec{F}_N = F \cos(\gamma) + F \sin(\gamma). \quad (5.3)$$

The force balance in Figure 5.2b is based on the following assumptions:

- Log position angle $\gamma = 45^\circ$,
- uniformly distributed hydraulic load, and
- eccentricity e , so $L_L = L_{L1} + L_{L2}$ and $L_{L1} > L_{L2}$.

For $\gamma = 45^\circ$ and e , the hydraulic load $F/L_{L,pr}$ results in a larger resulting force on the left side, leading to a counter-clockwise log rotation. If the log is still accumulated at the pier, a reactive drag force has to act to inhibit log detachment. In this simplified model, a reactive drag force is the friction force F_{friction} parallel to the log, defined as:

$$F_{\text{friction}} = \mu F_N, \quad (5.4)$$

with $\mu =$ constant roughness coefficient [–]. This coefficient depends on the two interacting materials and was set to $\mu = 0.6$ based on literature data for wood and aluminum (Hering *et al.* 1995).

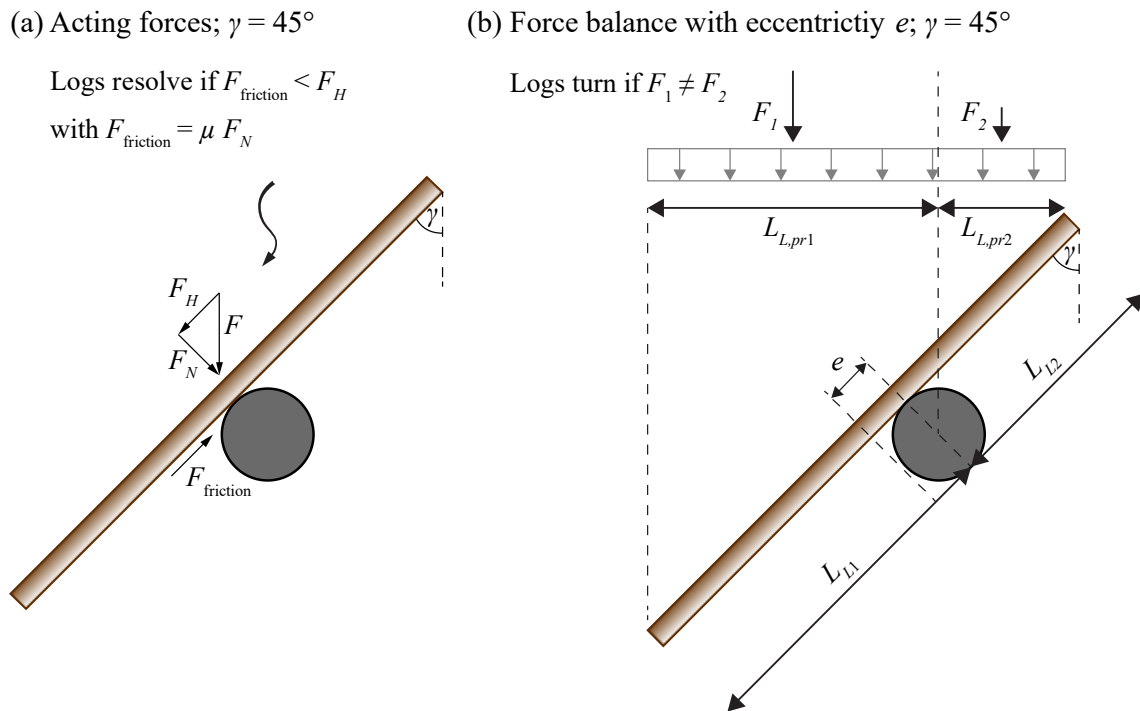


Figure 5.2 (a) Acting forces on an accumulated log with $\gamma = 45^\circ$, and (b) simplified force balance for an accumulated log with eccentricity and $\gamma = 45^\circ$.

During the flume experiments, it was observed that accumulated logs remained in an eccentric position (0.005...0.04 m) for $\gamma \leq 40^\circ$. The incipient log detachment was experimentally investigated for different L_L and v_o . A transparent tapeline was mounted on a log and the eccentricity was manually increased until the log detached from the idealized pier (e.g. $e = 0.02$ m in Figure 5.3). The values for the maximum eccentricity e_{max} and the

respective critical log position angle γ_{cr} were noted and are listed in Table 5.1. The observed e_{max} lie in the range of $e_{max}/L_L = 0.025 \dots 0.125$, and e_{max} increases up to 0.04 m for increasing L_L and decreasing v_o . Longer logs transported with low flow velocities may hit the bridge pier with an eccentricity of $\pm 20\%$, but still remain attached to the pier. Given the reactive drag force, i.e. $F_{friction}$, a log therefore detaches from the pier, if the horizontal force component exceeds the friction force $F_H > F_{friction}$.

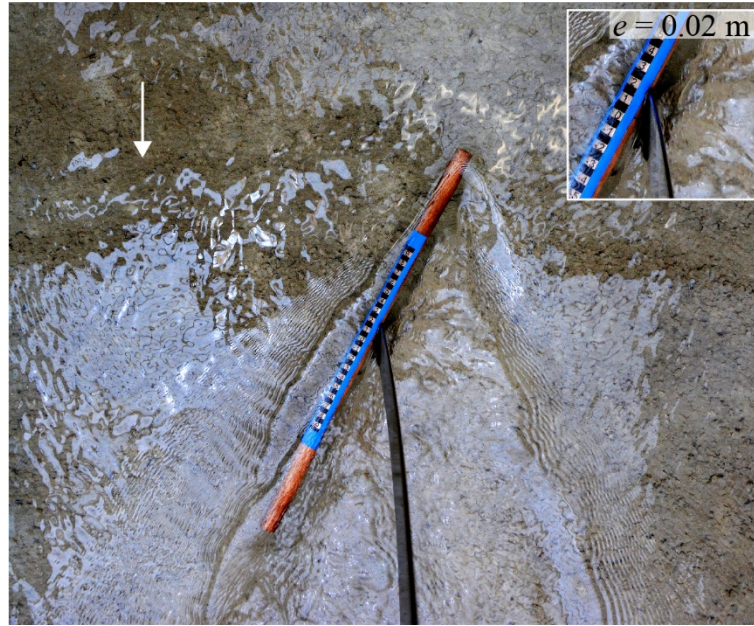


Figure 5.3 Flume experiments on log eccentricity e at an idealized pier, $v_o = 0.20$ m/s, $h_o = 0.10$ m, $L_L = 0.40$ m

Table 5.1 Experimental results for observed maximum eccentricity and critical log position angle γ_{cr} , where the log remained attached; theoretical values for γ_{cr} are marked in bold.

R [-]	v_o [m/s]	L_L [m]	e_{max} [m]	e_{max}/L_L [m]	γ_{cr} [°]	F [N]	F_H [N]	F_N [N]	$F_{friction}$ [N]	$F_{friction} - F_H$ [N]
3.9·10 ⁴	0.20	0.20	0.025	0.125	60	0.04	0.02	0.04	0.02	0.00
					40	0.03	0.03	0.02	0.01	-0.01
1.0·10 ⁵	0.50	0.20	0.005	0.025	60	0.30	0.15	0.26	0.15	0.01
					20	0.12	0.11	0.04	0.02	-0.09
7.8·10 ⁴	0.20	0.40	0.04	0.100	60	0.09	0.04	0.08	0.05	0.01
					40	0.07	0.05	0.04	0.03	-0.03
2.0·10 ⁵	0.50	0.40	0.03	0.075	60	0.59	0.30	0.51	0.31	0.01
					25	0.29	0.26	0.12	0.07	-0.19

The required (subscript req) critical log position angle for incipient log detachment $\gamma_{cr\text{-req}}$ was calculated based on Eq. (5.4) to meet $F_H \approx F_{\text{friction}}$ and are marked in bold in Table 5.1. Given a constant roughness coefficient $\mu = 0.6$, $\gamma_{cr\text{-req}}$ resulted in $\approx 60^\circ$, which is up to 3 times higher compared to the observed values $\gamma_{cr} \approx 20^\circ \dots 40^\circ$. This points at additional, indeterminable forces and processes inhibiting log detachment. If the log rotates, the downstream part of the log can be in the wake area of the pier (Figure 5.1c), exposed to lower flow velocities compared to the upstream part of the log. Due to the difference in flow velocity along the log length, the force acting on the upstream part of the log is higher compared to the force on the downstream part. Given that the log rotation due to eccentricity is counter-clockwise (Figure 5.3), the upstream force would then lead to a clockwise rotation, and the log may remain accumulated. Due to the velocity and hydraulic force fluctuations, respectively, the log starts a rotational movement with alternating directions (counter- versus clockwise). This specific log movement has been observed for a number of physical model tests, especially for longer logs and low v_o . In addition, a complex three dimensional flow field establishes around the pier, including vortex structures as a function of R . The resulting vortex structures in combination with the vortex shedding frequency may affect the force balance (acting forces) and therefore log detachment. However, the complex flow structures and forces acting on an accumulated log, as well as dynamic forces based on vortex shedding, were not the focus of this present thesis.

5.2.2 General process description: Log transport

For the majority of the flume experiments, the logs were added perpendicular to the flow 1 m upstream of the bridge pier to obtain maximum p , corresponding to the worst-case scenario. This setup was evaluated by testing p for a single log with $L_L = 0.40$ m added to the flow with $\gamma = 90^\circ$ (perpendicular to the flow), $\gamma = 45^\circ$, and $\gamma = 0^\circ$. For $\gamma = 90^\circ$ and $v_o = 0.20 \dots 0.50$ m/s, p increased by a factor of ≈ 2 and ≈ 6 compared to $\gamma = 45^\circ$ and $\gamma = 0^\circ$, respectively (Figure 5.4a). Tests A10-A18 therefore confirmed the setup with $\gamma = 90^\circ$ as a worst-case scenario of p .

In addition, a log with $L_L = 0.40$ m was added to the flow 4 m upstream of the bridge pier to investigate whether γ changes until the log reaches the bridge pier. The test was conducted for initial (subscript IC) log position angles of $\gamma_{IC} = 90^\circ$ (Figure 5.4b), $\gamma_{IC} = 45^\circ$ (Figure 5.4c), and $\gamma_{IC} = 0^\circ$ (Figure 5.4d) with $N = 40$. For more than half of the

tests ($\geq 55\%$), the log was transported with γ_{IC} along the channel length, indicating a homogeneous velocity profile in the transverse direction. The ratio between channel width B and approach flow depth h_o is $B/h_o = 10$. Because this ratio is $\gg 1$, it represents shallow flow, characterized as unidirectional (Jirka and Uijttewaal 2004). This is supported by velocity measurements (v_x and v_y) $x = 0.5$ m upstream of the bridge pier for a transverse cross-section at $y = 1/4, 2/4$, and $3/4$ of B (y -position 0 is set at glass-wall side of the flume; Figure 4.1) and $z = 0.05$ m (Tests A10-A18; Figure 5.5). The flow velocity in x -direction v_x is constant ($\pm 3\%$) over the transverse cross-section. In addition, the flow velocity in y -direction v_y is close to zero, with v_y ranging from $0.011 \dots 0.023$ m/s. Due to the unidirectional flow, the position of transported logs remained constant.

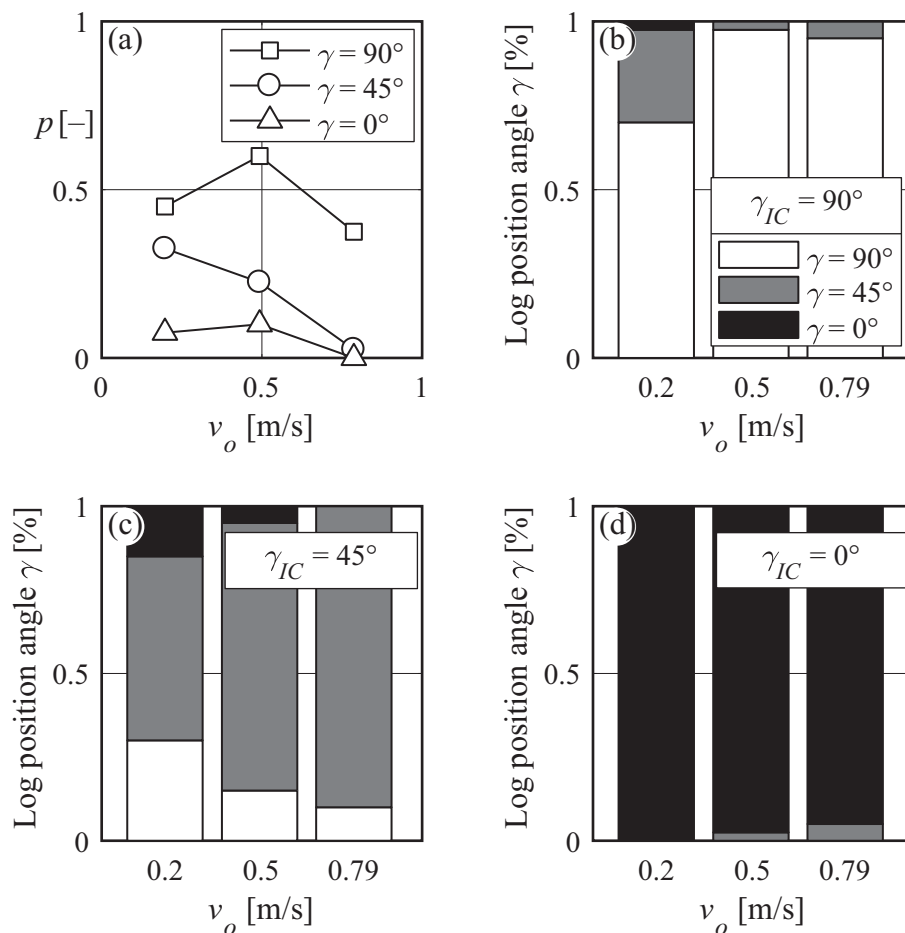


Figure 5.4 (a) Accumulation probability p versus v_o for different log position angles γ and (b-d) observed log position angle γ in [%] at pier versus v_o for different initial γ_{IC} (A10-A18)

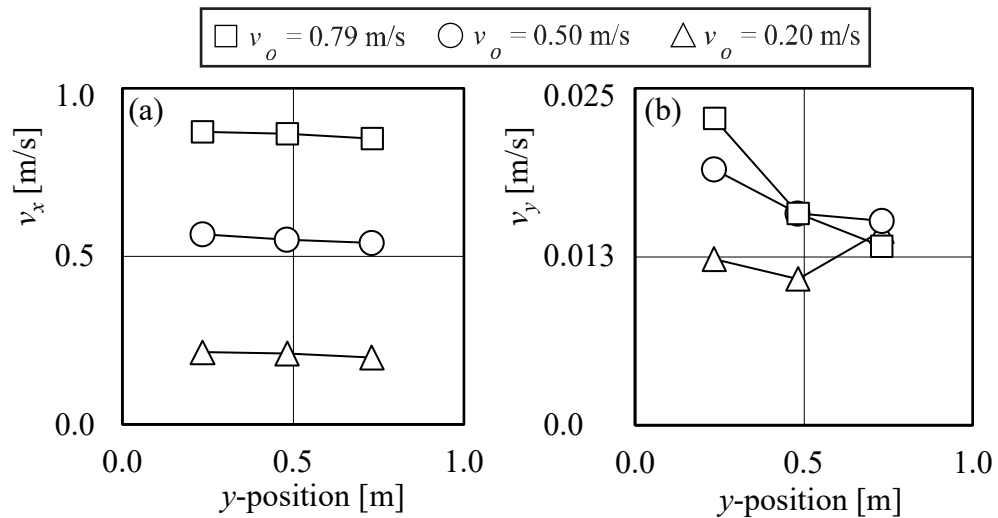


Figure 5.5 Transverse cross-section 0.50 m upstream of the bridge pier of flow velocities in (a) x-direction v_x and (b) y-direction v_y at $z = 0.05$ m

5.2.3 Approach flow conditions and log dimensions

The effect of the approach flow conditions and log dimensions on p was studied in test series B (Table 4.2; Section 4.4.4). Figure 5.6 shows a photo series of approach flow conditions during flume experiments with $v_o = 0.20$ m/s up to 0.97 m/s (a-d).

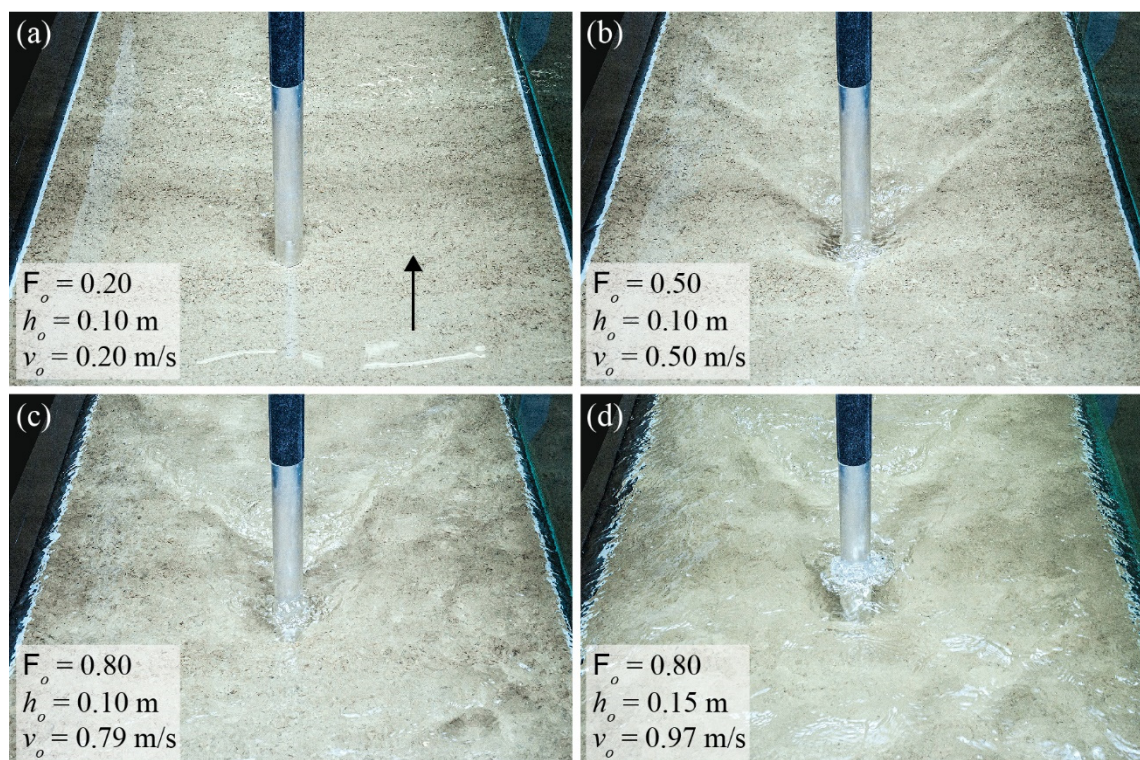


Figure 5.6 Approach flow conditions during flume experiments with increasing v_o (a) $v_o = 0.20$ m/s (B5), (b) $v_o = 0.50$ m/s (B16), (c) $v_o = 0.79$ m/s (B28), and (d) $v_o = 0.97$ m/s (B31)

With increasing v_o , the flow around the bridge pier becomes more turbulent. In addition, the surface roller upstream of the pier (Figure 5.6c and d) is more prominent and surface waves occur.

The accumulation probability p is plotted in Figure 5.7a as a function of v_o for $L_L = 0.20$ m and $F_o = 0.08 \dots 1.20$, ranging from subcritical to slightly supercritical flow. The accumulation probability p decreases with increasing v_o . Given a constant $L_L = 0.20$ m and $F_o = 0.50$, p varied between 10% to 38%. For the lowest tested $F_o = 0.08$ with $v_o = 0.08$ m/s and $L_L = 0.20$, the maximum accumulation probability p_{\max} amounts to 40%. In contrast, p approaches zero for $v_o \geq 0.8$ m/s and results in $p = 0\%$ for $F_o = 1.2$, i.e. slightly supercritical flow regime. For small v_o , logs tend to accumulate as soon as any of their parts touch the bridge pier. In contrast, logs transported with high v_o may touch the bridge pier, but disperse due to increased turbulence and waves. The more prominent surface roller and the surface wave for large flow velocities result in an increased eccentricity, thereby decreasing the accumulation probability. As described in Section 5.2.1, the observed maximum eccentricity e_{\max} for incipient log detachment also decreased with increasing v_o , thereby supporting the results illustrated in Figure 5.7a.

The effect of the approach flow conditions on p was further investigated by keeping v_o constant and varying h_o and F_o . In Figure 5.7b, p is plotted versus h_o for $L_L = 0.20$ m and $v_o = \text{constant} = 0.45$ m/s. The accumulation probability p varies by $\pm 5\%$ for $h_o = 0.04 \dots 0.52$ m, which is below the range of reproducibility ($\pm 10\%$). This trend can be further confirmed by Figure 5.7c, where p is plotted versus $F_o = 0.20 \dots 0.70$ and does not change significantly. If logs are transported at a fully floating stage, they do not interact with the channel bottom. Hence, the effect of h_o and consequently F_o on p is negligible for a given flow velocity and log length.

Figure 5.8 illustrates an accumulated log with $L_L = 0.10$ m versus $L_L = 0.40$ m at the model bridge pier. Note that the pier diameter d_P was kept constant in test series B to $d_P = 0.05$ m, resulting in ratios of $d_P/L_L = 0.5$ to 0.125 . A longer log is transported with more stability in the flow, exhibits a larger eccentricity before detaching (Section 5.2.1), and is therefore more likely to hit the bridge pier and stay accumulated compared to shorter logs.

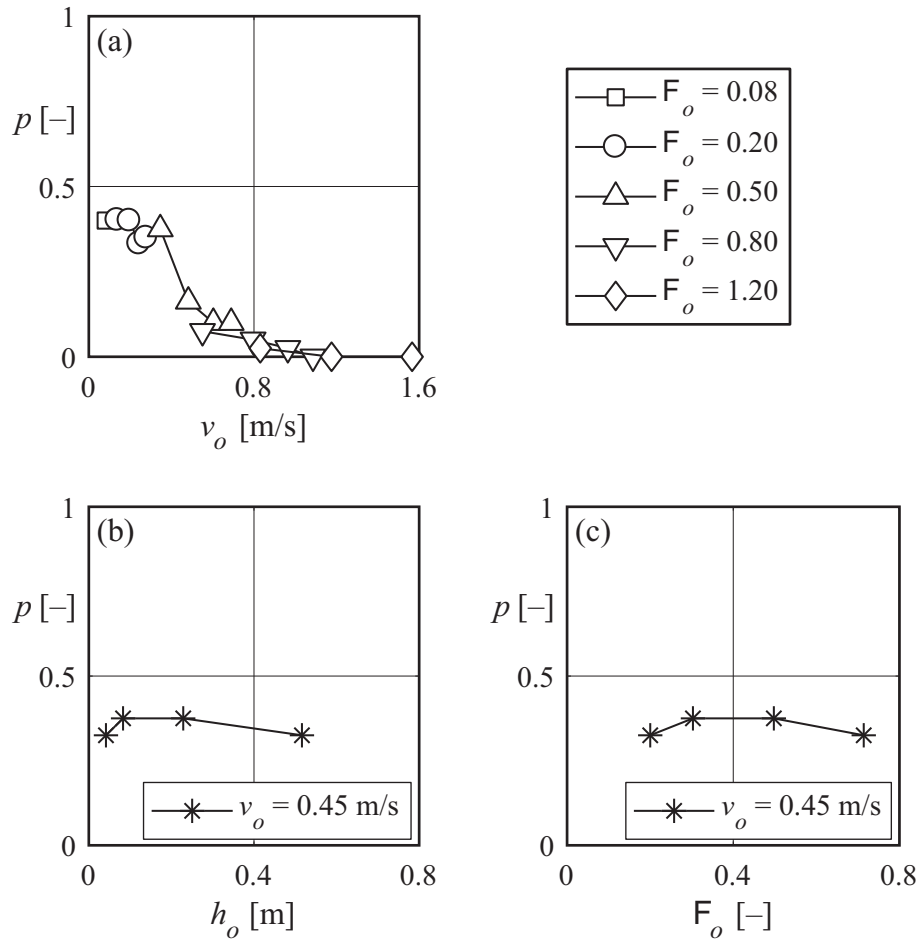


Figure 5.7 Accumulation probability p for $L_L = 0.20$ m versus (a) v_o and various F_o (A1, B1-B39), (b) h_o and constant $v_o = 0.45$ m/s (B40-B43), (c) F_o and constant $v_o = 0.45$ m/s (B40-B43)

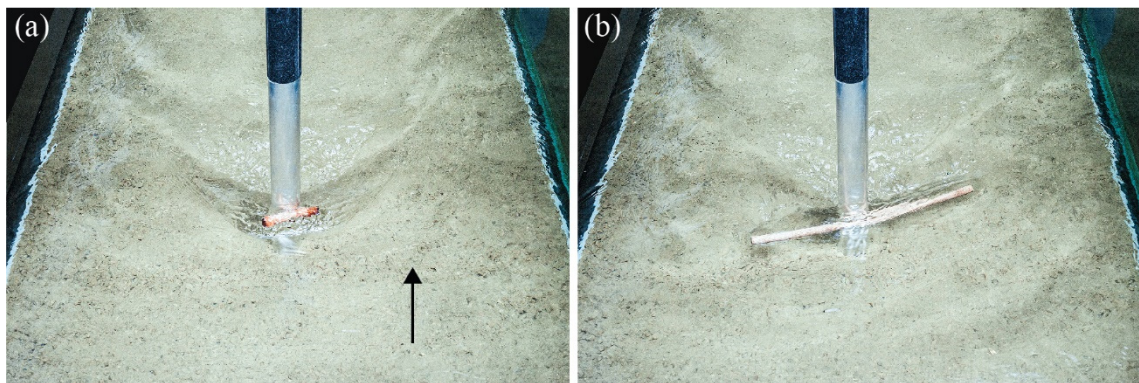


Figure 5.8 Plan view of accumulated log with (a) $L_L = 0.10$ m (B19) and (b) $L_L = 0.40$ m (B21)

Figure 5.9a shows p as a function of v_o for $L_L = 0.10$ m, 0.20 m, and 0.40 m (B2-B36, A1). The accumulation probability for $v_o = 0.14$ m/s is $p = 21\%$ ($L_L = 0.10$ m), 40% ($L_L = 0.20$ m), and 58% ($L_L = 0.40$ m), demonstrating a governing effect of the log length. Furthermore, p is decreasing with increasing v_o for all tested log lengths. Therefore, a governing effect of v_o on p can be deduced, whereas various p result for the same F_o . The

effect of v_o on p is not linear (Figure 5.9a), and p significantly decreases for $v_o > 0.50$ m/s (model scale), as surface waves and turbulence increase (Figure 5.6b-d compared to lower v_o in Figure 5.6a). Considering the various tested L_L , accumulation probability is $p \leq 15\%$ for a threshold value of $v_o \geq 0.80$ m/s (model scale).

The effect of the log diameter d_L on p was tested for $d_L = 0.03$ m, 0.015 m, and 0.004 m with two different log lengths $L_L = 0.20$ m and 0.40 m (Figure 5.9b). For $v_o = 0.20$ m/s, p varies between $\pm 15\%$ for both L_L , whereas p is almost independent of d_L for larger velocities. On average, the deviation of p is $\pm 5\%$. As this average deviation is within the range of reproducibility and no general trend of d_L can be deduced, the effect of d_L on p is of minor importance within the tested range. As the tested logs exhibit similar densities, they are transported in a comparable pattern and d_L does not affect p . According to Eq. (5.1), the projected area A_{pr} increases with increasing d_L , leading to a higher hydraulic force F acting on the log, possibly affecting the accumulation process. However, no differences in the accumulation or detachment process were observed during the flume experiments.

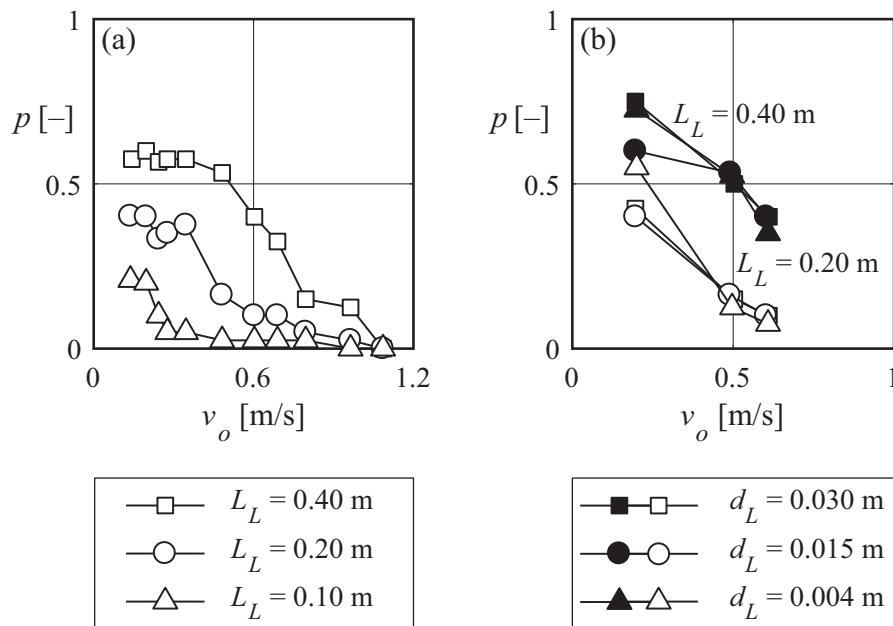


Figure 5.9 Accumulation probability p versus v_o for (a) various L_L with $d_L = 0.015$ m (B2-B36, A1) and (b) various d_L with $L_L = 0.20$ m and 0.40 m (B6-B7, B17-B18, B20-B21, B44-B55)

In summary, p increases with increasing L_L and decreasing v_o , whereas no effect of h_o or d_L was observed. Past studies often used F_o as the governing parameter for the accumulation probability. However, the current tests showed that a constant F_o results in a

large range of accumulation probabilities for a given L_L . Consequently, no governing effect of F_o on p can be concluded, and v_o is used as the decisive parameter for the design equation (Section 5.2.7). These results confirm the findings by Lyn *et al.* (2003), as they also defined v_o instead of F_o as the governing parameter for LW accumulation probability.

5.2.4 Pier characteristics

The effect of the pier characteristics, comprised of pier roughness (Figure 5.10), –number (Figure 5.11), –shape (Figure 5.12), and –diameter (Figure 5.13), on p was tested for various v_o and L_L (Test series C, Table 4.2 and Section 4.4.4).

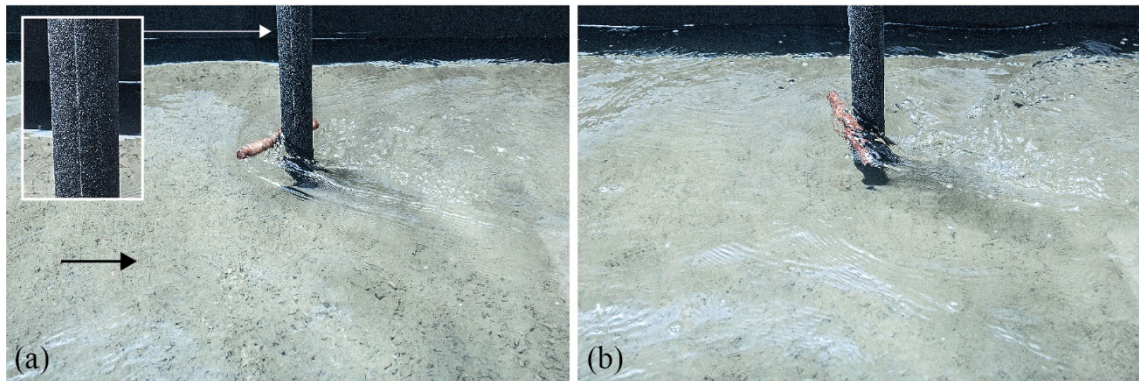


Figure 5.10 Side view of LW accumulation with a rough bridge pier with $L_L = 0.20$ m and (a) $v_o = 0.60$ m/s (C3) versus (b) $v_o = 0.70$ m/s (C4)

The results of p with a smooth versus a rough bridge pier for $L_L = 0.20$ m are depicted in Figure 5.14a. In prototype, the smooth bridge pier corresponds to steel and the rough bridge pier to concrete, thereby representing common materials for bridge piers. For the majority of the tested v_o , p is slightly higher for the rough bridge pier. Due to the increased pier roughness, the friction between log and pier is increased. The constant roughness coefficient μ between wood and concrete amounts to ~ 0.90 (Schneider 2001), leading to an increased reactive friction force compared to wood and aluminum (Section 5.2.1). Hence, accumulation probability generally increases for rougher piers. However, the mean difference between smooth and rough pier is $\approx 8.4\%$ of p , and consequently within the range of test reproducibility. The tested bridge pier roughness in the present study has no governing effect on p .

In Figure 5.14b, p is plotted versus v_o for a test setup with two circular piers compared to one circular pier. The two piers were placed into the flume with an axial spacing

of 0.33 m (Figure 5.11). Similar to the test procedure with one pier, logs with $L_L = 0.40$ m were added 1 m upstream of the bridge piers in the centerline of the flume to investigate maximum accumulation probability p . The log length was chosen to allow for a spanwise accumulation (i.e. $L_L >$ axial pier spacing) compared to a single log accumulation in front of a single pier. The mean accumulation probability with two piers is $\approx 24\%$ higher, whereas the difference in p increases with increasing v_o from 17.5% up to 35%. The accumulation process can be described as follows: the log was added to the flow with $\gamma_{IC} = 90^\circ$, and for $\gamma = \gamma_{IC} = 90^\circ$, the log touched the two piers with both log ends, leading to a spanwise accumulation. For $\gamma < \gamma_{IC} = 90^\circ$, one log end touched one of the two piers, resulting in either (1) a tilting log movement and again in a spanwise accumulation, or (2) the log being transported between the two piers further downstream. For increasing v_o , the flow is more turbulent and surface waves occur. Therefore, logs may slightly turn and are transported between the two bridge piers with $\gamma < \gamma_{IC} = 90^\circ$, resulting in lower p . Compared to the setup with one pier, a spanwise accumulation leads to increasing p , given the logs approach the two piers with $\gamma = \gamma_{IC} = 90^\circ$ and $L_L >$ axial pier spacing.

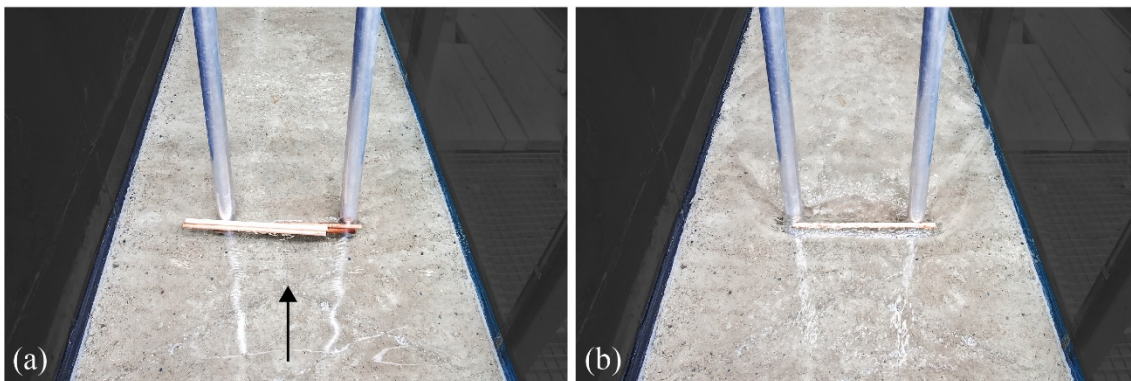


Figure 5.11 Plan view of LW accumulation with two bridge piers with $L_L = 0.40$ m and (a) $v_o = 0.20$ m/s and 5 logs (C7) versus (b) $v_o = 0.50$ m/s and 1 log (C8)

The effect of the pier shape on p versus v_o is plotted in Figure 5.14c for $L_L = 0.20$ m and 0.40 m. For both tested L_L , the square pier shape (Figure 5.12a) exhibits the largest p , followed by the triangular (Figure 5.12b) and circular pier shape. The contact area between pier and log is higher for a square bridge pier compared to a triangular or circular pier shape. This leads to increased friction force and eccentricity (Section 5.2.1), thereby favoring log attachment and hence increasing p . The deviations of p between a square and triangular pier shape are 2.5...15% for $L_L = 0.20$ m and 5...7.5% for $L_L = 0.40$ m. In comparison, p for a circular pier is 2.5...18.75% smaller with $L_L = 0.20$ m and 0.08...2.5%

smaller with $L_L = 0.40$ m than p for a square pier shape. On average, the deviations between all shapes in p are $\pm 8.5\%$ for $L_L = 0.20$ m and $\pm 4\%$ for $L_L = 0.40$ m, and consequently within the range of test reproducibility. The deviations decrease with increasing log length and flow velocity. A governing effect of the pier shape on the accumulation probability consequently cannot be derived for the present model test. According to the findings by De Cicco (2017), p varied between 0...5% for the different pier shapes and the two tested F_o . These deviations are rather small, so for both studies, no governing effect of the pier shape on p can be deduced.

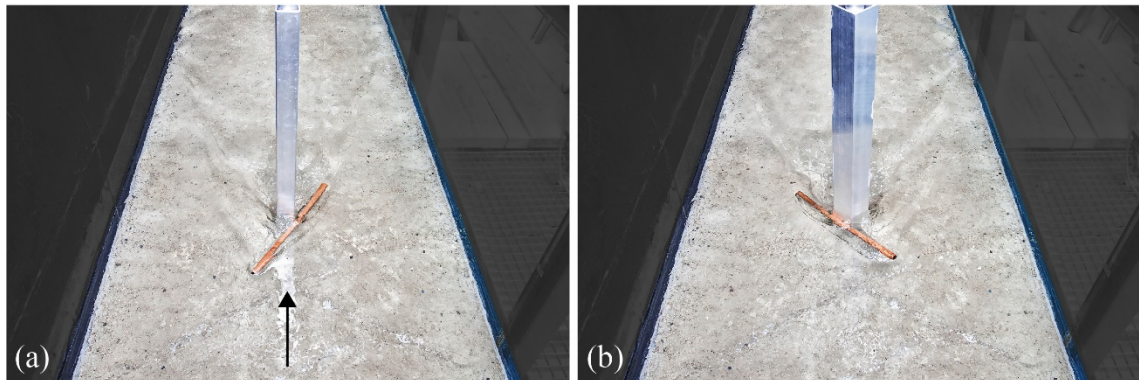


Figure 5.12 Plan view of LW accumulation with $L_L = 0.40$ m and $v_o = 0.50$ m/s for (a) square (C26) and (b) triangular bridge pier (C20)

The setup of the physical tests with pier diameters $d_P = 0.01$ m compared to 0.025 m is shown in Figure 5.13. Figure 5.14d illustrates p versus v_o for different pier diameters $d_P = 0.01$ m, 0.025 m, and 0.05 m. The effect of d_P was investigated by keeping the ratios of pier diameter to log length constant with $d_P/L_L = 0.125$ versus 0.250, resulting in tested L_L varying from 0.08 m to 0.40 m. Note that for $d_P = 0.01$ m only $d_P/L_L = 0.125$ was investigated, as the required $L_L = 0.04$ m for $d_P/L_L = 0.250$ was very unstable in the flow and the log transport was not comparable to other tested log lengths. The accumulation probability p increases with decreasing ratio d_P/L_L . For $d_P/L_L = 0.250$, p is 2.5...6.25% higher ($\approx 4.6\%$ on average) for $d_P = 0.05$ m compared to $d_P = 0.025$ m. The differences in p between $d_P = 0.05$ m and $d_P = 0.025$ m increase for $d_P/L_L = 0.125$ in a range of 2.5...15% ($\approx 8.4\%$ on average). The resulting p for $d_P = 0.010$ m with $d_P/L_L = 0.125$ is 20...40.8% lower compared to the other two pier diameters, indicating a stronger effect of L_L on p compared to d_P . In addition, the flow around the pier may be different for increasing pier diameter, due to an increase in flow acceleration at the pier sides.

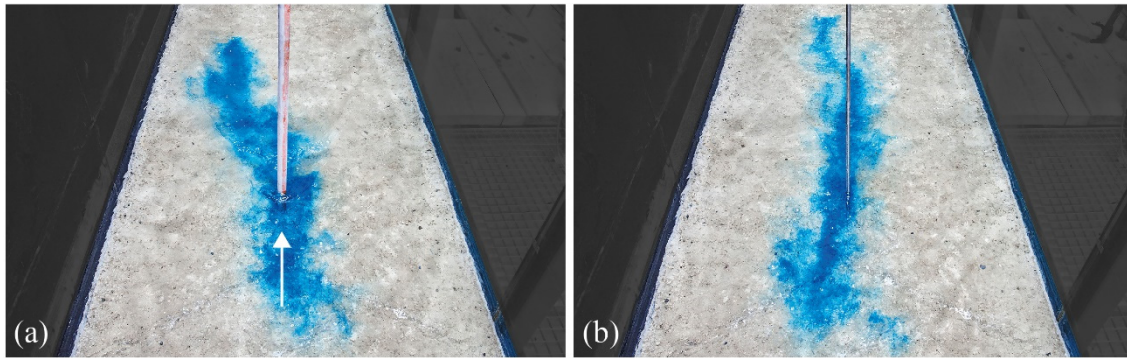


Figure 5.13 Plan view of flow around pier with $v_o = 0.50$ m/s for (a) $d_p = 0.025$ m (C34) and (b) $d_p = 0.01$ m (C30)

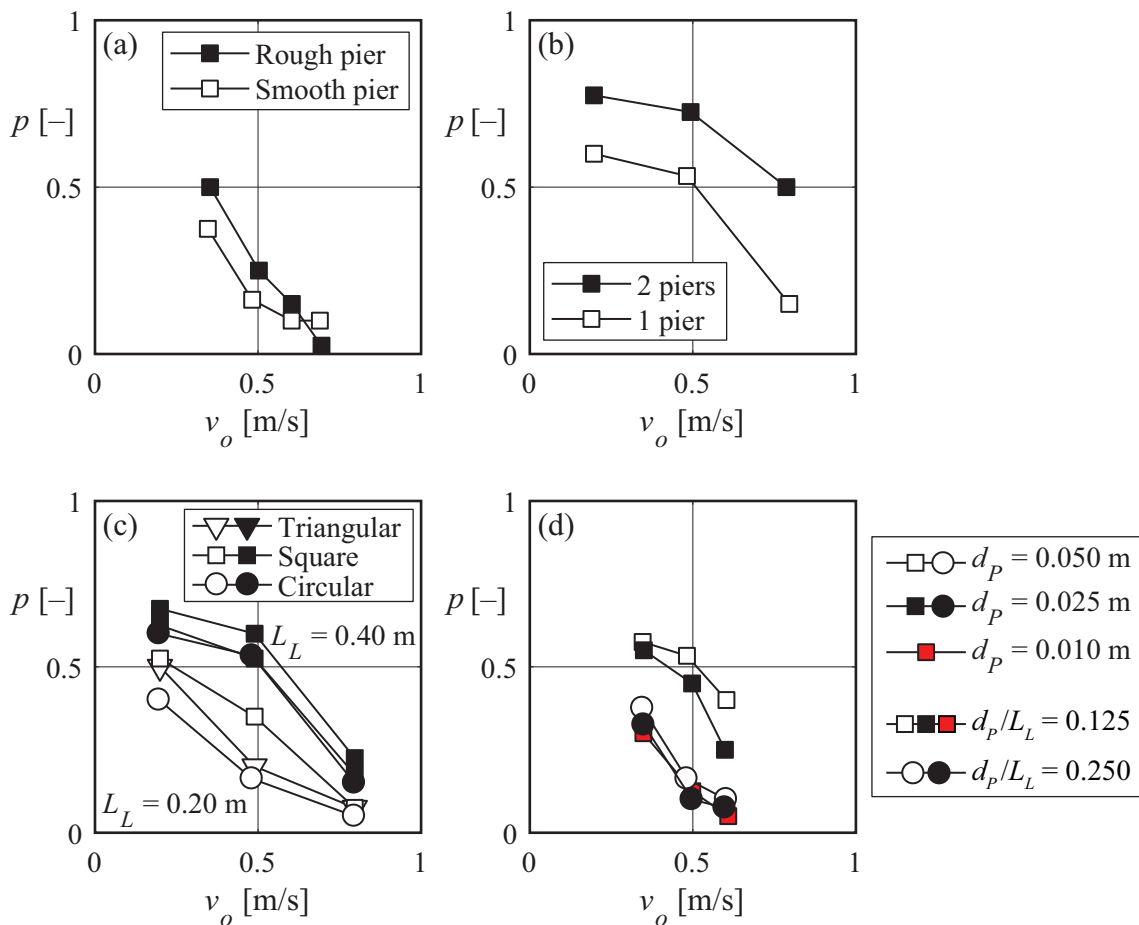


Figure 5.14 Accumulation probability p versus v_o for (a) smooth (B14, B17, B20, B23) versus rough pier with $L_L = 0.20$ m (C1-C4), (b) one versus two circular bridge piers with $L_L = 0.40$ m (B7, B18, B30 versus C5, C8, C11), (c) circular, triangular, and square pier shape with $L_L = 0.20$ m and $L_L = 0.40$ m (B6-B7, B17-B18, B29-B30 vs. C17-C22 vs. C23-C28), (d) $d_p/L_L = 0.125$ and 0.250 , i.e. $d_p = 0.05$ m vs. $d_p = 0.025$ m vs. $d_p = 0.010$ m (B14-B15, B17-B18, B20-B21 vs. C29-C31 vs. C32-C37)

In summary, p increases with increasing number of piers and decreasing ratio d_p/L_L , whereas only a minor effect on p was observed for bridge pier roughness and pier shapes.

5.2.5 Large wood characteristics

The tested LW characteristics include logs with branches (Figure 5.15), different log densities, semi-congested, and congested LW transport. The experiments were conducted for various v_o , L_L , and with one versus two circular bridge piers (Test series D and E, Table 4.2).

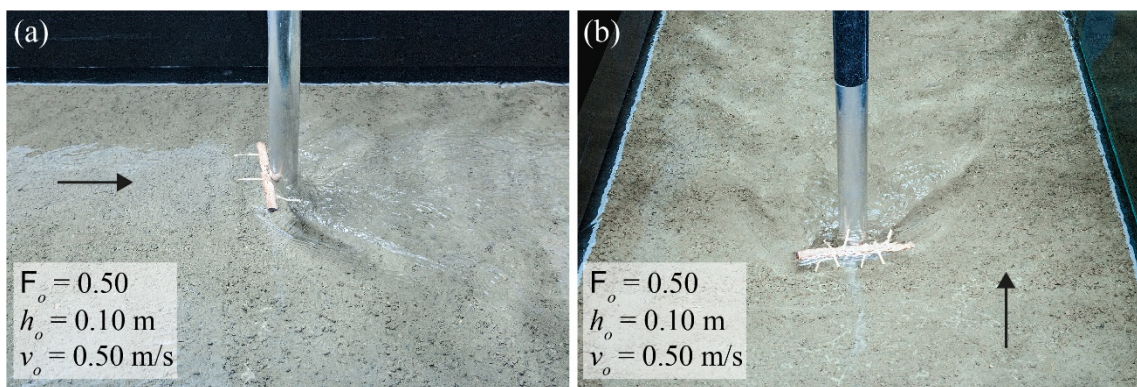


Figure 5.15 Accumulated log with $L_L = 0.20$ m and (a) 2D versus (b) 3D branches (Tests D2-D3)

The effect of single logs with and without branches on p is shown in Figure 5.16a. Regular logs ($L_L = 0.20$ m) without branches are compared to logs with two types of branches (2D and 3D in Figure 4.2; Test series B vs. D1-D7; Section 4.4.4). No experiments with alternate branches of type 3D were conducted for $v_o < 0.50$ m/s ($h_o < 0.10$ m), since the branches touched the channel bed and the logs were not fully floating. For $v_o = 0.50 \dots 0.61$ m/s, p is 2.5% to 8.75% higher for logs with branches (2D and 3D) compared to regular logs, whereas p is 5% lower for $v_o = 0.70$ m/s. The branches exhibit an alternating effect on p . Depending on how the logs accumulated at the pier; branches either entangled on both sides of the pier, or pushed the log away from the pier. The former process led to increasing p , whereas the latter to decreasing p . In prototype, branches may break, when touching the pier (Section 4.2). This process was not observed during the flume experiments, as the material of the branches was too stiff. However, as the spacing of natural branches is very random, a general behavior of branches favoring accumulation probability is rather difficult to deduce. It can be hypothesized, though, that

logs with branches favor the accumulation of approaching logs, once one log is accumulated, as the interrelation between logs with branches increases. Based on the results of the flume experiment, no clear trend of the effect of branches on p was observed and the differences are within the range of test reproducibility. Similar to the findings by Lyn *et al.* (2003), the effect of branches on p is negligible for uncongested LW transport.

Figure 5.16b compares p for logs with different densities ρ_L (Test series B vs. D8-D11). For the majority of the experiments, the logs were not watered and the measured log density resulted in $\rho_L = 460 \text{ kg/m}^3$. In comparison, logs watered for a duration of $t_W = 2$ months resulted in $\rho_L = 850 \text{ kg/m}^3$, and $t_W = 5$ months in $\rho_L = 1'320 \text{ kg/m}^3$. The accumulation probability p for logs with $\rho_L = 460 \text{ kg/m}^3$ compared to $\rho_L = 850 \text{ kg/m}^3$ varies on average by $\pm 3.75\%$. For $\rho_L < 1'000 \text{ kg/m}^3$, log density does not affect p , as the logs are all fully floating and transported in a same manner. For $\rho_L = 1'320 \text{ kg/m}^3$, logs were not fully floating and transported at the channel bottom, resulting in an increase of p by 7.5% for $v_o = 0.61 \text{ m/s}$. As rolling or sliding LW transport was not the focus of this study, p for logs with $\rho_L \geq 1'000 \text{ kg/m}^3$ was only investigated for a selected $v_o = 0.61 \text{ m/s}$.

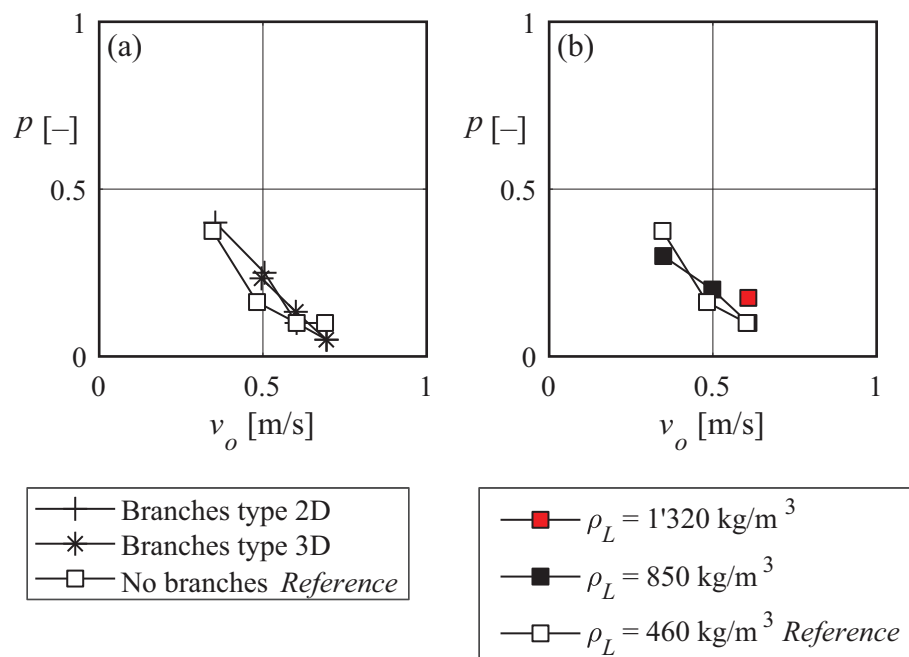


Figure 5.16 Accumulation probability p versus v_o for (a) logs without branches versus logs with 2D and 3D branches, $L_L = 0.20 \text{ m}$ (B14, B17, B20, B23 vs. D1-D7), (b) logs with different densities, $L_L = 0.20 \text{ m}$ (B14, B17, B20 vs. D8-D11)

The LW transport types are illustrated in Figure 5.17a-b for semi-congested, in Figure 5.17c for continuous, and in Figure 5.17d for congested LW transport. The effect of LW transport type on p is plotted in Figure 5.18 (Test series B vs. E) for the setup with one pier. The investigated LW transport types comprise uncongested and semi-congested transport for logs with $L_L = 0.20$ m (Figure 5.18a) and $L_L = 0.40$ m (Figure 5.18b). For semi-congested LW transport, 3 or 5 regular logs, as well as 3 logs with 3D branches were added to the flume. Note that for semi-congested LW transport, it was sufficient to count as accumulated, if at least one log accumulated at the pier. Logs with 3D branches were only tested for $L_L = 0.20$ m (Figure 5.18a).

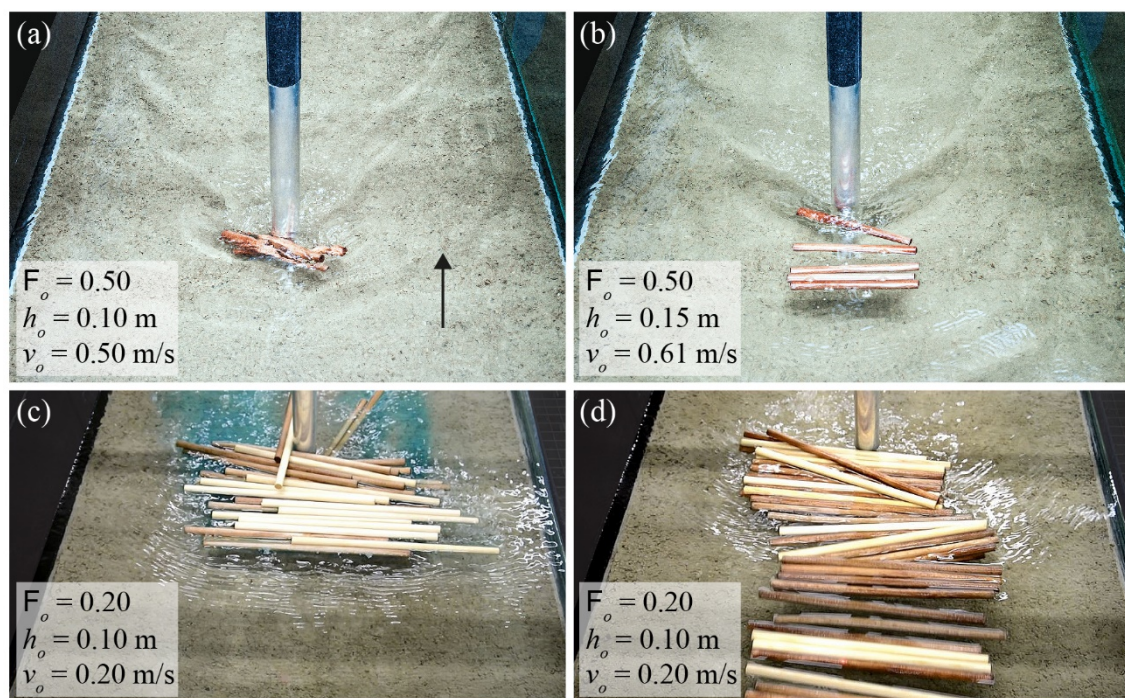


Figure 5.17 (a) Semi-congested LW transport with 3 regular logs and $L_L = 0.20$ m (E3), (b) semi-congested LW transport with 5 regular logs and $L_L = 0.20$ m (E7), (c) LW accumulation after continuous addition of 40 regular logs with $L_L = 0.40$ m (E19), (d) congested LW transport with 40 regular logs and $L_L = 0.40$ m (E23)

For $L_L = 0.20$ m, p increases by 5% to 33.75% for congested LW transport (average increase of + 20.7%). The increase in p is higher for smaller v_o and increasing number of added logs. For $v_o \geq 0.5$ m/s, p is also higher for logs with branches, as the interrelations between the single logs improved, leading to an increased stability of the accumulation. The higher velocity further results in a more compressed accumulation. However, the model branches were rather stiff and did not break as they hit the bridge pier, which may

be the case in prototype (Section 4.2). In addition, the symmetrical arrangement of the model branches may have favored the accumulation, leading to an overestimation of p . For $L_L = 0.40$ m (Figure 5.18b), p increases by 10% to 26.7% for congested LW transport with an average increase of +17.2%. Again, the increase in p is higher for smaller v_o , whereas p was similar for both 3 and 5 added logs. For semi-congested LW transport, the total length of e.g. 5 accumulated logs or blocked area in flow direction, respectively, was higher compared to the individual log length. Due to the increase in length, e_{\max} increases, which may further inhibit log detachment.

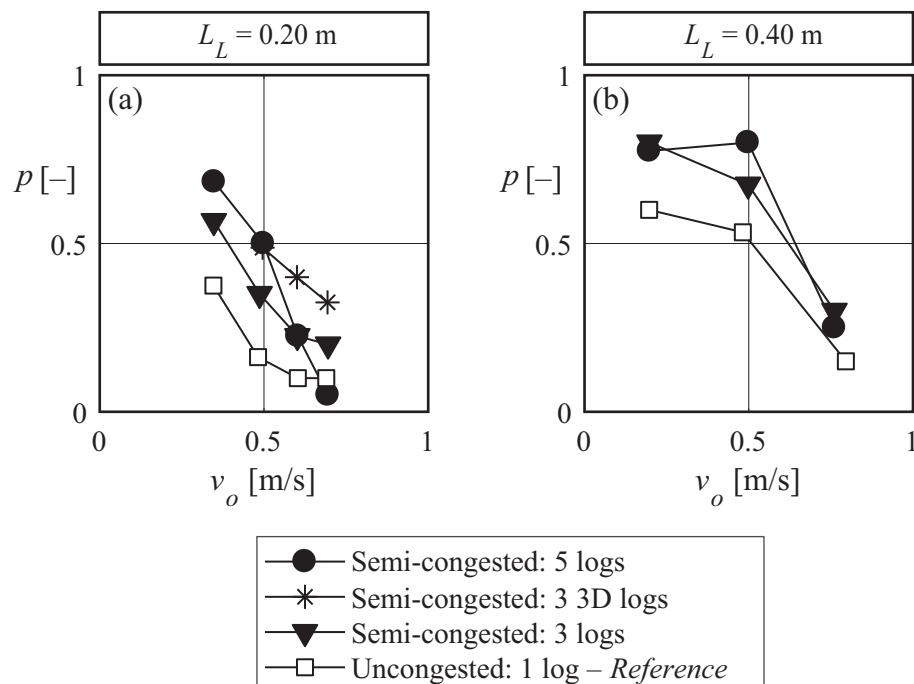


Figure 5.18 Accumulation probability p versus v_o with 1 pier for uncongested versus semi-congested LW transport with (a) $L_L = 0.20$ m (B14, B17, B20, B23 vs. E1-E5, E6-E8, E9-E11), (b) $L_L = 0.40$ m (B7, B18, B30 vs. E12-E17)

In Figure 5.19, p is illustrated versus v_o for semi-congested and uncongested LW transport with $L_L = 0.40$ m and with two piers (Test series C). Similar to the setup with one pier, p increases with increasing number of added logs. Compared to uncongested LW transport, p increases up to 30% for congested LW transport with an average increase of +17.5%. For $v_o = 0.5$ m/s and 5 added logs, p reaches a maximum of 100%. In addition, the setup with two piers results in $p \geq 77.5\%$ for $v_o = 0.97$ m/s, whereas $p \leq 12.5\%$ for one bridge pier. Note that for $L_L \geq$ axial spacing of bridge piers and semi-congested LW transport, $p \geq 75\%$, thereby significantly increasing the flood hazard.

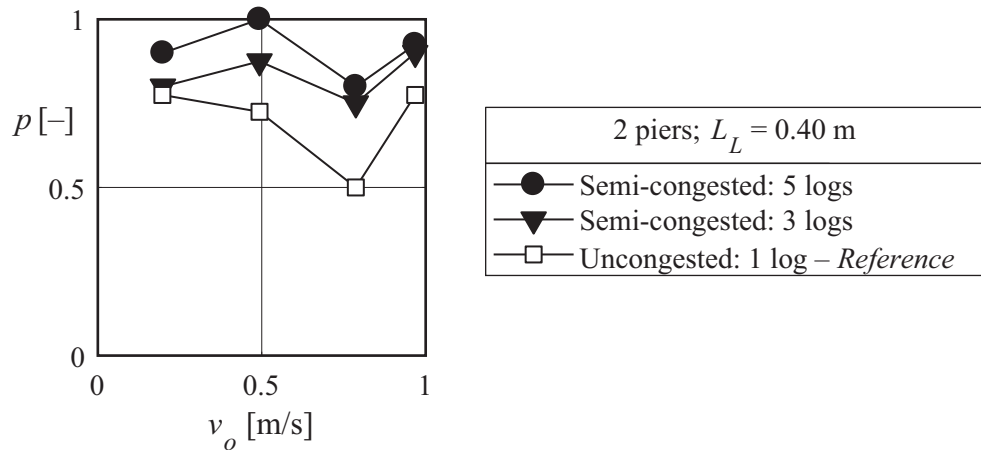


Figure 5.19 Accumulation probability p versus v_o with 2 piers for uncongested versus semi-congested LW transport with $L_L = 0.40$ m (C5-C16)

The effect of continuous addition of 40 logs and congested LW transport (i.e. addition of 40 logs in bulk) on p was investigated for selected approach flow conditions and for one pier (Figure 5.20). For both L_L , the continuous addition of LW led to an increase of p up to 33% compared to uncongested LW transport. Compared to semi-congested LW transport and $v_o = 0.20$ m/s, p is $\approx 20\%$ higher for continuous transport, but decreases by $\approx 5\%$ for $v_o = 0.5$ m/s. For semi-congested and continuous transport, p increases with increasing number of added logs. In contrast, congested LW transport resulted in $p = 3\dots23\%$ for $L_L = 0.20$ m and $p = 41\dots47\%$ for $L_L = 0.40$ m, which is on average $\approx 15\%$ lower compared to p for uncongested LW transport. The transport of 40 logs in bulk was rather difficult to reproduce in model tests. During the flume experiments, part of the LW bulk touched the pier, but bounced off due to the subsequent approaching logs. In addition, the interrelation between the model logs was observed to be different compared to natural logs. The variety in natural log roughness (i.e. due to bark), geometry, flexibility, and density was not modeled in the flume experiments, but may form a more compact accumulation body and result in higher p . Therefore, no general conclusion on the effect of congested LW transport on p can be drawn for this selected set of approach flow conditions and LW characteristics.

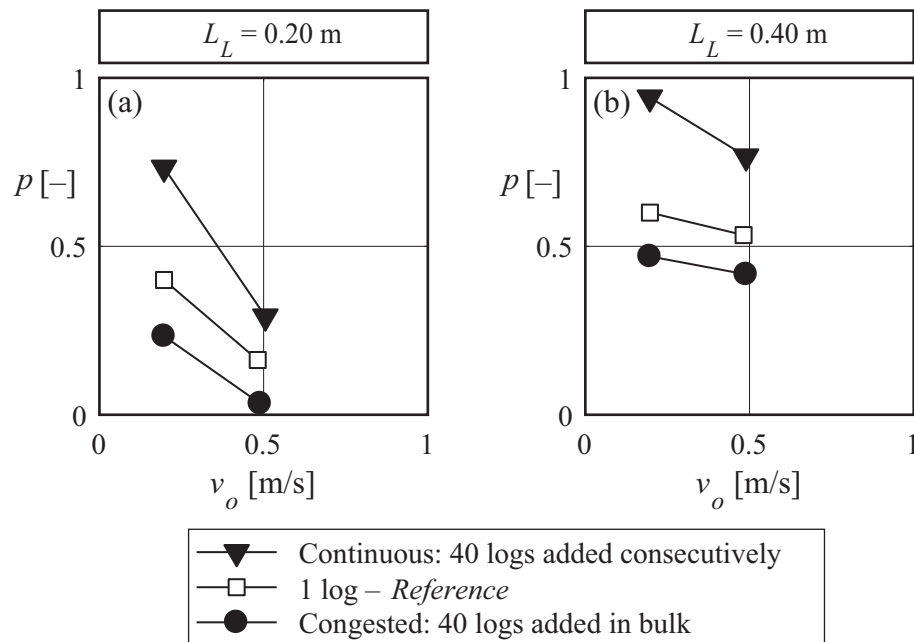


Figure 5.20 Accumulation probability p versus v_o with 1 pier for uncongested versus continuous and congested LW transport with (a) $L_L = 0.20$ m (B6+B17 vs. E18+E20 vs. E22+E24), (b) $L_L = 0.40$ m (B7+B18 vs. E19+E21 vs. E23+E25)

In summary, accumulation probability increases for continuous LW addition and semi-congested LW transport. The combination of two bridge piers and semi-congested LW transport results in the highest observed accumulation probability. The first experiments on congested LW transport resulted in comparatively low accumulation probabilities, which may be due to the interrelation between model logs, as the entire bulk bounced off the bridge pier. Only a minor effect of LW branches on p was observed for uncongested and semi-congested LW transport.

5.2.6 Movable bed

The effect of a movable bed and the resulting scour on p was studied for selected approach flow conditions in test series F (Table 4.2; Section 4.4.4; Figure 5.21). Scour evolved around the bridge pier for approach flow conditions set to $F_o = 0.8$, $h_o = 0.10$ m, and $v_o = 0.79$ m/s. The approach flow conditions were set, so the respective bed shear stress amounted to $\theta = 0.061$ and was higher than θ for incipient motion with $\theta_{cr} = 0.047$. After an equilibrium scour developed, p was determined for $v_o = 0.79$ m/s. To test p for $v_o = 0.50$ m/s and $v_o = 0.20$ m/s, Q and J_o were decreased. The flow velocities were chosen, so θ was smaller than 0.047, to keep the scour formed for $v_o = 0.79$ m/s. For $v_o = 0.20$ m/s (Figure 5.21a) and $v_o = 0.50$ m/s (Figure 5.21b), observed log transport and

accumulation processes were similar to the setup with a fixed bed. For $v_o = 0.79$ m/s (Figure 5.21c), logs were pulled downward to the bottom as they touched the bridge pier, indicating a more prominent downward flow upstream of the pier. Resulting scour topography is illustrated in Figure 5.21d and plotted in Figure 5.22. The maximum scour depth was $S_{\max} = 0.045$ m or put as the ratio between scour depth and mean grain size diameter $S_{\max}/d_m = 6.82$. The eroded material deposited downstream of the pier with a maximum deposition height of $D_{\max} = 0.0185$ m ($D_{\max}/d_m = 2.80$).

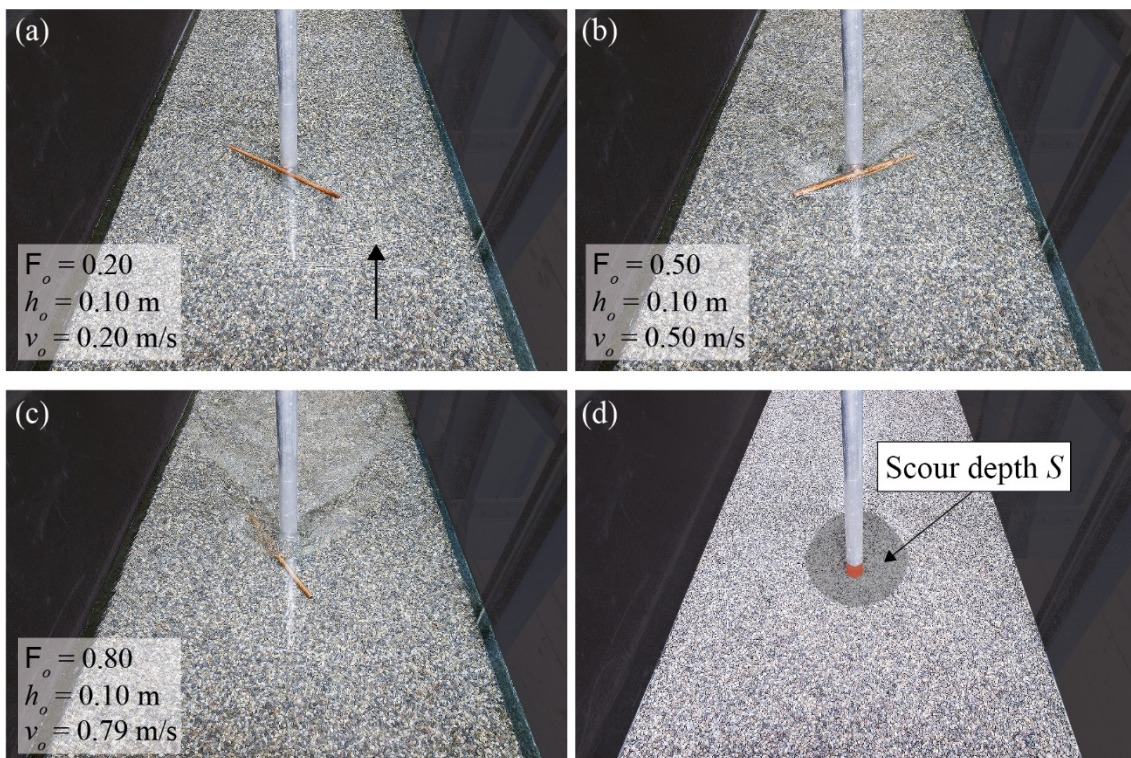


Figure 5.21 Photo series of flume experiments with movable bed; (a)-(c) accumulated log with $L_L = 0.40$ m and increasing approach flow velocity v_o , (d) final scour depth S (F1-F6)

Accumulation probability p is plotted versus v_o for fixed and movable bed and for logs with $L_L = 0.20$ m and $L_L = 0.40$ m in Figure 5.23a and Figure 5.23b, respectively. The deviations in p between fixed and movable bed are on average $\pm 12\%$ and slightly above the reproducibility range of $\pm 10\%$. Note that p for a movable bed and $v_o = 0.50$ m/s is higher for $L_L = 0.20$ m, whereas it is lower for $L_L = 0.40$ m compared to p for a fixed bed. The resulting scour did not strongly affect the flow around the bridge pier and had therefore only a small effect on p . As no governing trend can be deduced and the deviations are close to reproducibility range, the effect of a movable bed on p can be neglected for the present model tests. However, given a larger scour and increasing flow velocity,

the downward flow may further increase. Consequently, logs would be pulled toward the bottom and stay accumulated due to lower flow velocity at the bottom.

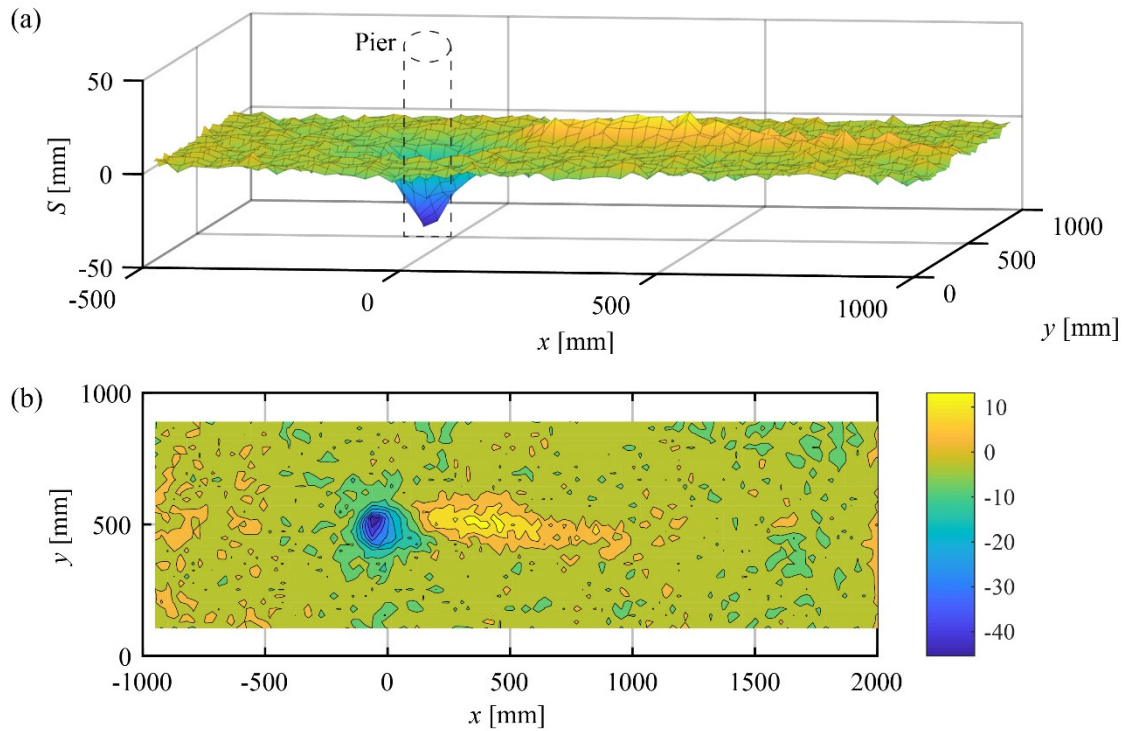


Figure 5.22 Topography of final scour around bridge pier (F5-F6)

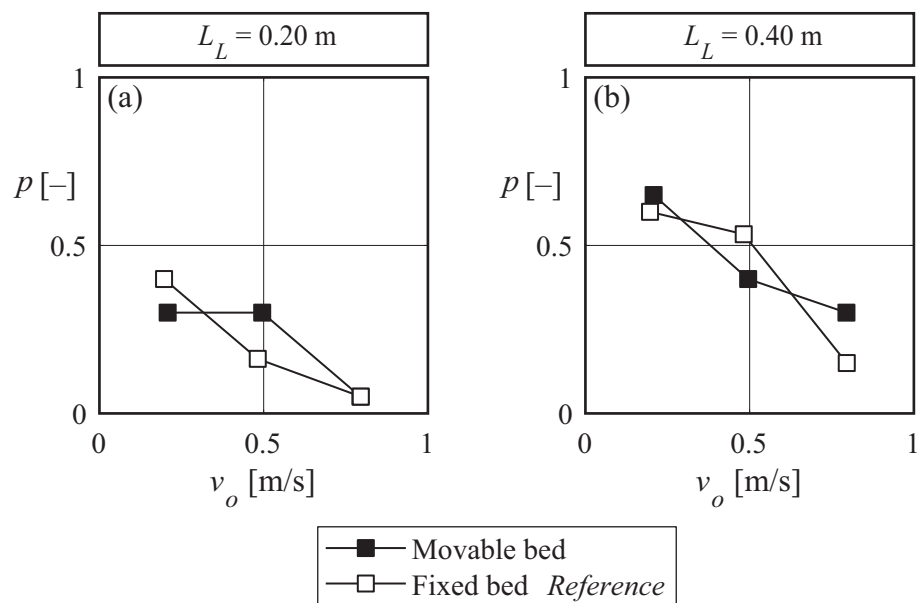


Figure 5.23 Accumulation probability p versus v_o with 1 pier for fixed bed versus movable bed (a) $L_L = 0.20$ m (B6, B17, B29 vs. F1, F3, F5), (b) $L_L = 0.40$ m (B7, B18, B30 vs. F2, F4, F6)

5.2.7 Normalized large wood accumulation probability: Design equation

To generalize and predict the obtained results on LW accumulation probability, the governing parameters are discussed hereafter. LW accumulation probability p can be described by the basic parameters listed in Table 5.2 and by Eq. (5.5):

$$p = f(L_L, d_L, d_P, v_o, h_o, \rho_W, \rho_L, g, \sigma, \nu). \quad (5.5)$$

The selected $n = 10$ independent parameters include $r = 3$ reference dimensions ([M] mass, [L] length, [T] time). Therefore, $n - r = 7$ non-dimensional parameters Π_{1-7} need to be defined based on a dimensional analysis. Π_{1-7} are the relative velocity head $\Pi_1 = v_o^2/(2gL_L)$, relative pier diameter $\Pi_2 = d_P/L_L$, approach flow Froude number $\Pi_3 = v_o/(gh_o)^{1/2}$, relative LW density $\Pi_4 = \rho_L/\rho_W$, relative log length $\Pi_5 = L_L/d_L$, Reynolds number $\Pi_6 = (v_o d_L)/\nu$, and Weber number $\Pi_7 = (\rho_W v_o^2 h_o)/\sigma$. The non-dimensional parameters were defined based on the experimental results. The flow velocity and log length indicated a governing effect on p . Therefore, the velocity head was normalized using the log length to define Π_1 . As the flume experiments were primarily conducted to study floating logs, the approach flow depth and log density had no significant effect on p . In addition, the log diameter, pier shape, branches, and the movable bed exhibited no apparent effect on p . The water viscosity and surface tension are assumed constant for all tests. Therefore, $\Pi_3 \dots \Pi_7$ are not included in the further analysis.

Table 5.2 Basic parameters for LW accumulation probability p

Parameters	
Log length	L_L [m]
Log diameter	d_L [m]
Pier diameter	d_P [m]
Approach flow velocity	v_o [m/s]
Approach flow depth	h_o [m]
Water density	ρ_W [kg/m ³]
Log / wood density	ρ_L [kg/m ³]
Gravitational acceleration	g [m/s ²]
Water surface tension	σ [kg/s ²]
Water viscosity	ν [m ² /s]

In addition to the non-dimensional parameters Π_{1-2} , a pre-factor x_n is introduced to account for uncongested versus semi-congested LW transport. Note that tests C29-C31 ($d_P = 0.01$ m), D11 ($\rho_L > 1'000$ kg/m³), and E22-E25 (congested LW transport) are not included in the fit equation, as the type of LW transport was not comparable to the majority of the test runs. The pre-factors and exponents of the governing parameters were quantified with a non-linear regression analysis. Accumulation probability p can therefore be defined by the normalized LW accumulation probability parameter LW_P :

$$LW_P = x_n \left(\frac{v_o^2}{2gL_L} \right)^{0.43} \left(\frac{d_P}{L_L} \right)^{0.60}$$

with

$$\begin{aligned} x_n &= 1.00 && \text{for uncongested LW transport} \\ x_n &= 0.65 && \text{for semi-congested and continuous LW transport} \end{aligned}$$

According to Eq. (5.6), L_L exhibits the largest effect on p , with an exponent of -1.03 , followed by v_o with an exponent of 0.86 , and d_P with 0.60 . For the present test range (Test series B-F, Table 4.2), LW accumulation probability at a single bridge pier for uncongested, semi-congested, and continuous LW transport can be described by the following relationship for $F_o = 0.08 \dots 1.2$ and $0 \leq LW_P \leq 0.53$ ($R^2 = 0.83$):

$$p = e^{-12.7 LW_P} .$$

Figure 5.24 shows p as a function of LW_P for uncongested, semi-congested, and continuous LW transport for test series B-F and Eq. (5.7). The Root Mean Squared Error (RMSE) of Eq. (5.7) is 0.094. The maximum accumulation probability $p_{\max} = 94\%$ results for $v_o = 0.20$ m/s, $L_L = 0.40$ m, and continuous addition of 40 logs with $LW_P = 0.019$. For $v_o \geq 1.0$ m/s (model scale) and $LW_P \geq 0.25$, p tends to zero.

For increasing number of bridge piers, the following recommendations can be summarized based on the relation between log length L_L and axial spacing between the piers:

- $L_L > axial\ spacing$: p resulted in $p \geq 50\%$ for uncongested and $p \geq 75\%$ for semi-congested LW transport for flow velocities ranging from $v_o = 0.20$ m/s up to ≈ 1 m/s (model scale). Therefore, cross-sections with two or more bridge piers are prone for LW accumulations. Further steps to evaluate the hazard potential are deemed necessary. As a next step it is recommended to estimate expected backwater rise due to spanwise accumulation and evaluate the adjacent flood embankments (Section 5.3.1.7).

- $L_L < \text{axial spacing}$: p should be determined using Eq. (5.7), as the accumulation process can be compared to the experiments with a single bridge pier. Given $p \geq 30\%$, backwater rise (Section 5.3.1.7) should be determined, as a LW accumulation can likewise form at a single bridge pier.

The practical application of Eq. (5.7) to determine the accumulation probability at bridge piers is demonstrated in a computational example, provided in Section 6.

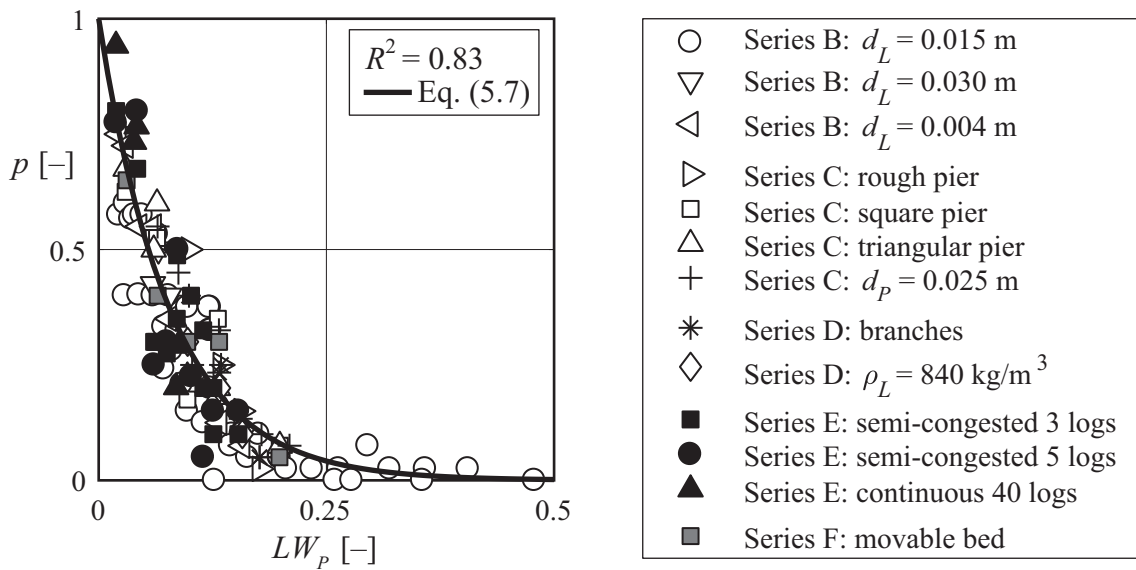


Figure 5.24 Normalized LW accumulation probability at a single bridge pier for Test series B-F, and Eq. (5.7) (black line)

As the experimental setup represents a worst-case scenario for p (non-parallel log placement directly upstream of bridge pier), the application of Eq. (5.7) is considered a conservative estimation. In Figure 5.25a, relative prediction error ε is plotted versus measured LW accumulation probability p . ε is defined as

$$\varepsilon = \frac{\text{predicted value} - \text{observed value}}{\text{observed value}} = \frac{e^{-12.7 LW_p} - p}{p}, \quad (5.8)$$

and describes the relative deviation of the proposed fit equation (Eq. (5.7)) compared to the observed accumulation probabilities p . The majority of the data points are within a $\pm 30\%$ prediction range, and ε decreases with increasing p . Note that seven data points are not shown in Figure 5.25a, as $\varepsilon > 1$. The residuals r defined as

$$r = p - e^{-12.7 LW_p}, \quad (5.9)$$

are plotted as a function of p in Figure 5.25b. A positive value of r indicates an underestimation of p , whereas a negative value of r corresponds to an overestimation of p . Based on the residuals plot, the proposed Eq. (5.7) tends to generally overestimate p , confirming a conservative approach. The residuals plot further indicates no clear pattern, and is clustered in the range of $r \pm 0.15$. However, the x -axis exhibits a slight unbalance, which is due to the majority of measurements in the range of $p < 0.5$.

An error propagation analysis was conducted for Eq. (5.7) to estimate the target value p and is summarized in Table 5.3. The procedure and formula are described in Section 4.3 and Eq. (4.6), respectively. The total error of p (e_{xp}) was determined for a range of input parameters, namely approach flow velocity v_o , gravitational acceleration g , log length L_L , pier diameter d_P , and pre-factor x_n . The corresponding total errors of the input parameters were estimated according to Section 4.3 and set to:

- v_o : ± 0.05 m/s
- g : ± 0 m/s²
- L_L : ± 0.001 m
- d_P : ± 0.001 m
- x_n : ± 0

The total error e_{xp} depends on p obtained with Eq. (5.7). The relative total errors $e_{xp,r}$ ($e_{xp,r} = e_{xp} / \bar{x}$) vary between 5.3% and 17.2% for the different input parameters; $e_{xp,r}$ is higher for low v_o and L_L . On average, $e_{xp,r}$ obtained with Eq. (4.6) of $\pm 10\%$ is small compared to the scatter of the final data evaluation (Figure 5.24 and Figure 5.25), but similar to the RMSE = 0.094 of Eq. (5.7).

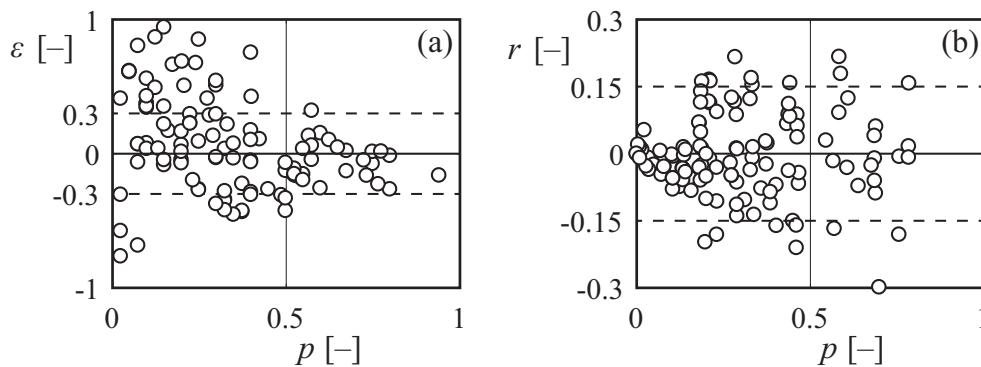


Figure 5.25 (a) relative prediction error ε versus measured LW accumulation probability p , and (b) residuals r versus p

Table 5.3 Total and relative error e_{xp} to estimate p with Eq. (5.7) for various input parameters

Input parameters					Eq. (5.7)	Total error	Relative error
v_o	g	L_L	d_P	x_n	p	e_{xp} Eq. (4.6)	$e_{xp,r}$
[m/s]	[m/s ²]	[m]	[m]	[-]	[-]	[-]	[%]
0.20	9.81	0.40	0.05	1	0.686	±0.056	8.1
0.50	9.81	0.40	0.05	1	0.437	±0.031	7.2
0.79	9.81	0.40	0.05	1	0.293	±0.020	6.9
0.97	9.81	0.40	0.05	1	0.231	±0.016	6.7
0.08	9.81	0.20	0.05	1	0.771	±0.133	17.2
0.20	9.81	0.10	0.05	1	0.421	±0.070	16.7
0.20	9.81	0.20	0.05	1	0.565	±0.077	13.6
0.20	9.81	0.10	0.025	1	0.285	±0.021	7.4
0.20	9.81	0.20	0.025	1	0.437	±0.033	7.5
0.20	9.81	0.40	0.05	0.65	0.783	±0.041	5.3

5.3 Large wood accumulation characteristics – Backwater rise and local scour

Parts of this subsection have been published in

- *Schalko et al. (2018a): “Backwater rise due to large wood accumulations”. Journal of Hydraulic Engineering.*
- *Schalko et al. (2018b): “Hazards due to large wood accumulations: Local scour and backwater rise”, in the proceedings of the 9th River Flow Congress in Lyon, France.*
- *Schalko et al. (2016): “Modeling the effect of organic fine material in a driftwood accumulation on backwater rise”, in the proceedings of the 8th River Flow Congress in St. Louis, USA.*

5.3.1 Backwater rise

Backwater rise due to LW accumulations was investigated in three test series (A-C; Section 4.5 and Table 4.3-Table 4.5). First, the results for series A with a predefined LW accumulation and a fixed bed are summarized and discussed in Sections 5.3.1.1-5.3.1.4. Second, the findings of series B with a natural LW accumulation and a fixed bed are presented in Section 5.3.1.5, followed by the results of series C with a natural LW accumulation and a movable bed in Section 5.3.1.6. The normalized results for all test series are summarized in Section 5.3.1.7.

5.3.1.1 Approach flow conditions

The effect of approach flow conditions, namely approach flow depth h_o and approach flow Froude number F_o , on backwater rise Δh was investigated in small-scale model tests with $\lambda = 30$ (A16-A21; Table 4.3; Section 4.5.6). The flume experiments were conducted in the range of $h_o = 0.05$ m, 0.10 m, 0.15 m and $F_o = 0.2 \dots 1.4$. Figure 5.26 shows two photos of test A47 with $F_o = 0.20$ compared to $F_o = 0.80$. In Figure 5.27a, Δh is plotted as a function of F_o for various h_o with all other parameters kept constant (A16-A18). The experiments for $h_o = 0.10$ m and 0.15 m could only be conducted for $F_o \leq 1.20$ and $F_o \leq 0.60$, respectively, as otherwise the 0.40 m high accumulation would have been overtopped.

According to Figure 5.26 and Figure 5.27, Δh increases linearly with increasing F_o . For $h_o = 0.10$ m and $F_o = 1.2$, Δh is 6.5 times higher compared to $F_o = 0.2$ (Figure 5.27a). Given a constant h_o , v_o and consequently the velocity head are higher for increasing F_o .

Due to the LW accumulation, v_o is reduced and the flow depth upstream of the accumulation h increases up to the energy head. The increase in energy for increasing F_o results in higher backwater rise. The flow depth downstream of the accumulation is equivalent to the approach flow depth h_o (Figure 4.9a). Given a constant h_o , the pressure gradient $\Delta p/\rho g = (h_o + \Delta h) - h_o = \Delta h$ increases for increasing F_o due to increased Δh . In contrast to the accumulation probability p (Section 5.2.3), F_o has a governing effect on backwater rise Δh . Based on Figure 5.27b, the data for all three h_o collapse when plotted against the relative backwater rise $\Delta h/h_o$. Consequently, h_o has no effect on $\Delta h/h_o$ for a given F_o .

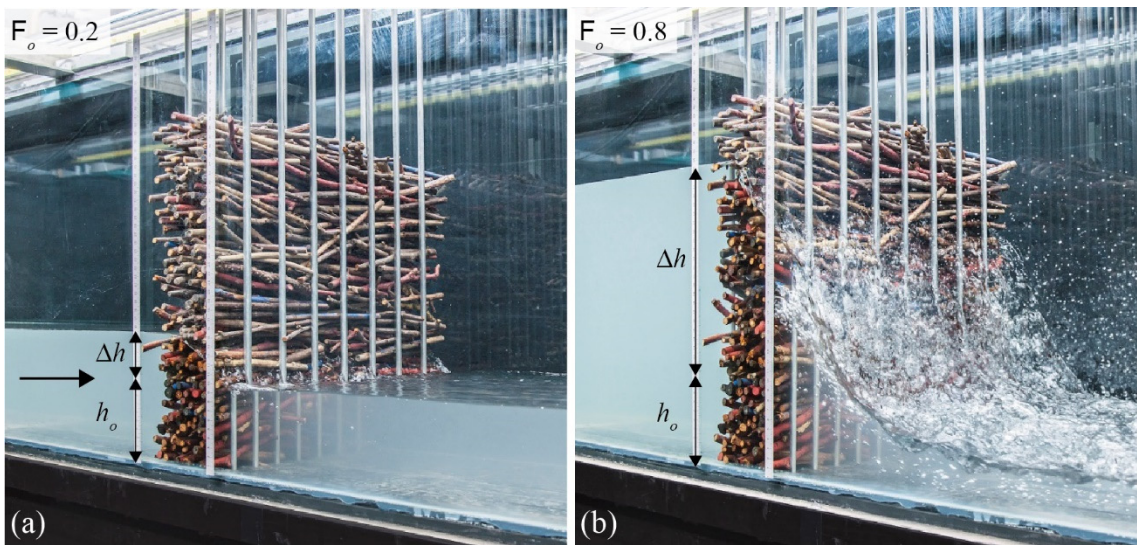


Figure 5.26 Δh for (a) $F_o = 0.2$, $Q = 8$ l/s and (b) $F_o = 0.8$, $Q = 32$ l/s with all other parameters kept constant ($h_o = 0.10$ m, $a = 3.3$, $L_A = 0.10$ m, and $d_{Lm} = 7$ mm; A47)

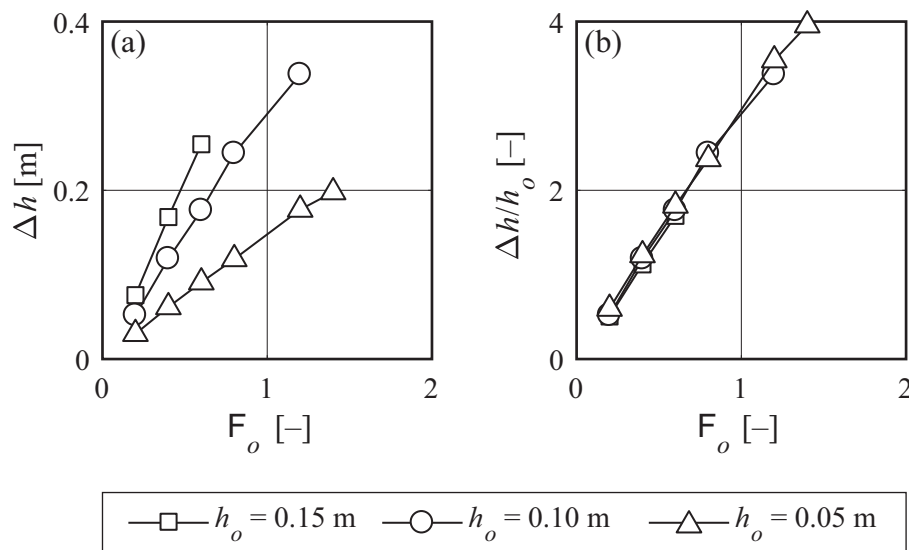


Figure 5.27 (a) Δh and (b) $\Delta h/h_o$ versus F_o for three different h_o with all other parameters kept constant ($d_{Lm} = 3.7$ mm, $L_A = 0.10$ m, and $a = 3.6$; A16-A18)

5.3.1.2 Large wood accumulation characteristics

The impact of (1) bulk factor a (Figure 5.28), (2) accumulation length L_A (Figure 5.29), and (3) mean log diameter d_{Lm} (Figure 5.30) on Δh were analyzed in tests A7-A15 and A22-A43 (Table 4.3; Section 4.5.6).

The compactness of a LW accumulation is described by the bulk factor a (Eq. (3.12)). It is comparable with the porosity parameter in groundwater flow, as it describes the flow through a certain medium. The two photos in Figure 5.28 indicate an increase of Δh for $a = 2.5$ (dense accumulation, A8) compared to $a = 4.3$ (loose accumulation, A11). In Figure 5.31a, $\Delta h/h_o$ is plotted as a function of F_o for various a with all other parameters kept constant (A8, A11, and A13). The experiments for $a = 2.5$ and $a = 3.3$ were limited to $F_o \leq 0.8$ to prevent an overtopping of the LW accumulation. For $F_o = 0.8$, Δh amounted to 0.30 m for $a = 2.5$ compared to $\Delta h = 0.14$ m for $a = 4.3$. Hence, Δh increases with decreasing a . A compact LW accumulation body represents a higher flow resistance due to lower porosity, leading to higher Δh . These findings were observed for all tested log diameters and approach flow conditions.

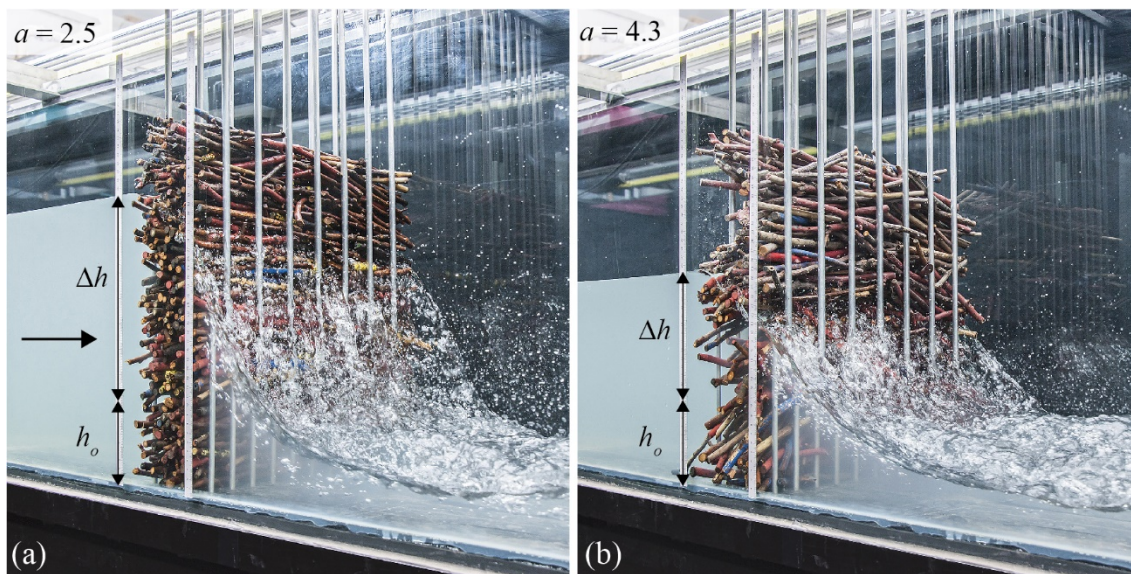


Figure 5.28 Δh for (a) $a = 2.5$ and (b) $a = 4.3$ with all other parameters kept constant ($h_o = 0.10$ m, $F_o = 0.8$, $L_A = 0.10$ m, $d_{Lm} = 7$ mm; A8 and A11)

The accumulation length was predefined based on the distance between the two racks and varied between $L_A = 0.05$ m (Figure 5.29a), 0.10 m, and 0.20 m (Figure 5.29b). In Figure 5.31b, $\Delta h/h_o$ is plotted as a function of F_o for various L_A , with all other parameters kept constant (A4, A34-35). The experiments for $L_A = 0.20$ m were limited to $F_o \leq 1.2$ to prevent an overtopping of the LW accumulation. For $F_o = 0.6$, Δh resulted in 0.08 m for $L_A = 0.05$ m compared to $\Delta h = 0.13$ m for $L_A = 0.20$ m. Since a long accumulation body exhibits a higher flow resistance, Δh increases linearly with increasing L_A .

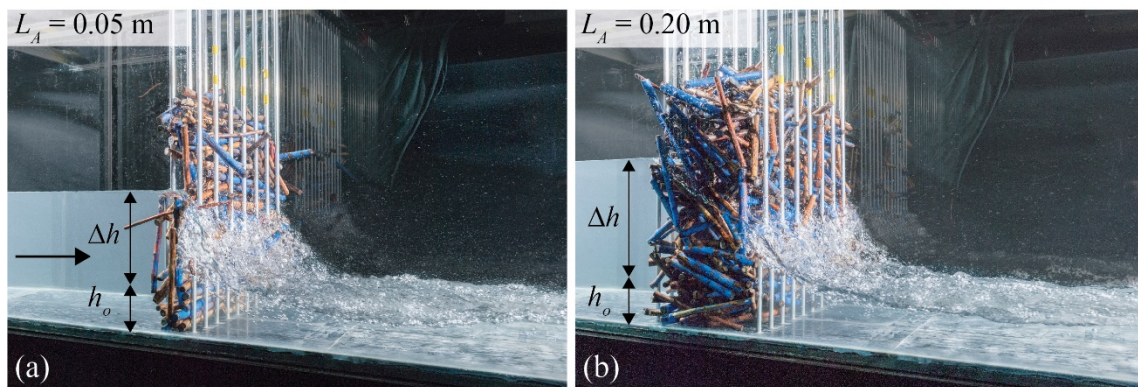


Figure 5.29 Δh for (a) $L_A = 0.05$ m and (b) $L_A = 0.20$ m with all other parameters kept constant ($h_o = 0.10$ m, $F_o = 1.2$, $d_{Lm} = 10.3$ mm, $a = 3.8$; A34-A35)

The effect of d_{Lm} on Δh was investigated in tests A39-A43 (Figure 5.30). The experiments were conducted for various d_{Lm} with all other parameters kept constant. In Figure 5.31c, $\Delta h/h_o$ is plotted as a function of F_o for the log diameters $d_{Lm} = 2.3$, 8.5 and 14 mm (A39-A41). For $F_o = 0.8$, $\Delta h = 0.24$ m for $d_{Lm} = 2.3$ mm compared to $\Delta h = 0.15$ m for $d_{Lm} = 14$ mm. Consequently, Δh increases with decreasing d_{Lm} . A small log diameter allows for more individual logs within an accumulation. Due to the higher number of logs, the flow is diverted more often and friction losses of the seepage flow increase, resulting in higher Δh . The accumulation with small d_{Lm} represents a consistent accumulation body whereas large d_{Lm} form a more inhomogeneous accumulation body. The overall flow resistance is consequently higher for smaller d_{Lm} .

In summary, backwater rise Δh increases with increasing F_o and L_A and decreasing a and d_{Lm} . Compared to F_o and a , the effect of L_A and d_{Lm} on Δh is rather small.

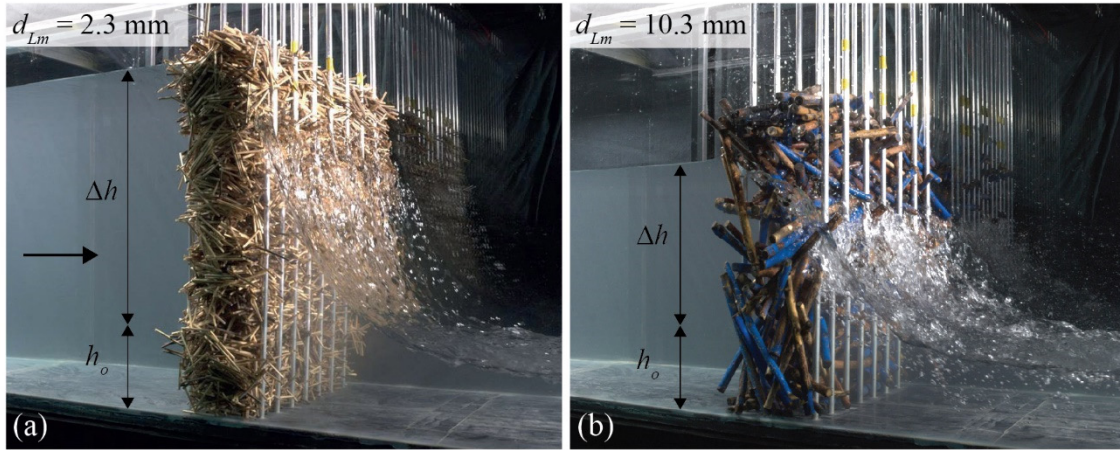


Figure 5.30 Δh for (a) $d_{Lm} = 2.3$ mm (A39) and (b) $d_{Lm} = 10.3$ mm (A4) with all other parameters kept constant ($h_o = 0.10$ m, $F_o = 1.2$, $L_A = 0.10$ m, $a \approx 3.7$)

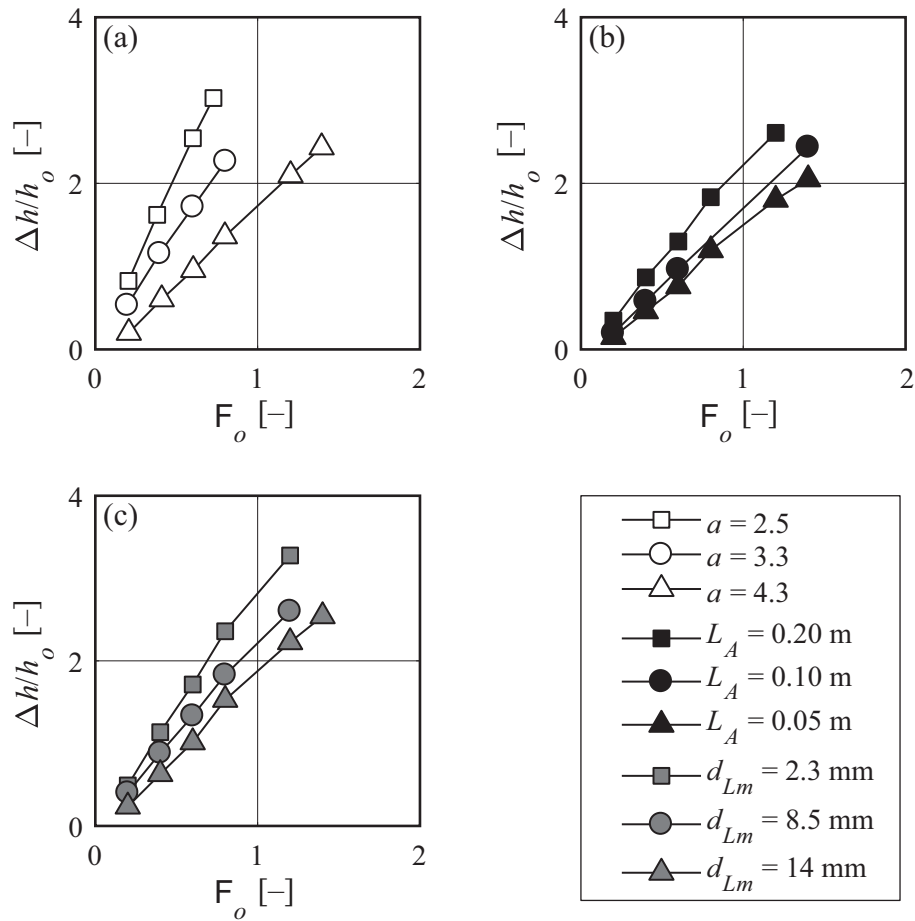


Figure 5.31 $\Delta h/h_o$ versus F_o for (a) three different a , $L_A = 0.10$ m, and $d_{Lm} = 7$ mm (Tests A8, A11, and A13), (b) three different L_A , $a = 3.8$, and $d_{Lm} = 10.3$ mm (A4, A34-A35), (c) three different d_{Lm} , $a = 3.6$, and $L_A = 0.10$ m (A39-A41)

5.3.1.3 Organic fine material

The effect of organic fine material FM in LW accumulations on backwater rise Δh was investigated in both small ($\lambda = 30$) and close-to-prototype ($\lambda = 6$) scale experiments (A44-A66, A75-94; Table 4.3). Branches and leaves were defined as FM (Section 4.5.6), so the effect of suspended fine material was not considered in this present study. Due to the ease of measurement, FM was included as a separate parameter (Section 4.5.4) and the parameters a and d_{Lm} correspond to the accumulation characteristics prior to the FM addition.

Figure 5.32a-d shows a photo series of the small-scale model tests and the increase of Δh for 0%, 2.5%, 5%, and 7.5% FM with all other parameters kept constant ($d_{Lm} = 13$ mm, $F_o = 0.4$, $h_o = 0.10$ m, $L_A = 0.10$ m, $a = 4.2$). The same parameter configuration but for $F_o = 0.8$ is illustrated in Figure 5.32e-h. For both $F_o = 0.4$ and $F_o = 0.8$, Δh is increasing with increasing FM .

In comparison, Figure 5.33a-h shows the increase of Δh for 0%, 5.5%, 11%, and $\approx 16.5\%$ FM in close-to-prototype model tests. The other parameters are $d_{Lm} = 65$ mm, $F_o = 0.30$, $h_o = 0.36$ m, and $a = 4.2$. In Figure 5.33a-d, FM consists of fir branches, whereas willow branches are illustrated in Figure 5.33e-h.

For all tested FM types, Δh increases with increasing FM . The branches and leaves within an accumulation decrease the porosity (i.e. decrease the bulk factor) and generate a higher flow resistance and a more heterogeneous flow path. This results in an increase of friction losses and consequently an increased Δh , as more potential energy and thus hydraulic head is required for the flow to seep through the accumulation body.

In Figure 5.34, $\Delta h/h_o$ is plotted as a function of F_o for increasing FM with all other parameters kept constant and $\lambda = 30$ (A63-A66). To prevent an overtopping of the accumulation body, the experiments for 5% and 7.5% FM were limited to $F_o \leq 1.2$ and $F_o \leq 0.8$, respectively. For $a = 4.2$ and $F_o = 0.6$, $\Delta h = 0.087$ m for $FM = 0\%$ compared to $\Delta h = 0.182$ m for $FM = 7.5\%$ (Figure 5.34a). In comparison, for $a = 2.8$ and $F_o = 0.6$, $\Delta h = 0.187$ m for $FM = 0\%$ compared to $\Delta h = 0.305$ m for $FM = 7.5\%$ (Figure 5.34b). Hence, Δh increases linearly with increasing FM .

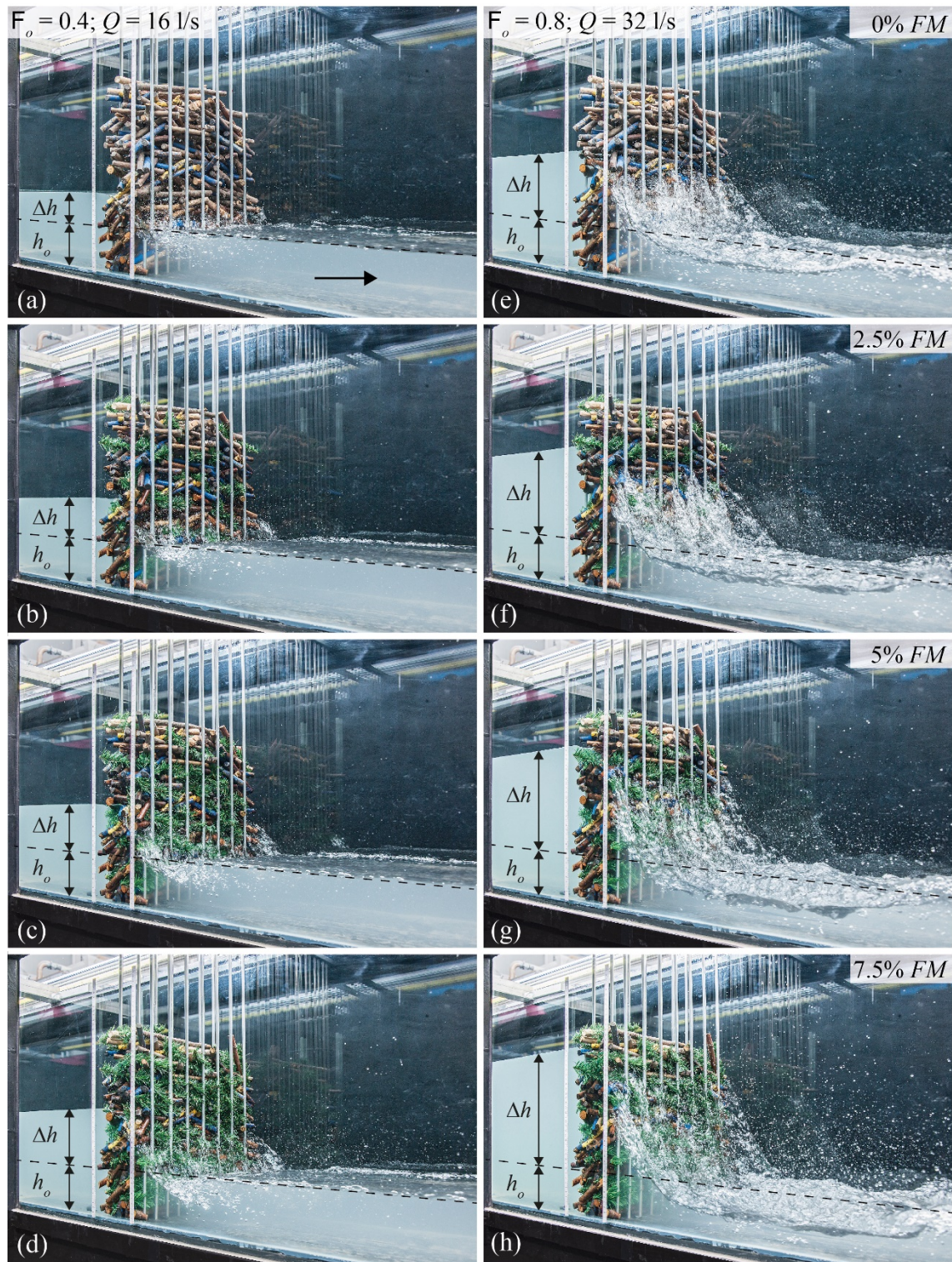


Figure 5.32 Δh with increasing FM and all other parameters kept constant ($h_o = 0.10 \text{ m}$, $a = 4.2$, $L_A = 0.10 \text{ m}$, and $d_{Lm} = 13 \text{ mm}$; A63-A66); (a-d) $F_o = 0.4$; (e-h) $F_o = 0.8$

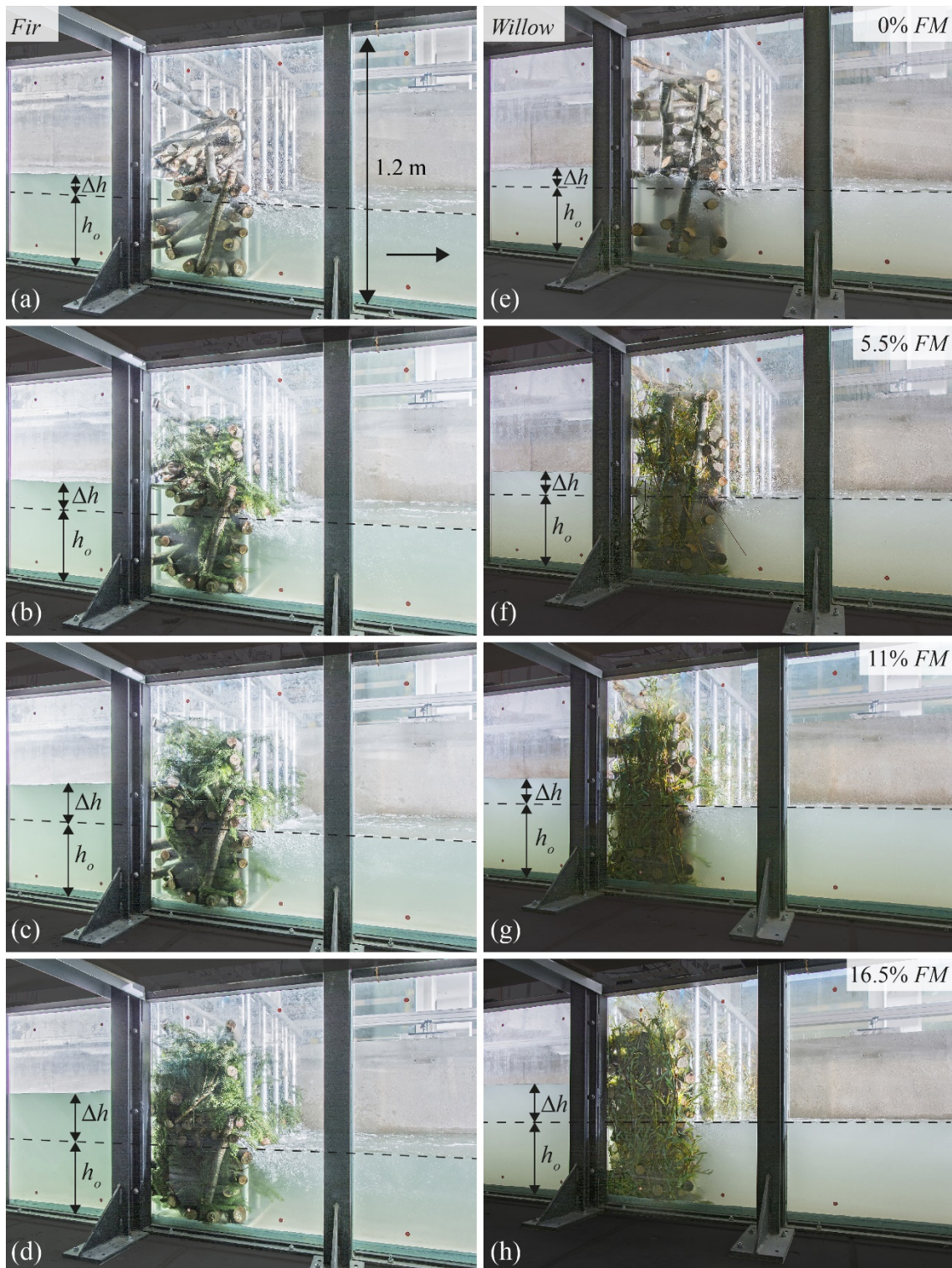


Figure 5.33 Δh with increasing FM and all other parameters kept constant ($F_o = 0.3$, $h_o = 0.36$ m, $a = 4.2$, $L_A = 0.50$ m, and $d_{Lm} = 65$ mm); (b-d) fir branches (A91-A94), and (f-h) willow branches (A83-A86)

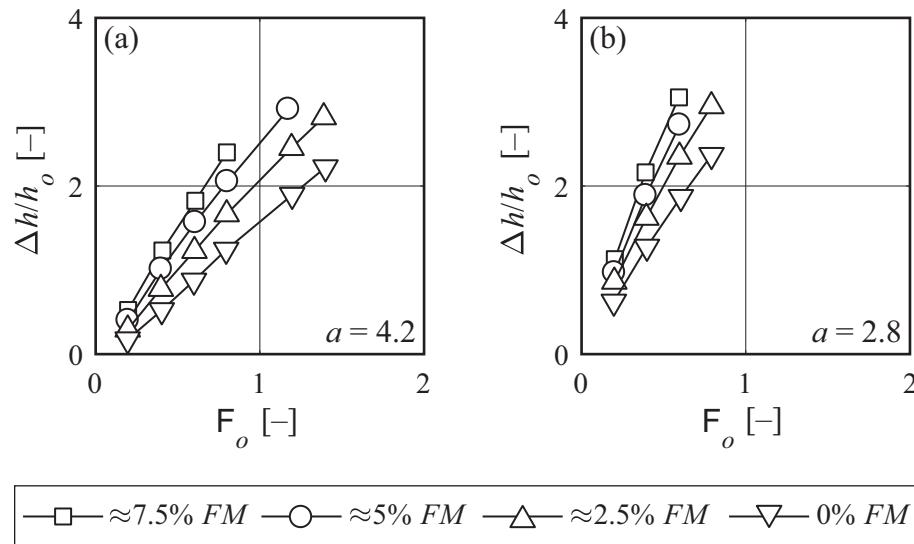


Figure 5.34 $\Delta h/h_o$ versus F_o for different % of organic fine material (FM) with all other parameters kept constant ($L_A = 0.10$ m, $d_{Lm} = 7$ mm); (a) loose LW accumulation $a = 4.2$ (A63-A66), (b) dense LW accumulation $a = 2.8$ (A55-A58)

To compare the effect of fir to willow branches, Δh is plotted as a function of h_o for various percentages of FM , with all other parameters kept constant and $\lambda = 6$ in Figure 5.35. The reproducibility tests without FM (A83, A91) resulted in an average relative standard error for Δh of 12%. For 5.5%, 11%, and $\approx 17\%$ FM , the relative standard errors for Δh varied between 0.2%...9.5% (A84-A86, A92-A94). The deviations in Δh decrease with increasing FM , as a more homogeneous accumulation is easier to install for higher FM percentages. Backwater rise was slightly higher for fir branches, due to the increased cumulative area of fir branches compared to willow branches. As the density of fir and willow branches are similar ($\rho_{FM,w} = 610$ kg/m³ and $\rho_{FM,f} = 600$ kg/m³), no effect of ρ_{FM} on Δh can be deduced. According to Figure 5.35, both types of FM are suited to model branches and leaves in an accumulation body, as both types result in a comparable backwater rise, and the deviations are within the range of reproducibility.

The results highlight the relevance of accounting for FM when estimating Δh . Based on the results for series A, FM affects the LW accumulation characteristics, leading to a smaller porosity (smaller a) and an increased flow diversion due to a longer and more sinuous flow path.

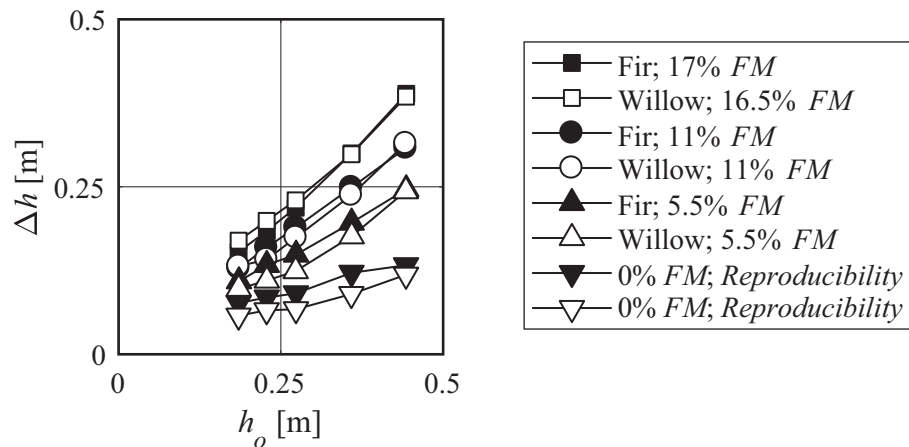


Figure 5.35 Δh versus h_o for different types and percentages of *FM* with all other parameters kept constant ($F_o = 0.3$, $a = 4.2$, $L_A = 0.50$ m, $d_{Lm} = 65$ mm; A83-A86 versus A91-A94)

5.3.1.4 Scale series

To determine possible scale effects, a scale series was investigated for different approach flow conditions and LW characteristics. The flume experiments were conducted for $\lambda = 50$ (A95-A106; Table 4.3), $\lambda = 30$ (A47-A49, A63-A65), and $\lambda = 6$ (A67, A75-A76, A83-A84). A photo series of the flume experiments with the three scale factors $\lambda = 6$, $\lambda = 30$, and $\lambda = 50$ is illustrated in Figure 5.36.

The results were upscaled to prototype dimensions according to Froude similitude (Heller 2011). Potential scale effects exist, if the results of the small-scale ($\lambda = 50$ and/or $\lambda = 30$) deviate significantly from the close-to-prototype model ($\lambda = 6$). In Figure 5.37a and b, Δh is plotted as a function of h_o for all investigated scale factors, with $a = 4.2$, without *FM* (A63, A91, A98), and with $\approx 5\%$ *FM* (A65, A92, A100), respectively. Backwater rise Δh is slightly smaller for $\lambda = 30$ compared to $\lambda = 50$ and $\lambda = 6$ (Figure 5.37a). The results for $a \approx 3.2$ are depicted in Figure 5.37c and d, comparing experiments without *FM* (A47, A83, A104) and with 5% *FM* (A49, A84, A106), respectively. The relative standard errors for Δh range from 2% up to 27% with an average relative standard error of 8.6%. The deviations decrease with increasing compactness (i.e. decreasing a) and increasing *FM*. For $a \approx 3.2$ and 5% *FM*, the average relative standard error amounts to 2.8% compared to 22% for $a \approx 4.2$ and 0% *FM*.

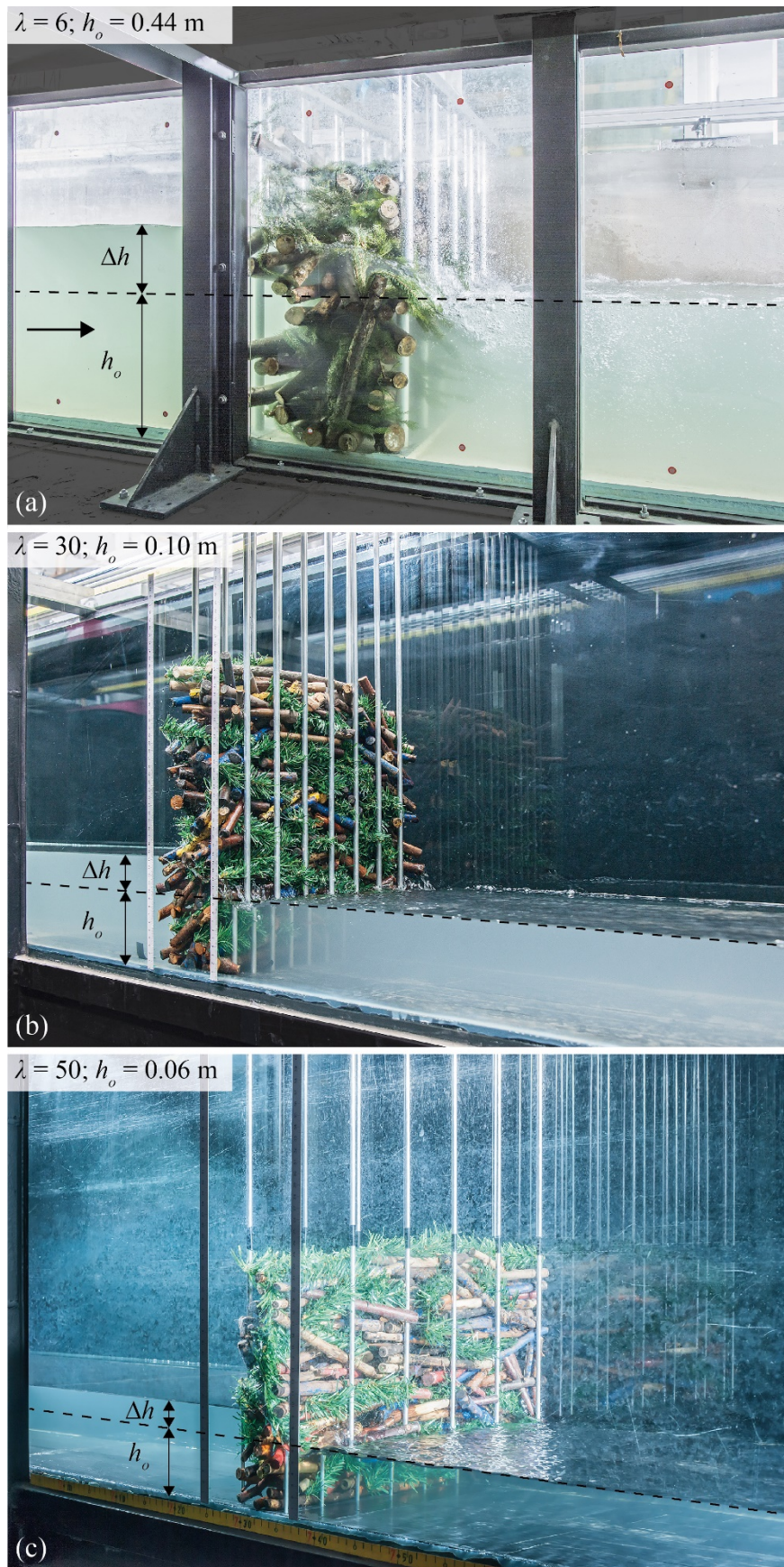


Figure 5.36 Δh for scale series with all other parameters kept constant ($F_o \approx 0.2$, $a \approx 4.2$, 5% FM); (a) $\lambda = 6$ (A92), (b) $\lambda = 30$ (A65), (c) $\lambda = 50$ (A100)

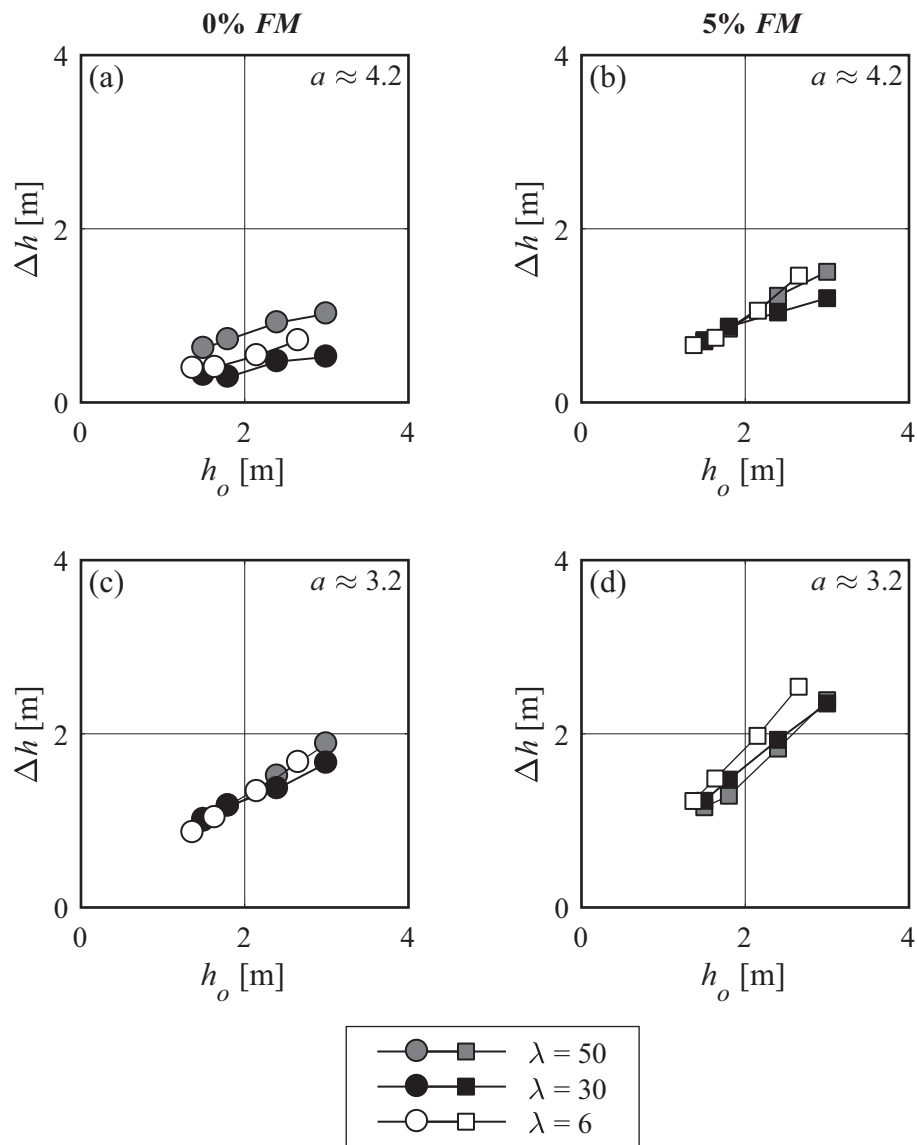


Figure 5.37 Δh versus h_o (prototype values) for three model scales ($\lambda = 50, 30, 6$); (a) $a = 4.2$ and 0% *FM* (A98, A63, A91), (b) $a = 4.2$ and 5% *FM* (A100, A65, A92), (c) $a \approx 3.2$ and 0% *FM* (A104, A47, A83), (d) $a \approx 3.2$ and 5% *FM* (A106, A49, A84)

Note that the comparably high deviations for a rather loose accumulation (e.g. for $a \approx 4.2$ and 0% *FM*) are due to the tests with $\lambda = 50$ and their manual model setup. For $\lambda = 50$, it was rather difficult to install an evenly distributed accumulation, especially close to the bottom. To allow an upscaling of the results with $\lambda = 50$, flow depths of $h_o \geq 0.03$ m had to be investigated, resulting in small effective flow cross-sections compared to the other two tested scales. However, the results from $\lambda = 50$ do not generally deviate from the two other scales and no scale effect can be identified based on the observed backwater rise.

The physical experiments were scaled according to Froude similitude (Section 4.2). As the flow through an accumulation is comparable to groundwater flow, possible scale

effects may exist due to the force ratio of inertia to viscosity, described by the Reynolds number R . The Reynolds number $R = (v_A d_{Lm})/\nu$ in the accumulation, with flow velocity in the accumulation $v_A = v_o/\phi$, and viscosity of water $\nu = 1.01 \cdot 10^{-6} \text{ m}^2\text{s}^{-1}$ for $T = 20^\circ\text{C}$, varied for all tests between $R = 375 \dots 3'200$ for $\lambda = 50$, compared to $R = 210 \dots 8'300$ for $\lambda = 30$, and $R = 6'000 \dots 37'000$ for $\lambda = 6$. $\Delta h/h_o$ is plotted versus R in Figure 5.38a for all tests, indicating two areas: $R < 10'000$ for $\lambda = 50$ and $\lambda = 30$ and $R > 5'000$ for $\lambda = 6$. The flow is in the fully turbulent regime for $R > 10'000$ (Section 4.2), so for $\lambda = 6$ the viscous force is largely independent of R . Given the same initial conditions, no clear trend of $\Delta h/h_o$ versus R , hence no viscous effects, for the different scales can be deduced (Figure 5.38b for $a \approx 3.2$ and Figure 5.38c for $a = 4.2$). As the relative standard errors for Δh are still within the range of reproducibility, it is assumed that possible scale effects can be neglected. Based on the conducted flume experiments and due to the ease of measurement and log dimensions, scale factors ≤ 50 are recommended.

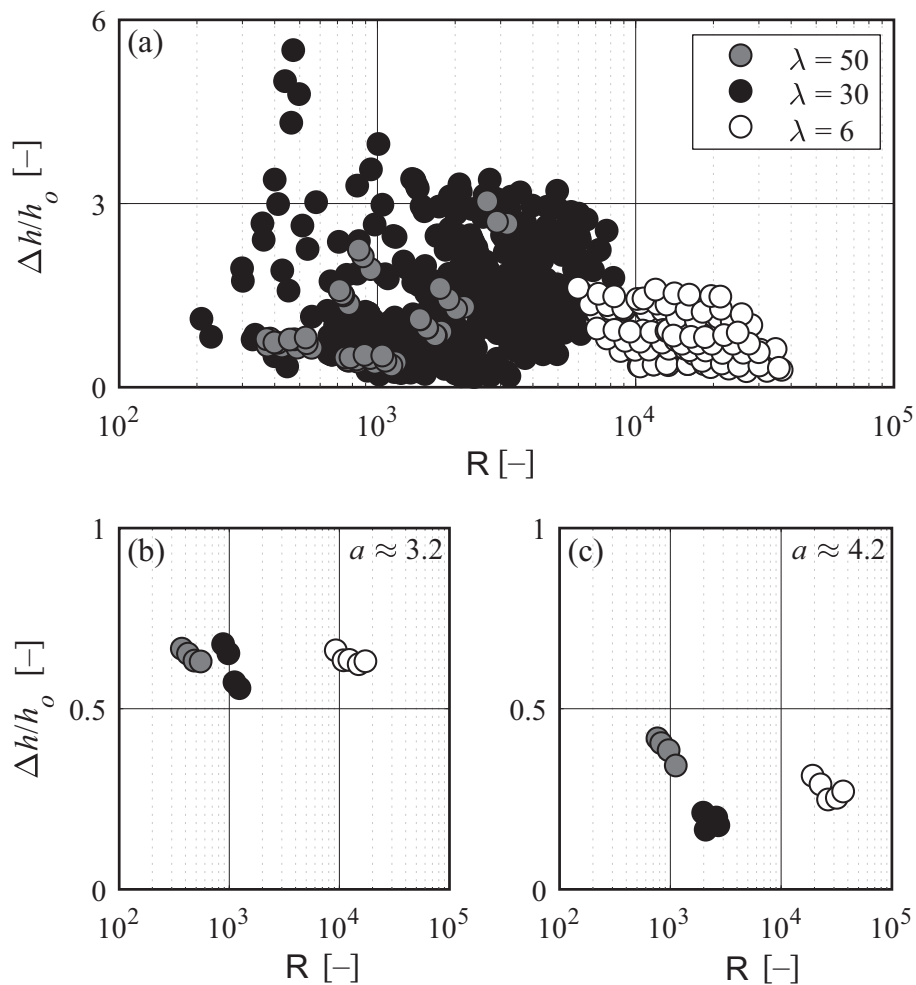


Figure 5.38 $\Delta h/h_o$ versus R for three model scales ($\lambda = 50, 30, 6$); (a) entire range of tested R , (b) $a \approx 3.2$ (A104, A47, A83), (c) $a = 4.2$ (A98, A63, A91)

5.3.1.5 Natural large wood accumulation

The impact of a natural LW accumulation on Δh was analyzed in test series B for $\lambda = 30$ and $\lambda = 6$ and a fixed bed (Table 4.4; Section 4.5.6), as well as in test series C for $\lambda = 30$ and a movable bed (Table 4.5; Section 4.5.6). To model a natural LW accumulation, a given LW volume was added continuously along the transverse section of the flume to achieve a homogeneous accumulation across the rack (Figure 5.39a). In comparison, test series A simplified the LW accumulation as box-shaped (Figure 5.39b).

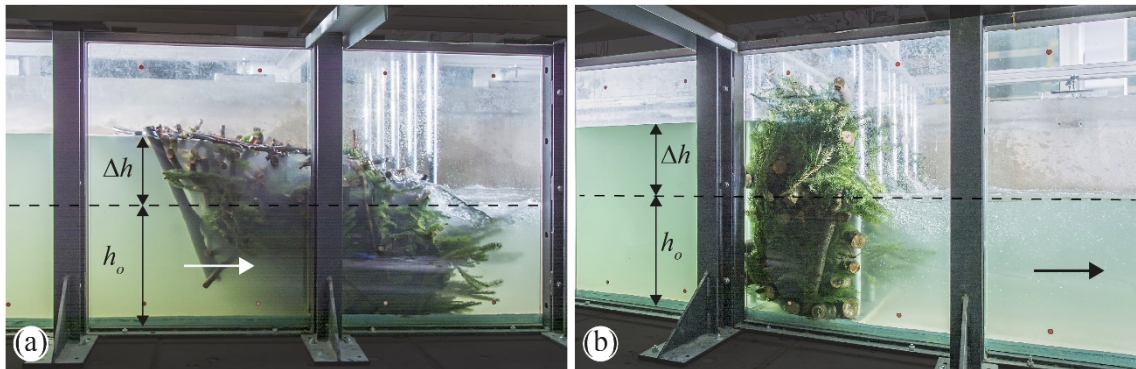


Figure 5.39 (a) Natural (B5) and (b) predefined LW accumulation (A94) with $V_s = 0.240 \text{ m}^3$, $\lambda = 6$, $Q = 370 \text{ l/s}$, $h_o = 0.440 \text{ m}$, $d_L = 35 \text{ mm}$, and $FM \approx 17\%$

A photo series of the formation of a LW accumulation and backwater rise Δh for increasing relative added LW volume, i.e. $V_{s,rel} = V_s/(Bh_o^2)$ (total added $V_s = 0.540 \text{ m}^3$) is illustrated in Figure 5.40 (B6). The first 10% to 20% of added LW (Figure 5.40a) hit the retention rack at water level h_o . As the upper portion of the rack is blocked, the flow velocity below the accumulation is increasing and the flow is deflected downward. Additional LW is dragged to the bottom part of the cross-section, thereby extending the LW accumulation vertically downwards. For $V_{s,rel} \leq 40\%$ (Figure 5.40b), the shape can be approximated as box-like. Once the entire cross-section is blocked (Figure 5.40c and d), the LW accumulation changes to a trapezoidal or triangular shape. Additional LW then starts to form a “LW carpet”. Backwater rise due to the formation of the LW carpet leads only to a minor decrease of flow velocity (Figure 5.40e) compared to the first percentages of added LW. However, additional LW volume still increases flow resistance and compactness of the LW accumulation, thereby increasing backwater rise. Due to the smaller accumulated area for the natural setup, the resulting backwater rise for the same amount of wood was lower ($\Delta h = 0.29 \text{ m}$; B5) compared to the predefined, box-shaped setup ($\Delta h = 0.39 \text{ m}$; A94).

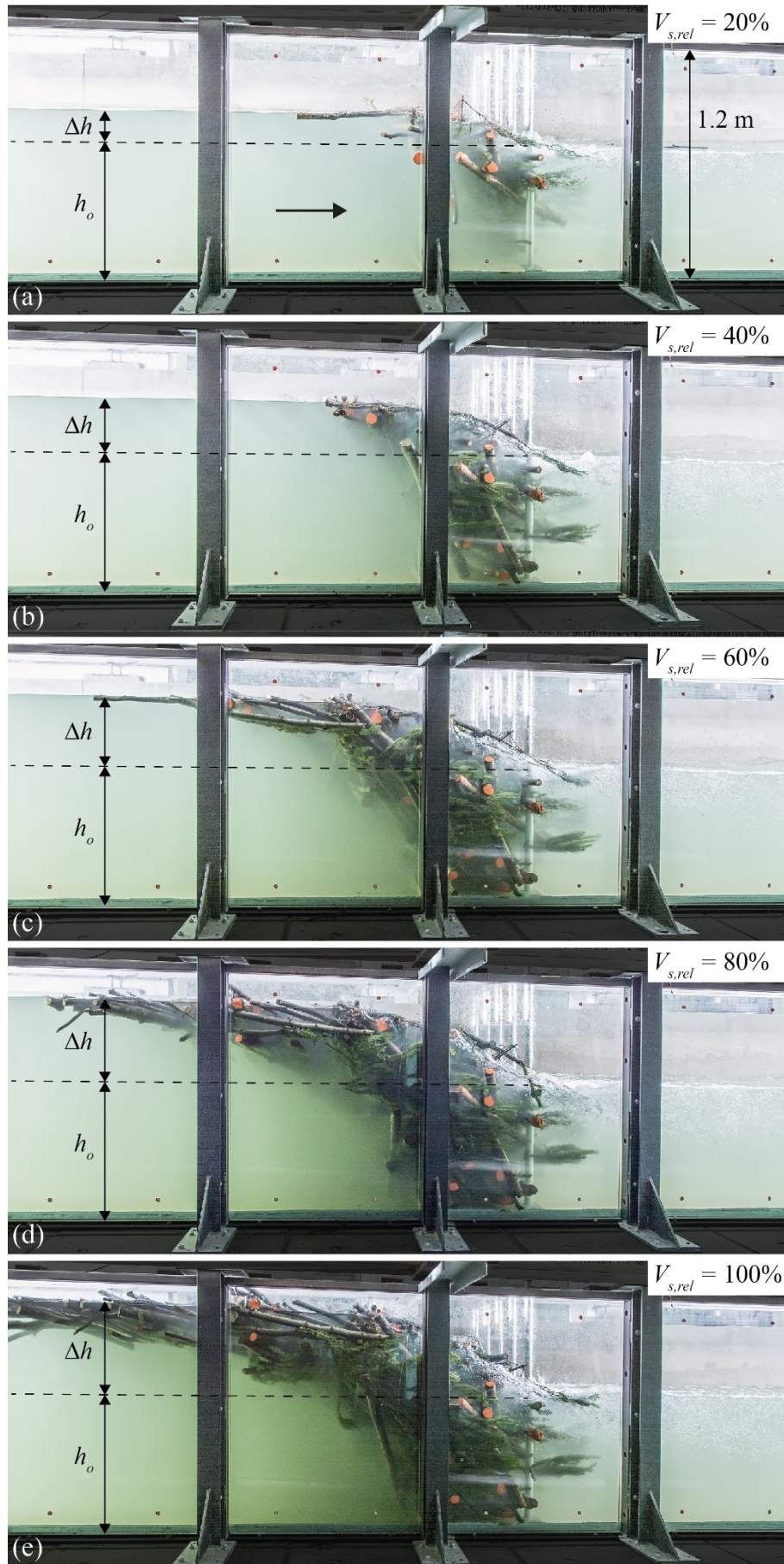


Figure 5.40 Development of a LW accumulation for (a)-(e) $V_{s,rel} = 20-100\%$ and $\lambda = 6$ (B6)

The definition of the LW volume generating the primary backwater rise prior to the formation of a LW carpet is of particular relevance for flood hazard assessment. This volume is herein defined as the characteristic LW volume V_c , leading to the main increase of backwater rise and attributed to the LW volume accumulated along the rack. V_c was determined for the experiments with a natural LW accumulation, i.e. test series B and C.

- (1) *Reference development of $\Delta h/h_o = f(V_{s,rel})$* : For the majority of the model tests in series B, the amount of added LW volume was equal to test series A. This enabled a direct comparison of the effect of LW accumulation shape on $\Delta h/h_o$. However, the formation of a LW carpet was not observed for all tests, as the amount of added wood was too small. For test series C, the added LW volume was increased by a factor of 5 to exhibit a LW carpet. Relative backwater rise as a function of the relative added LW volume $V_{s,rel}$, was plotted for every test (series B and C) and the development approximated with a fit equation in the general form of:

$$\frac{\Delta h}{h_o} = a \cdot \left(\frac{V_s}{Bh_o^2} \right)^b. \quad (5.10)$$

The pre-factor and exponents (a , b) were altered for each test to best fit the development of $\Delta h/h_o = f(V_{s,rel})$. An example for series B and C is illustrated in Figure 5.41.

- (2) *Definition of V_c for $\Delta h/h_o = f(V_{s,rel})$* : The derivatives of Eq. (5.10) y' were obtained to illustrate the relative change of $\Delta h/h_o$ as a function of $V_{s,rel}$ for all tests (Figure 5.41). The characteristic LW volume V_c corresponds to $V_{s,rel}$, where the derivate, or relative change of $\Delta h/h_o = 0.10$. Given two times the volume of V_c , $\Delta h/h_o$ then only increases by 10%. V_c therefore corresponds to the primary backwater rise. Based on the values for $V_{s,rel}$ at $y' = 0.10$, V_c was then determined for all tests. The values for V_c , relative characteristic LW volume V_c/Bh_o^2 , F_o , and d_m are summarized in Table 5.4. In both test series, relative V_c increases with increasing F_o . The V_c corresponds to the start of the LW carpet formation (i.e. decreased flow velocities upstream of the accumulation). For low F_o , v_o is smaller and may decrease sooner to allow the formation of a LW carpet, so the corresponding wood volume, i.e. V_c is smaller. In addition, tests with smaller grain size diameter $d_m = 2.65$ mm (e.g. $F_o = 0.47$) indicate a slightly higher V_c compared to tests with $d_m = 13.1$ mm (e.g. $F_o = 1.53$). As scour formation increases for decreasing d_m , the flow cross-section below the accumulation increases, and logs are pulled downwards. This process may

delay the LW carpet formation, so the required wood volume to block the cross-section, i.e. V_c , increases.

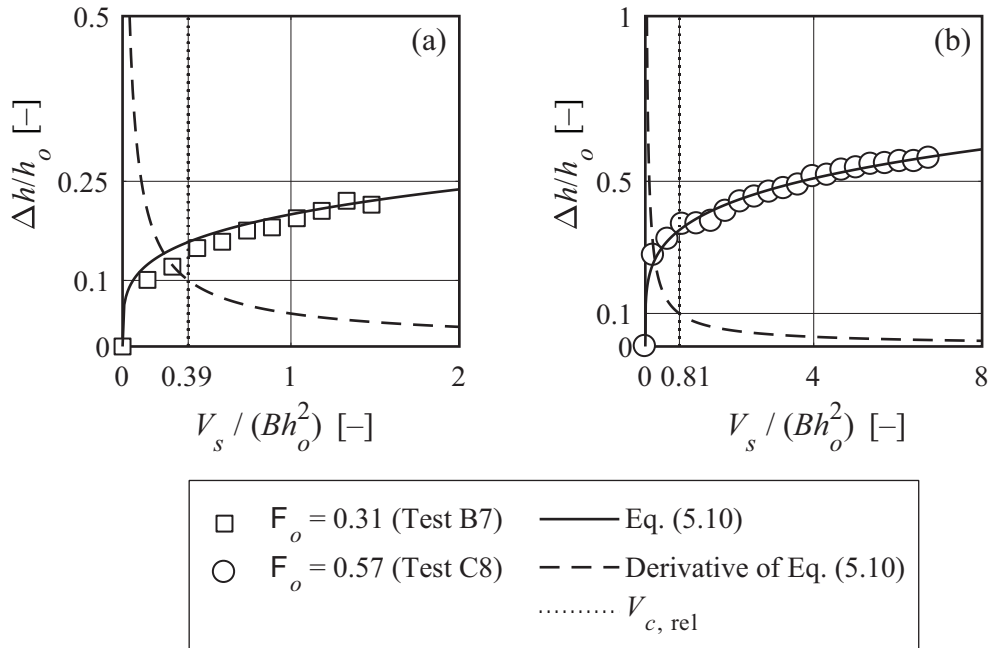


Figure 5.41 Relative backwater rise $\Delta h/h_o$ versus relative solid LW volume $V_{s,rel}$ with Eq. (5.10), derivative of Eq. (5.10), and characteristics LW volume V_c for test (a) B7, and (b) C8

Table 5.4 Relative characteristic LW volume, F_o , and d_m for test series B and C

Tests (Table 4.4/Table 4.5)	V_c [m ³]	$V_c/(Bh_o^2)$ [-]	F_o [-]	d_m [mm]
B1-B3	0.247	0.86	0.27	
B4	1.487	1.75	0.30	
B5	1.342	4.54	0.27	
B6	2.651	4.91	0.28	
B7	0.002	0.39	0.31	
B8	0.005	1.31	0.62	
B9	0.019	4.71	1.46	
B10	0.010	2.39	0.63	
C1-C3	0.004	1.45	0.74	5.4
C4-C5	0.004	0.78	0.68	5.4
C6-C7	0.008	1.07	0.65	5.4
C8	0.003	0.81	0.57	2.7
C9	0.004	0.65	0.51	2.7
C10	0.005	0.47	0.47	2.7
C11	0.003	3.68	1.53	13.1
C12	0.006	2.94	1.24	13.1

(3) *Normalized V_c* : The obtained V_c were then normalized as a function of the approach flow conditions (F_o and h_o), channel width B , and bed material characteristics (d_m).

The ratio of V_c/Bh_o^2 (relative V_c) corresponds to the required wood volume to block an idealized box-shape cross-section of the dimensions $B \times h_o \times h_o$. As only selected experiments were conducted with FM (B5, B6, B10), the effect of FM on V_c has not yet been included. For series B, V_c can be expressed for $F_o = 0.3 \dots 1.5$ ($R^2 = 0.89$) as

$$\frac{V_c}{Bh_o^2} = 3.1F_o. \quad (5.11)$$

For test series C, V_c can be described for $F_o = 0.5 \dots 1.5$ ($R^2 = 0.98$) as

$$\frac{V_c}{Bh_o^2} = 3.1F_o \left(\frac{h_o}{d_m} \right)^{-0.20}. \quad (5.12)$$

Note that Eq. (5.11) describes a linear relationship between relative V_c and F_o . In comparison, Eq. (5.12) further includes the relative submergence h_o/d_m to account for the effect of the bed material. The data points and Eqs. (5.11)-(5.12) are illustrated in Figure 5.42. The application of Eqs. (5.11)-(5.12) allows the estimation of the required wood volume to block a box-shape cross-section until a LW carpet forms, corresponding to the main increase in backwater rise. This simplifies the flood hazard assessment, as the estimation of the effective or potential LW volume (Section 2.4) is associated with high uncertainties. For further analyses in the present thesis, the ratio of V_s/V_c will be used instead of V_s in percentages. Note that the ratio of $V_s/V_c = 1$, corresponds to the main increase in backwater rise. In contrast, the percentage of V_s is only based on the total amount of added LW during the flume experiment, which was randomly selected and has no physical meaning.

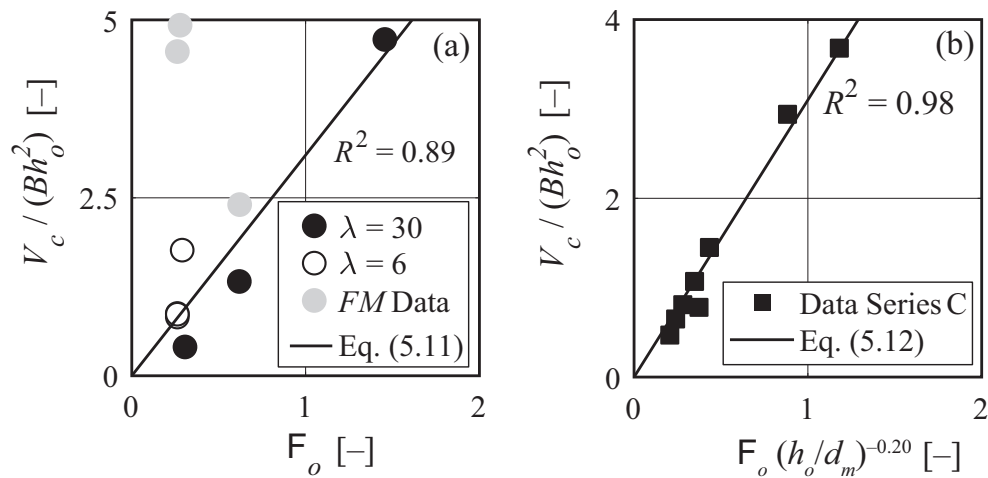


Figure 5.42 V_c / Bh_o^2 versus (a) F_o for test series B (data with FM are plotted in grey), Eq. (5.11); (b) $F_o (h_o/d_m)^{-0.20}$ for test series C, Eq. (5.12)

During floods, the compactness of LW accumulations may exhibit values of $a = 2 \dots 5$; $a = 2$ represents a dense and $a = 5$ a loose accumulation (Lange and Bezzola 2006). Figure 5.43 shows a box-plot of the bulk factors a of the natural accumulations, obtained with the videometric analysis for test series B and C. On average, $a \approx 4$ for both series B and C. With increasing V_s/V_c , the scatter and values decrease. As the accumulation becomes more compact, a decreases, leading to an increase of Δh .

The LW accumulation Froude number $F_A = v_A/(gh)^{1/2}$ with $v_A = Q/(Bh)$ and $h = \Delta h + h_o$ is plotted as a function of V_s/V_c for different initial approach flow Froude numbers F_o and test series B in Figure 5.44a compared to test series C in Figure 5.44b. For $V_s/V_c \geq 0.20$, the approach flow conditions already change due to the LW accumulation and backwater rise. F_A decreases rapidly until reaching a value of $\approx 0.20 \dots 0.40$ for $V_s/V_c \geq 1$, which corresponds to the initiation of the LW carpet.

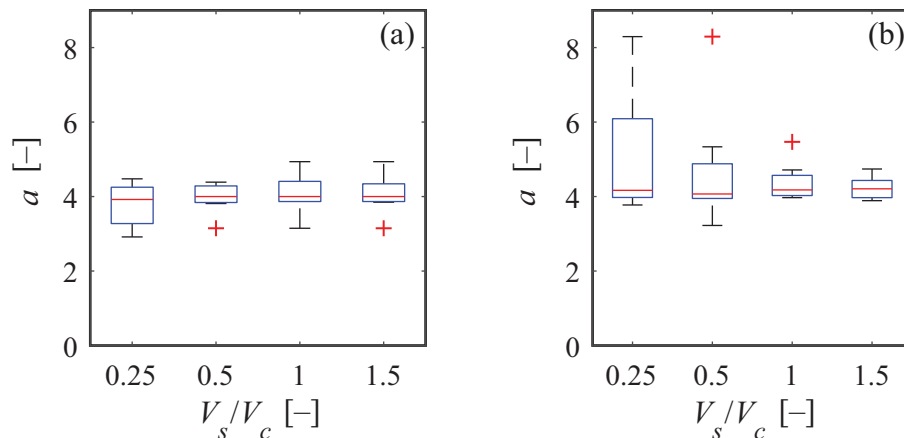


Figure 5.43 a versus V_s/V_c for (a) test series B (B1-B4; B7-B9), (b) test series C

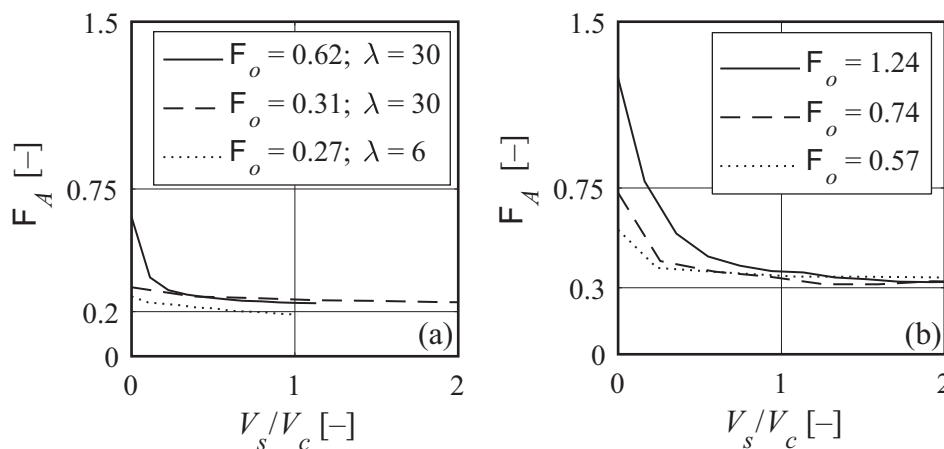


Figure 5.44 F_A versus V_s/V_c for (a) test series B (B1-B4; B7-B9), (b) test series C

In Figure 5.45a, $\Delta h/h_o$ is plotted as a function of V_s/V_c for test series B, $\lambda = 30$, $F_o = 0.31$, $F_o \approx 0.62$ with 0% *FM* compared to 8% *FM*, and $F_o = 1.46$. Similar to test series A, $\Delta h/h_o$ increases with increasing F_o . For $V_s/V_c = 0.3$, $\Delta h/h_o \approx 0.10$ for $F_o = 0.31$ compared to $\Delta h/h_o = 0.71$ for $F_o = 0.62$, and $\Delta h/h_o = 1.96$ for $F_o = 1.46$. For $V_s/V_c = 0.5$ and $F_o \approx 0.62$, $\Delta h/h_o$ resulted in 0.80 for *FM* = 0% compared to $\Delta h/h_o = 1.5$ for *FM* \approx 8%. Hence, $\Delta h/h_o$ increases with increasing *FM*. The results confirm the findings of series A (Section 5.3.1.3). The accumulation becomes more compact and the flow path more heterogeneous due to the addition of *FM*. The results further foster the relevance to account for *FM* when estimating Δh . In Figure 5.45b, $\Delta h/h_o$ is shown as a function of V_s/V_c for test series B, both model scales (\bullet for $\lambda = 30$ versus \circ for $\lambda = 6$), and $F_o \approx 0.30$. The development as well as the value of $\Delta h/h_o$ for $V_s/V_c = 0.5$ are similar for both scales. Given $V_s/V_c = 0.5$, $\Delta h/h_o = 0.12$ for $\lambda = 30$ compared to $\Delta h/h_o = 0.18$ for $\lambda = 6$. Backwater rise Δh is higher for $\lambda = 6$. Schmocker and Hager (2013) also investigated two different scales ($\lambda = 1$ and 2) for Δh due to natural LW accumulations. The final value for $V_s = 50 \text{ dm}^3$ resulted in $\Delta h/h_o = 1.5$ for $\lambda = 1$ and $\Delta h/h_o = 1.3$ for $\lambda = 2$. Their findings confirm that $\Delta h/h_o$ can also be investigated in small-scale model tests (Section 5.3.1.4).

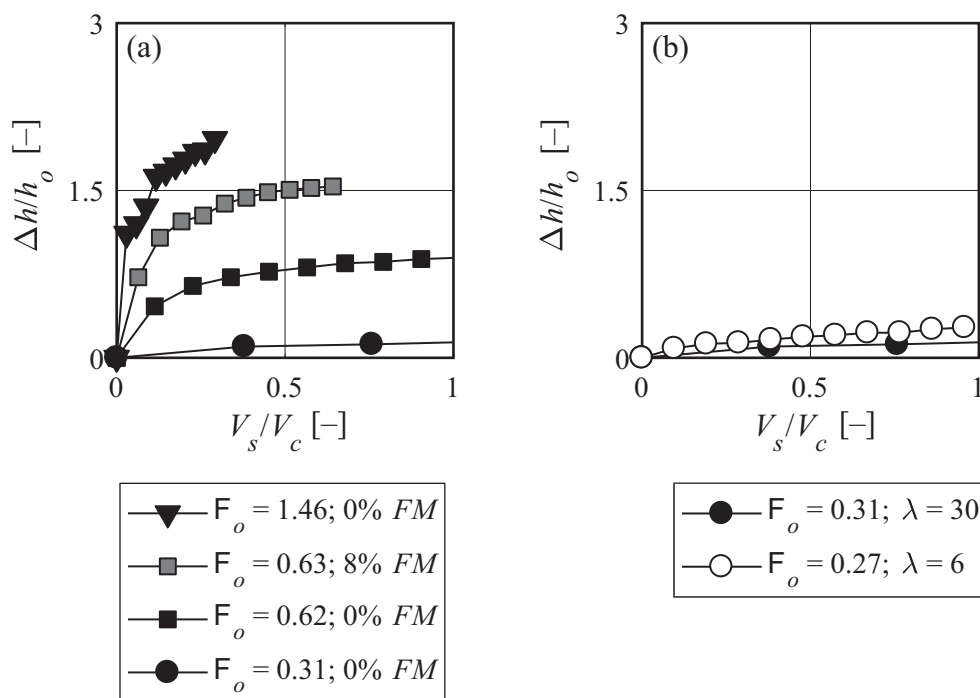


Figure 5.45 $\Delta h/h_o$ versus V_s/V_c with (a) $F_o = 0.31$, $F_o \approx 0.62$ with 0% *FM* compared to 8% *FM*, and $F_o = 1.46$ for $\lambda = 30$ (B1-B4), (b) $F_o \approx 0.30$ and $\lambda = 30$ compared to $\lambda = 6$ (B1 versus B7)

5.3.1.6 Bed material

The formation of a natural LW accumulation with a movable bed is illustrated in a photo series for increasing V_s in Figure 5.46 (C10, Table 4.5).

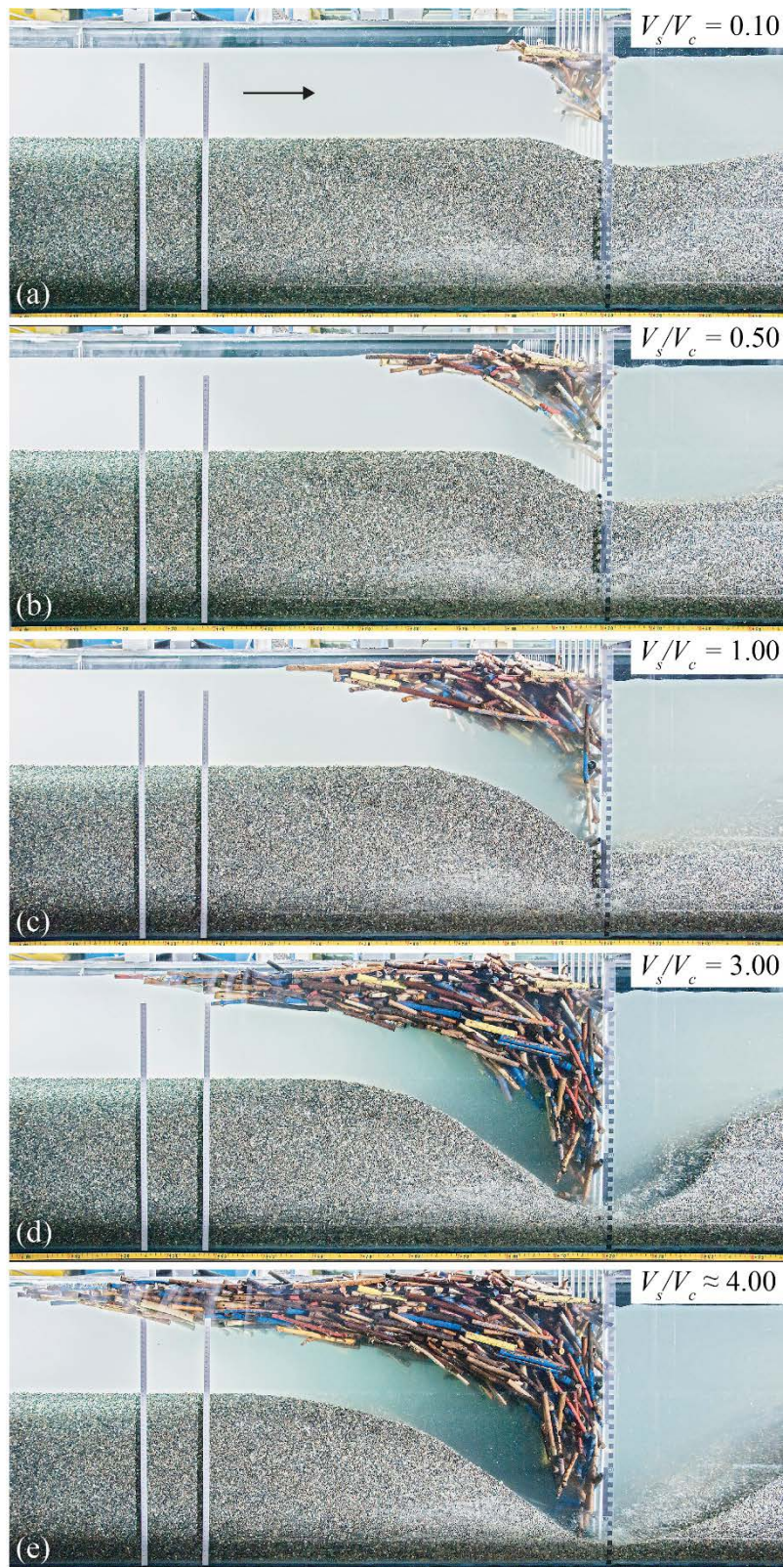


Figure 5.46 LW accumulation with a movable bed for (a)-(e) $V_s/V_c = 0.10-4.00$ and $\lambda = 30$ (C10)

The LW accumulation forms similar to test series B (Figure 5.40). However, due to the movable bed, every LW package leads to a scour formation. Compared to a fixed bed, the LW accumulation extends further vertically downwards, as the scour increases the open cross-sectional area (Figure 5.46a and b). The LW accumulation shape is triangular for $V_s/V_c = 0.50$ (Figure 5.46b). A “LW carpet” starts forming for $V_s/V_c \geq 1.00$ (Figure 5.46c). Due to the increasing scour depth for increasing V_s , logs may still be dragged to the bottom part of the cross-section for $V_s/V_c = 3.00 \dots 4.00$ (Figure 5.46d and e). The accumulation body consequently expands both vertically towards the bottom and horizontally backwards as a LW carpet, with a final quasi-triangular shape.

Figure 5.47a compares $\Delta h/h_o$ versus V_s/V_c for a fixed and a movable bed with $F_o \approx 0.60$ and $\lambda = 30$. The development of $\Delta h/h_o$ as a function of V_s/V_c is similar for both bed types. However, for $V_s/V_c = 1$, $\Delta h/h_o = 0.89$ for a fixed bed compared to $\Delta h/h_o = 0.37$ for a movable bed. A movable bed enables scour formation, thereby increasing the open flow cross-section of the retention structure and its discharge capacity. Figure 5.47b shows the relative backwater rise $\Delta h/h_o$ as a function of V_s/V_c for various F_o and uniform bed material with $d_m = 2.7$ mm (C8-C10). Similar to the results with a fixed bed (Figure 5.45), $\Delta h/h_o$ increases with increasing F_o . It can be observed that $V_s/V_c \leq 1$ generate the main increase of Δh (Section 5.3.1.5).

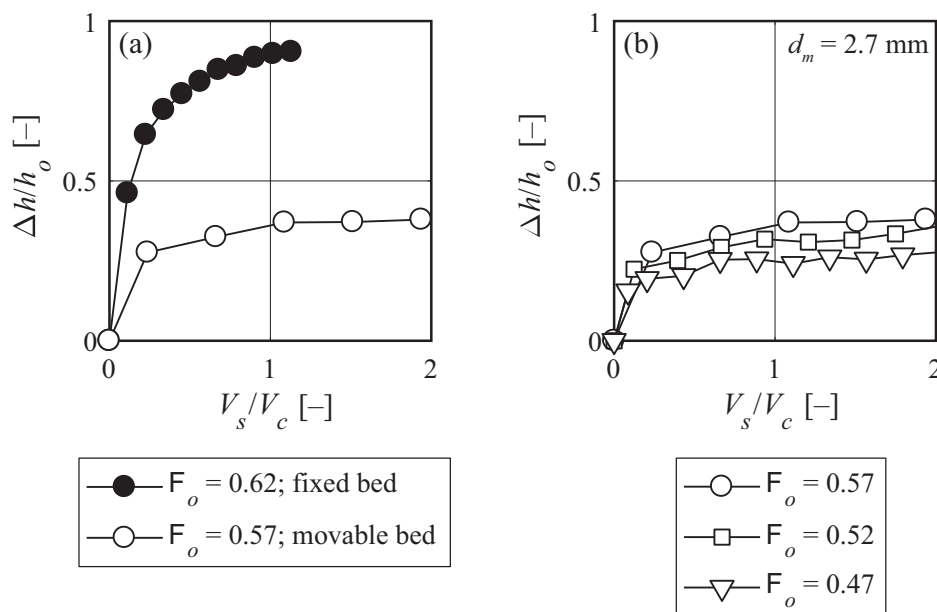


Figure 5.47 $\Delta h/h_o$ versus V_s/V_c with (a) fixed (B8) and movable bed (C8), $F_o \approx 0.60$, and $\lambda = 30$, (b) movable bed, different F_o , $d_m = 2.7$ mm, and $\lambda = 30$ (C8-C10)

5.3.1.7 Normalized backwater rise: Design equations

The governing parameters are discussed in order to generalize from and predict the observed effects on backwater rise resulting from LW accumulations. First, the results are normalized for series A with a predefined LW accumulation and a fixed bed. Second, normalized backwater rise is presented for series B and C with a natural LW accumulation and a fixed versus a movable bed. Third, backwater rise is normalized as a function of LW volume.

Predefined LW accumulation with a fixed bed

Backwater rise Δh is described by the basic parameters listed in Table 5.5 and by Eq. (5.13):

$$\Delta h = f(L_A, d_L, L_L, V_{FM}, V_l, V_s, h_o, v_o, \rho_w, \rho_L, g, \sigma, \nu). \quad (5.13)$$

Table 5.5 Basic parameters for backwater rise due to LW accumulation with a fixed bed

Parameters	
Accumulation length	L_A [m]
Log diameter	d_L [m]
Log length	L_L [m]
Organic fine material volume	V_{FM} [m ³]
Loose large wood volume	V_l [m ³]
Solid large wood volume	V_s [m ³]
Approach flow depth	h_o [m]
Approach flow velocity	v_o [m/s]
Water density	ρ_w [kg/m ³]
Wood density	ρ_L [kg/m ³]
Gravitational acceleration	g [m/s ²]
Water surface tension	σ [kg/s ²]
Water viscosity	ν [m ² /s]

The selected $n = 13$ independent parameters include $r = 3$ reference dimensions ([M] mass, [L] length, [T] time). Therefore, $n - r = 10$ non-dimensional parameters Π_{1-10} need to be defined based on a dimensional analysis. Π_{1-10} are the approach flow Froude

number $\Pi_1 = v_o/(gh_o)^{1/2}$, flow diversion u $\Pi_2 = L_A/d_L$, relative organic fine material volume FM $\Pi_3 = V_{FM}/V_s$, bulk factor a $\Pi_4 = V_l/V_s$, relative LW density $\Pi_5 = \rho_L/\rho_w$, relative accumulation length $\Pi_6 = L_A/L_L$, relative log length $\Pi_7 = L_L/d_L$, relative velocity head $\Pi_8 = v_o^2/(2gL_L)$, Reynolds number $\Pi_9 = (v_A d_{Lm})/\nu$, and Weber number $\Pi_{10} = (\rho_w v_o^2 h_o)/\sigma$. The log length and wood density were not varied systematically in this study. The water viscosity and surface tension are assumed constant for all tests. The Reynolds number for the three investigated scales varied in a wide range, but has no significant effect on the resulting backwater rise. Therefore, $\Pi_5 \dots \Pi_{10}$ are not included in the further analysis. Backwater rise due to LW accumulation can be described as a functional relationship with parameters increasing backwater rise in the numerator and parameters decreasing backwater rise in the denominator, i.e.

$$\text{Backwater rise} \sim \frac{F_o, u, FM}{a} \quad (5.14)$$

Based on the dimensional analysis, the exponents of the governing parameters were quantified with a non-linear regression analysis. The dimensionless LW accumulation factor LW_A is defined as:

$$LW_A = \frac{F_o u^{1/3} (9FM + 1)}{a^{4/3}} \quad (5.15)$$

According to Eq. (5.15), a exhibits the largest effect on Δh with an exponent of $-4/3$, followed by the linear effects of both F_o and FM percentage. The flow diversion $u = L_A/d_{Lm}$ shows a minor effect on Δh with an exponent of $1/3$. Based on LW_A , $\Delta h/h_o$ can be described by a linear relationship for $F_o = 0.2 \dots 1.4$ and $LW_A = 0 \dots 1.0$ ($R^2 = 0.95$):

$$\frac{\Delta h}{h_o} = 5.4LW_A \quad (5.16)$$

In Figure 5.48, $\Delta h/h_o$ is plotted as a function of LW_A for series A ($\lambda = 50$, $\lambda = 30$, and $\lambda = 6$), Eq. (5.16), and $\pm 20\%$ prediction range. All data collapse with the proposed design equation. The standard errors of the determined coefficients (i.e. governing parameters) vary between 0.008 and 0.29, whereas the lowest value represents the flow diversion u and the highest value the organic fine material FM . The higher standard error for FM is due to the uncertainties in the experimental determination of the FM percentages. The Root Mean Square Error (RMSE) of Eq. (5.16) applied to the experimental data amounts to 0.185.

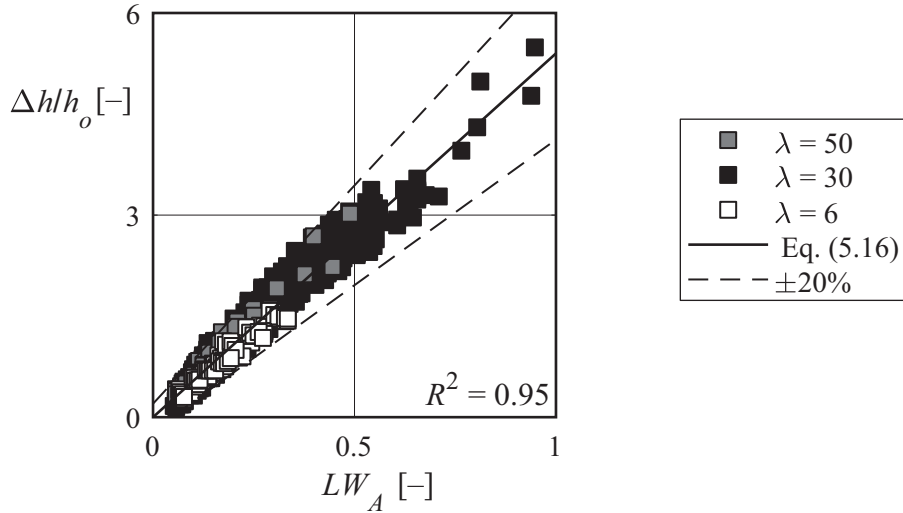


Figure 5.48 $\Delta h/h_o$ versus LW_A for series A ($\lambda = 50$, $\lambda = 30$, and $\lambda = 6$), Eq. (5.16), and $\pm 20\%$ prediction range

In Figure 5.49, relative prediction error ε is plotted versus measured relative backwater rise $\Delta h/h_o$, with ε defined as:

$$\varepsilon = \frac{\text{predicted value} - \text{observed value}}{\text{observed value}} = \frac{5.4LW_A - \Delta h/h_o}{\Delta h/h_o}. \quad (5.17)$$

In addition, ε is plotted for the different scales (Figure 5.49b for $\lambda = 50$, Figure 5.49c for $\lambda = 30$, and Figure 5.49d for $\lambda = 6$). A positive value of ε indicates an overestimation of $\Delta h/h_o$, whereas a negative value of ε corresponds to an underestimation of $\Delta h/h_o$. The majority of the data points are within a $\pm 30\%$ prediction range, and ε decreases with increasing $\Delta h/h_o$. Note that for $\lambda = 30$ and $\Delta h/h_o < 0.50$, data points exhibit $1 \geq \varepsilon > 0.3$. These comparably high deviations are due to IDM fluctuations for $Q < 10$ l/s. For low Q , the effective LW volume is small and it was rather difficult to install a homogeneous compactness of the accumulation, especially in the lower part. However, Eq. (5.16) overestimates $\Delta h/h_o$ (positive values for ε), so the application is a conservative approach.

The residuals $r = \text{observed value} - \text{predicted value}$, i.e.:

$$r = \frac{\Delta h}{h_o} - 5.4LW_A, \quad (5.18)$$

are plotted as a function of $\Delta h/h_o$ in Figure 5.50a for all data. Again, r is illustrated separately for the different investigated scales in Figure 5.50b-d. In contrast to ε , a positive value of r indicates an underestimation of $\Delta h/h_o$. The residuals plot indicates no clear pattern (Figure 5.50a) and the majority of the data points are clustered in the range of $r \pm 0.30$.

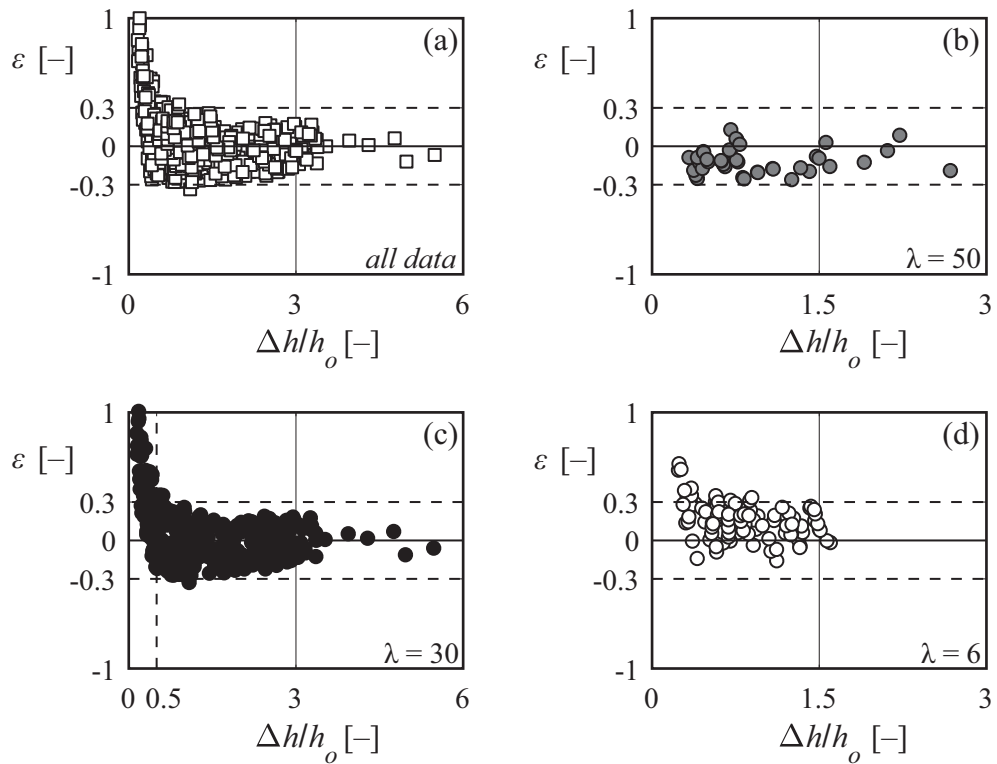


Figure 5.49 Relative prediction error ε versus measured relative backwater rise $\Delta h/h_o$ for (a) all data, (b) $\lambda = 50$, (c) $\lambda = 30$, and (d) $\lambda = 6$

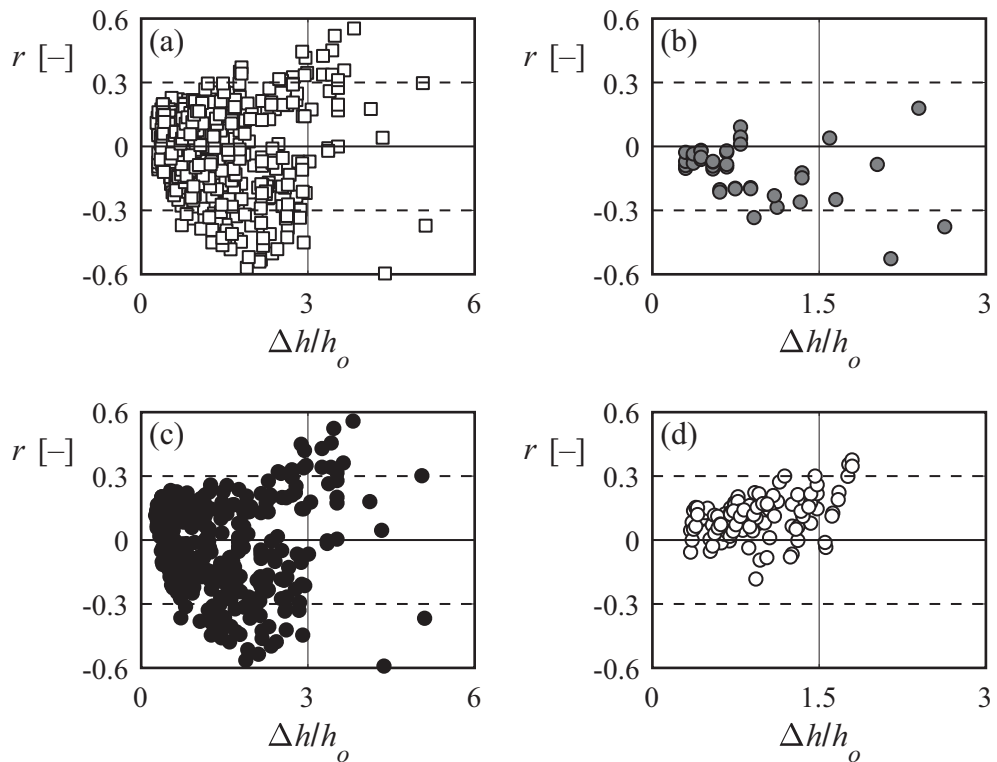


Figure 5.50 Residuals r versus measured relative backwater rise $\Delta h/h_o$ for (a) all data, (b) $\lambda = 50$, (c) $\lambda = 30$, and (d) $\lambda = 6$

An error propagation analysis was conducted for Eq. (5.16). As the target value $\Delta h/h_o$ also exhibits an error due to the measurement of the flow depths, an error propagation was also performed for $\Delta h/h_o$. The resulting total ($e_{X\Delta h}$) and relative errors ($e_{X\Delta h,r} = e_{X\Delta h}/\bar{x}$) are then a sum of the errors obtained for Eq. (5.16) and $\Delta h/h_o$. The error propagation analysis was conducted for a range of input parameters, summarized in Table 5.6 and Table 5.7. The total errors for the input parameters were set to:

- Q : $\pm 1\%$ – h_o : ± 0.001 m – d_L : ± 0.001 m
- B : ± 0.002 m – a : $\pm 10\%$ – FM : $\pm 5\%$
- g : ± 0 m/s² – L_A : ± 0.001 m – Δh : ± 0.001 m

Note that the total error for the approach flow Froude number F_o consists of the errors for Q , B , g , and h_o . Based on $e_{X\Delta h}$ for the various input parameter configurations, a regression analysis was performed to determine the prediction range. Compared to the relative errors of Eq. (5.16) with $\pm 13.4\% \dots 19.8\%$, the resulting relative errors of $\Delta h/h_o$ are rather small with $\pm 0.3\% \dots 5.8\%$. The sum of relative errors $e_{X\Delta h,r}$ vary between 13.9% and 22.3% for the different input parameters, resulting in a prediction range of $\pm 20\%$, similar to the scatter of the final data evaluation (Figure 5.48).

Table 5.6 Total and relative error $e_{X\Delta h}$ of Eq. (5.16) for various input parameters

Input parameters								Eq. (5.16)	Total error	Relative error
Q	B	g	h_o	a	L_A	d_L	FM	LW_A	$e_{X\Delta h}$ Eq. (4.6)	$e_{X\Delta h,r}$
[l/s]	[m]	[m/s ²]	[m]	[-]	[m]	[mm]	[%]	[-]	[-]	[%]
48	0.4	9.81	0.10	3.6	0.10	3.7	0	0.655	± 0.106	16.1
32	0.4	9.81	0.10	3.3	0.10	7	0	0.397	± 0.057	14.2
55	0.4	9.81	0.10	3.8	0.10	10.3	0	0.498	± 0.069	13.8
8	0.4	9.81	0.10	2.4	0.10	10.3	0	0.133	± 0.018	13.8
16	0.4	9.81	0.10	3.9	0.05	2.3	0	0.183	± 0.036	19.7
6	0.4	9.81	0.05	4.0	0.20	2.3	0	0.296	± 0.059	19.8
3	0.4	9.81	0.05	4.2	0.10	13	5	0.090	± 0.013	14.0
301	1.5	9.81	0.39	3.1	0.50	35	15	0.329	± 0.045	13.7
165	1.5	9.81	0.27	4.2	0.50	65	5	0.104	± 0.014	13.4
1.3	0.4	9.81	0.03	3.2	0.06	4	2.5	0.134	± 0.022	16.5

Table 5.7 Total and relative error $e_{X\Delta h}$ of $\Delta h/h_o$ for various input parameters

Input parameters		Measured data	Total error	Relative error
h_o	Δh	$\Delta h/h_o$	$e_{X\Delta h}$ Eq. (4.6)	$e_{X\Delta h,r}$
[m]	[m]	[-]	[-]	[%]
0.10	0.335	3.535	± 0.035	1.0
0.10	0.227	2.144	± 0.025	1.2
0.10	0.244	2.689	± 0.026	1.0
0.10	0.085	0.721	± 0.013	1.8
0.10	0.082	0.986	± 0.013	1.3
0.05	0.086	1.597	± 0.040	2.5
0.05	0.024	0.488	± 0.022	4.5
0.39	0.561	1.776	± 0.004	0.3
0.27	0.164	0.560	± 0.004	0.8
0.03	0.023	0.724	± 0.042	5.8

As the experimental setup represents a worst-case scenario (Figure 5.39b), the application of Eq. (5.16) is a conservative estimation. The proposed design equation is especially useful for flood hazard assessment. For a given LW accumulation, the resulting backwater rise (Eq. (5.16)) can be estimated for varying approach flow conditions. Based on the topography of the surroundings, critical cross-sections or river infrastructures can be identified. In addition, the pole height of LW retention racks can be designed with Eq. (5.16). To apply Eq. (5.16), the approach flow Froude number and flow depth can be estimated using discharge measurements of previous floods. The log diameter can be derived from forest inventories. Values for the accumulation length and the bulk factor should be based on collected data of floods with extensive LW transport. If no data are available, L_A and a can be estimated with a sensitivity analysis. For added safety, a should be chosen in the range of 2 to 3. In addition, the effect of branches and leaves should be considered for the estimation of Δh . Again, a sensitivity analysis on the effect of varying percentages of FM on Δh is recommended.

Natural accumulation, fixed versus movable bed

Backwater rise due to a predefined LW accumulation can be estimated with Eq. (5.16). Due to the setup of a natural accumulation, the bulk factor a and the accumulation length L_A are not predefined, but rather a function of approach flow conditions and LW volume. To estimate $\Delta h/h_o$ for a natural accumulation, the following approximations are made:

The bulk factor a was obtained with a videometric analysis for test series B (B7-B9). Based on a regression analysis, a can be approximated for $F_o = 0.3 \dots 1.5$ ($R^2 = 0.87$) using

$$a \approx (5 - 1.35F_o). \quad (5.19)$$

Similar to Eq. (3.13) to estimate the LW carpet length by Schmocker and Hager (2013), an increasing F_o leads to a more compact accumulation body. Given the same h_o , increasing F_o implies increasing v_o , so the acting hydraulic force (Eq. (5.2)), i.e. drag force is likewise higher, resulting in a denser accumulation.

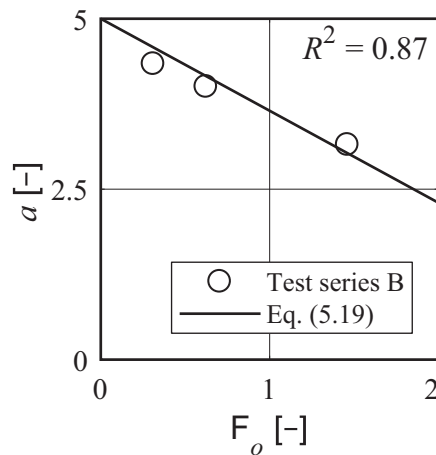


Figure 5.51 Bulk factor a versus F_o for test series B (B7-B9) and Eq. (5.19)

As the shape of a natural accumulation is not rectangular, an equivalent LW accumulation length L_A was defined. This equivalent length L_A corresponds to an ideal rectangular LW accumulation with a defined height of h_o and width B . Therefore, an equivalent $u = L_A/d_{Lm}$ can also be obtained for irregular, non-box-shaped LW accumulation shapes. L_A is then calculated using V_l , h_o , and B as:

$$L_A = \frac{V_l}{h_o B} \quad \text{and} \quad u = \frac{L_A}{d_{Lm}} = \frac{V_l}{h_o B d_{Lm}} = \frac{a V_s}{h_o B d_{Lm}}. \quad (5.20)$$

In Figure 5.52a, $\Delta h/h_o$ is plotted as a function of the dimensionless LW accumulation factor LW_A (Eq. (5.16)). In the plot are included tests with a predefined accumulation

(test series A), a natural accumulation with a fixed bed (test series B), and a movable bed (test series C). For a given V_s , d_{Lm} , and a , $\Delta h/h_o$ can be compared for the different setups. The experiments with the predefined accumulation (selected tests of series A with similar d_{Lm} and a compared to series B and C) are defined as a reference with the slope for LW_A of 1. The resulting slope for the natural accumulation of LW_A equals $\approx 3/5$ for a fixed bed and $\approx 1/3$ for a movable bed. Therefore, a natural accumulation results in smaller backwater rise compared to a predefined accumulation, mainly due to the larger open flow area and a decrease in flow resistance. A movable bed further decreases backwater rise due to scour formation. To account for the natural LW accumulation and the movable bed in Eq. (5.16), an accumulation type factor f_A ($R^2 = 0.97$) can be added. Combined with Eq. (5.20), it results to:

$$\frac{\Delta h}{h_o} = 5.4 f_A LW_A = 5.4 f_A \frac{F_o u^{1/3} (9FM + 1)}{a^{4/3}} = 5.4 f_A \frac{F_o (L_A/d_L)^{1/3} (9FM + 1)}{a^{4/3}}, \quad (5.21)$$

$$\frac{\Delta h}{h_o} = 5.4 f_A \frac{F_o (aV_s/h_o B d_L)^{1/3} (9FM + 1)}{a^{4/3}} = 5.4 f_A \frac{F_o (V_s/h_o B d_L)^{1/3} (9FM + 1)}{a}$$

$f_A = 1.00$ for predefined accumulation (test series A),

$f_A = 0.55$ for natural accumulation with fixed bed (test series B), and

$f_A = 0.30$ for natural accumulation with movable bed (test series C).

Figure 5.52b shows $\Delta h/h_o$ as a function of $f_A LW_A$ for selected data points of test series A (similar d_{Lm} and a), test series B and C, Eq. (5.21), and $\pm 20\%$ prediction range. All data collapse with the proposed design equation and the Root Mean Square Error (RMSE) of Eq. (5.21) applied to the experimental data amounts to 0.15. Eq. (5.21) extends the area of application to estimate $\Delta h/h_o$ as it includes the effect of the natural shape of an accumulation as well as a movable bed. The effect of ρ_L on $\Delta h/h_o$ has not been studied in this present thesis. It can be hypothesized that ρ_L affects the LW accumulation shape. With increasing ρ_L , logs are further pulled downwards along the rack, reducing the open flow cross-section and therefore increasing $\Delta h/h_o$. To account for increasing ρ_L in Eq. (5.21), it is recommended to increase f_A .

The main input data for Eq. (5.21) are the expected approach flow conditions during floods. The expected LW volume can be estimated with simple formulas (e.g. Rickenmann 1997 or Steeb *et al.* 2017) or a GIS analysis (Ruiz-Villanueva *et al.* 2014a or Schalko *et al.* 2017). The average log dimensions and FM percentages can be determined based on forest inventories.

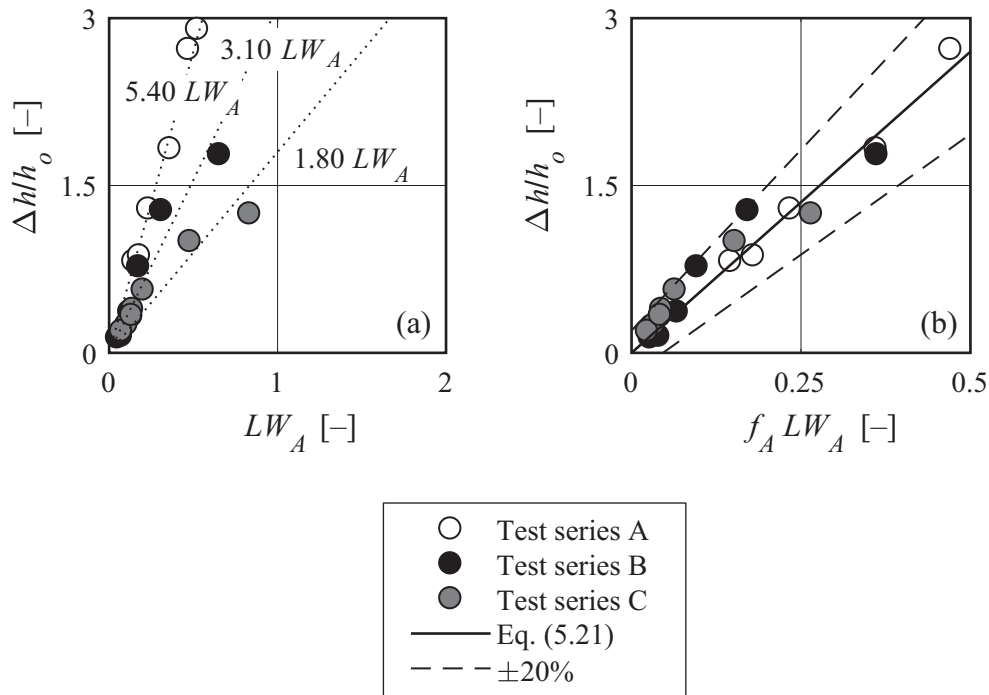


Figure 5.52 (a) $\Delta h/h_o$ versus LW_A for test series A, B, and C (b) $\Delta h/h_o$ versus $f_A LW_A$, Eq. (5.21), and $\pm 20\%$ prediction range

For a given LW volume, $\Delta h/h_o$ should be calculated with a sensitivity analysis of f_A . The following recommendations are made:

- *Worst-case scenario:* A box-shaped LW accumulation with a fixed bed can be assumed and the expected backwater rise calculated with $f_A = 1$ (i.e. Eq. (5.16)).
- *Average-case scenario:* For river infrastructures where no scour may occur (e.g. with large connected foundation elements), the effect of a movable bed can be neglected and a natural accumulation expected: $f_A \approx 3/5$;
- *Best-case scenario:* For river infrastructures where scour is expected and tolerable (e.g. with single or deeply placed foundation elements), f_A can be set to $\approx 1/3$. For the design of a retention rack or bridge pier, a deeply placed foundation can be chosen to allow for a defined scour formation, thereby increasing morphological heterogeneity while reducing backwater rise.

Effect of LW volume on backwater rise

For a flood hazard assessment, the expected LW volume V_s exhibits high uncertainties. To reduce these uncertainties, the effect of varying LW volume on backwater rise is essential. The characteristic LW volume V_c generates the primary, characteristic backwater rise Δh_c prior to the formation of a LW carpet and is a function of B , F_o , d_m , and h_o

(Eqs. (5.11)-(5.12)). Additional LW accumulates at the accumulation tail, thereby only minimally contributing to an additional backwater rise. The backwater rise ratio $\eta = \Delta h/\Delta h_c$ is plotted versus the relative LW volume V_s/V_c for test series B and C in Figure 5.53. For $F_o = 0.3 \dots 1.5$, $\eta = \Delta h/\Delta h_c$ is then represented by ($R^2 = 0.93$):

$$\eta = \frac{\Delta h}{\Delta h_c} = \left(\frac{V_s}{V_c} \right)^{1/4}. \quad (5.22)$$

All data agree well with the design equation and RMSE = 0.10.

As a first estimate, backwater rise Δh can be determined using Eq. (5.16) or Eq. (5.21). To analyze the effect of varying LW volume on Δh , Eq. (5.22) can be applied. Only the ratio of V_s/V_c has to be selected, e.g. to 0.5 and 2 given a scatter range of the expected LW volume by a factor of 3. For $V_s/V_c = 0.5$, $\eta = 0.84$ compared to $\eta = 1.19$ for $V_s/V_c = 2$. The variation of the LW volume V_s allows for a scenario-based flood risk assessment and is useful for engineering application. So the design of LW retention structures, i.e. the rack height as well as the height of the required flood embankments can be analyzed in more detail. The practical application of Eq. (5.16), Eq. (5.21), and Eq. (5.22) to estimate backwater rise due to LW accumulations is demonstrated in a computational example, provided in Section 6.

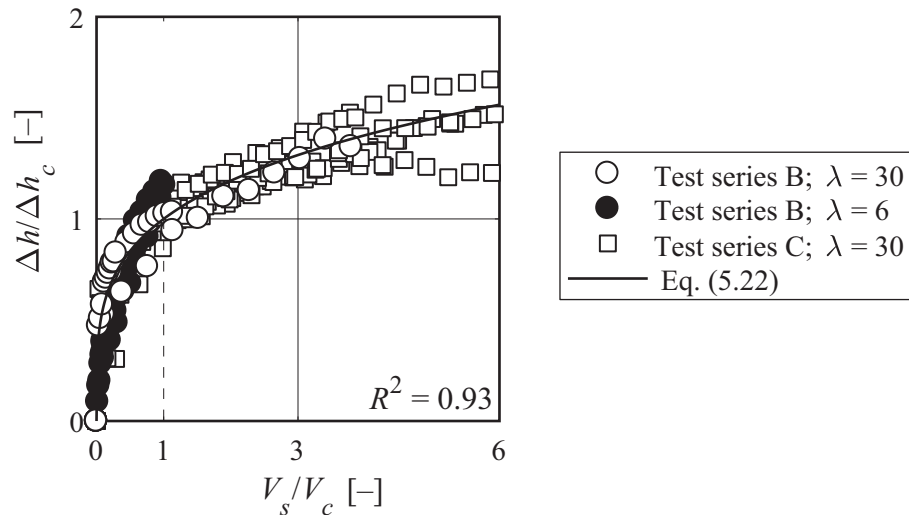


Figure 5.53 Backwater rise ratio $\eta = \Delta h/\Delta h_c$ versus relative LW volume V_s/V_c for test series B ($\lambda = 6$ and $\lambda = 30$), C ($\lambda = 30$), and Eq. (5.22)

5.3.2 Local scour

5.3.2.1 Approach flow conditions and bed material

Figure 5.46 illustrates the formation of a natural LW accumulation with a movable bed for increasing V_s (C10; Table 4.5). In addition, the scour formation and scour depth at the rack S_r can be observed in Figure 5.46. For test C10 ($d_m = 2.7$ mm), $S_r = 0.14$ m for $V_s/V_c = 0.5$, $S_r = 0.28$ m for $V_s/V_c = 2$, increasing up to $S_r = 0.34$ m for $V_s/V_c \approx 4.3$. For the experiments on local scour, the initial bed shear stress θ_{IC} was set slightly below the threshold value for incipient motion (Section 4.5.5). With increasing V_s , the flow upstream of the accumulation is altered. Due to increasing backwater rise, bed shear stress θ increases, so $\theta > \theta_{IC}$ and also $\theta > \theta_{cr}$ for incipient motion, thereby initiating scour formation. Every added LW package leads to increasing backwater rise (Section 5.3.1.5), increasing θ , and therefore increasing S_r (Figure 5.46a versus Figure 5.46e).

Figure 5.54 shows S_r for $V_s/V_c = 2$, $d_m = 2.7$ mm, and different Q (C8-C10). S_r is increasing with increasing Q or unit discharge $q = Q/B$, respectively (Figure 5.54a versus Figure 5.54c). For $d_m = 2.7$ mm and $V_s/V_c = 2$, $S_r = 0.16$ m for $Q = 20$ l/s ($q = 0.05$ m²/s), compared to $S_r = 0.22$ m for $Q = 30$ l/s ($q = 0.075$ m²/s), and $S_r = 0.28$ m for $Q = 40$ l/s ($q = 0.10$ m²/s). Similar to increasing V_s , hydraulic load likewise increases with increasing q , leading to larger S_r .

In Figure 5.55, a photo series of S_r is illustrated for $V_s/V_c = 1$, $Q = 30$ l/s, and different mean grain size diameters $d_m = 2.7$ mm, $d_m = 5.4$ mm, and $d_m = 13.1$ mm (C9, C4, C12). S_r is decreasing with increasing d_m (Figure 5.55a compared to Figure 5.55c). For $V_s/V_c = 1$ and $Q = 30$ l/s, $S_r = 0.22$ m for $d_m = 2.7$ mm compared to $S_r = 0.14$ m for $d_m = 5.4$ mm, and $S_r = 0.07$ m for $d_m = 13.1$ mm. Given the same flow conditions, a larger grain size diameter d_m results in smaller θ compared to smaller d_m . If θ is only slightly above θ_{cr} for incipient motion, weak sediment transport occurs, resulting in smaller scour depths compared to conditions with $\theta \gg \theta_{cr}$. In addition, a large d_m represents a greater resistance, resulting in smaller scour depths.

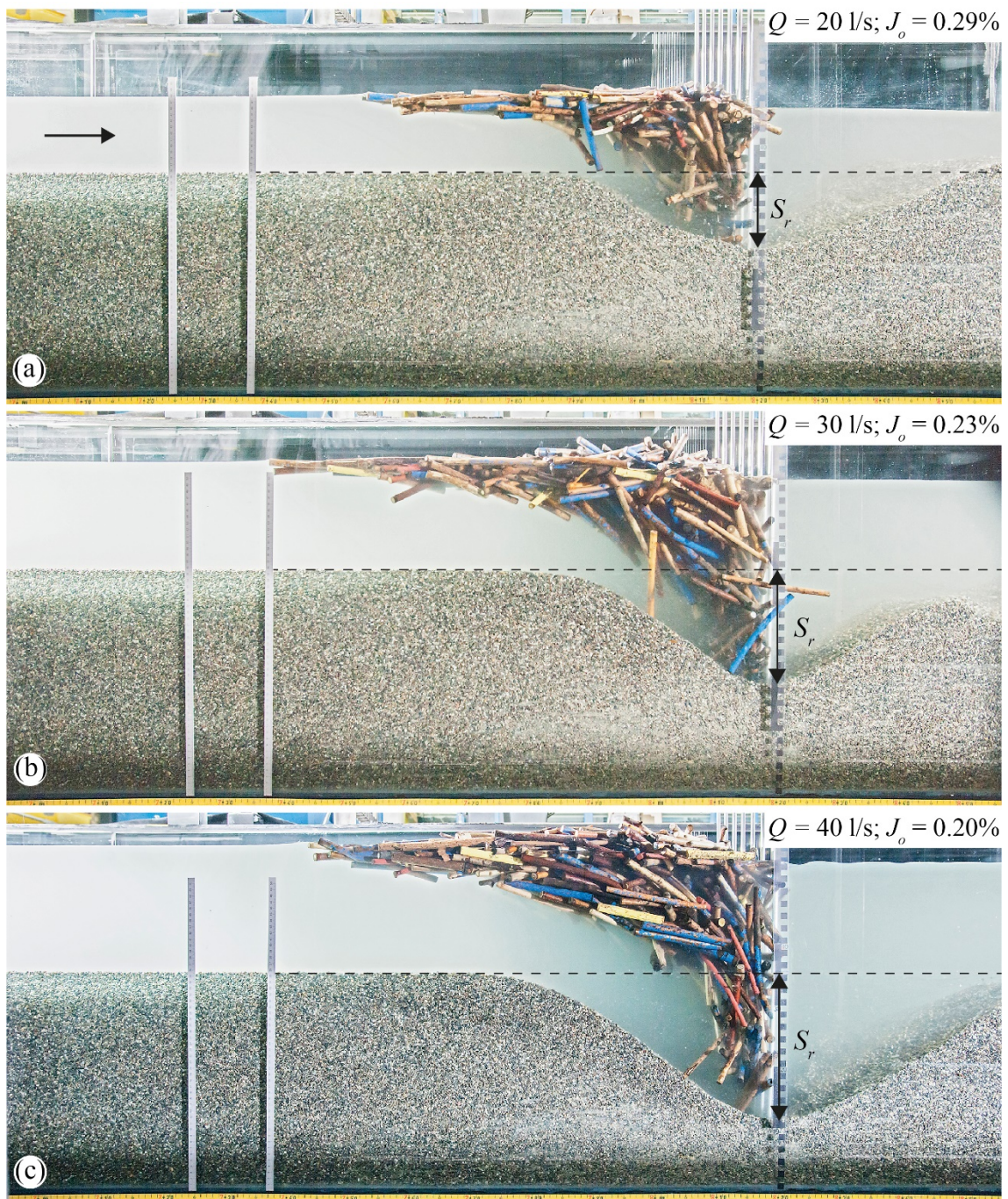


Figure 5.54 Scour with uniform bed material for $V_s/V_c = 2$, $d_m = 2.7 \text{ mm}$, and (a) $Q = 20 \text{ l/s}$ (C8), (b) $Q = 30 \text{ l/s}$ (C9), and (c) $Q = 40 \text{ l/s}$ (C10); Initial bed shear stress was set to $\theta_{IC} = 0.04$ for $d_m = 2.7 \text{ mm}$.

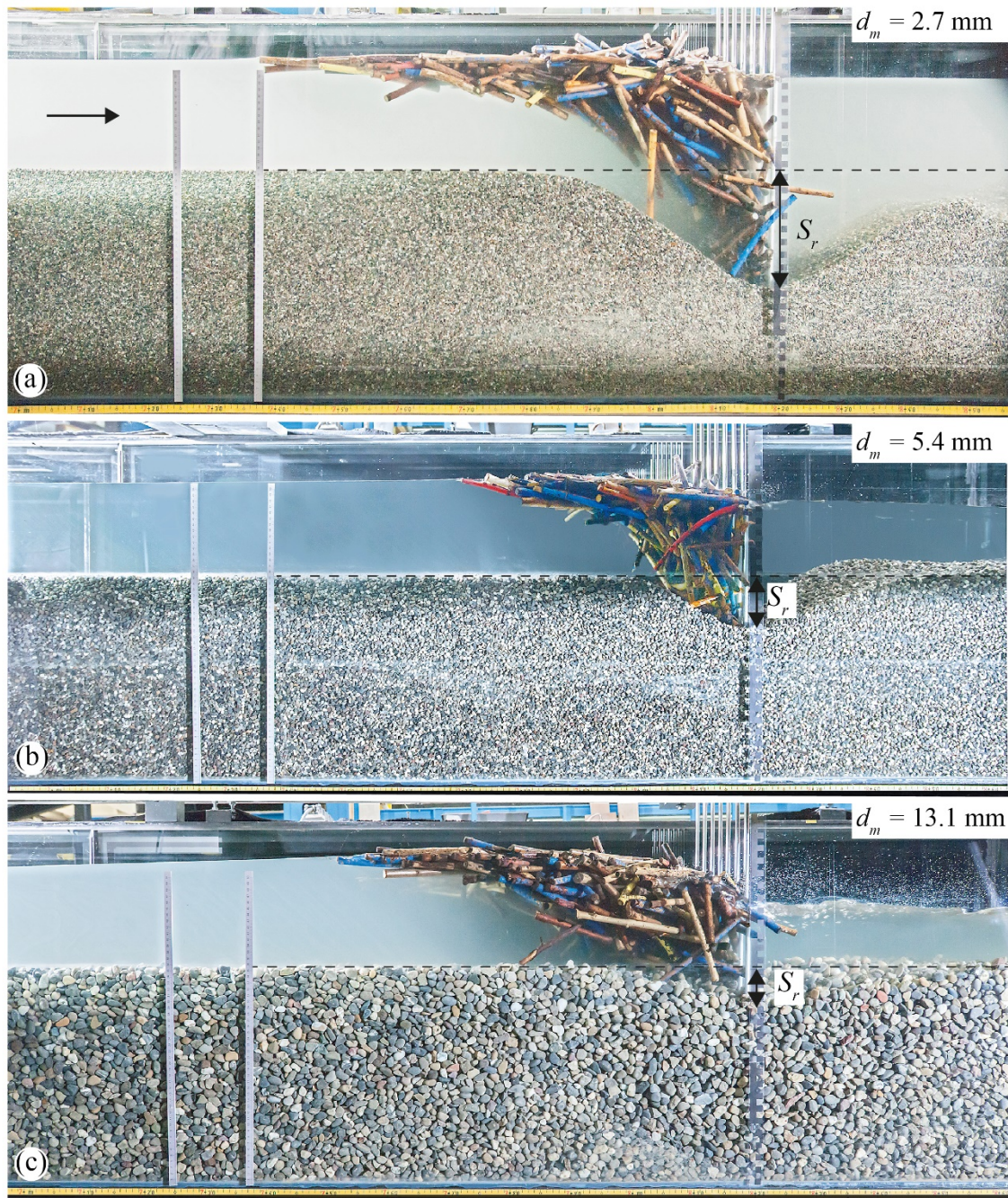


Figure 5.55 Scour for various uniform bed material for $V_s/V_c = 1$, $Q = 30$ l/s, and (a) $d_m = 2.7$ mm (C9), (b) $d_m = 5.4$ mm (C4), and (c) $d_m = 13.1$ mm (C12); Initial bed shear stresses were set to $\theta_{IC} = 0.04$ for $d_m = 2.7$ mm and 5.4 mm, and $\theta_{IC} = 0.05$ for $d_m = 13.1$ mm

The topography of the final scour S (after the addition of $V_s = 0.023 \text{ m}^3$) is shown in Figure 5.56 to Figure 5.59 for tests C1, C6, C8 and C10. For $d_m = 2.7 \text{ mm}$, the maximum scour depth $S_{\max} = 0.20 \text{ m}$ for $Q = 20 \text{ l/s}$, whereas $S_{\max} = 0.34 \text{ m}$ for $Q = 40 \text{ l/s}$. In comparison, for a larger grain size diameter $d_m = 5.4 \text{ mm}$, $S_{\max} = 0.17 \text{ m}$ for $Q = 20 \text{ l/s}$, compared to $S_{\max} = 0.29 \text{ m}$ for $Q = 40 \text{ l/s}$. Therefore, scour increases with increasing q and decreasing d_m . Scour volume V_{scour} for $d_m = 2.7 \text{ mm}$ increased from $V_{\text{scour}} = 29.1 \text{ dm}^3$ for $Q = 20 \text{ l/s}$ to $V_{\text{scour}} = 69.9 \text{ dm}^3$ for $Q = 40 \text{ l/s}$. In comparison, given $Q = 20 \text{ l/s}$, $V_{\text{scour}} = 29.1 \text{ dm}^3$ for $d_m = 2.7 \text{ mm}$ compared to $V_{\text{scour}} = 17.1 \text{ dm}^3$ for $d_m = 5.4 \text{ mm}$. The increase in V_{scour} for increasing Q and decreasing d_m was observed for all other tests. According to Figure 5.56 to Figure 5.59, a symmetric scour along the transverse cross-section developed, i.e. a 2D scour. So possible 3D or wall effects can be neglected for this setup.

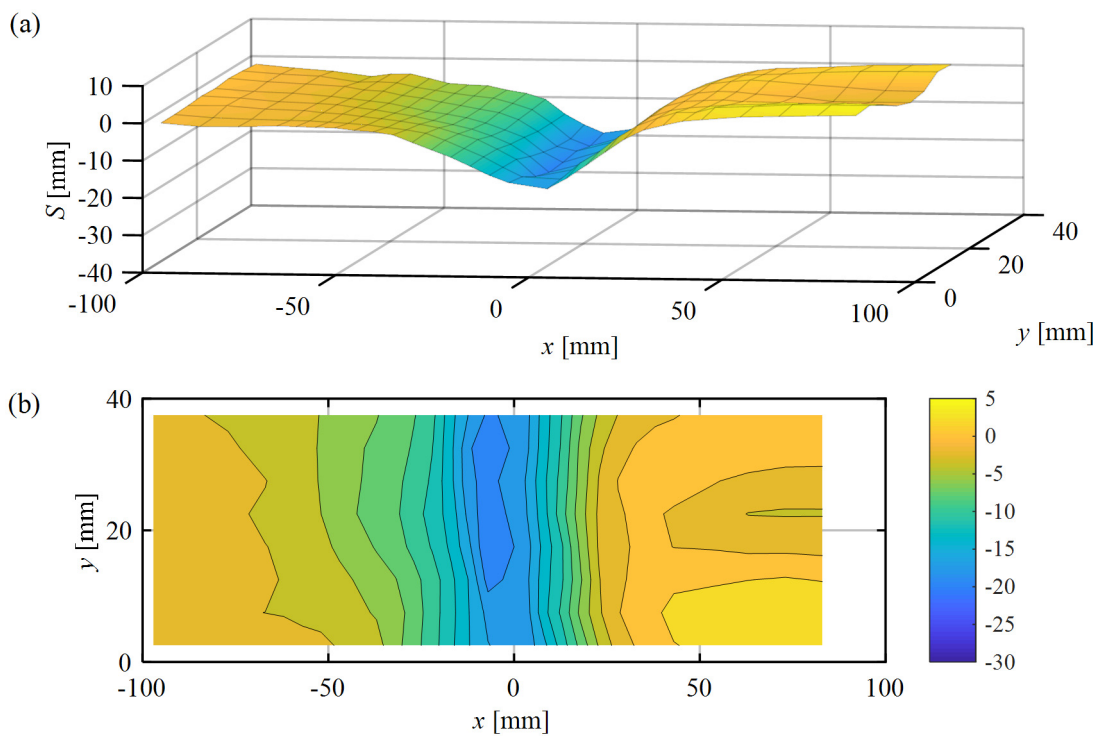


Figure 5.56 Topography of final scour S for $Q = 20 \text{ l/s}$ and $d_m = 2.7 \text{ mm}$ (C8)

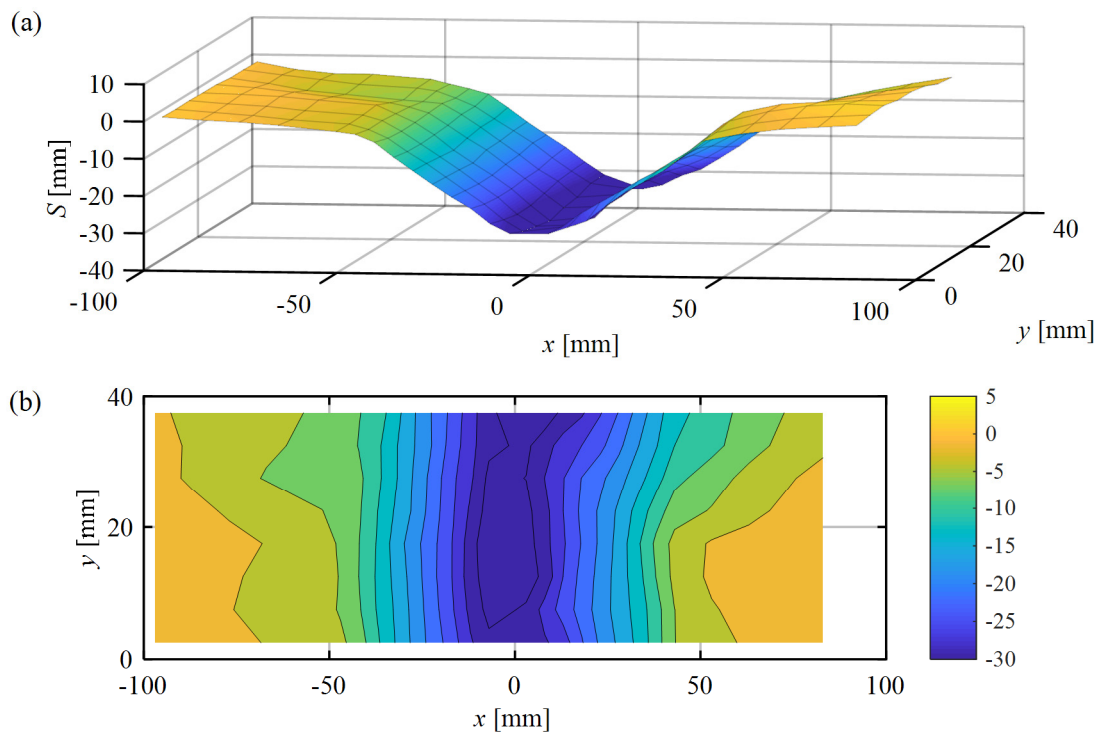


Figure 5.57 Topography of final scour S for $Q = 40$ l/s and $d_m = 2.7$ mm (C10)

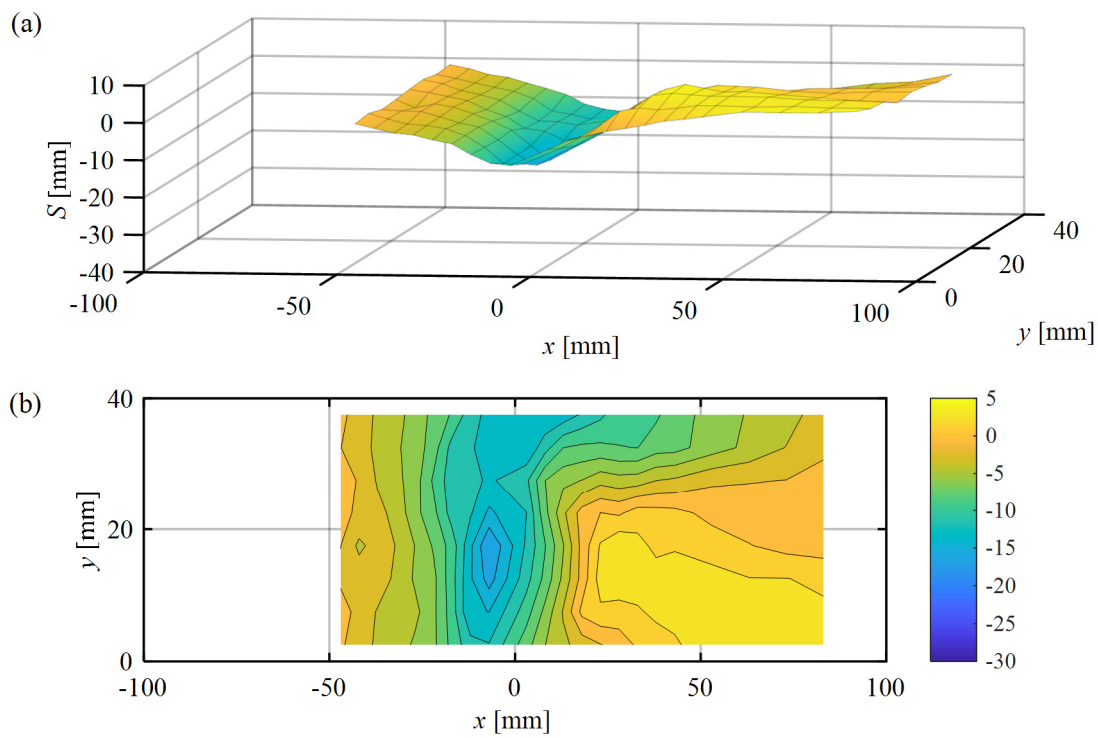


Figure 5.58 Topography of final scour S for $Q = 20$ l/s and $d_m = 5.4$ mm (C1)

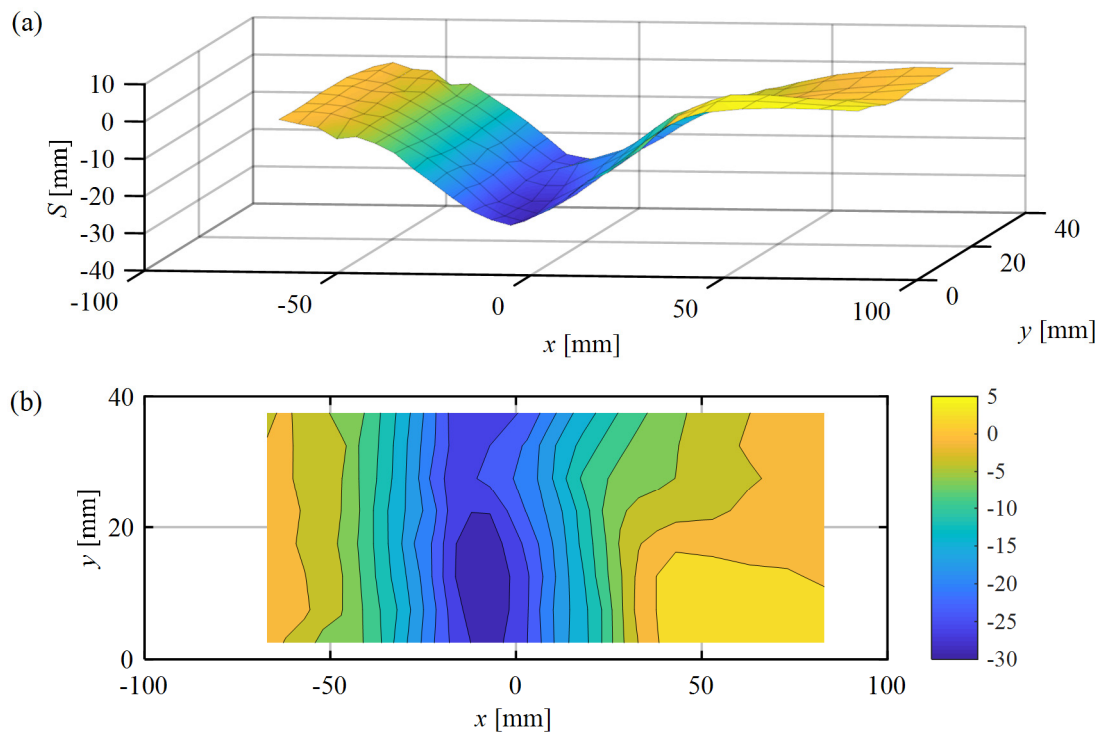


Figure 5.59 Topography of final scour S for $Q = 40$ l/s and $d_m = 5.4$ mm (C6)

In Figure 5.60a, the scour depth at the rack S_r normalized with d_{90} is plotted as a function of V_s/V_c for $d_m = 2.7$ mm and different $Q = 20$ l/s...40 l/s ($F_o = 0.57...0.47$). The development of S_r/d_{90} is comparable to $\Delta h/h_o$ as a function of V_s/V_c (Figure 5.47). For the majority of the tests, $V_s/V_c \leq 1$ generates not only the main increase of Δh , but also the main increase of S_r . For $V_s/V_c = 1$, $S_r/d_{90} \approx 49$ for $Q = 20$ l/s and increases up to $S_r/d_{90} \approx 70$ for $Q = 40$ l/s.

The effect of different grain size diameters d_m on S_r/d_{90} is illustrated in Figure 5.60b. Given $Q = 20$ l/s and $V_s/V_c = 1$, $S_r/d_{90} \approx 49$ for $d_m = 2.7$ mm, $S_r/d_{90} \approx 19$ for $d_m = 5.4$ mm, and decreases to $S_r/d_{90} \approx 1.3$ for $d_m = 13.1$ mm. According to Figure 5.60a and b, grain size diameter d_m imposes a stronger effect on S_r compared to the approach flow conditions, i.e. Q or q .

A longitudinal section of the average cross-sectional scour depth S_m is shown in Figure 5.60c and d. The position of the maximum scour depth ($x = -7$ cm) can be approximated at the rack with $x = 0$ cm, i.e. $S_{\max} \approx S_r$.

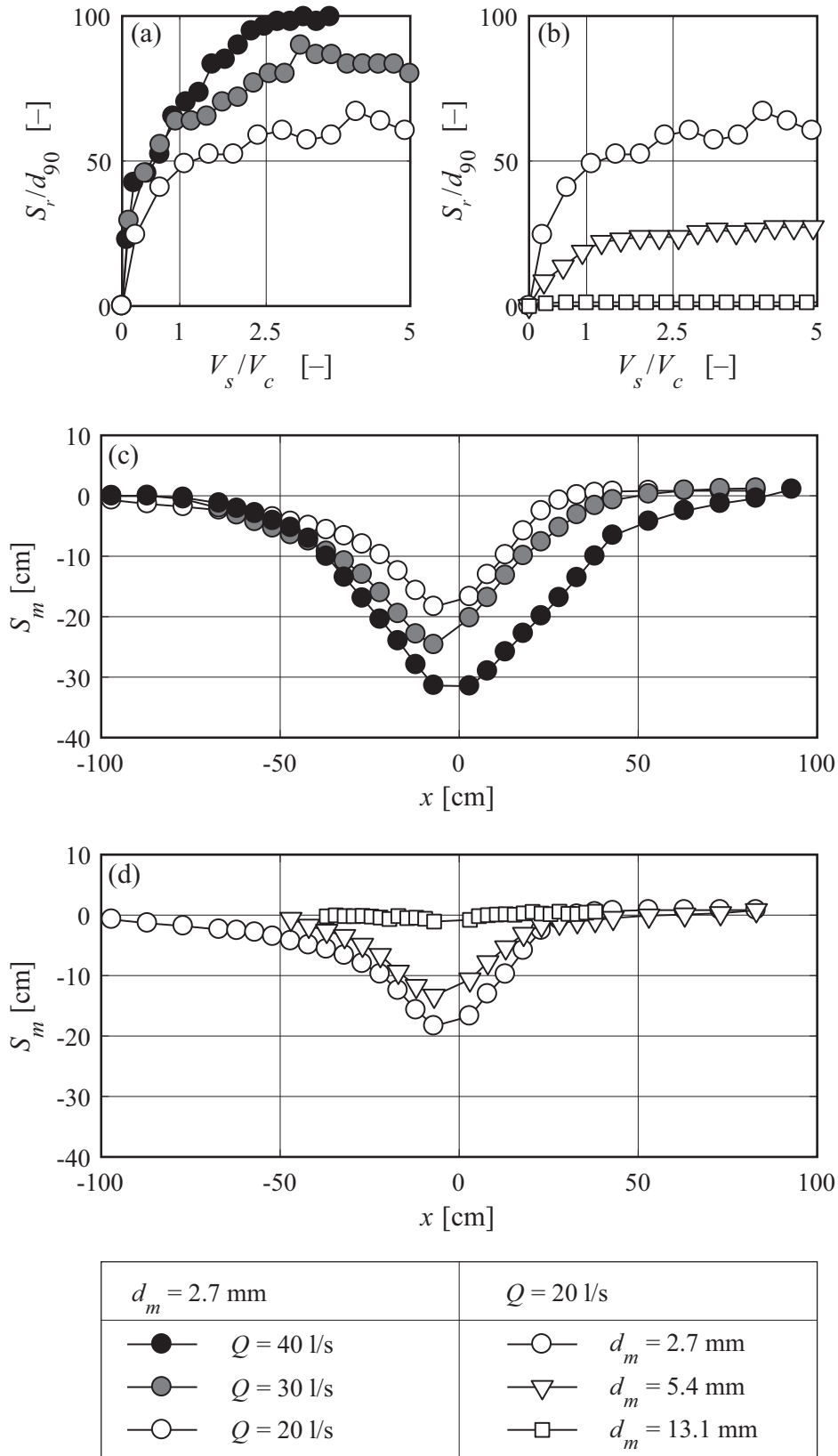


Figure 5.60 (a) S_r/d_{90} versus V_s/V_c with $d_m = 2.7 \text{ mm}$ and different $Q = 20 \text{ l/s} \dots 40 \text{ l/s}$ (C8-C10), (b) S_r/d_{90} versus V_s/V_c with $Q = 20 \text{ l/s}$ and different d_m (C1, C8, C11), (c) and (d) longitudinal section of the average cross-sectional scour depth S_m for tests C1, C8-C11. Initial bed shear stresses were set to $\theta_{IC} = 0.04$ for $d_m = 2.7 \text{ mm}$ and 5.4 mm , and $\theta_{IC} = 0.05$ for $d_m = 13.1 \text{ mm}$

5.3.2.2 Normalized local scour depth: Design equation

To generalize the results, the governing parameters for local scour due to LW accumulation ($\theta_{IC} = 0.04$ for $d_m = 2.7$ and 5.4 mm, $\theta_{IC} = 0.05$ for $d_m = 13.1$ mm) with uniform bed material (Tests B1-B12) are discussed hereafter. The maximum scour depth S_{\max} , i.e. scour depth at the rack S_r , can be described by the basic parameters in Table 5.8.

Table 5.8 Basic parameters for scour due to LW accumulation

Parameters	
Log diameter	d_L [m]
Log length	L_L [m]
Characteristic large wood volume	V_c [m ³]
Solid large wood volume	V_s [m ³]
Unit discharge	q [m ² /s]
Mean grain size diameter	d_m [m]
Characteristic grain size diameter	d_{84} [m]
Characteristic grain size diameter	d_{16} [m]
Water density	ρ_w [kg/m ³]
Wood density	ρ_L [kg/m ³]
Sediment density	ρ_{sed} [kg/m ³]
Gravitational acceleration	g [m/s ²]

The selected $n = 12$ independent parameters include $r = 3$ reference dimensions ([M] mass, [L] length, [T] time). Based on a dimensional analysis, $n - r = 9$ non-dimensional parameters Π_{1-9} need to be defined. These Π_{1-9} are the relative unit discharge $\Pi_1 = q/(gd_m^3)^{0.5}$, relative sediment density $\Pi_2 = \rho_{sed}/\rho_w = s$, relative LW volume $\Pi_3 = V_s/V_c$, standard deviation σ_g of the grain size distribution $\Pi_4 = (d_{84}/d_{16})^{0.5}$, relative log length $\Pi_5 = L_L/d_L$, relative LW density $\Pi_6 = \rho_L/\rho_w$, ratio between sediment and LW density $\Pi_7 = \rho_{sed}/\rho_L$, relative sediment diameter $\Pi_8 = d_m/d_L$, and ratio between log length and sediment diameter $\Pi_9 = L_L/d_m$. As the log diameter, log length, and wood density were not varied systematically in this study, $\Pi_5 \dots \Pi_{10}$ are not included in the further analysis. As described in Section 5.3.1.7, ρ_L may affect the LW accumulation shape, and therefore may alter the scour depth. For increasing ρ_L , increasing $\Delta h/h_o$ can be expected and hence, increasing scour depth S . However, to test this hypothesis, flume experiments with varying ρ_L are deemed necessary. All tests were conducted for uniform bed material,

so Π_4 will not be considered. Scour due to LW accumulation can therefore be described by $\Pi_1 \dots \Pi_3$. The exponents of the governing parameters were quantified with a non-linear regression analysis and the dimensionless scour factor S_A is defined as:

$$S_A = 0.86 \left(\frac{q}{\sqrt{(s-1)gd_m^3}} \right)^{0.85} \left(\frac{V_s}{V_c} \right)^{0.30}. \quad (5.23)$$

According to Eq. (5.23), d_m exhibits the largest effect on S_A with an exponent of -1.28 , followed by q with an exponent of 0.85 , and the relative LW volume with an exponent of 0.30 . The governing parameters (unit discharge and grain size diameter) are comparable to Eq. (3.20), describing local scour due to horizontal jets (Eggenberger and Müller 1944). Previous studies on the effect of LW on scour were mainly conducted for bridge pier scour (Eqs. (3.17)-(3.19)). To include the effect of LW, the pier diameter was increased and defined as an effective pier diameter (Melville and Dongol 1992, Lagasse *et al.* 2010). In Eq. (5.23), however, LW is considered as a separate parameter with the ratio of V_s/V_c . Based on S_A , the relative maximum scour depth S_{\max}/d_{90} at the rack can be described by a linear relationship for $F_o = 0.5 \dots 1.5$ and $S_A = 0 \dots 120$ ($R^2 = 0.97$) with:

$$\frac{S_{\max}}{d_{90}} = S_A. \quad (5.24)$$

In Figure 5.61, S_{\max}/d_{90} is plotted as a function of S_A for test series C with Eq. (5.24), and $\pm 30\%$ prediction range. All data agree with the proposed design equation and $RMSE = 5.2$.

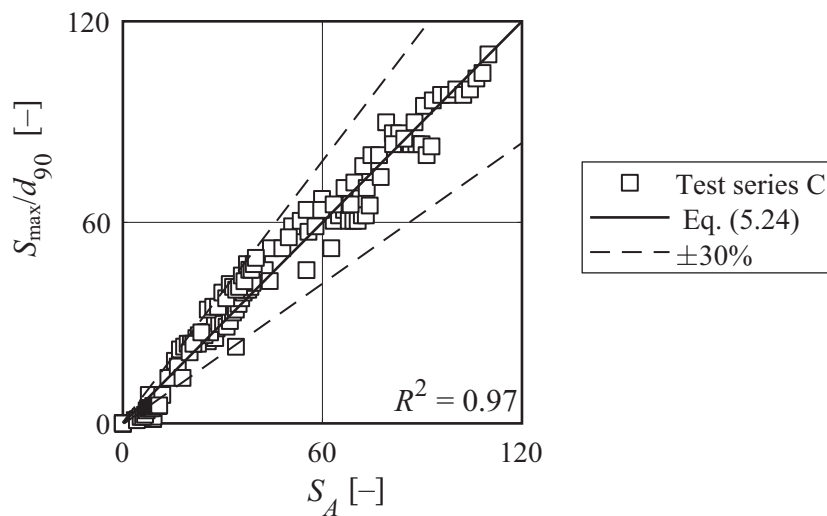


Figure 5.61 S_{\max}/d_{90} versus S_A for test series C, Eq. (5.24), and $\pm 30\%$ prediction range

In Figure 5.62a, relative prediction error ε is plotted versus measured relative scour depth S_{\max}/d_{90} , with ε defined as:

$$\varepsilon = \frac{S_A - S_{\max}/d_{90}}{S_{\max}/d_{90}}. \quad (5.25)$$

$\varepsilon > 0$ corresponds to an overestimation of S_{\max}/d_{90} , whereas $\varepsilon < 0$ is an underestimation of S_{\max}/d_{90} . The majority of the data points are within a $\pm 30\%$ prediction range. In addition, ε decreases with increasing S_{\max}/d_{90} . Note that for $d_m = 13.1$ mm (grey data points) and $S_{\max}/d_{90} \leq 2$, data points exhibit $6.0 \geq \varepsilon > 2.1$. Therefore, it is further recommended to apply Eq. (5.24) for $S_{\max}/d_{90} > 2$.

The residuals $r = \text{observed value} - \text{predicted value}$, i.e.:

$$r = S_{\max}/d_{90} - S_A, \quad (5.26)$$

are plotted as a function of S_{\max}/d_{90} in Figure 5.62b. The residuals plot indicates no clear pattern and the majority of the data points are clustered in the range of $r \pm 10$.

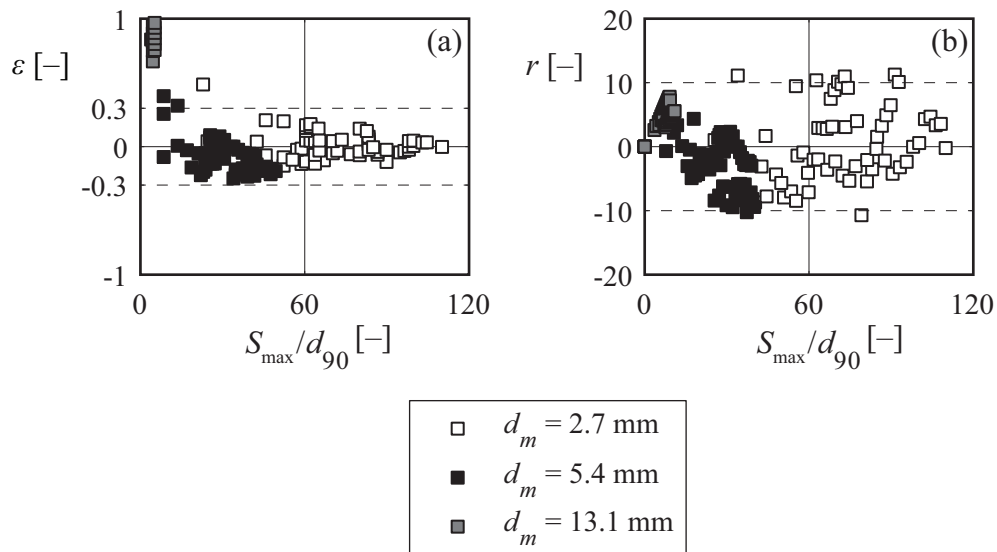


Figure 5.62 (a) Relative prediction error ε versus measured relative scour depth S_{\max}/d_{90} for the tested d_m , (b) residuals r versus S_{\max}/d_{90} for the tested d_m

An error propagation analysis was conducted for Eq. (5.24) and the target value S_{\max}/d_{90} . The input parameter range is summarized in Table 5.9 and Table 5.10. The total errors for the input parameters were set to:

- Q : $\pm 1\%$ – g : $\pm 0 \text{ m/s}^2$ – V_c : $\pm 10\%$
- B : $\pm 0.002 \text{ m}$ – d_m : $\pm 0.0005 \text{ m}$ – d_{90} : $\pm 0.0005 \text{ m}$
- s : ± 0 – V_s : $\pm 5\%$ – S_{\max} : $\pm 0.001 \text{ m}$

Compared to the relative errors of Eq. (5.24) with $\pm 6.0\% \dots 23.9\%$, the relative errors of S_{\max}/d_{90} result in $\pm 6.0\% \dots 16.4\%$. The sum of relative errors $e_{XS,r}$ varies between 11.9% and 40.2% for the different input parameters, resulting in a prediction range of $\pm 27\%$, similar to the scatter of the final data evaluation (Figure 5.61).

Table 5.9 Total and relative error e_{XS} of Eq. (5.24) for various input parameters

Input parameters							Eq. (5.24)	Total error	Relative error
Q	B	s	g	d_m	V_s	V_c	S_A	e_{XS} Eq. (4.6)	$e_{XS,r}$
[l/s]	[m]	[-]	[m/s ²]	[mm]	[dm ³]	[dm ³]	[-]	[-]	[%]
20	0.4	2.65	9.81	2.7	3	5.3	32.78	± 7.82	23.87
40	0.4	2.65	9.81	2.7	9.3	4.6	86.56	± 20.66	23.87
20	0.4	2.65	9.81	5.4	6.8	6.8	16.07	± 1.98	12.31
40	0.4	2.65	9.81	5.4	19.1	6.2	40.59	± 5.00	12.31
20	0.4	2.65	9.81	13.1	19.7	12.7	5.92	± 0.36	5.99

Table 5.10 Total and relative error e_{XS} of S_{\max}/d_{90} for various input parameters

Input parameters		Measured data	Total error	Relative error
S_{\max}	d_{90}	S_{\max}/d_{90}	e_{XS} Eq. (4.6)	$e_{XS,r}$
[m]	[mm]	[-]	[-]	[%]
0.15	3.06	49.02	± 8.02	16.35
0.26	3.06	84.97	± 13.89	16.34
0.14	5.89	23.77	± 2.02	8.52
0.27	5.89	45.84	± 3.90	8.50
0.02	15.40	1.30	± 0.078	5.96

The scour due to LW accumulations can be estimated for varying approach flow conditions, bed material, and LW volume. The maximum scour depth S_{\max} is further useful for the estimation of backwater rise, as a large S_{\max} may suggest a lower value for f_A , e.g. $\approx 1/3$ (Eq. (5.21)). The input data for the approach flow conditions and LW volume can be obtained similar to the procedure for the estimation of backwater rise (Section 5.3.1.7). The values for the bed material can be assessed by granulometric analyses (e.g. line-sampling method).

5.4 Measures for large wood accumulation risk reduction

The efficiency of two types of measures for LW accumulation risk reduction at bridge piers was investigated using physical modeling. The measures are A = LW fin mounted upstream of the bridge pier and B = bottom sill mounted on the channel bottom (Figure 4.11; Section 4.6). The results are subsequently presented for the LW fin (Section 5.4.1) and the bottom sills (Section 5.4.2), including design recommendations and limitations.

5.4.1 Large wood fin

The model LW fin is made of PVC and was mounted upstream of the bridge pier (Figure 4.11a). The variations (A.1-A.6) are listed in Table 4.7 and the test program is summarized in Table 4.8 (Section 4.6).

A photo series of LW fin configurations to reduce LW accumulation probability p at a bridge pier is illustrated in Figure 5.63. The LW fin was placed against flow direction with a horizontal fin angle $\delta_2 = 90^\circ$ (Figure 5.63a, e-f), or with $\delta_2 = 30^\circ$ (Figure 5.63b-d). In addition, the vertical fin angle δ_1 varied between $\delta_1 = 45^\circ$ (Figure 5.63a-d) and $\delta_1 = 20^\circ$ (Figure 5.63e-f). It was hypothesized that transported logs may hit the LW fin, but disperse due to the sharp edges of the LW fin and the small width in comparison to the bridge pier. Due to the LW fin geometry, an accumulated log is more unstable, leading to an increased eccentricity, and hence decreased p . The variation of δ_2 and the Λ -shaped top should further foster the imbalance of an accumulated log, so logs are guided on the sides of the bridge pier. In the following, p is compared between setups with and without measures.

The results of p with measure A.1 (Table 4.7, Table 4.8, and Figure 4.11) versus reference tests without measures (i.e. *Ref*) are depicted in Figure 5.64 for $L_L = 0.20$ m, $L_L = 0.40$ m, uncongested, and semi-congested LW transport. For uncongested LW transport (Figure 5.64a-b), p only deviates for $v_o = 0.50$ m/s ($p \pm 17\%$), in which p increases for measure A.1 for $L_L = 0.20$ m and decreases for $L_L = 0.40$ m. However, for uncongested LW transport, the mean difference between A.1 and the reference test is $p \pm 8.3\%$, and consequently within the range of test reproducibility ($\pm 10\%$). For semi-congested LW transport (Figure 5.64c-d), the mean deviations are higher with $p \pm 14.6\%$. As no systematic trend can be determined, measure A.1 has no governing effect on p . The

efficiency of A.1 was also not observed during the model tests. In contrast to the hypothesis, logs accumulated at the LW fin similar to the bridge pier.

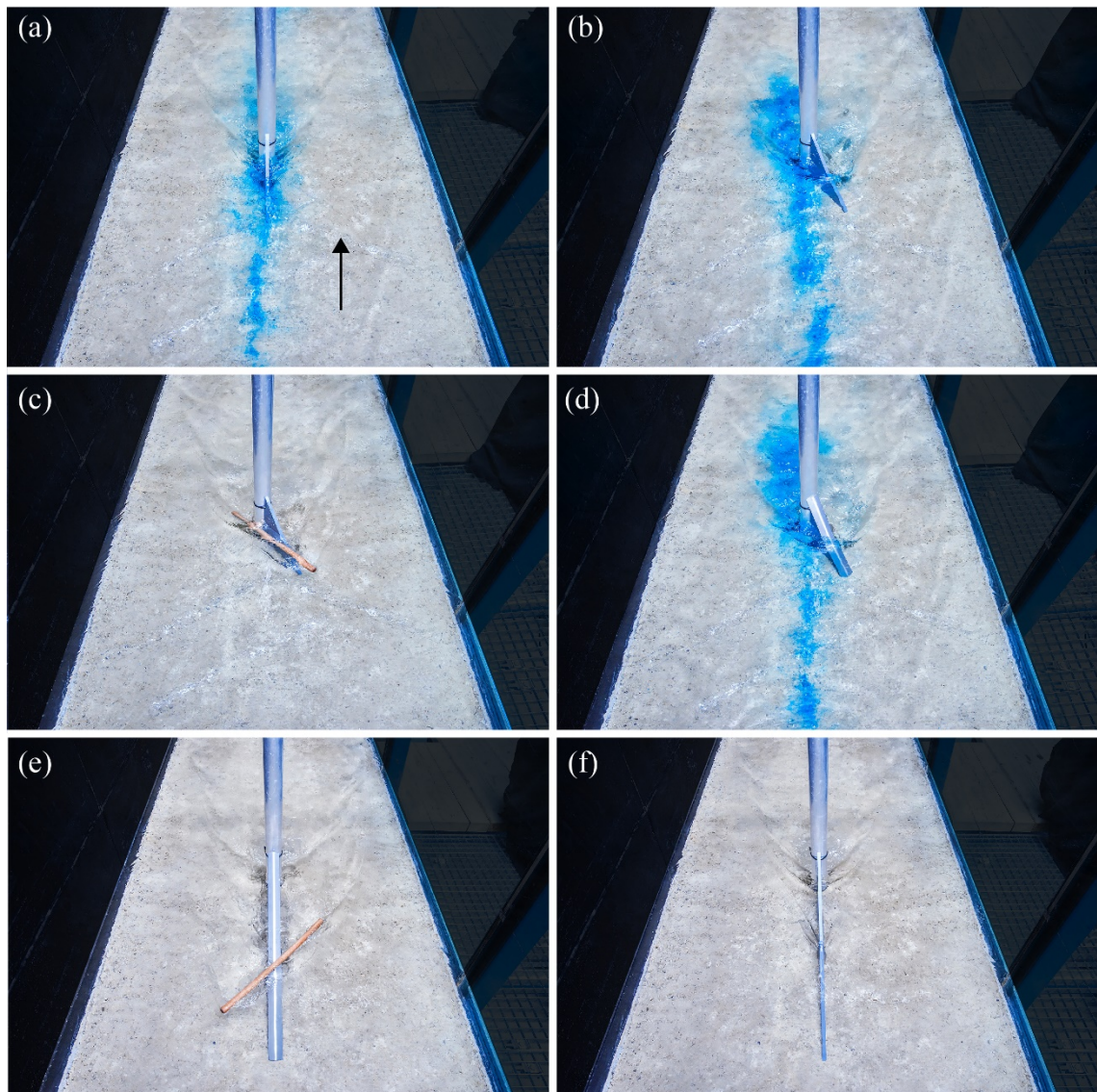


Figure 5.63 Measures for LW accumulation risk reduction with $h_o = 0.10$ m, $v_o = 0.50$ m/s, (a) A.1 (b)-(c) A.2, (d) A.4, (d) A.5, and (e) A.6 (Table 4.7)

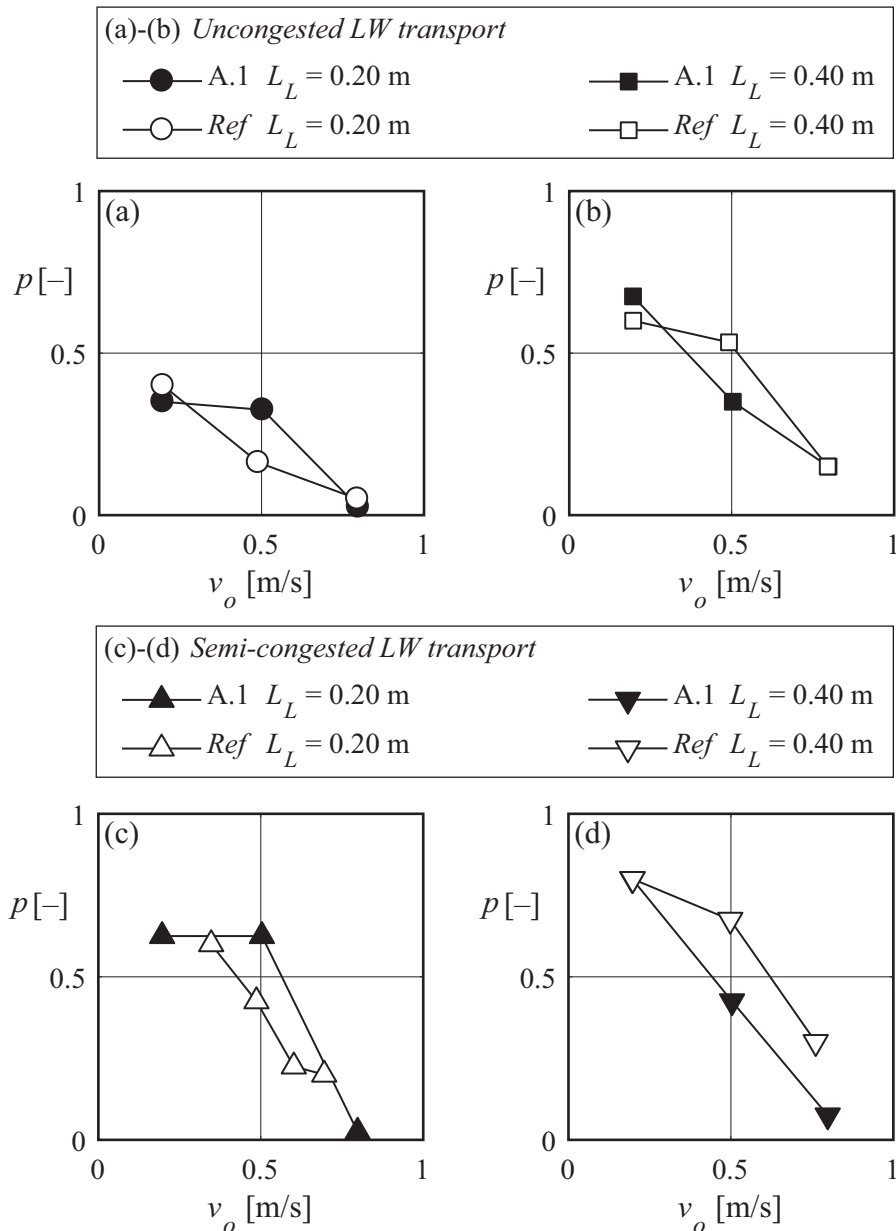


Figure 5.64 Accumulation probability p versus v_o with measure A.1 and reference tests (*Ref*) for (a)-(b) uncongested and (c)-(d) semi-congested LW transport, (a)-(c) $L_L = 0.20$ m, and (b)-(d) $L_L = 0.40$ m (M1-M12 vs. B6-B7, B17-B18, B29-B30, and vs E1, E3, E6, E9, E12, E14, E16)

In Figure 5.65, p is plotted as a function of v_o for measures A.2-A.6 (Table 4.7, Table 4.8, and Figure 4.11) versus reference tests for selected approach flow conditions, L_L , and uncongested LW transport. For measures A.2 and A.3 (Figure 5.65a), p is similar to the reference test for $v_o = 0.20$ m/s and $L_L = 0.20$ m ($p \pm 2.5\%$). For $v_o = 0.50$ m/s, $L_L = 0.40$ m, and measure A.2, p is $\approx 8\%$ lower compared to the reference test. As the deviations are within the reproducibility range, no governing effect can be concluded. Neither the variation of δ_2 , nor a Λ -shaped top led to a significant reduction of p . The Λ -shaped top was adapted to be sharper for measure A.4 and tested for

$v_o = 0.20$ m/s... 0.50 m/s and $L_L = 0.40$ m. According to Figure 5.65b, p decreases $\approx 13\%$ for $v_o = 0.50$ m/s, but is similar for $v_o = 0.20$ m/s, resulting in an average deviation of only 6%. The effect of δ_1 (measures A.5 and A.6), i.e. a longer LW fin, on p is also illustrated in Figure 5.65b. The resulting p are higher with A.5 and A.6 compared to the reference tests. Therefore, the variation of δ_1 does not reduce p .

In summary, the various LW fin configurations (geometry, orientation, aluminum top) did not significantly affect the stability of accumulated log and contradicted the proposed hypothesis. According to Lyn *et al.* (2003), a vertical cylindrical deflector reduced p (Figure 3.3), but logs were still retained at the deflector itself. LW retention at a LW fin or deflector may reduce the impact force of accumulated logs acting on a bridge pier. Furthermore, it can prevent structural damages of a bridge pier itself by reducing scour.

Possible scale effects may exist due to the roughness of the LW fin as well as the aluminum top in model compared to prototype. An aluminum top in prototype may be smooth enough for logs to be guided on the sides of the bridge pier. The efficiency of a LW fin to guide rootstocks farther downstream was not part of this present thesis. The center of gravity is different for a rootstock compared to a log, which may affect the resulting accumulation probability and hence the efficiency of the LW fin.

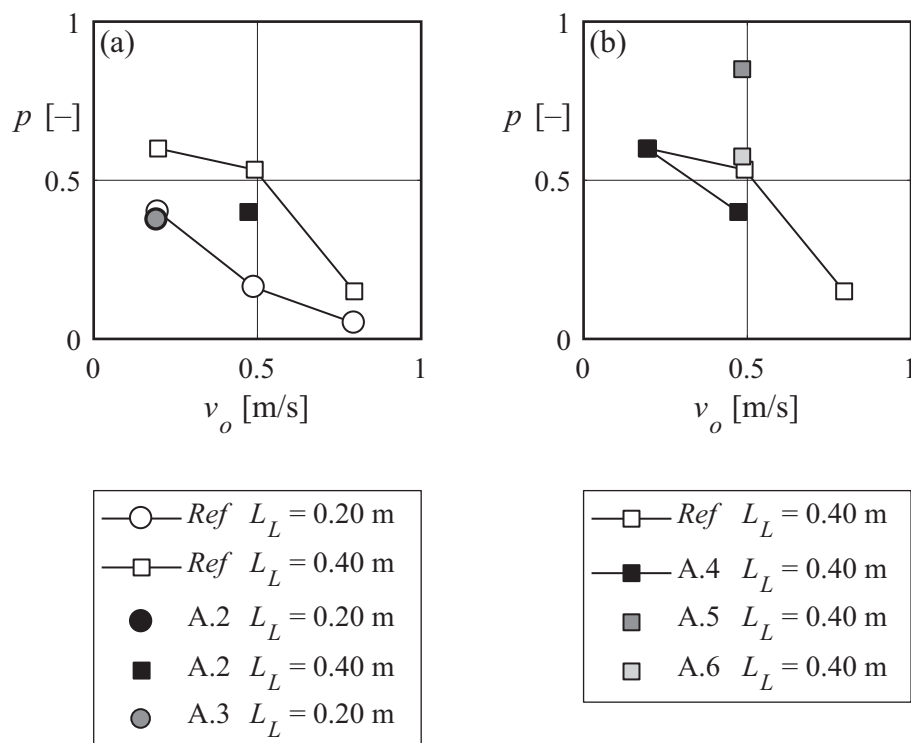


Figure 5.65 Accumulation probability p versus v_o with (a) A.2-A.3 vs. Ref, $L_L = 0.20$ m and $L_L = 0.40$ m, and (b) A.4-A.6 vs. Ref, $L_L = 0.40$ m (M13-M19 vs. B6+B7, B17+B18)

5.4.2 Bottom sills

The bottom sill configurations are illustrated in Figure 4.11b and Figure 5.66. The different setups are listed in Table 4.7 (Section 4.6) and include a cross-sill (B.1; Figure 5.66a), single and double declined sills (B.2 and B.3 Figure 5.66b-f). For the double declined sills (B.3), the distance Δx between sill and pier was varied to $\Delta x = 0$ m, $\Delta x = 0.15$ m, and $\Delta x = 0.30$ m (Figure 5.66 and Figure 5.67). Similar to the concept of “instream river training structures” (Section 3.5), the bottom sills are supposed to alter the flow by inducing secondary currents so transported logs do not accumulate at the pier. The flow is diverted normal to the bottom sill, so depending on the position of the bottom sill, logs may turn and are then guided at the side of the pier. In addition, the flow around the pier may become more turbulent and surface waves increase. These flow conditions lead to a more unstable accumulated log, thereby reducing accumulation probability. In Figure 5.66c, dye was added to visualize the flow, indicating a prominent flow alteration due to the declined bottom sill. To test their efficiency, p was determined for $L_L = 0.40$ m, $v_o = 0.50$ m/s and varying $h_o = 0.05$ m, 0.10 m, and 0.20 m (Table 4.8).

The accumulation probability p is plotted in Figure 5.68 as a function of F_o for $v_o = 0.50$ m/s and $L_L = 0.40$ m with measures B.1-B.3 versus a reference test. Note that the dashed line represents an assumption of p versus F_o based on the results illustrated in Figure 5.7c, i.e. p without any measures is similar for a wide range of F_o . Given $p_{Ref} = 53\%$ for $F_o \approx 0.20 \dots 0.70$, accumulation probability decreases due to B.1 by $8.3\% \dots 25.8\%$ with an average decrease of 16.6% (Figure 5.68a). For B.2, p decreases in a similar range ($3.3\% \dots 23.3\%$) with an average reduction of 12.5% (Figure 5.68a). Both measures indicate the strongest effect to reduce p for $F_o \approx 0.67$, corresponding to $h_o = 0.05$ m. For measure B.3 (Figure 5.67 and Figure 5.68b), the effect of various distances to the bridge pier Δx on p was tested. On average, p decreases by 17.5% for $\Delta x = 0.00$ m, by 20.3% for $\Delta x = 0.15$ m, and by 29.1% for $\Delta x = 0.30$ m. The average decrease in p due to measures B.3 is higher than the reproducibility range ($\pm 10\%$). The best results to reduce p were obtained with B.3 and $\Delta x = 0.30$ m. Given $\Delta x = 0.30$ m and $F_o \approx 0.50$ ($h_o = 0.10$ m; Figure 5.67c), $p = 10\%$ compared to $p_{Ref} = 53\%$. According to Figure 5.68, the efficiency of bottom sills strongly depends on F_o and h_o , respectively. The efficiency further tends to increase with increasing F_o or decreasing ratio of sill height (subscript S) to flow depth h_S/h_o ($h_S/h_o = 13.3$ for $h_o = 0.20$ m, $h_S/h_o = 6.6$ for $h_o = 0.10$ m, and $h_S/h_o = 3.3$ for $h_o = 0.05$ m).

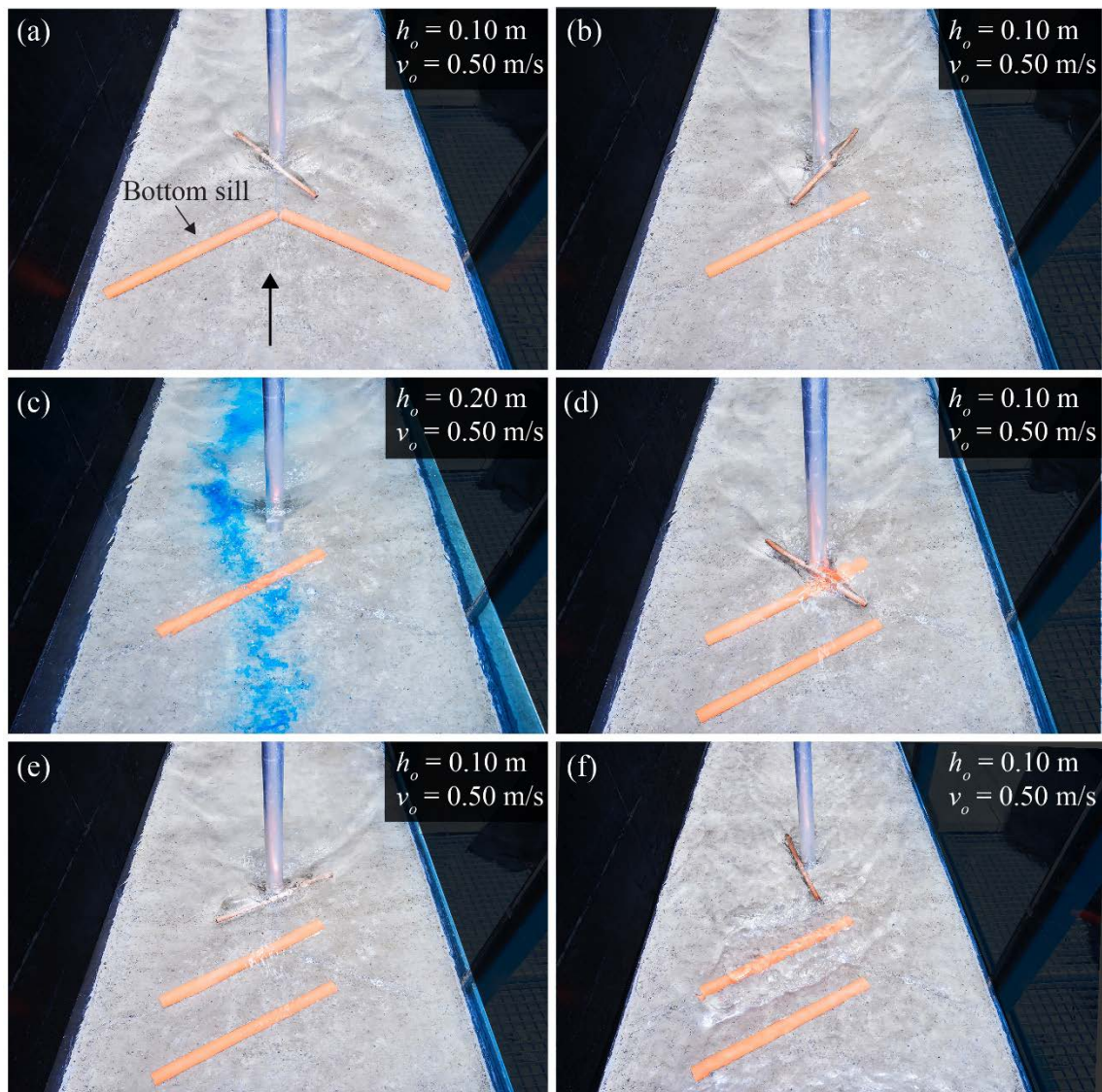


Figure 5.66 Measures for LW accumulation risk reduction with $h_o = 0.10$ m, $v_o = 0.50$ m/s for (a) B.1, (b) B.2, (d) B.3 with $\Delta x = 0$ m, (e) B.3 with $\Delta x = 0.15$ m, (f) B.3 with $\Delta x = 0.30$ m, and $h_o = 0.20$ m, $v_o = 0.50$ m/s for (c) B.2

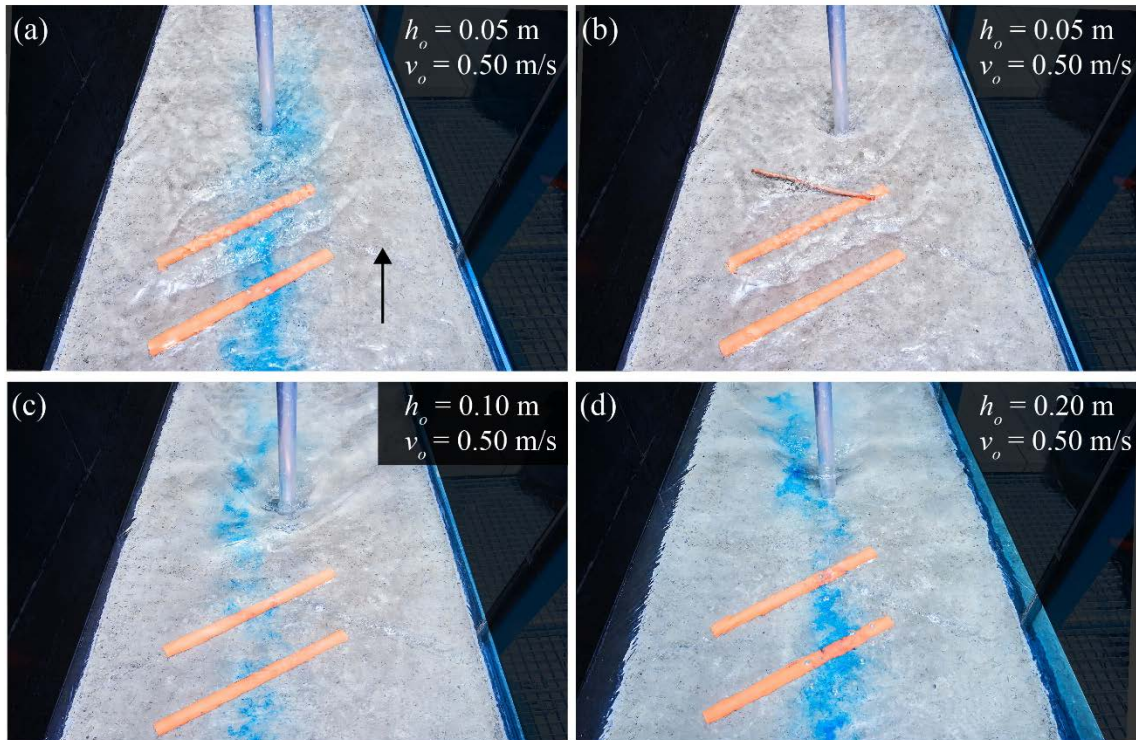


Figure 5.67 Measure B.3 with $\Delta x = 0.30$ m, $v_o = 0.50$ m/s, (a)-(b) $h_o = 0.05$ m, (c) $h_o = 0.10$ m, and (d) $h_o = 0.20$ m

Bottom sills are consequently a promising measure to reduce p . The efficiency of this measure can be described by two governing effects: (1) flow diversion and (2) increased turbulence. (1) The slightly shifted arrangement of the sills compared to the pier centerline diverts the flow normal to the sill, generating a transversal flow component (Figure 5.67c). Therefore, approaching logs are rotated normal to the bottom sill, i.e. \sim parallel to the flow, which reduces accumulation probability p (Figure 5.4). (2) The installed sills lead to increased turbulence downstream of the structure. Depending on the sill position with respect to the bridge pier (i.e. Δx), increased turbulence occurs right in front of the bridge pier (Figure 5.67d). The flow velocity fluctuations can lead to varying hydraulic forces acting on the log (Eq. (5.2)). These variations cause a rotating movement of the log and log detachment. Accumulated logs are then unstable and disperse faster compared to flow conditions without a bottom sill.

In contrast to a LW fin, p decreases due to the bottom sills. However, as the efficiency of bottom sills depends on the approach flow conditions, the design has to be further analyzed for a respective river topography and designated flow conditions. The efficiency can only be recommended for a small range of boundary conditions. In addition, the flume experiments were conducted with a fixed bed, thereby neglecting the effect of

a movable bed. Scour or deposition changes the sill geometry and consequently affects the wood diversion efficiency. The sill can further have a negative effect on the pier stability as the increased turbulence may lead to larger scour depths. Moreover, the construction of a fixed sill in the middle of the river in prototype may pose several challenges.

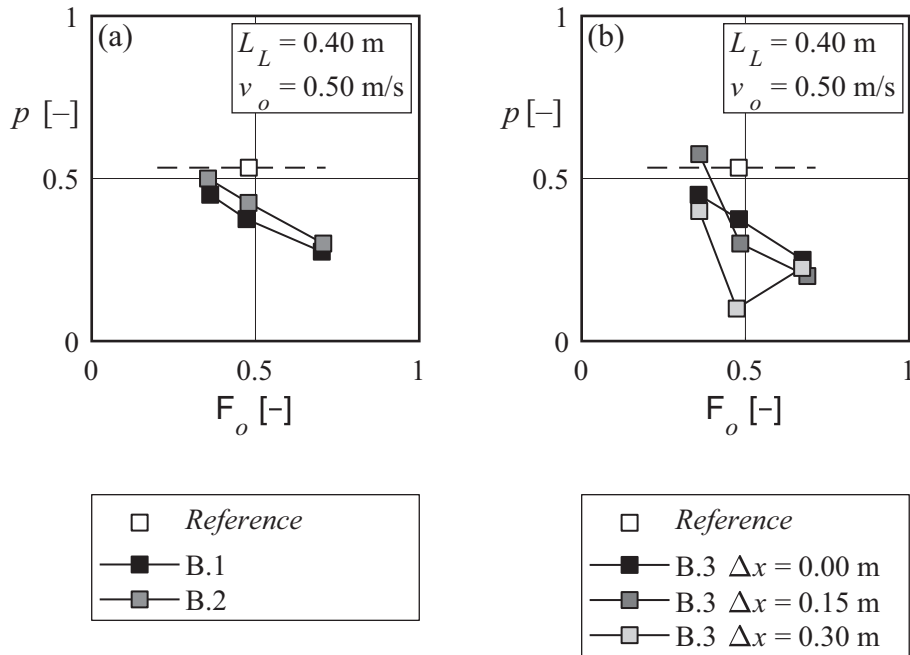


Figure 5.68 Accumulation probability p versus F_o for $v_o = 0.50$ m/s and $L_L = 0.40$ m with measures (a) B.1-B.2 versus *Ref*, and (b) B.3 versus *Ref* (M20-34 vs. B18); note that ---- is an assumption of p as a function of F_o according to Figure 5.7c.

5.5 Numerical modeling of large wood accumulation

The application of the 2D numerical simulation model ‘IberWood’ (Section 3.6 and Section 4.7) was evaluated by comparing simulation results to selected physical model test results. The preliminary results are subsequently presented for LW accumulation probability (Section 5.5.1) and backwater rise due to LW accumulation at a retention rack (Section 5.5.2), followed by an evaluation of the applicability of ‘IberWood’ (Section 5.5.3).

5.5.1 Large wood accumulation probability at bridge piers

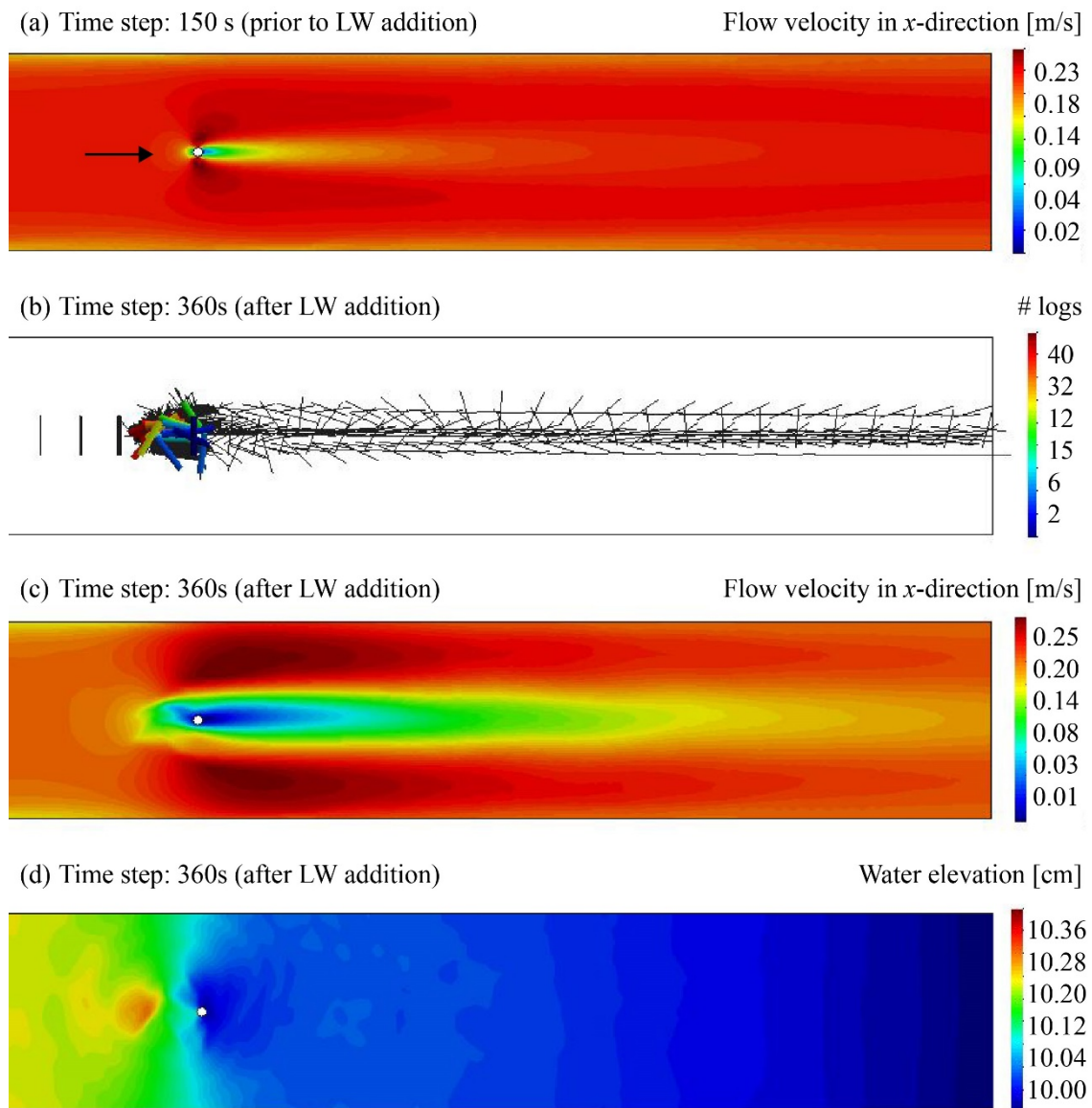
The model setup and numerical mesh to simulate LW accumulation probability p is illustrated in Figure 4.12a. The test program is listed in Table 4.10 and comprises the simulation of a single circular bridge pier (N1-N2), and two circular bridge piers (N3). The test procedure is described in Section 4.7.1 and can be defined as a continuous addition of LW (Section 4.4.4). The corresponding physical model tests are E18-E19 for N1-N2, and C5 for N3 (Table 4.2 versus Table 4.10).

In general, the approach flow conditions were established after 150 s simulation time (Figure 5.69a and Figure 5.70a). Previous studies also confirmed that the flow conditions can be reproduced well using Iber (Ruiz-Villanueva *et al.* 2014c, De Cicco 2018). For tests N1-N2, a log was transported to the pier perpendicular to the flow. Similar to the flume experiments, the log orientation remained constant for the distance between log addition and pier (Section 5.2.2). Depending on the flow velocity fluctuations, some logs hit the bridge pier with a slight eccentricity (Section 5.2.1), turned and dispersed. However, if one log accumulated, the subsequently approaching logs formed a small accumulation at the bridge pier. This process was also observed during the flume experiments for continuous LW transport (Section 5.2.5). The first blocked log then acts as a ‘key log’ and initiates the accumulation. The resulting p are summarized in Table 5.11.

For N1 (Figure 5.69) with the log addition 1 m upstream of the bridge pier, the mean accumulation probability p_m is 23.3%. The simulation was repeated (with $N = 3$) by adding the logs 0.20 m upstream of the bridge pier, resulting in p_m of 63.3%. In contrast to the flume experiments, the position of log addition highly affected p . With a shorter distance to the pier, the log orientation and position relative to the pier are more probable to stay constant, so the logs can hit the pier at its centerline. The high fluctuations between the obtained p for the 3 repetitions are mainly due to the enabled turbulence. If turbulence is enabled, logs are transported with the mean flow velocity plus fluctuations.

Table 5.11 Accumulation probabilities using ‘IberWood’

Tests	N [-]	p [-]	p_m [-]	Flume experiments p [-] and test number
N1	1	0.00		
Log addition 1 m up- stream of pier	2	0.00	0.23	0.73 (E18)
	3	0.70		
N1	1	0.65		
Log addition 0.20 m upstream of pier	2	0.50	0.63	0.73 (E18)
	3	0.75		
N2	1	0.45	0.41	0.94 (E19)
	2	0.00		
	3	0.78		
N3	1	1.00	1.00	0.79 (C5)

**Figure 5.69** Test N1 with log addition 1 m upstream of pier; (a) flow velocity in x -direction v_x prior to LW addition, (b) final LW accumulation, (c) v_x and, (d) water elevation after LW addition

Therefore, logs may be added at the same position for the different runs, but are transported with different flow velocities. Compared to the physical model tests, p is $\approx 10\text{-}50\%$ lower (N1 vs. E18). After 360s (Figure 5.69b), the logs form a small accumulation in front of the bridge pier. This leads to a decrease in flow velocity and increase in depth upstream of the pier, which can be observed in Figure 5.69c and d. Downstream of the pier, the approach flow conditions are established. Note that the black lines in Figure 5.69b are the log trajectories. For N2, all logs were added 1 m upstream of the pier and p_m resulted in 40.9%, which is $\approx 40\%$ lower compared to E19. The deviations in p are mainly due to the missing friction force between pier and log. In addition, the 3D flow field cannot be reproduced by ‘IberWood’, lacking the prominent downward flow in front of the bridge pier. Similar to the physical model tests, p increases with increasing L_L .

For N3 (Figure 5.70), all logs accumulated and p is $\approx 21.1\%$ higher using ‘IberWood’. This can be explained due to the test procedure. With ‘IberWood’, the logs were added continuously, whereas for the flume experiments, a log was extracted, before adding the next log. The continuous LW addition increases p (Section 5.2.5).

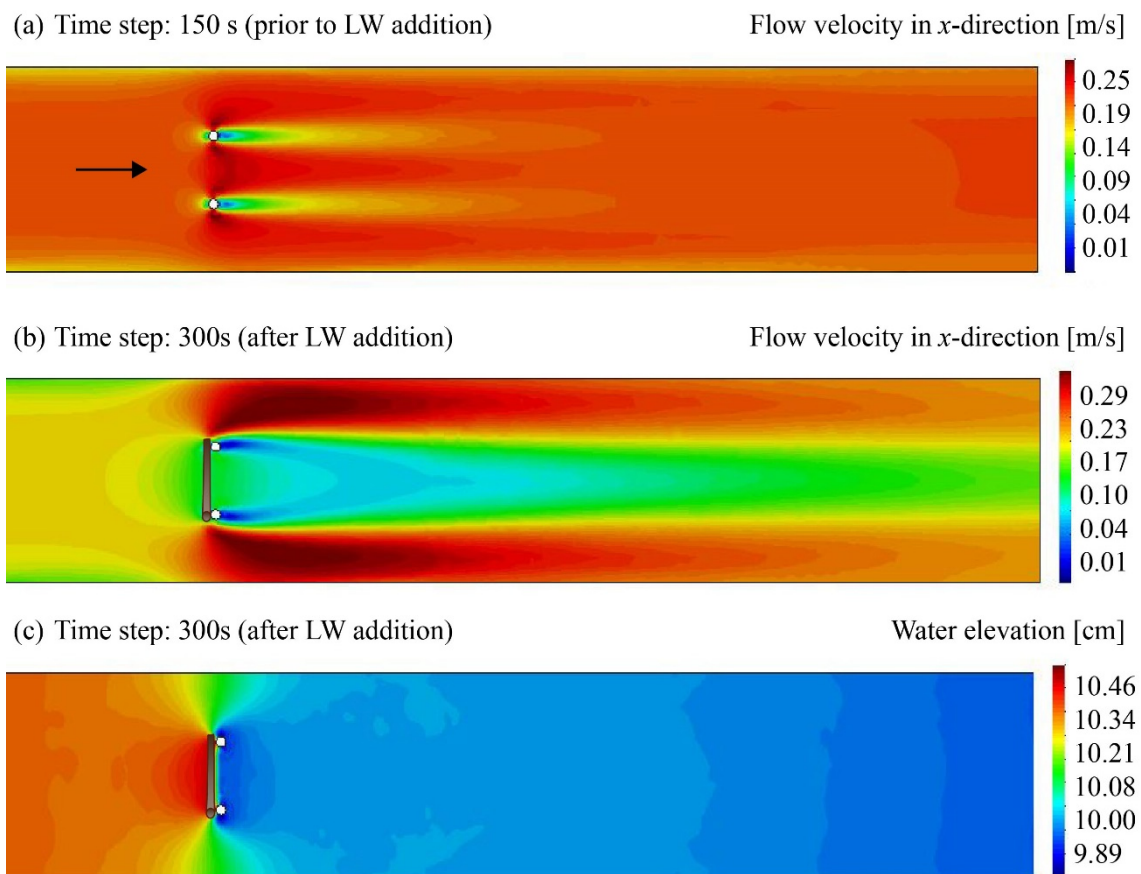


Figure 5.70 Test N3 with (a) flow velocity in x -direction v_x prior and (b) after LW addition, (c) water elevation; model log for visualization

The effect of the accumulation on the hydrodynamics can be observed in Figure 5.70b and c. Due to the spanwise blockage, the flow velocity increases at both log ends and decreases upstream of the accumulation, similar to the flume experiments.

5.5.2 Backwater rise at a retention rack

The numerical model setup for backwater rise due to LW accumulation is illustrated in Figure 4.12b, and the test program is listed in Table 4.10. A first simulation of a retention rack with a LW accumulation was conducted for test N4. The approach flow conditions and LW dimensions are based on the physical model test B7 (Table 4.4). To model the same LW accumulation, ≈ 990 logs ($V_s = 0.0056 \text{ m}^3$ and $\rho_L = 600 \text{ kg/m}^3$) were added homogeneously across the transverse cross-section at the channel inlet. The log position angle varied between 0° and 90° . The first logs passed through the spacing between the rack poles. As soon as one log accumulated, the following logs formed a rather homogeneous accumulation across the rack. Due to the LW accumulation, flow depth 1.5 m upstream of the rack increases to $h_o + \Delta h = 0.141 \text{ m}$ compared to the approach flow depth of $h_o = 0.105 \text{ m}$ (Figure 5.71). Resulting backwater rise with ‘IberWood’ amounts to $\Delta h = 3.54 \text{ cm}$ compared to $\Delta h = 2.10 \text{ cm}$ in test B7. The backwater rise is therefore over-estimated by $\approx 40\%$ with ‘IberWood’, which is above test reproducibility of the physical model tests ($\approx 15\%$; Section 4.5.7), and larger than $\pm 20\%$ prediction range of Eq. (5.16) (Section 5.3.1.7). The approach flow conditions are illustrated in Figure 5.72a and the resulting LW accumulation in Figure 5.72b. The altered hydrodynamics due to the LW accumulation can be observed in Figure 5.72c-d.

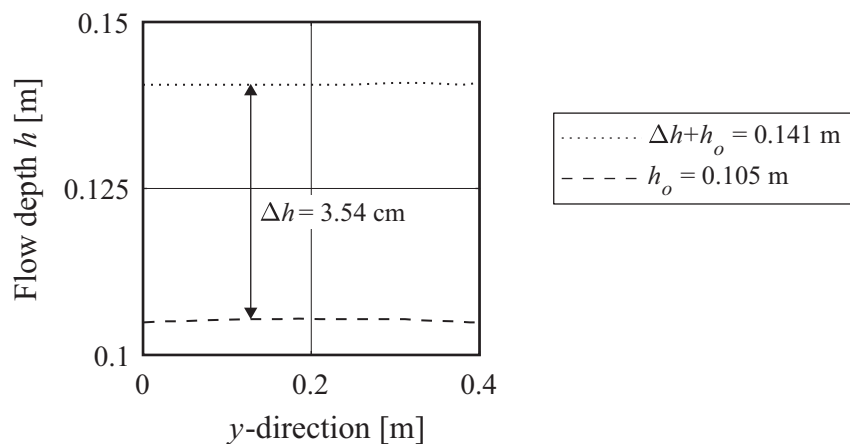


Figure 5.71 Approach flow depth and resulting flow depth 1.5 m upstream of rack using ‘IberWood’

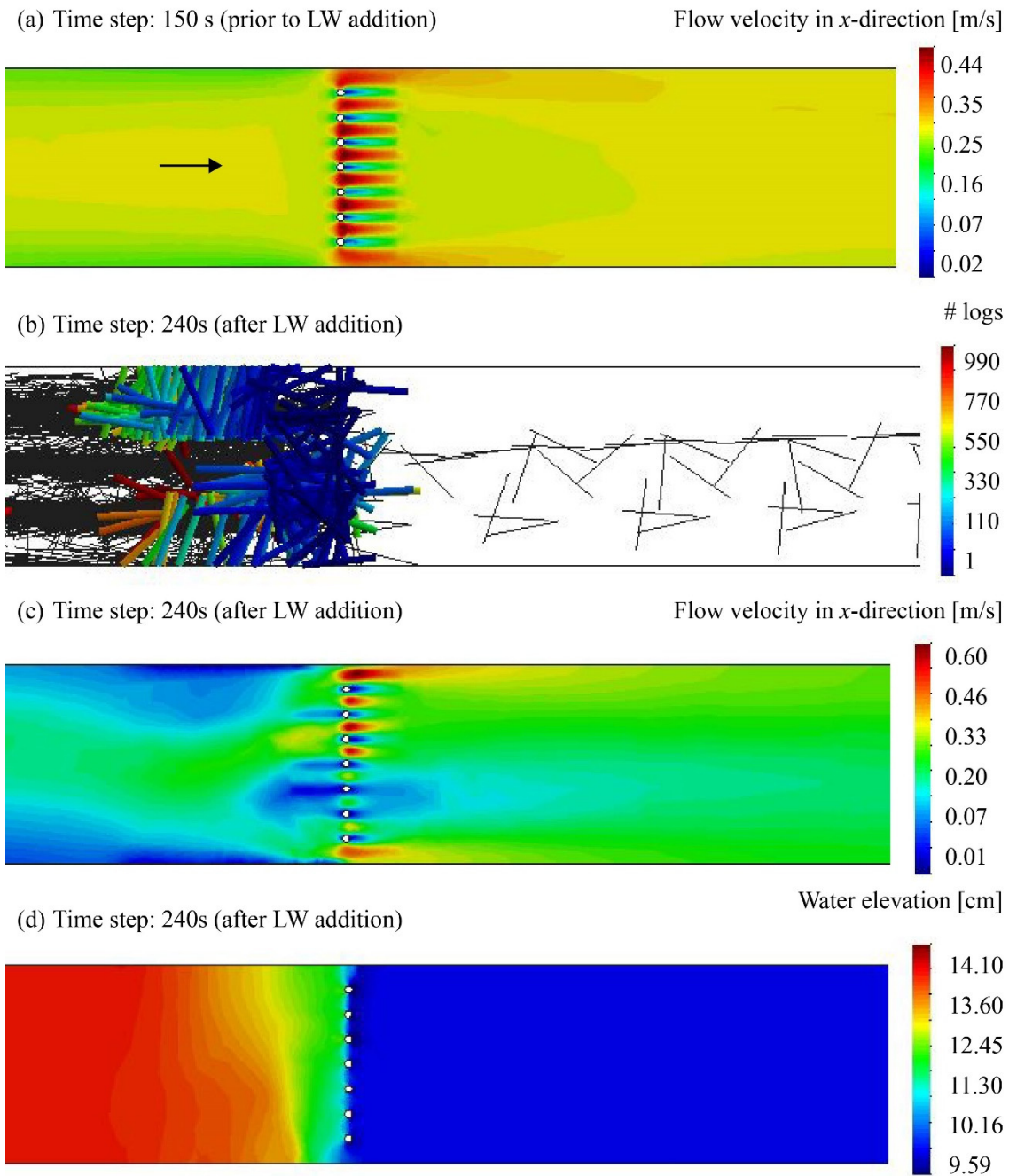


Figure 5.72 Test N4 with (a) flow velocity in x -direction v_x prior to LW addition, (b) final LW accumulation with black lines as log trajectories, (c) v_x and, (d) water elevation after LW addition

Flow velocity decreases upstream of the rack and especially upstream of larger clusters of log accumulations. The LW accumulation length is shorter in the numerical model (Figure 5.72b) and no LW carpet forms, which was observed in the flume experiments for low F_o . In addition, the compactness of the accumulation cannot be accounted for with a 2D simulation model, leading to an overestimation of backwater rise.

5.5.3 Evaluation of 'IberWood'

The experimental results on LW accumulation probability and backwater rise were used to evaluate the application of the 2D numerical simulation model 'IberWood'. The preliminary results can be concluded as follows:

- The simulation approach of 'IberWood' showed first promising results.
- The application and interface of 'IberWood', including the pre- and post-processing tool GiD, is user-friendly and allows rapid analysis of the results.
- The log movement can be reproduced well using 'IberWood'. Similar to the physical model tests, logs were transported with their initial orientation for a short distance. Depending on the transverse velocity distribution in the channel, logs may rotate to align parallel to the flow.
- If turbulence is enabled, repetitions are required to obtain statistically significant results of the accumulation probability p .
- On average, p differed by $\approx 33\%$ compared to the physical model tests, thereby mainly underestimating p . The log-structure interaction still needs to be improved, e.g. as the friction between log and structure is not included. Another option would be to include an empirical equation (Eq. (5.7), Section 5.2.7) or an expert criteria (e.g. Mazzorana *et al.* 2011) to determine the accumulation probability in 'IberWood'.
- The effect of logs on the hydrodynamics is well implemented in 'IberWood'. For a selected set of boundary conditions, a LW accumulation formed upstream of a retention rack, resulting in backwater rise of 3.54 cm, which is $\approx 40\%$ higher compared to the physical model tests. The porosity cannot be accounted for in a 2D model, leading to an overestimation of backwater rise. Natural LW accumulations are a 3D phenomenon. However, the resulting backwater rise with a 2D model can be useful as a first estimate and seems to correspond to a conservative approach.

In general, 'IberWood' is a promising tool to simulate wood transport, deposition, and their effect on the hydrodynamics. However, further validation tests with varying (1) approach flow conditions, (2) LW characteristics, and (3) pier or rack dimensions are deemed necessary to allow the practical application of 'IberWood' in the near future.

6 Computational example

The developed design equations presented in Section 5 aim to improve the flood hazard assessment of transported LW and are summarized in Table 6.1. The applicability of the design equations and the required steps for a LW hazard and risk assessment will be demonstrated in the following computational example.

Table 6.1 Design equations for LW accumulation probability, backwater rise and local scour due to LW accumulations

Description and application range	Equation	Eq. (#)
LW accumulation probability $0 \leq LW_p \leq 0.53$; $R^2 = 0.83$	$p = e^{-12.7 LW_p} = e^{-12.7 x_n \left(\frac{V_o^2}{2gL_L} \right)^{0.43} \left(\frac{d_p}{L_L} \right)^{0.60}}$ $x_n = 1.00$ for uncongested, and $x_n = 0.65$ for congested LW transport	Eq. (5.7)
Backwater rise: box-shape accumulation $F_o = 0.2 \dots 1.4$; $R^2 = 0.95$	$\frac{\Delta h}{h_o} = 5.4 LW_A = 5.4 \frac{F_o u^{1/3} (9FM + 1)}{a^{4/3}}$	Eq. (5.16)
Backwater rise: natural accumulation $F_o = 0.2 \dots 1.5$; $R^2 = 0.97$	$\frac{\Delta h}{h_o} = 5.4 LW_A f_A = 5.4 f_A \frac{F_o u^{1/3} (9FM + 1)}{a^{4/3}}$	Eq. (5.21)
Bulk factor a (accumulation compactness) $F_o = 0.3 \dots 1.5$; $R^2 = 0.87$	$a \approx (5 - 1.35 F_o)$	Eq. (5.19)
Flow diversion factor u and accumulation length L_A	$L_A = \frac{V_l}{h_o B} \text{ and } u = \frac{L_A}{d_{Lm}} = \frac{V_l}{h_o B d_{Lm}} = \frac{a V_s}{h_o B d_{Lm}}$	Eq. (5.20)
Characteristic LW volume: fixed bed $F_o = 0.3 \dots 1.5$; $R^2 = 0.89$	$\frac{V_c}{B h_o^2} = 3.1 F_o$	Eq. (5.11)
Characteristic LW volume: movable bed $F_o = 0.5 \dots 1.5$; $R^2 = 0.98$	$\frac{V_c}{B h_o^2} = 3.1 F_o \left(\frac{h_o}{d_m} \right)^{-0.20}$	Eq. (5.12)
Effect of LW volume on back- water rise $F_o = 0.5 \dots 1.5$; $R^2 = 0.93$	$\eta = \frac{\Delta h}{\Delta h_c} = \left(\frac{V_s}{V_c} \right)^{1/4}$	Eq. (5.22)
Local scour $F_o = 0.5 \dots 1.5$; $S_A = 0 \dots 120$; $R^2 = 0.97$	$\frac{S_{\max}}{d_{90}} = 0.86 \left(\frac{q}{\sqrt{(s-1)gd_m^3}} \right)^{0.85} \left(\frac{V_s}{V_c} \right)^{0.30}$	Eq. (5.24)

The River Glatt is located in the Canton of Zurich, Switzerland, and is 37.5 km long, starting from the Greifensee to the River Rhine. Restoration and local recreation measures are planned at the River Glatt in the area of the city of Zurich (Grün Stadt Zürich 2015, Figure 6.1a). Both river banks are vegetated with bushes and trees, which may increase in subsequent years due to restoration measures. Several cross-sections of the River Glatt are characterized by a series of bridge piers (Figure 6.1b and c). The combination of (1) riverine vegetation, i.e. LW potential, (2) bridge piers and casing upstream of a bridge pier, i.e. hot spots for LW accumulation, and (3) proximity to densely populated area, i.e. potential damage, demands for a LW hazard and risk assessment.



Figure 6.1 (a) Map of River Glatt in Zurich (swisstopo 2017), (b) and (c) circular bridge pier

(1) Hazard identification

- Approach flow conditions (Scherrer AG 2002)

Discharge $HQ_{100} = 93 \text{ m}^3/\text{s}$

Approach flow velocity $v_o = 1.6 \text{ m/s}$

Approach flow depth $h_o = 3.9 \text{ m}$

Approach flow Froude number $F_o = 0.32$

- River infrastructure

Pier diameter $d_P = 1.2 \text{ m}$

Cross-sectional width $B = 12 \text{ m}$

- LW dimensions

Log length $L_L = 3 \dots 6 \text{ m}$ (estimate)

Log diameter $d_L = 0.10 \text{ m}$ (based on Bezzola and Hegg 2007)

(2) Risk analysis

LW accumulation probability can be estimated using Eq. (5.7) for uncongested and semi-congested LW transport. For the risk analysis, Figure 5.24 can be divided into three areas (Figure 6.2), with $p \geq 30\%$ corresponding to high (red area), $p \approx 10\% \dots 30\%$ to medium (blue area), and $p \leq 10\%$ to low probability (yellow area). Depending on the log length, the following accumulation probabilities p result for uncongested LW transport:

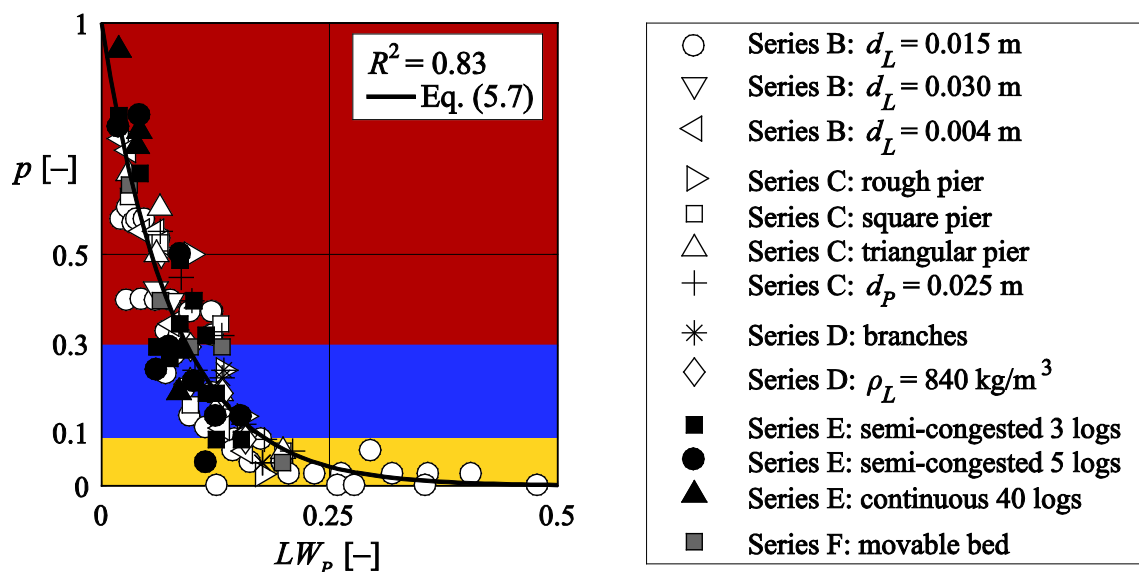


Figure 6.2 Areas for LW accumulation probability risk assessment

$$p_{L_L=3} = e^{-12.7 x_n \left(\frac{v_o^2}{2gL_L} \right)^{0.43} \left(\frac{d_P}{L_L} \right)^{0.60}} = e^{-12.71 \cdot 1.0 \left(\frac{1.6^2}{2g \cdot 3} \right)^{0.43} \left(\frac{1.2}{3} \right)^{0.60}} = 10\%$$

$$p_{L_L=6} = e^{-12.71 \cdot 1.0 \left(\frac{1.6^2}{2g \cdot 6} \right)^{0.43} \left(\frac{1.2}{6} \right)^{0.60}} = 40\%$$

For semi-congested LW transport, p increases to

$$p_{\text{semi-con}, L_L=3} = e^{-12.7 \cdot 0.65 \left(\frac{1.6^2}{2g \cdot 3} \right)^{0.43} \left(\frac{1.2}{3} \right)^{0.60}} = 30\%$$

$$p_{\text{semi-con}, L_L=6} = e^{-12.7 \cdot 0.65 \left(\frac{1.6^2}{2g \cdot 6} \right)^{0.43} \left(\frac{1.2}{6} \right)^{0.60}} = 60\%$$

The maximum accumulation probability amounts to $p_{\max} = 60\%$, corresponding to a high accumulation probability according to Figure 6.2. A casing with a utility cable is positioned upstream of the bridge pier (Figure 6.1b). Depending on the flow depth, this obstruction can lead to a spanwise accumulation. Therefore, it is recommended to estimate backwater rise due to LW accumulation.

- **Backwater rise due to LW accumulation** upstream of the bridge pier and the casing can be estimated for different scenarios (Eq. (5.21)). The required input parameters are defined based on existing flow data and suitable assumptions. Approach flow Froude number and flow depth can be determined based on flow measurement data. For the flow diversion $u = L_A/d_L$, the following assumptions are made: The accumulation length L_A is an uncertain parameter. For this computational example, L_A was calculated with Eq. 5.20 ($L_A = V_{l,\text{eff}}/h_o B$). The potential LW volume $V_{\text{pot}} \approx 2,800 \text{ m}^3$ was determined using Eq. (2.6) (forested stream length; $V_{\text{pot}} = V_l$). The effective LW volume was estimated to amount to 5% of V_{pot} , i.e. $V_{l,\text{eff}} \approx 140 \text{ m}^3$, based on previous studies on the ratio between $V_{\text{eff}}/V_{\text{pot}}$ (Schalko *et al.* 2017). The log diameter d_L was estimated based on values obtained after the 2005 flood (Bezzola and Hegg 2007) and set to $d_L = 0.10 \text{ m}$. For the organic fine material, a percentage of 2.5% was estimated. The bulk factor a can be determined using Eq. (5.19). Given a worst-case scenario with a box-shaped accumulation and a fixed bed, the accumulation type factor f_A amounts to 1 and relative backwater rise results to

$$\frac{\Delta h}{h_o} = 5.4 f_A \frac{F_o u^{1/3} (9FM + 1)}{a^{4/3}} \text{ with } a = (5 - 1.35F_o) = (5 - 1.35 \cdot 0.32) = 4.6 \text{ and}$$

$$u = \frac{L_A}{d_L} = \frac{3 \text{ m}}{0.1 \text{ m}} = 30$$

$$\rightarrow \frac{\Delta h}{h_o} = 5.4 \cdot 1.0 \frac{0.32 \cdot 30^{1/3} (9 \cdot 0.025 + 1)}{4.6^{4/3}} = 0.86$$

For a natural LW accumulation with a fixed bed $f_A = 0.55$, and $\Delta h/h_o$ decreases to 0.47. Given a natural LW accumulation with local scour, $f_A = 0.30$ and $\Delta h/h_o = 0.26$. Compared to the height of the flood embankment (4.3 m), the resulting flow depth with accumulation h is higher for all scenarios, specifically +3 m ($f_A = 1.0$), +1.5 m ($f_A = 0.55$), and +0.7 m ($f_A = 0.3$). LW accumulation therefore intensifies the flood hazard and would lead to flooding of the surrounding area.

- The **characteristic LW volume** V_c , generating the primary backwater rise, can be calculated using Eq. (5.11), assuming a fixed bed. V_c results in

$$\frac{V_c}{h_o^2 B} = 3.1 F_o = 3.1 \cdot 0.32 = 1.00$$

$$V_c = 1.00 \cdot h_o^2 B = 1.00 \cdot 3.90^2 \cdot 12.0 = 181.8 \text{ m}^3$$

The corresponding backwater rise for V_c is $\Delta h_c = 3.66$ m (Eq. (5.21) with $f_A = 1.0$ and $L_A = V_c/Bh_o = 3.9$ m). The effect of varying LW volume on backwater rise can be estimated with the backwater rise ratio η , illustrated in Figure 5.53. The backwater rise ratio amounts to $\eta = \Delta h/\Delta h_c = 0.92$, indicating that the backwater rise for the worst-case scenario ($f_A = 1.0$) is in the range of the characteristic backwater rise.

- **Local scour due to LW accumulation** cannot be estimated, as $F_o = 0.32$ is smaller than the application range of Eq. (5.24) with $F_o \geq 0.50$. In addition, Eq. (5.24) rather applies to local scour at LW retention racks than bridge piers.

(3) Risk evaluation

The resulting accumulation probability and backwater rise in combination with the height of the current flood embankment indicate an increased flood hazard due to LW. Based on the results of the risk analysis, possible measures to ensure the safe downstream guidance of LW or for the retention of LW can be deduced.

The computational example demonstrates the applicability of the proposed design equations, in particular to estimate the accumulation probability, backwater rise due to LW accumulation, and effect of LW volume on backwater rise. It further demonstrates the need for sensitivity analyses of various input parameters.

7 Conclusions and outlook

7.1 Conclusions

Physical experiments were conducted in three different flumes and a 2D numerical simulation was performed with ‘IberWood’ to study hazards related to large wood (LW) in rivers. The thesis comprises the following topics: (1) LW accumulation probability at bridge piers, (2) LW accumulation characteristics at transverse river structures, resulting backwater rise and local scour, (3) design of suitable measures at bridge piers for LW accumulation risk reduction, and (4) numerical simulation of LW accumulation. For the physical model investigations, a model setup was established to study the LW accumulation process at model river infrastructures and its hydraulic and geomorphic impact. All results were summarized in dimensionless design equations. Their practical application is demonstrated in a computational example (Section 6).

(1) Large wood accumulation probability

The objectives of the model tests were to improve the general process understanding of LW accumulations at bridge piers, identify the governing parameters of LW accumulation probability at bridge piers and combine the results in a design equation. The model tests were conducted with a scale factor of 20. The effect of varying approach flow conditions, LW and pier characteristics, and a movable bed on the accumulation probability was investigated. The main findings on LW accumulation probability p are:

- The required number of model test repetitions to obtain statistically significant accumulation probabilities was determined to be $N \geq 40$. Thereby, the reproducibility range results in $\pm 10\%$.
- The flume experiments were conducted in a conservative manner, as the logs were inserted perpendicular to the flow and centered to the bridge pier axis. Logs transported in flow direction resulted in ≈ 6 times lower accumulation probabilities p .
- The accumulation process of a single log at a bridge pier is described in terms of the acting forces: A log detaches from the pier, if the horizontal force component exceeds the friction force $F_H > F_{\text{friction}}$. Thereby, the log exceeds a critical log position angle γ_{cr} . Given a constant roughness coefficient $\mu = 0.6$, $\gamma_{cr\text{-req}}$ resulted in $\approx 60^\circ$, which is up to 3 times higher compared to the observed values, pointing at additional forces and processes inhibiting log detachment.

- LW accumulation probability p increases with increasing log length L_L , decreasing approach flow velocity v_o , for semi-congested and continuous LW transport, and with increasing number of bridge piers.
- The approach flow Froude number and flow depth (F_o, h_o) generally had a negligible effect on the accumulation probability p .
- The bridge pier roughness, logs with branches, pier shape, and a movable bed (i.e. scour) indicated a minor effect on the accumulation probability p .
- Based on a dimensional analysis, the results for uncongested, semi-congested, and continuous LW transport were summarized in a design equation to estimate the accumulation probability p at a single bridge pier (Eq. (5.7)). The governing parameters are log length L_L , approach flow velocity v_o , pier diameter d_P , and LW transport type. L_L exhibits the largest effect on p , with an exponent of -1.03 , followed by v_o with an exponent of 0.86 , and d_P with 0.60 . The effect of LW transport can be considered with a pre-factor x_n , set to $x_n = 1.0$ for uncongested and $x_n = 0.65$ for semi-congested and continuous LW transport. The design equation can be applied for $F_o = 0.08 \dots 1.2$ and $LW_P = 0 \dots 0.53$ ($R^2 = 0.83$) with a prediction range of $\pm 30\%$.
- The recommendations for LW accumulation probability p for more than one bridge pier are summarized based on the relation between log length L_L and axial spacing between the piers to:
 - $L_L > axial\ spacing$: LW accumulation probability resulted in $p \geq 50\%$ for uncongested and $p \geq 75\%$ for semi-congested LW transport for flow velocities ranging from $v_o = 0.20$ m/s up to ≈ 1 m/s (model scale). Therefore, cross-sections with two or more bridge piers are prone to LW accumulations and require further evaluations regarding their hazard potential.
 - $L_L < axial\ spacing$: LW accumulation probability p should be determined using Eq. (5.7), as the accumulation process can be compared to the experiments with a single bridge pier.

(2) Large wood accumulation characteristics – Backwater rise and local scour

The objectives of this part were to examine LW accumulation characteristics and in particular backwater rise and local scour due to LW accumulations. The model tests were conducted in two model flumes and were divided in three test series (Figure 7.1).

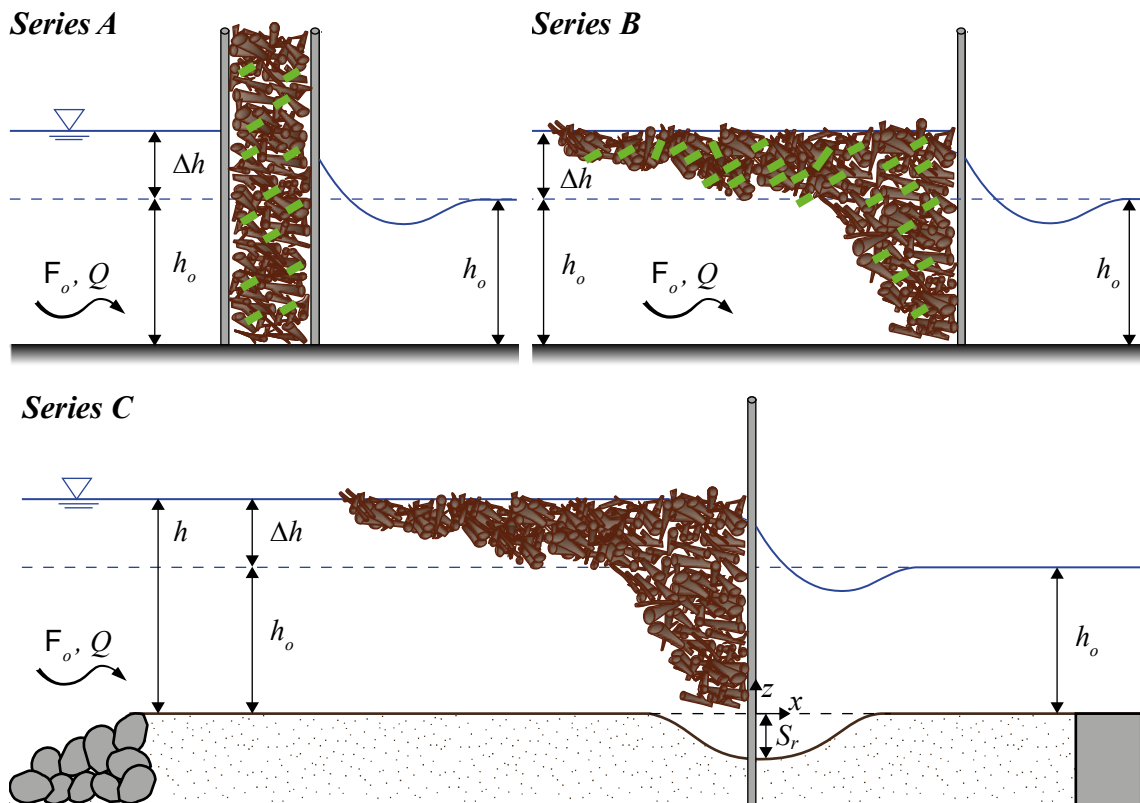


Figure 7.1 Setup for test series A, B, and C on backwater rise and local scour due to LW accumulations

Series A modeled a **predefined LW accumulation with a fixed bed** and studied the effect of approach flow conditions and LW accumulation characteristics on **backwater rise Δh** in a scale series (model scale factor $\lambda = 50$, $\lambda = 30$, and $\lambda = 6$).

Series B investigated **natural LW accumulations with a fixed bed** and the effect of approach flow conditions and LW accumulation volume on **Δh** with $\lambda = 30$ and $\lambda = 6$.

Series C studied **natural LW accumulations with a movable bed** and the effect of approach flow conditions, LW accumulation volume, and bed material on **Δh and local scour S** with $\lambda = 30$.

The main findings can be summarized as follows:

Series A:

- The setup and procedure of the flume experiments can be simplified as a predefined LW accumulation placed between two racks, representing a worst-case scenario that results in the highest backwater rise.
- Based on the results of the investigated scale series, backwater rise is slightly smaller for $\lambda = 30$ compared to $\lambda = 50$ and $\lambda = 6$. However, the variations of $\Delta h/h_o$

for the different model scales are within the reproducibility range. Therefore, possible scale effects are assumed negligible.

- Organic fine material (*FM*; branches and leaves) were modeled using plastic fir trees and natural fir and willow branches. All types of *FM* are suited to model branches and leaves in an accumulation, when added as a volume percentage of the solid LW volume V_s to the accumulation. *FM* affects the LW accumulation characteristics, leading to a smaller porosity and an increased flow diversion due to a longer and more sinuous flow path.
- The approach flow Froude number F_o , bulk factor a (compactness of LW accumulation), accumulation length L_A (representing the expected LW volume), mean log diameter d_{Lm} , and the volume percentage of organic fine material *FM* were identified as the governing parameters for backwater rise Δh .
- Backwater rise Δh increases with increasing approach flow Froude number F_o , accumulation length L_A , and organic fine material *FM* and with decreasing bulk factor a and mean log diameter d_{Lm} . Bulk factor a exhibits the largest effect on Δh with an exponent of $-4/3$, followed by the linear effects of both F_o and *FM* percentage. The flow diversion $u = L_A/d_{Lm}$ shows a minor influence on Δh with an exponent of $1/3$. The governing parameters were combined to a dimensionless LW accumulation factor LW_A , which correlates linearly with the relative backwater rise $\Delta h/h_o$ for $F_o = 0.2 \dots 1.4$ (Eq. (5.16); $R^2 = 0.95$). The prediction range of Eq. (5.16) amounts to $\pm 20\%$.

Series B and C:

- The LW accumulation shape can be approximated as box-like for the first percentages of added LW blocking the main flow cross-section. As soon as a “LW carpet” forms, the LW accumulation shape changes from box-like to a trapezoidal or triangular. The LW carpet leads only to a minor additional increase of backwater rise compared to the first percentages of added LW. With a movable bed, added LW increases the hydraulic load, leading to scour formation. Compared to a fixed bed, scour increases the open cross-sectional area and the LW accumulation extends further vertically downwards.
- The LW volume generating the primary backwater rise prior to the formation of a LW carpet is herein defined as the characteristic LW volume V_c . It can be normalized as a function of the approach flow conditions (F_o and h_o), channel width

B , and bed material characteristics (d_m); Eqs. (5.11)-(5.12) for $F_o = 0.3 \dots 1.5$. The estimation of V_c is especially useful for flood hazard assessment.

- Compared to pre-installed LW accumulations, natural LW accumulations with a fixed bed reduce backwater rise Δh to $\approx 3/5$. Local scour S decreases backwater rise Δh to $\approx 1/3$. Eq. (5.16) was extended by the accumulation type factor f_A to include the effects of a natural accumulation and a movable bed (Eq. (5.21) for $F_o = 0.3 \dots 1.5$; $R^2 = 0.97$). Based on f_A , the following scenarios can be distinguished:
 - *Worst-case scenario*: Box-shaped LW accumulation with a fixed bed is assumed and expected backwater rise Δh calculated with $f_A = 1$ (Eq. (5.16)).
 - *Average-case scenario*: For river infrastructures where no scour may occur, the effect of a movable bed can be neglected and $f_A \approx 3/5$ for natural LW accumulations.
 - *Best-case scenario*: For river infrastructures where scour is expected and tolerable, f_A can be chosen to $\approx 1/3$.
- The variation of the relative LW volume V_s/V_c allows for a scenario-based flood risk assessment and is useful for engineering application. Eq. (5.22) can be applied for $F_o = 0.3 \dots 1.5$ ($R^2 = 0.93$) and enables the analysis of the effect of varying LW volume on Δh .
- The governing parameters to describe the maximum local scour S_{\max} due to LW accumulation are unit discharge q , mean grain size diameter d_m , and relative characteristic LW volume V_s/V_c .
- Local scour increases with increasing q and V_s/V_c , and decreasing d_m . Based on a dimensional analysis, a design equation was deduced to estimate maximum local scour depth S_{\max} due to LW accumulations at retention racks (Eq. (5.24)). The grain size diameter d_m exhibits the largest effect on S_{\max} with an exponent of -1.21 , followed by q with an exponent of 0.85 , and the relative characteristic LW volume with an exponent of 0.30 . Based on a dimensionless scour accumulation factor S_A , the relative maximum scour depth S_{\max}/d_{90} can be described by a linear relationship for $F_o = 0.5 \dots 1.5$ and $S_{\max}/d_{90} > 2$ ($R^2 = 0.97$). The application of this equation is mainly recommended for LW retention racks.

The results of test series A-C improve the process understanding of the formation of LW accumulations at river infrastructures. The design equations enable the prediction

of backwater rise and local scour for floods with considerable LW transport. The results are especially useful for practitioners, as they increase the efficient planning of robust LW retention structures. The data set may further be relevant for the validation of numerical simulation models.

(3) Measures for large wood accumulation risk reduction

The objective of this part was to examine and evaluate existing and new measures at bridge piers regarding their accumulation risk reduction effect. The efficiency of a LW fin and bottom sills was investigated using physical modeling. The resulting accumulation probability p was then compared to the setup without measures. The findings can be summarized as follows:

- The tested configurations of a LW fin did not decrease accumulation probability p , supporting the findings that the pier shape did not affect p . For selected approach flow conditions, accumulation probability p even increased for a LW fin. Based on the tested parameter range, LW fin cannot be recommended as an efficient measure to reduce accumulation probability p .
- Bottom sills are a promising measure to reduce accumulation probability p for a defined range of boundary conditions. The installed sills led to flow diversion and increased turbulence. The best results to reduce LW accumulation probability p were obtained with two consecutive sills (measure B.3), leading to a reduction of accumulation probability p by 30%. The efficiency of bottom sills strongly depends on the approach flow conditions (F_o and h_o) and distance to the bridge pier.

(4) Numerical modeling of large wood accumulation

The experimental results on LW accumulation probability and backwater rise were used to evaluate the 2D numerical simulation model 'IberWood'.

- Similar to the physical model tests, repetitions are required to obtain statistically significant results of the accumulation probability p .
- On average, p was underestimated with 'IberWood' by $\approx 30\%$, as the log-structure interaction still needs to be improved (friction between log and structure is not included). Alternatively, an empirical equation (Eq. (5.7), Section 5.2.7) to determine the accumulation probability in 'IberWood' can be included.

- The effect of logs on the hydrodynamics is well implemented in 'IberWood'. However, backwater rise was overestimated by $\approx 30\%$, as a 2D model cannot reproduce the 3D characteristics of a natural LW accumulation.
- In general, 'IberWood' is a promising tool to simulate wood transport, deposition, and their effect on the hydrodynamics. Further validation tests are required to allow the practical application of 'IberWood' in the near future.

7.2 Outlook

In addition to the findings of the present thesis, the following topics would further improve the process understanding of large wood accumulations and add to the flood hazard assessment:

- Examine the flow conditions in the vicinity of a bridge pier to derive the acting forces on an accumulated log. A more detailed analysis of the log-structure interactions will certainly improve the understanding of the large wood accumulation process at bridge piers.
- Investigate the effect of the strength characteristics (tensile, bending, and flexural), Young's modulus, and density of the model logs on the transport and accumulation behavior.
- Provide estimates for backwater rise and local scour due to large wood accumulations considering unsteady flow conditions (i.e. flood hydrograph), hyper-congested large wood transport, varying log densities, and suspended sediment.
- Conduct experiments with sediment feeding to evaluate the sediment continuity of retention structures or check dams, given a large wood accumulation.
- Analyze the efficiency of bottom sill measures with a movable bed, thereby quantifying the effect of scour and deposition.
- Continue to investigate large wood accumulations using a combined approach of hydraulic and numerical modeling as well as field tests to further improve the process understanding and flood risk assessment.

Furthermore, future research regarding the flood hazard assessment of large wood should aim to put more emphasis on the safe downstream guidance compared to large wood retention and removal, as large wood provides various ecological benefits in river ecosystems.

Notation

Symbols

a	=	Bulk factor [-]
A	=	Area [m ²]
A_{BE}	=	Hazard area due to bank erosion [m ²]
A_{catch}	=	Catchment area [km ²]
$A_{f,catch}$	=	Forested catchment area [km ²]
A_{LS}	=	Hazard area due to landslides [m ²]
A_{pr}	=	Projected area [m ²]
A_{rec}	=	Recruitment area [m ²]
A_s	=	Lateral area [m ²]
A_{sub}	=	Submerged area [m ²]
b	=	Constant to estimate solid large wood volume [-]
b_l	=	Constant to estimate loose large wood [-]
B	=	Width [m]
\bar{B}	=	Average width [m]
B_{Parker}	=	Regime width [m]
B_r	=	Width of retention rack [m]
C	=	Vegetation type coefficient [-]
C_d	=	Drag coefficient [-]
C_{fr}	=	Friction coefficient [-]
d	=	Diameter [m]
d_A	=	Diameter of large wood accumulation [m]
d_{eff}	=	Effective pier diameter [m]
d_{eff}^*	=	Modified effective pier diameter [m]
d_i	=	Grain size diameter at which i-% of the sample is finer [m]
$d_{i,AL}$	=	Grain size diameter of armor layer [m]
d_L	=	Log diameter [m]
d_{Lm}	=	Mean log diameter [m]
d_m	=	Mean grain size diameter [mm]
d_P	=	Pier diameter [m]
d_r	=	Rack pole diameter [m]
d_R	=	Rootstock diameter [m]

d_{R^*}	=	Geometric mean of maximal and minimal rootstock dimensions [m]
D	=	Deposition height [m]
DR	=	Debris roughness index [-]
e	=	Eccentricity [m]
e_{\max}	=	Maximum eccentricity [m]
e^*	=	Relative standard error [-]
$\overline{e^*}$	=	Average relative standard error [-]
e_s	=	Standard error [Unit of the respective variable]
e_x	=	Total error [Unit of the respective variable]
e_X	=	Total error of target value X [Unit of the respective variable]
$e_{X,r}$	=	Relative total error of target value X [%]
e_{xn}	=	Total error of measured parameter x_n [Unit of the respective variable]
f	=	Reduction ratio [-]
F	=	Froude number [-]
FA	=	Froude number within the accumulation [-]
F_o	=	Approach flow Froude number [-]
F	=	Hydraulic force [N]
F_B	=	Buoyancy force [N]
F_{drag}	=	Drag force [N]
$F_{friction}$	=	Friction force [N]
F_G	=	Gravity force [N]
F_H	=	Horizontal force [N]
F_{lift}	=	Lift force [N]
F_N	=	Normal force [N]
f_A	=	Accumulation type factor [-]
f_{eff}	=	Reduction ratio for the effective large wood volume [-]
f_{LS}	=	Landslides reduction ratio [-]
FM	=	Organic fine material [-]
g	=	Gravitational acceleration [m/s^2]
h	=	Flow depth [m]
h_b	=	Height of movable bed [m]
h_B	=	Buoyancy depth [m]
h_A	=	Height of large wood accumulation [m]
h_o	=	Approach flow depth [m]

h_o/H_{Bridge}	=	Relative approach flow depth [-]
h_S	=	Height of sill [m]
h_2	=	Downstream flow depth [m]
H_{Bridge}	=	Clearance height at the bridge [m]
HQ_i	=	Flood with a return period of i -years [m^3/s]
J_o	=	Bottom slope [-]
k_{St}	=	Channel roughness [$\text{m}^{1/3}/\text{s}$]
k_s	=	Equivalent sand roughness [mm]
K_1	=	Accumulation shape factor [-]
K_2	=	Accumulation flow factor [-]
K_d	=	Ratio between scour depth with and without LW accumulation [-]
L	=	Length [m]
L_b	=	Length of movable bed [m]
L_A	=	Length of large wood accumulation [m]
L_C	=	Length of large wood carpet [m]
L_F	=	Forested stream length [km]
L_L	=	Log length [m]
L_P	=	Pier length [m]
LW_A	=	Large wood accumulation factor [-]
LW_{dc}	=	Large wood decay [$\text{m}^3/\text{m s}$]
LW_{in}	=	Large wood input [$\text{m}^3/\text{m s}$]
$LW_{in, FC}$	=	Large wood input from fluvial corridor [$\text{m}^3/\text{m s}$]
$LW_{in, HS}$	=	Large wood input from hillslope [$\text{m}^3/\text{m s}$]
LW_{out}	=	Large wood output [$\text{m}^3/\text{m s}$]
LW_P	=	Large wood probability factor [-]
M	=	Torque [Nm]
n	=	Number of samples [-]
N	=	Number of repetitions [-]
N_{req}	=	Number of required repetitions [-]
p	=	Accumulation probability [-]
p_L	=	Accumulation probability of single logs [-]
p_m	=	Mean / average accumulation probability [-]
p_{min}	=	Minimum accumulation probability [-]
p_{max}	=	Maximum accumulation probability [-]

p_R	=	Accumulation probability of single rootstocks [-]
q	=	Unit discharge [m^2/s]
Q	=	Discharge [m^3/s]
Q_o	=	Approach flow discharge [m^3/s]
$Q_{LW,in}$	=	Wood input rate [m^3/s]
$Q_{LW,out}$	=	Wood output rate [m^3/s]
r	=	residuals [Unit of the respective variable]
R	=	Reynolds number [-]
R_h	=	Hydraulic radius [m]
s	=	Relative sediment density [-]
S	=	Scour depth [m]
S_A	=	Scour accumulation factor [-]
S_m	=	Average cross-sectional scour depth [m]
S_{\max}	=	Maximum scour depth [m]
S_r	=	Scour depth at the rack [m]
SL	=	Sediment load [m^3]
t_T	=	Test duration [s]
t_W	=	Watering time of wood [s]
T	=	Temperature [$^{\circ}\text{C}$]
u	=	Flow diversion factor [-]
v	=	Flow velocity [m/s]
v_A	=	Flow velocity in large wood accumulation [m/s]
v_o	=	Approach flow velocity [m/s]
v_x	=	Flow velocity in x -direction [m/s]
v_y	=	Flow velocity in y -direction [m/s]
V	=	Volume [m^3]
V_c	=	Characteristics large wood volume [m^3]
V_d	=	Volume of discharge [m^3]
V_{eff}	=	Effective large wood volume [m^3]
V_{FM}	=	Volume of organic fine material [m^3]
V_l	=	Volume of loose large wood [m^3]
V_{pot}	=	Potential large wood volume [m^3]
V_s	=	Volume of solid large wood [m^3]
$V_{s,rel}$	=	Relative solid large wood volume [-]

V_{scour}	=	Volume of scour [m^3]
W	=	Constant for scour due to horizontal jets [$\text{m}^{0.3}/\text{s}^{0.6}$]
x	=	Measured quantity [Unit of the respective variable]
x_n	=	Pre-factor for large wood transport type [-]
\bar{x}	=	Mean or expected value [Unit of the respective variable]
X	=	Target value [Unit of the respective variable]
z	=	Constant based on bridge type [-]

Greek symbols

α	=	Normalized height difference [-]
β	=	Bed angle [$^\circ$]
γ	=	Log position angle [$^\circ$]
γ_{cr}	=	Critical log position angle [$^\circ$]
γ_{IC}	=	Initial log position angle [$^\circ$]
δ_1	=	Vertical large wood fin angle [$^\circ$]
δ_2	=	Horizontal large wood fin angle [$^\circ$]
Δ	=	Difference [-]
ΔA	=	Ratio of large wood accumulation area to the flow area [-]
Δh	=	Backwater rise [m]
$\Delta h/h_o$	=	Relative backwater rise [-]
ΔLW	=	Difference in large wood storage [m^3/m]
Δt	=	Difference in time [s]
Δx	=	Difference in length [m]
ε	=	Relative prediction error [-]
η	=	Backwater rise ratio [-]
θ	=	Bed shear stress [-]
θ_{cr}	=	Critical bed shear stress [-]
θ_{IC}	=	Initial bed shear stress [-]
λ	=	Scale factor [-]
μ	=	Friction coefficient [-]
μ_{bed}	=	Bed friction coefficient [-]
ν	=	Kinematic viscosity [m^2/s]
Π_{n-r}	=	non-dimensional parameters of Π -theorem [-]
ρ_{FM}	=	Density of organic fine material [kg/m^3]

ρ_L	=	Density of logs [kg/m ³]
ρ_{sed}	=	Density of sediment [kg/m ³]
ρ_W	=	Density of water [kg/m ³]
σ	=	Water surface tension [kg/s ²]
σ_n	=	Standard deviation of sample [-]
σ_g	=	Standard deviation of the grain size distribution $\sigma_g = (d_{84}/d_{16})^{0.5}$ [-]
τ_{Wood}	=	Wood shear stress [N/m ²]
ϕ	=	Porosity or void fraction of large wood accumulation [-]
Ω_{LW}	=	Stock of large wood [m ³ /m ²]

Subscripts

<i>A</i>	accumulation
<i>AL</i>	armor layer
<i>b</i>	bed
<i>B</i>	Buoyancy
<i>BE</i>	bank erosion
<i>c</i>	characteristic
<i>cr</i>	critical
catch	catchment
<i>C</i>	carpet
<i>dc</i>	decay
<i>d</i>	discharge
eff	effective
<i>f</i>	forested
<i>f,catch</i>	forested catchment
<i>fr</i>	friction
<i>FC</i>	fluvial corridor
<i>FM</i>	organic fine material
<i>FM,f</i>	organic fine material, fir
<i>FM,PVC</i>	organic fine material, PVC
<i>FM,w</i>	organic fine material, willow
<i>g</i>	grain
<i>G</i>	gravity
<i>h</i>	hydraulic

<i>H</i>	horizontal
<i>HS</i>	hillslope
<i>i</i>	certain quantity
<i>in</i>	input
<i>IC</i>	Initial condition
<i>l</i>	loose
<i>L</i>	log
<i>LS</i>	landslides
<i>LW</i>	large wood
<i>m</i>	mean
max	maximum
min	minimum
<i>n</i>	sample
<i>N</i>	normal
<i>o</i>	approach flow
<i>out</i>	output
<i>P</i>	pier
pot	potential
<i>pr</i>	projected
<i>r</i>	rack
rec	recruitment
rel	relative
req	required
<i>R</i>	rootstock
<i>s</i>	solid
<i>sed</i>	sediment
<i>S</i>	sill
sub	submerged
<i>T</i>	test
<i>X</i>	target value
<i>W</i>	water

Abbreviations

ADV	Acoustic Doppler Velocimeter
c	Circular
CG	Center of gravity
Cong.	Congested
Cont.	Continuous
CWD	Coarse woody debris
FOEN	Swiss Federal Office for the Environment
IDM	Electromagnetic Flow Meter
LDS	Laser Distance Sensor
LiDAR	Light detection and ranging
LW	Large wood
LWD	Large woody debris
MW	Medium wood
r	rectangular
Reg.	Regular
Repr.	Reproducibility
RMSE	Root Mean Square Error
sq	Square
SW	Small wood
tr	Triangular
UDS	Ultrasonic Distance Sensor
VAW	Laboratory of Hydraulics, Hydrology and Glaciology

References

- Abbe T.B. and Montgomery D.R. (2003). Patterns and processes of wood debris accumulation in the Queets river basin, WA. *Geomorphology* 51: 81–107.
- Andreoli A., Comiti F., Lenzi M.A. (2007). Characteristics, distribution and geomorphic role of large woody debris in a mountain stream of the Chilean Andes. *Earth Surf. Process. Landforms* 32: 1675–1692.
- Bänziger R. (1989). Schwemmholz, Ursachenanalyse Hochwasser 1987 (Large wood, analysis of the flood 1987). Swiss Federal Institute for Forest, Snow, and Landscape Research WSL. *WSL Report* (in German).
- Benda L.E. and Sias J.C. (2003). A quantitative framework for evaluating the mass balance of in-stream organic debris. *Forest Ecology and Management* 172: 1–16.
- Bertoldi W., Gurnell A.M., Welber M. (2013). Wood recruitment and retention: The fate of eroded trees on a braided river explored using a combination of field and remotely-sensed data sources. *Geomorphology* 180-181: 146–155.
- Bertoldi W., Welber M., Mao L., Zanella S., Comiti F. (2014). A flume experiment on wood storage and remobilization in braided river systems. *Earth Surf. Process. Landforms* 39: 804–813.
- Bertoldi W., Welber M., Gurnell A.M., Mao L., Comiti F., Tal M. (2015). Physical modelling of the combined effect of vegetation and wood on river morphology. *Geomorphology* 246: 178–187.
- Bertram K. and Schärer N. (2015). Aufstau infolge Schwemmholzverkläusungen: Der Einfluss von Feinmaterial (Backwater rise due to large wood accumulations: effect of organic fine material). *Project Thesis*. VAW, ETH Zurich, Switzerland (in German).
- Bezzola G.R. (2017). Flussbau (River engineering). *Lecture notes*, fall semester 2017. ETH Zurich, Switzerland (in German).

- Bezzola G.R., Gantenbein S., Hollenstein R., Minor H.-E. (2002). Verklausung von Brückenquerschnitten (Blocking of bridge cross-sections). *Proc. Intl. Symposium "Moderne Methoden und Konzepte im Wasserbau"*, VAW-Mitteilung 175: 87–97 (H. E. Minor, ed.). ETH Zurich, Switzerland (in German).
- Bezzola G.R. and Hegg C. (2007). Ereignisanalyse Hochwasser 2005 Teil 1: Prozesse, Schäden und erste Einordnung (Analysis of 2005 flood, Part 1: Processes, damages and classification). Federal Office for the Environment FOEN, Swiss Federal Institute for Forest, Snow, and Landscape Research WSL. *Umwelt-Wissen*: 0825 (in German).
- Bezzola G.R. and Hegg C. (2008). Ereignisanalyse Hochwasser 2005 Teil 2: Analyse von Prozessen, Massnahmen und Gefahregrundlagen (Analysis of 2005 flood, Part 2: Analysis of processes, measures and hazard principles). Federal Office for the Environment FOEN, Swiss Federal Institute for Forest, Snow, and Landscape Research WSL. *Umwelt-Wissen*: 0825 (in German).
- Bladé E., Cea L., Corestein G., Escolano E., Puertas J., Vázquez-Cendón M.E., Dolz J., Coll A. (2014). Iber: herramienta de simulación numérica del flujo en ríos (Iber — River modeling simulation tool). *Revista Internacional de Métodos Numéricos para Cálculo y Diseño en Ingeniería* 30(1): 1–10 (in Spanish).
- Bladé E., Sánchez-Juny M., Ruiz-Villanueva V. (2016). Strategies in the 2D numerical modelling of wood transport in rivers. *Proc. 8th River Flow Congress*. St. Louis, MO, USA.
- Bocchiola D., Catalano F., Menduni G., Passoni G. (2002). An analytical–numerical approach to the hydraulics of floating debris in river channels. *Journal of Hydrology* 269: 65–78.
- Bocchiola D., Rulli M.C., Rosso R. (2006a). Flume experiments on wood entrainment in rivers. *Advances in Water Resources* 29: 1182–1195.
- Bocchiola D., Rulli M.C., Rosso R. (2006b). Transport of large woody debris in the presence of obstacles. *Geomorphology* 76: 166–178.

- Bocchiola D., Rulli M.C., Rosso R. (2008). A flume experiment on the formation of wood jams in rivers. *Water Resources Research* 44(2): W02408.
- Bradley J.B., Richards D.L., Bahner C.D. (2005). Debris control structures: Evaluation and countermeasures. *Report No.: FHWA-IF-04-016, U.S. Dept, Transportation, Federal Highway Administration*. Washington, D.C., USA.
- Brändli D. (2014). Aufstau infolge Schwemmh Holzverklausungen (Backwater rise due to large wood accumulations). *Master Thesis*. VAW, ETH Zurich, Switzerland (in German).
- Braudrick C.A., Grant G.E., Ishikawa Y., Ikeda H. (1997). Dynamics of wood transport in streams: A flume experiment. *Earth Surf. Process. Landforms* 22, 669–683.
- Braudrick C.A. and Grant G.E. (2000). When do logs move in rivers? *Water Resources Research* 36(2): 571–583.
- Braudrick C.A. and Grant G.E. (2001). Transport and deposition of large woody debris in streams: a flume experiment. *Geomorphology* 41: 263–283.
- Buckingham E. (1914). On physically similar systems; illustrations of the use of dimensional equations. *Physical Review* 4(4): 345–376.
- Bundesamt für Wasser und Geologie (BWG) (2001). Hochwasserschutz an Fließgewässern (Flood Control at Rivers and Streams). *BWG Guideline*. Biel, Switzerland (in German).
- Chiew Y.M. (1984). Local scour at bridge piers. *Doctoral thesis*. Auckland University, Auckland, New Zealand.
- Comiti F., Andreoli A. Lenzi M.A., Mao L. (2006). Spatial density and characteristics of woody debris in five mountain rivers of the Dolomites (Italian Alps). *Geomorphology* 78: 44–63.
- Comiti F., Lucía A., Rickenmann D. (2016). Large wood recruitment and transport during large floods: A review. *Geomorphology* 269: 23–39.

- Crosato A., Rajbhandari N., Comiti F., Cherradi X., Uijttewaal W.S.J. (2013). Flume experiments on entrainment of large wood in low-land Rivers. *Journal of Hydraulic Research* 51(5): 581–588.
- Curran J.C. (2010). Mobility of large woody debris (LWD) jams in a low gradient channel. *Geomorphology* 116: 320–329.
- Davidson S.L., MacKenzie L.G., Eaton B.C. (2015). Large wood transport and jam formation in a series of flume experiments. *Water Resources Research* 51: 10065–10077.
- De Cicco P.N., Paris E., Solari L. (2016). Wood accumulation at bridges: Laboratory experiments on the effect of pier shape. *Proc. 8th River Flow Congress*. St. Louis, MO, USA.
- De Cicco P.N. (2017). Experimental and numerical investigations on wood accumulation at bridge piers with different shapes. *Doctoral thesis*. TU Braunschweig, Germany and University of Florence, Italy.
- Diehl T. H. (1997). Potential drift accumulation at bridges. *Rep. FHWA-RD-97-028*. U.S. Dept. of Transportation, Federal Highway Administration, Washington, D.C., USA.
- Dixon S. J. and Sear D. A. (2014). The influence of geomorphology on large wood dynamics in a low gradient headwater stream. *Water Resources Research* 50(12): 9194–9210. <https://doi.org/10.1002/2014WR015947>
- Eggenberger W. and Müller R. (1944). Die Kolkbildung beim reinen Unterströmen und allgemeinere Behandlung des Kolkproblems (Scour due to flow under a structure and general analysis of the scour phenomenon). *VAW-Mitteilung* 5. ETH Zurich, Switzerland (in German).
- Elliot R.C., Froehlich D.C., MacArthur R.C. (2012). Calculating the potential effects of large woody debris accumulations on backwater, scour, and hydrodynamic loads. *Proc. World Environmental and Water Resources Congress 2012: Crossing Boundaries*. Albuquerque, NM, USA.
- Ferziger J.H. and Peric M. (2008). Numerische Strömungsmechanik (Computational methods for fluid dynamics). *Springer*, Berlin Heidelberg, Germany (in German).

- Flussbau AG (2012). Ereignisanalyse Hochwasser vom 4. Juli 2012 in der Zulg (Analysis of the flood on July 4, 2012 at the River Zulg). *Report* (in German).
- Franzetti S., Radice A., Rabitti M., Rossi G. (2011). Hydraulic design and preliminary performance evaluation of countermeasure against debris accumulation and resulting local pier scour on River Po in Italy. *Journal of Hydraulic Engineering* 137(5): 615–620.
- Furlan P., Pfister M., Matos J., Amado C., Schleiss T. (2018). Experimental repetitions and blockage of large stems at ogee crested spillways with piers. *Journal of Hydraulic Research*, DOI: 10.1080/00221686.2018.1478897.
- Gems B., Sendlhofer A., Achleitner S., Huttenlau M., Aufleger M. (2012). Evaluierung verklausungsinduzierter Überflutungsflächen durch Kopplung eines physikalischen und numerischen Modells (Evaluation of floodplain areas due to large wood accumulation using hybrid modeling). *Proc. 12th Congress Interpraevent*. Grenoble, France (in German).
- GiD (2012). User Manual of GiD 11. www.gidhome.com (Status: 2018-04-09, 10.30 am)
- Gippel C.J. (1995). Environmental hydraulics of large woody debris in streams and rivers. *Journal of Environmental Engineering* 121(5): 388–395.
- Gippel C.J., O’Neill I.C., Finlayson B.L., Schnatz I. (1996). Hydraulic guidelines for the reintroduction and management of large woody debris in lowland rivers. *Regulated Rivers: Research and Management* 12: 223–236.
- Graf W.H and Altinakar M.S. (2017). Local Scour. *River System Analysis and Management* (Nayan Sharma, ed.). Springer Science+Business Media, Singapore. Chapter 8: 145–166.
- Grün Stadt Zürich (2015). Fil Bleu, Überregionales Freiraumkonzept Glattraum (Fil Bleu, nationwide public space concept in the Glatt area). *Technical Report*. Zurich, Switzerland.
- Gschnitzer T., Gems B., Aufleger M., Mazzorana B., Comiti F. (2013). Physical Scale Model Test on Bridge Clogging. *Proc. 35th IAHR World Congress*. Chengdu, Beijing.

- Gurnell A.M. (2015). Large wood and river morphodynamics. *Engineering Geology for Society and Territory* (G. Lollino, ed.). Springer International, Switzerland. Volume 3, Chapter 25: 131–134.
- Gurnell A.M. and Sweet R. (1998). The distribution of large woody debris accumulations and pools in relation to woodland stream management in a small, low-gradient stream. *Earth Surf. Process. Landforms* 23: 1101–1121.
- Gurnell A.M., Petts G.E., Hannah D.M., Smith B.P.G., Edwards P.J., Kollmann J., Ward J.V., Tockner K. (2000). Wood storage within the active zone of a large European gravel-bed river. *Geomorphology* 34: 55–72.
- Gurnell A.M., Piégay H., Swanson F.J., Gregory S.V. (2002). Large wood and fluvial processes. *Freshwater Biology* 47(4): 601–619.
- Haga H., Kumagai T., Otsuki K., Ogawa S. (2002). Transport and retention of coarse woody debris in mountain streams: An in situ field experiment of log transport and a field survey of coarse woody debris distribution. *Water Resources Research* 38(8): 1029–1044.
- Hager W.H. and Hutter K. (1984). On pseudo-uniform flow in open channel hydraulics. *Acta Mechanica* 53(3-4): 183–200.
- Hager W.H. and Unger J. (2010). Bridge pier scour under flood waves. *Journal of Hydraulic Engineering* 136(10): 842–847.
- Hartlieb A. and Bezzola G.R. (2000). Ein Überblick zur Schwemmholzproblematik (Overview of problems associated with large wood). *Wasser, Energie, Luft* 92(1–2): 1–5 (in German).
- Hartlieb A. (2012). Large scale hydraulic model tests for floating debris jams at spillways. *Proc. 2nd IAHR Europe Congress*. Munich, Germany.
- Hartlieb A. (2015). Schwemmholz in Fließgewässern - Gefahren und Lösungsmöglichkeiten (Large wood in rivers – hazards and possible solutions). *Report 133*. Versuchsanstalt Oberrach, TU Munich, Germany (in German).

- Hassan M.A., Bird S., Reid D., Hogan D. (2016). Simulated wood budgets in two mountain streams. *Geomorphology* 259: 119–133.
- Heller V. (2011). Scale effects in physical hydraulic engineering models. *Journal of Hydraulic Research*. 49(3): 293–306.
- Hering E., Rolf M., Stohrer M. (1995). *Physikalisch-technisches Taschenbuch* (Physical technical practice manual). VDI-Verlag, Düsseldorf, Germany (in German).
- Hughes S.A. (2005). *Physical models and laboratory techniques in coastal engineering*. Advanced series on ocean engineering 7, World Scientific, Singapore.
- Hygelund B. and Manga M. (2003). Field measurements of drag coefficients for model large woody debris. *Geomorphology* 51: 175–185.
- Ishikawa Y. (1990). Studies on Disasters Caused by Debris Flows Carrying Floating Logs Down Mountain Streams. *Doctoral thesis*. Kyoto University, Japan.
- Jegorow S.A. (1941). Versuche über den der Wasserströmung voreilenden Baumstamm (Experiments on logs leading the water flow). *Wasserkraft und Wasserwirtschaft* 1: 17–22.
- Jirka G.H. and Uijtewaal W.S.J. (2004). Shallow flows: a definition. In *Shallow Flows* (G.H. Jirka and W.S.J. Uijtewaal, ed.). Taylor & Francis: 3–11.
- Keller E.A. and Swanson F.J. (1979). Effects of large organic material on channel form and fluvial processes. *Earth Surf. Process. Landforms* 4: 361–380.
- Knauss J. (1995). Von der oberen zur unteren Isar (From the upper to the lower Isar). *Report 76*: 23–66. Versuchsanstalt Obernach, TU Munich, Germany (in German).
- Kramer N. and Wohl E. (2015). Driftcretions: The legacy impacts of driftwood on shoreline morphology. *Geophys. Res. Lett.* 42(14): 5855–5864.
- Lagasse P.F., Zevenbergen L.W., Clopper P.E. (2010). Impacts of debris on bridge pier scour. *Proc. 5th International Conference on Scour and Erosion*. San Francisco, CA, USA.

- Lageder C. (2016). Geschiebedurchgängigkeit von Schwemmholzrechen (Sediment continuity at large wood retention racks). *Master Thesis*. VAW, ETH Zurich, Switzerland (in German).
- Lange D. and Bezzola G.R. (2006). Schwemmholz: Probleme und Lösungsansätze (Large wood: problems and countermeasures). *VAW-Mitteilung* 188 (H.-E. Minor, ed.). ETH Zurich, Switzerland (in German).
- Lassette N.S., Piégay H., Dufour S., Rollet A.J. (2008). Decadal changes in distribution and frequency of wood in a free meandering river, the Ain River, France. *Earth Surf. Process. Landforms* 33: 1098–1112.
- Laursen E.M. and Toch A. (1956). Scour around bridge piers and abutments. *Bulletin No. 4, Iowa Highway Research Board*. Iowa Institute of Hydraulic Research in cooperation with the Iowa State Highway Commission and the Bureau of Public Roads, IA, USA.
- Lienkamper G.W. and Swanson F.J. (1987). Dynamics of large woody debris in streams in old-growth Douglas-fir forests. *Can. J. For. Res.* 17: 150–156.
- Lucía A., Comiti F., Borga M., Cavallo M., Marchi L. (2015). Dynamics of large wood during a flash flood in two mountain catchments. *Nat. Hazards Earth Syst. Sci.* 15: 1741–1755.
- Lyn D.A., Cooper T., Yi Y.K., Sinha R., Rao A.R. (2003). Debris accumulation at bridge crossings: Laboratory and field studies. *Report No.: FHWA/IN/JTRP-2003/10*. Joint Transportation Research Program, Purdue University, West Lafayette, IN, USA.
- MacVicar B.J., Piégay H., Henderson A., Comiti F., Oberlin C., Pecorari E. (2009). Quantifying the temporal dynamics of wood in large rivers: field trials of wood surveying, dating, tracking, and monitoring techniques. *Earth Surf. Process. Landforms* 34: 2031–2046.
- Mächler M. (2009). GIS-Modellierung von potentiellm Schwemmholzeintrag von Rutschungen (GIS modeling of potential large wood entrainment due to landslides). *ZAHW term paper*, Wädenswil, Switzerland (in German).

- Manners R.B., Doyle M.W., Small M.J. (2007). Structure and hydraulics of natural woody debris jams. *Water Resources Research* 43: W06432.
- Manners R.B. and Doyle M.W. (2008). A mechanistic model of woody debris jam evolution and its application to wood-based restoration and management. *River Res. Appl.* 24(8): 1104–1123.
- Martin H. and Pohl R. (2015). *Technische Hydromechanik 4* (Technical hydromechanics 4). Verlag Bauwesen. Berlin, Germany (in German).
- Mazzorana B., Zischg A., Largiader A., Hübl J. (2009). Hazard index maps for woody material recruitment and transport in alpine catchments. *Nat. Hazards Earth Syst. Sci.* 9: 197–209.
- Mazzorana B., Hübl J., Zischg A., Largiader A. (2011). Modelling woody material transport and deposition in alpine rivers *Nat. Hazards* 56: 425–449.
- Melville B.W. and Sutherland A.J. (1988). Design method for local scour at bridge piers. *Journal of Hydraulic Engineering* 114(10): 1210–1226.
- Melville B.W. and Dongol D.M. (1992). Bridge pier scour with debris accumulation. *Journal of Hydraulic Engineering* 118(9): 1306–1310.
- Melville B.W. and Chiew Y.M. (1999). Time scale for local scour at bridge piers. *Journal of Hydraulic Engineering* 125(1): 59–65.
- Melville B.W. and Coleman S.E. (2000). *Bridge scour*. Water Resources Publication, LLC. CO, USA. 550 p.
- Merten E., Finlay J., Johnson L., Newman R., Stefan H., Vondracek B. (2010). Factors influencing wood mobilization in streams. *Water Resources Research* 46(10): W10514.
- Meyer J. and Rimböck A. (2014). GIS basierter Ansatz zur Abschätzung des Schwemmh Holzpotenzials in Wildbächen (GIS based method to estimate large wood potential in torrents). *Proc. Intl. Symposium "Wasser- und Flussbau im Alpenraum"*, VAW-Mitteilung 228: 443–452 (R.M. Boes, ed.). ETH Zurich (in German).

- Meyer-Peter E. and Müller R. (1948). Formulas for bed-load transport. *Proc. 2nd IAHR Congress, Vol. A2, IAHR*. Delft, Netherlands. 1–26.
- Nakamura F. and Swanson F.J. (1994). Distribution of coarse woody debris in a mountain stream, western Cascade Range, Oregon. *Can. J. For. Res.* 24: 2395–2403.
- Oliveto G. and Hager W.H. (2002). Temporal evolution of clear-water pier and abutment scour. *Journal of Hydraulic Engineering* 128(9): 811–820.
- Pagliara S. and Carnacina I. (2011). Influence of wood debris accumulation on bridge pier scour. *Journal of Hydraulic Engineering* 137(2): 254–261.
- Panici D. and de Almeida G.A.M. (2017). Understanding the formation of woody debris jams at bridge piers. *Proc. 37th IAHR World Congress*. Kuala Lumpur, Malaysia.
- Parker G. (1979). Hydraulic geometry of active gravel rivers. *Journal of the Hydraulics Division* 105(9): 1185–1201.
- Perham R. E. (1987). Floating debris control: A literature review. *Rep. REMR-HY-3, U.S. Army Corps of Engineers*. Washington, DC, USA.
- Piégay H. and Gurnell A.M. (1997). Large woody debris and river geomorphological pattern: examples from S.E. France and S. England. *Geomorphology* 19: 99–116.
- Piton G. and Recking A. (2015). Design of sediment traps with open check dams. II: Woody debris. *Journal of Hydraulic Engineering* 142(2): 04015046.
- Ravazzolo D., Mao L., Picco L., Lenzi M.A. (2015a). Tracking log displacement during floods in the Tagliamento River using RFID and GPS tracker devices. *Geomorphology* 228: 226–233.
- Ravazzolo D., Mao L., Picco L., Lenzi M.A. (2015b). Geomorphic effects of wood quantity and characteristics in three Italian gravel-bed rivers. *Geomorphology* 246: 79–89.
- Rickenmann D. (1997). Schwemmh Holz und Hochwasser (Large wood and floods). *Wasser Energie Luft* 89(5–6): 115–119 (in German).

- Rickli C. and Bucher H. (2006). Schutzwald und Schwemmholz in Wildbacheinzugsgebieten (Protection forest and large wood in mountainous catchment areas). *FAN-Agenda* 1 (July): 17–20 (in German).
- Rickli C., Kamm S., Bucher, H. (2008). Flachgründige Rutschungen, Ereignisanalyse Hochwasser 2005 (Shallow landslides, Analysis of the 2005 flood). Federal Office for the Environment FOEN, Swiss Federal Institute for Forest, Snow, and Landscape Research WSL. *WSL Report* (in German).
- Rimböck A. (2001). Luftbasierte Abschätzung des Schwemmholzpotentials (LASP) in Wildbächen (Aerial surveys to estimate the large wood potential in torrents). *Report* 91. Versuchsanstalt Obernach, TU Munich, Germany: 202–213 (in German).
- Rimböck A. (2003). Schwemmholzrückhalt in Wildbächen (Large wood retention in mountain torrents). *Report* 94. Versuchsanstalt Obernach, TU Munich, Germany (in German).
- Rinaldi M., Amponsah W., Benvenuti M., Borga M., Comiti F., Lucía A., Marchi L., Nardi L., Righini M., Surian N. (2016). An integrated approach for investigating geomorphic response to extreme events: methodological framework and application to the October 2011 flood in the Magra River catchment, Italy. *Earth Surf. Process. Landforms* 41: 835–846.
- Ruiz-Villanueva V. (2012). Nuevas metodologías en la evaluación de la peligrosidad y el riesgo por avenidas en cuencas de montaña (New methods for the analysis of flash flood hazard and risk in mountain basins). *Doctoral thesis*. Universidad Complutense de Madrid, Spain (in Spanish).
- Ruiz-Villanueva V., Díez-Herrero A., Ballesteros J.A., Bodoque J.M. (2014a). Potential large woody debris recruitment due to landslides, bank erosion and floods in mountain basins: A quantitative estimation approach. *River Res. Applic.* 30: 81–97.
- Ruiz-Villanueva V., Bladé Castellet E., Díez-Herrero A., Bodoque J.M., Sánchez-Juny M. (2014b). Two-dimensional modelling of large wood transport during flash floods. *Earth Surf. Process. Landforms* 39: 438–449.

- Ruiz-Villanueva V., Bladé-Castellet E., Sánchez-Juny M., Díez-Herrero A., and Bodoque J. M. (2014c). Two-dimensional numerical modeling of wood transport. *Journal of Hydroinformatics* 16(5): 1077–1096.
- Ruiz-Villanueva V., Badoux A., Boes R.M, Rickenmann D., Rickli C., Schalko I., Schmocker L., Schwarz M., Steeb N., Stoffel M., Weitbrecht V. (2016a). Large wood research in Swiss watercourses. *Proc. 8th River Flow Congress*. St. Louis, MO, USA.
- Ruiz-Villanueva V., Piégay H., Gurnell A., Marston R.A., Stoffel M. (2016b). Recent advances quantifying the large Wood dynamics in river basins: New methods and remaining challenges. *Rev. Geophys.* 54(3): 611–652.
- Ruiz-Villanueva V., Piégay H., Gaertner V., Perret F., Stoffel M. (2016c). Wood density and moisture sorption and its influence on large wood mobility in rivers. *Catena* (140): 182–194.
- Ruiz-Villanueva V., Wyzga B., Zawiejska J., Hajdukiewicz M., Stoffel M. (2016d). Factors controlling large-wood transport in a mountain river. *Geomorphology* 272: 21–31.
- Ruiz-Villanueva V., Mazzorana B., Mao L., Ravazzolo D., Wohl E., Bürkli L, Iribarren-Anacona, P., Nakamura F., Stoffel M. (2018). Observation, definition and characteristics of wood-laden flows using home videos: redefining flows in forested river basins?. *Geophys. Res. Lett.* (in review).
- SCD (2017). Floating debris at reservoir dam spillways. Swiss Committee on Dams, *Report*, www.swissdams.ch.
- Schalko I. (2017). Large wood accumulation probability at a single bridge pier. *Proc. of the 37th IAHR World Congress*, Kuala Lumpur, Malaysia: 1704-1713.
- Schalko I., Schmocker L., Weitbrecht V., Boes R. (2016). Modeling the effect of organic fine material in a driftwood accumulation on backwater rise. *Proc. River Flow 2016*, St. Louis, USA, Constantinescu, Garcia & Hanes (Eds.), ISBN 978-1-138-02913-2: 2326-2332.
- Schalko I., Schmocker L., Weitbrecht V., Boes R. (2017). Schwemmholz: Gefahrenbeurteilung und Massnahmenplanung am Fallbeispiel Renggbach, Kanton Luzern. (Large

- wood: Hazard assessment and action planning for the case study Renggbach, Canton Lucerne). *Wasser Energie Luft* 109(4): 271–278 (in German).
- Schalko I., Schmocker L., Weitbrecht V., Boes R. (2018a). Backwater rise due to large wood accumulations. *Journal of Hydraulic Engineering* 144(9): 04018056.
- Schalko I., Schmocker L., Weitbrecht V., Boes R. (2018b). Hazards due to large wood accumulations: Local scour and backwater rise. *Proc. River Flow 2018*, Lyon, France.
- Schaller D. (2015). Aufstau infolge Schwemmh Holzverklausung unter Berucksichtigung von Feinanteil (Backwater rise due to large wood accumulations considering the effect of organic fine material). *Master Thesis*. VAW, ETH Zurich, Switzerland (in German).
- Schenk E.R., Moulin B., Hupp C.R., Richter J.M. (2014). Large wood budget and transport dynamics on a large river using radio telemetry. *Earth Surf. Process. Landforms* 39: 487–498.
- Scherrer AG (2002). Der Einfluss der Siedlungsentwicklung auf die extremen Hochwasser der Glatt (ZH) (The effect of settlement development on extreme floods at the River Glatt). *Technical Report*. Switzerland (in German)
- Schmocker L. and Hager W.H. (2011). Probability of drift blockage at bridge decks. *Journal of Hydraulic Engineering* 137(4): 480–492.
- Schmocker L. and Weitbrecht V. (2013). Driftwood: Risk analysis and engineering measures. *Journal of Hydraulic Engineering* 139(7): 683–695.
- Schmocker L. and Hager W.H. (2013). Scale modelling of wooden debris accumulation at a debris rack. *Journal of Hydraulic Engineering* 139(8): 827–836.
- Schneider K.J. (2001). *Bautabellen fur Ingenieure* (Construction tables for engineers) (K.J. Schneider, ed.). Werner Verlag. 14th Edition. ISBN 3-8041-4184-6 (in German).

- Schütz T. (2013). *Hucho – Aerodynamik des Automobils* (Aerodynamics of road vehicles) (T. Schütz, ed.). Springer-Vieweg. 6th Edition. ISBN 978-3-8348-1919-2 (in German).
- Shields D.F. and Gippel C.J. (1995). Prediction of effects of woody debris removal on flow resistance. *Journal of Hydraulic Engineering* 121(4): 341–354.
- Shields D.F. and Alonso C.V. (2012). Assessment of flow forces on large wood in rivers. *Water Resources Research* 48: W045416. doi:10.1029/2011WR011547.
- Steeb N., Rickenmann D., Badoux A., Rickli C., Waldner P. (2017). Large wood recruitment processes and transported volumes in Swiss mountain streams during the extreme flood of August 2005. *Geomorphology* 279: 112–127.
- Stockstill R.L., Daly S.F., Hopkins M.A. (2009). Modeling floating objects at river structures. *Journal of Hydraulic Engineering* 135(5): 403–414.
- Swanson F.J. (2003). Wood in rivers: A landscape perspective. *American Fisheries Society Symposium* 37: 299–313.
- Uchiogi T., Shima J., Tajima H., Ishikawa Y. (1996). Design methods for wood-debris entrapment. *Proc. Intl. Symposium Interpraevent*. Volume 5: 279–288. Klagenfurt, Austria.
- Versuchsanstalt für Wasserbau, Hydrologie und Glaziologie (VAW) der ETH Zürich (1991). Umleitstollen Campo Vallemaggia (Sediment bypass tunnel Campo Callemaggia). *VAW-Report* 940. ETH Zurich, Switzerland (in German).
- Versuchsanstalt für Wasserbau, Hydrologie und Glaziologie (VAW) der ETH Zürich (2001). Schwemmholz Riemenstaldnerbach (Large wood at the River Riemenstaldnerbach). *VAW-Report* 4138. ETH Zurich, Switzerland (in German).
- Versuchsanstalt für Wasserbau, Hydrologie und Glaziologie (VAW) der ETH Zürich (2008). Ereignisanalyse Hochwasser 2005: Teilprojekt Schwemmholz (Analysis of the 2005 flood: Sub-project large wood). *VAW-Report* 4240. ETH Zurich, Switzerland (in German).

- Waldner P., Köchli D., Usbeck T., Schmocker L., Sutter F., Rickli C., Rickenmann D., Lange D., Hilker N., Wirsch A., Siegrist R., Hug C., Kaennel M. (2009). Schwemmholz des Hochwassers 2005 (Large wood during the 2005 flood). Federal Office for the Environment FOEN, Swiss Federal Institute for Forest, Snow, and Landscape Research WSL, Switzerland. *WSL Report* (in German).
- Wallerstein N.P. (2003). Dynamic model for constriction scour caused by large woody debris. *Earth Surf. Process. Landforms* 28(1): 49–68. <https://doi.org/10.1002/esp.426>
- Wallerstein N.P., Thorne C.R., Abt S.R. (1996). Debris control at hydraulic structures – management of woody debris in natural channels and at hydraulic structures. *Report prepared for the U.S. Army Corps of Engineers, Waterways Experiment Station*. Vicksburg, MS, USA.
- Wallerstein N.P., Thorne C.R., Abt S.R. (1997). Debris control at hydraulic structures in selected areas of the United States and Europe. *Report prepared for the U.S. Army Research Development & Standardization Group*. London, UK.
- Wallerstein N.P., Alonso C. V., Bennett S. J., Thorne C.R. (2001). Distorted Froude-scaled flume analysis of large woody debris. *Earth Surf. Process. Landforms* 26(12): 1265–1283. <https://doi.org/10.1002/esp.271>
- Wallerstein N.P., Alonso C.V., Bennett S.J., Thorne C.R. (2002). Surface wave forces acting on submerged logs. *Journal of Hydraulic Engineering* 128(3), 349–353.
- Werdenberg N., Mende M., Sindelar C. (2014). Instream river training: Fundamentals and practical example. *Proc. 7th River Flow Congress*. Lausanne, Switzerland.
- Wohl E. (2011). Threshold-induced complex behavior of wood in mountain streams. *Geology* 39(6): 587–590.
- Wohl E. and Goode J.R. (2008). Wood dynamics in headwater streams of the Colorado Rocky Mountains. *Water Resources Research* 44: W09429.
- Wohl E. and Jaeger K. (2009). A conceptual model for the longitudinal distribution of wood in mountain streams. *Earth Surf. Process. Landforms* 34: 329–344.

- Wohl E., Bledsoe B.P., Fausch K.D., Kramer N., Bestgen K.R., Gooseff M.N. (2016). Management of large wood in streams: an overview and proposed framework for hazard evaluation. *Journal of the American Water Resources Association (JAWRA)* 52(2): 315–335.
- Wyzga B. and Zawiejska J. (2005). Wood storage in a wide mountain river: case study of the Czarny Dunajec, Polish Carpathians. *Earth Surf. Process. Landforms* 30: 1475–1494.
- Xu Y. and Liu X. (2016). 3D computational modeling of stream flow resistance due to large woody debris. *Proc. 8th River Flow Congress*. St. Louis, MO, USA.
- Yano A., Kitagawa Y., Taniguchi H., Nishimura K., Dozono S. (2015). Estimation of drift woods discharge from A-class Rivers in the Ariake Sea by their numerical transport simulation. *Proc. 36th IAHR World Congress*. The Hague, the Netherlands.
- Young W.J. (1991). Flume study of the hydraulic effects of large woody debris in lowland rivers. *Regulated Rivers: Research & Management* 6: 203–211.
- Zarn B. (1992). Lokale Gerinneaufweitungen: Eine Massnahme zur Sohlenstabilisierung der Emme bei Utzendorf (Local river widenings: a measures to stabilize the bed of the River Emme in Utzendorf, Switzerland). *VAW-Mitteilung* 118. ETH Zurich, Switzerland (in German).
- Zollinger F. (1983). Die Vorgänge in einem Geschiebeablagerungsplatz (Processes in a sediment retention basin). *Doctoral thesis* Nr. 7419. ETH Zurich, Switzerland (in German).

Curriculum Vitae



Isabella Schalko

•
 Laboratory of Hydraulics, Hydrology and Glaciology (VAW)
 ETH Zurich
 Hönggerbergring 26, HIA C 53, 8093 Zurich

•
 Email: schalko@vaw.baug.ethz.ch

ORCID Profile: <https://orcid.org/0000-0002-4602-0758>

Education

- | | |
|-----------------|--|
| 09/2015-09/2018 | Doctoral candidate, ETH Zurich, Switzerland
Doctoral examination on September 12, 2018
Doctoral supervisor: Prof. Dr. Robert M. Boes
Dissertation title: Modeling hazards related to large wood in rivers |
| 11/2009-11/2011 | Master's degree with distinction, Environmental Engineering, University of Natural Resources and Life Sciences Vienna (BOKU) |
| 02/2009-08/2009 | Exchange semester at ETH Zurich |
| 10/2005-11/2009 | Bachelor's degree, Environmental Engineering, BOKU, Austria |
| 06/2005 | Matriculation examination with distinction, Vienna, Austria |
| 08/2003-06/2004 | Highschool exchange at Analy High School, CA-95472 Sebastopol |

Professional experience

- | | |
|-----------------|--|
| Since 09/2015 | Scientific assistant, River Engineering Division, VAW, ETH Zurich |
| 01/2014-08/2015 | Teaching assistant, Chair of Hydraulic Structures, VAW, ETH Zurich |
| 03/2012-12/2013 | Scientific assistant, Institute of Hydraulics and Rural Water Management, BOKU |

Teaching activities

- | | |
|-----------------|---|
| 01/2014-08/2015 | Lecture Assistance at VAW, ETH Zurich
Revitalisierung von Fließgewässern (River Revitalization)
Flussbau (River Engineering)
Wasserbau (Hydraulic Engineering) |
| 03/2012-12/2013 | Lecture Assistance at Institute of Hydraulics and Rural Water Management, BOKU
Hydrodynamik (Hydrodynamics; MSc; 120 students) |

Supervision of student theses in Civil Engineering and Environmental Engineering at ETH Zurich

Master theses

- | | |
|-------------|---|
| Fall 2018 | Sediment continuity and large wood retention at check dams
Sediment continuity of check dams in the Ct. Zurich |
| Spring 2017 | Flood protection and river revitalization at the River Chommlibach
Sediment continuity of large wood retention racks |

Fall 2016	Integral flood protection concept at the River Luthern (Ct. Lucerne) Effect of inclined large wood retention racks on sediment continuity
Spring 2016	Experimental investigation of large wood at fish guidance structures
Fall 2015	Backwater rise due to large wood accumulation
Spring 2015	Effect of hydropower plant expansion on waterfall appearance for the case study Diesbach (Ct. Glarus) Measures against reservoir sedimentation at reservoir Livigno (Ct. Grisons)
Spring 2014	Hydropower due to glacial retreat in Switzerland Hydropower at the Gorner glacier (Ct. Valais) Measures against reservoir sedimentation at Lai da Ova Spin (Ct. Grisons)

Supervision of **29 project theses students** and **9 bachelor theses students** on topics of flood protection, reservoir sedimentation, and large wood volume and retention racks.

Reviewer

[Geomorphology](#), [Water Resources Research \(WRR\)](#)

Active memberships

Since 2017	European Geosciences Union (EGU)
Since 2017	International Association for Hydro-Environment Engineering and Research (IAHR)
Since 2014	Academic Association of Scientific Staff at ETH Zurich (AVETH)

Prizes and awards

08/2017	1st Place at John F. Kennedy Student Paper Competition at 37 th IAHR World Congress, Kuala Lumpur, Malaysia (1,000 USD)
10/2016	Best Presentation Award at D-BAUG Meet & Share your Research Day, ETH Zurich (100 CHF)
06/2016	2 nd Place at Student Poster Competition at 13 th Congress Interpraevent, Lucerne, Switzerland (€ 1,000)

Engagement in university politics

Since 09/2016	AVETH (Academic Association of the Scientific Staff at ETH Zurich) Representative in "Forum Nachwuchsförderung" (Support of young researchers careers at ETH)
06/2016-12/2017	Project Manager Art of Leadership Award at ETH Zurich (former Golden Tricycle)
04/2016	KITE (Key Innovation in Teaching at ETH) Award Jury Member as a Representative of the Scientific Staff
02/2015-09/2016	AVETH Board Member and Politics Team Coordinator
02/2015-09/2016	AVETH Delegate in ActionUni (Representation of Scientific Staff in Switzerland)
02/2015-09/2016	Member of ETH University Assembly as a Representative of the Scientific Staff

